Prediction of the Recrystallised Grain Size Distribution after Deformation for the Nb Free and Nb Model Steel

By

Mususu Kosta Mpongo Kaonda

A thesis submitted to

The University of Birmingham

For the degree of

DOCTOR OF PHILOSOPHY

School of Metallurgy and Materials

College of Engineering and Physical Sciences

The University of Birmingham (UK)

October 2016

Abstract

Grain size refinement can be achieved by recrystallisation during hot deformation, with multiple deformation steps being used during rolling or forging to give a fine grain structure. Whilst the mode (or average) grain size after recrystallisation can be determined from standard equations the full grain size distribution is required for accurate prediction of mechanical properties.

In the present work, a method to predict the full grain size distribution after recrystallisation, taking into account variations in applied strain and initial grain size, has been developed and validated using a laboratory cast and hot rolled (70 % reduction) Fe - 30 wt - % Ni model steel and commercial steels. Reheating was carried out to generate different initial grain sizes at 1200 ^{o}C and 1300 ^{o}C. Strains of 0.08 - 0.3 were applied by cold deforming the specimens. Based on the equivalence of stored energy the cold strains were estimated to be equivalent to 0.15 - 0.7 strain at 850 ^{o}C. Cold deformation was carried out as a more uniform strain distribution is realised whereas during hot deformation barrelling of the cylindrical specimens occurs due to friction between the anvil and the specimen.

The accuracy of literature equations and approaches in predicting the full recrystallised grain size distribution has been examined. It was found that equations from the literature predict the recrystallised grain size distribution with significant discrepancies, although the average grain size can be well predicted. In the current work an approach (variable *D'* approach) has been developed for predicting the recrystallised grain size distribution after deformation by using a modified Sellars equation and the best fit *D'* values obtained for the $D_{5\%}$, D_{mode} and D_{max}, where $D_{5\%}$ is the grain size class constituting the first 5% of the total area measured, D_{mode} is the mode grain size class and D_{max} is the largest grain size class in the distribution. The

Sellars equations used for predicting the recrystallised grain size were modified by considering the exponents for strain and the initial grain size from the classical rate of nucleation by assuming that grain boundary nucleation is occurring. It has been found that *D'* is a function of strain at high strain values (above 0.3 equivalent hot strain) and the relative position of the grain size in the grain size range (D*). The best fitted *D'* values for $D_{5\%}$, D_{mode} and D_{max} were used to develop an approach for predicting the recrystallised grain size after deformation.

The variable *D'* approach has been verified for other steels by applying it to available data in the literature and measured in this work. Steels grades examined included a model Fe - Ni - Nb steel, commercial Nb-microalloyed plate, a high strength strip steel and a high alloy (9Cr) forging steel with different initial grain sizes and following deformation to different deformation strains. The results for the recrystallised grain size distributions showed that predicting the recrystallised grain size distribution after deformation using the variable *D'* approach gives reasonable agreement with the experimental data. The fits are significantly better than that obtained using literature equations. However, it was found that the variable *D'* approach becomes less accurate as the complexity of the alloy increases and at lower strains, although in almost all cases the fit is better than when equations from literature are used.

Acknowledgements

Special thanks go to Professor Claire Davis and Dr. Martin Strangwood for their support and guidance, of which I am eternally grateful; without them the work could not have been accomplished. I would also like to thank Dr. Carl Slater for his support (technical and academic) and all the encouragements rendered.

I would also like to thank the commonwealth scholarship commission for sponsoring the project and Tata steels for the supply of material.

Thank you to Dave Price, Tim Doel and Avril Rogers, Jasbinder Singh for providing help readily. Appreciation must also go to the phase transformation group and to each and every fellow student that helped me in one way or the other.

Without the ongoing love and support of friends and family the challenging times would definitely have not been less bearable. A special thank you must go to my husband Stephen, who gave up his job to come to the UK to support me in my endeavours and whose encouragement helped me through the stressful times; without them, I would not have achieved what I have today.

To my three children, Mercy, Lucheshi and Butemwe, thank you for being patient with me and so understanding and supportive of my work. I would like to thank my mum for going out of her way to ensure I finish this work - her encouragement, spiritual and financial support. Thank you for showing faith in me throughout and offering kind words which provided me the required motivation to succeed.

Table of contents

List of illustrations

List of tables

List of Symbols

Chapter 2 Microstructure formation during hot deformation of microalloyed steels

X_d	Dissolution distance
D_d	Diffusivity
t	Time
D	Final reheated grain size
D_o	Initial grain size
R	Universal gas constant
Q_g	Activation energy for grain growth
T	Absolute temperature
mg, A	Constants in the grain growth model
ng	Grain growth exponent
M	Boundary mobility
V	Moving boundary velocity
P	Driving pressure
M_o	constant
Q_{bm}	Activation energy for boundary migration
F_p	Total pinning force
r	Particle radius
Ns	Number of particles per unit area of boundary
γ	Interfacial energy per unit area of boundary
R	Maximum grain radius
f	The precipitate volume fraction
r_m	Mean particle radius
α	Constant
μ	Shear modulus

b	Burgers vector
τ	Flow stress
E_s	Stored energy
ρ	Dislocation density
F_R	Driving force for recrystallisation
ρ^G	Dislocation density for geometrically necessary dislocations
C_G	Constant in Ashby's model
γ_1	Shear strain
$\Delta\sigma$	Increase in dislocation density during work hardening
α_S, C_2	Constants in stored energy model
M_S	Constant
ε	Strain
P_r	Retarding force
σ_B	Specific boundary energy
τ_s	Applied stress
FS	Softened fraction
σ_m	Maximum stress of the first deformation
σ_2	Stress from the second deformation curve determined depending on the method used to calculate FS
σ_1	Stress from the first deformation curve determined depending on the method used to calculate FS
σ_{FS}	Stress
σ_{01}, σ_{03}	Instantaneous stress values in stage 1 and 3 of stress relaxation
α_1	Slope of the first curve of stress relaxation
α_3	Slope of the third curve of stress relaxation
X	Recrystallised fraction
σ_A	Stress for the first stage of stress relaxation
σ_B	Stress for the third stage of stress relaxation
σ	Stress for the second stage of stress relaxation

$t_{0.5}$	Time for 50 % recrystallisation
n	Avrami exponent
A_1, m, p, q	Constants in the empirical equation for determining $t_{0.5}$
Q_{rex}	Activation energy for static recrystallisation
R_s	Recrystallisation start time
R_f	Recrystallisation finish time
T_{def}	Temperature of deformation
Q_{def}	Activation energy for deformation
$\dot{\varepsilon}$	Strain rate
T_{NR}	No recrystallisation temperature
C_3, B	Constants in Dutta - Sellars equations
Z	Zener - Holloman parameter
K_s	Supersaturation ratio
P_s	Strain induced precipitation start time
D_{rex}	Recrystallised grain size
x	Initial grain size exponent
y	Strain exponent
D'	Constant in the empirical equation for determining D_{rex}

Chapter 4 Effect of strain and initial grain size distribution

B	Barrelling coefficient
h_f	Final height after deformation
d_f	Final diameter measured at the mid length of the deformed sample
h_i	Initial height
d_i	Initial diameter

Chapter 5 Modelling recrystallised grain size distribution

ΔG^*	Critical free energy
k	Boltzmann constant
v	Jump frequency

C_4	The factor that represents the number of nucleation sites per unit volume
ΔG	Free energy of activation for diffusion
N_v	Number of nuclei per unit volume per unit time
r^*	Critical radius
ΔG_v	Volumetric free energy
γ_2	The interfacial surface energy per unit area
D^*	Relative position of the grain size in the grain size range
$D_{5\%}$	Grain size class constituting the first 5 % of the total area measured
D_{max}	The largest grain size class in the distribution
D_{mode}	Mode grain size class

List of Abbreviations

Chapter 1	**Introduction**
TMCR	Thermomechanical controlled rolled
HSLA	High strength low alloy
Chapter 2	**Microstructure formation during hot deformation of microalloyed steels**
SEM	Scanning electron microscopy
TEM	Transmission electron microscopy
DSC	Differential scanning calorimetry
SDAS	Secondary dendritic arm spacing
DRV	Dynamic recovery
EBSD	Electron backscatter diffraction
SIP	Strain induced precipitation
DRX	Dynamic recrystallisation
SRX	Static recrystallisation
SFE	Stacking fault energy
RPTT	Recrystallisation precipitation temperature time
SRCT	Static recrystallisation critical temperature
RST	Recrystallisation start temperature
PSN	Particle stimulated nucleation
EDS	Energy dispersive spectrometry
SIBM	Strain induced grain boundary migration
SSD	Statically stored dislocations
GND	Geometrically necessary dislocations
DHT	Double deformation test
SRT	Stress relaxation test
RMS	Root mean square

Chapter 3	**Materials and experimental procedures**
EDM	Electro - discharge machine
PTFE	Polytetrafluoroethylene
ECD	Equivalent circle diameter
NRMS	Normalised root mean square
Chapter 6	**Prediction and verification of grain size distribution in different steel grades**
SRP	Solute retardation parameter

List of publications from this work

JOURNAL

- Modelling recrystallised grain size distributions in deformed and annealed Fe - 30Ni steel: Kaonda, M. K. M., Slater, C., Strangwood, M. and Davis, C.L., under preparation.

CONFERENCE PROCEEDINGINGS

- Study of grain structure development during deformation in Nb microalloyed steels, Kaonda, M. K. M., Strangwood, M. and Davis, C.L., Brunel University, UK, June 2013.

- Modelling the recrystallised grain size distribution after deformation: Kaonda, M. K. M., Slater, C., Strangwood, M. and Davis, C.L., Proceedings of the 6th International Conference (Steelsim), Lake Garda, Italy, August 2015.

CHAPTER – 1

Introduction

Currently about 1.8 * 10^8 tonnnes of microalloyed steel are produced in the world annually making up 12 % of the total world steel production (1,606 million tonnes) [1]. The continued demand for steel has led to extensive research on improving the mechanical properties of steel as well as improving production rates. Different steel grades have, over the years, found extensive use in the manufacturing of structural components for industries such as construction and transportation. Engineering applications using steels generally require high strength and good toughness the balance of which is controlled by their microstructures.

Microalloyed steels contain small amounts of alloying elements (other than carbon, silicon and manganese) such as niobium (Nb), vanadium (V) and titanium (Ti), which enhance their mechanical and physical properties and are as such suitable for most engineering applications that require high strength and toughness. Microalloyed steels undergo several stages of processing before the required fine and uniform microstructure is obtained. The process involves casting, reheating and hot rolling which determine the microstructure of the final product. For the majority of microalloyed steels, hot deformation via thermo-mechanical controlled rolling (TMCR) or forging is currently used to produce plate and strip steels with fine (typically 5 - 10 μm final ferrite grain size for TMCR high strength low alloy (HSLA) steels), uniform grain size distribution, required for high strength (yield strength greater than 275 MPa) and adequate toughness (e.g. 27 J at - 40 ^oC for pipeline steels). TMCR is commonly used because of its ability to control the microstructure whilst shaping the dimensions of steels. TMCR is designed in such a way that full recrystallisation occurs during

roughing rolling (in order to refine the grain size). Full recrystallisation is followed by no recrystallisation during finish rolling leading to a pancake austenite grain structure for subsequent transformation to fine grained ferrite [2].

Accurate prediction of the recrystallised grain size distribution obtained from such processing would allow for prediction of coarse grains in the distribution as well as allow for designing of the most efficient processing schedules in order to obtain a uniform fine grain size. Whilst it has been shown that mode / average grain sizes mostly determine the strength of the steel, toughness has a greater dependence on the large grains in the grain size distribution [3, 4]. Therefore, any grain size prediction modelling will need to incorporate the full distribution modelling, rather than just mode, which is the more common current method [4].

Different equations based on Sellars equations and approaches have been proposed in the open literature for predicting recrystallised grain sizes [3 - 10]. These equations show that applied strain and initial grain size have an influence on the recrystallised grain size [3 - 10]. Most of these equations are developed for predicting mode / average recrystallised grain sizes and are valid for specific strains, initial grain sizes and steel grades. The equations from the literature such as those proposed by Sellars [5], do predict the recrystallised mode grain size well however not many approaches and equations have been proposed for modelling the recrystallised grain size distributions [4]. Kundu [3, 4] proposed the individual grain size class approach for predicting grain size distributions using a Nb-containing HSLA (high strength low alloy) steel with an initial grain size of 240 - 280 μm deformed to a strain of 0.3. However, the proposed approach did not consider different strain levels and a range of initial grain sizes as well as the effect of high strain values on nucleation site density, which may lead to discrepancies in predicted recrystallised grain size distributions. Therefore, a more

robust approach for modelling recrystallised grain size distributions after deformation is required.

In the present work, the influence of prior austenite grain size and strain on recrystallisation will be investigated using a model Nb-free (Fe - 30 wt - % Ni) and a Nb-containing model steel. The model alloy will be used because it retains the austenitic microstructure upon cooling or heating which makes direct observation of the grain size distributions after deformation easier, whereas low alloy steels undergo a transformation from austenite to ferrite on cooling from hot deformation temperatures [4]. The data generated from carrying out tests on the Fe - 30 wt - % Ni steel will be used to develop an approach for modelling recrystallised grain size distributions after deformation. The proposed approach will be validated using various strains, initial grain sizes and steel grades. The accuracy of approaches [3, 4] and equations given in open literature [5, 6] in predicting grain size distributions will also be assessed.

1.1 Thesis structure

- Chapter 2 contains a description of the investigation of the key metallurgical processes during and after deformation in greater detail through an examination of literature published by peers in both industry and academia. The chapter includes findings from the literature and a critical analysis of the historical research studied.
- Chapter 3 comprises a discussion of experimental procedures used to gather data for both material characterisation and developing equations / approaches for modelling grain size distributions after deformation. The chapter provides details for the different steel grades examined in this work.

- Chapter 4 discusses the findings from the experiments in Chapter 3. The chapter discusses the influence of strain and initial grain size on recrystallisation as well as the accuracy of literature equations [5] and approaches [3, 4] in predicting recrystallised grain size distributions after deformation.
- Chapter 5 discusses the modification of Sellars equation [5], based on the classical rate of nucleation (assuming that nucleation occurs by boundary migration).
- Chapter 6 discusses the prediction of grain size distributions for different steel grades, strains and initial grain sizes using the modified Sellars equation. The chapter also discusses the validity and limitations of the modified approach.
- Finally, in Chapter 7 and 8 conclusions and a brief overview of potential future work are given.

CHAPTER – 2

Microstructure formation during hot deformation of microalloyed steels

2.1 Introduction

As stated in Chapter one, the most common deformation route used to produce plate and strip steels is thermo-mechanical controlled rolling which involves the interaction between recrystallisation and precipitation effects [11, 12]. TMCR, shown in Figure 2.1 [2, 13], has the ability to extensively refine grains whilst shaping the dimensions of the steel compared with conventional hot rolling. This is achieved by using finish rolling deformation at temperatures below the recrystallisation start temperature (RST) to produce pancaked austenite grains with a large number of nucleation sites for subsequent ferrite formation [13, 14, 15]. The process consists of preliminary continuous casting, then reheating the steel at about 1150 - 1250 ^{o}C, followed by deformations through multiple stages with different holding times in between deformation passes. Typical TMCR temperatures for rough rolling are 1000 to 1100 ^{o}C and 750 - 850 ^{o}C for finishing rolling with strains of 0.15 to 0.3 (with strain rate of 1 to 20 / s for plate rolling) [2, 16], for static recrystallisation. In TMCR processes prior austenite grain boundaries act as ferrite nucleation sites with typical final ferrite grain size after deformation being 5 - 10 μm [17].

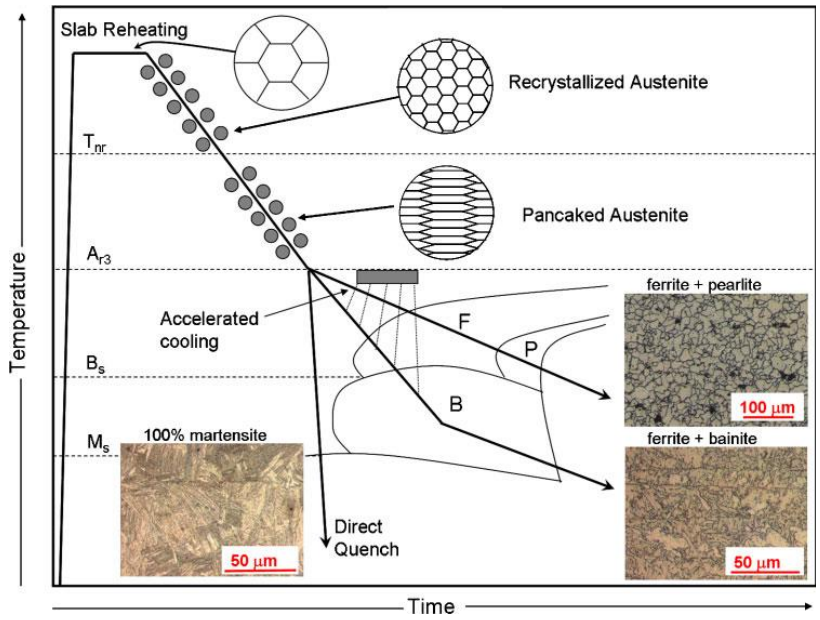

Figure 2.1: Schematic representation of thermo-mechanical controlled processing (TMCR). Obtained microstructures (T_{NR}: non-recrystallisation temperature, B_s: Bainite start temperature, A_{r3}: Austenite to ferrite transformation start temperature, M_s: Martensite start temperature, F: Ferrite, B: Bainite, P: Pearlite) are also shown [2].

Figure 2.1 shows the changes in microstructure, that is, grain size change (e.g. pancaking, recrystallisation and transformation) during the different processing parameters in TMCR [2, 13]. It is important to understand how the microstructure evolves during and after deformation through the key metallurgical processes operating during TMCR, such as recovery, recrystallisation, grain growth and precipitation, to be able to design an appropriate rolling schedule [1, 4, 18]. However, the grain-coarsening behaviour of steels during reheating before rolling is also an important factor to consider in obtaining a fine-grained product [19] and is therefore considered in the next section.

2.2 Microstructure development during reheating

As stated in Section 2.1 continuous casting is the preliminary stage to TMCR and involves solidification of molten metal into semi-finished billet bloom, or slab for subsequent rolling followed by reheating. During continuous casting, dendritic solidification is predominant and occurs due to constitutional super cooling in the liquid, which leads to the formation of primary and secondary dendrites [20]. The spacing between primary and secondary branches is termed dendritic arm spacing and is widely used to measure the effects of solidification conditions on dendrite structures [21]. Differences in the solubility of alloying elements in the solid and the liquid metal during casting leads to alloying elements segregating preferentially into the solid or liquid. Segregation takes place during freezing of an alloy and refers to any non-uniformity of chemical composition. During continuous casting steels may undergo either micro segregation (typically on the scale of 10 - 100 μm) or macro segregation which is typically on the scale of 1 - 1000 mm. Macro segregation is as a result of non-uniformity of composition in the cast material on a larger scale whereas micro segregation is due to freezing the solute enriched liquid in the inter dendritic spaces [21]. For more information on solidification of castings the reader should refer to [21].

A detailed discussion on grain structure development during solidification is given by Kundu [4]. She stated that avoiding micro segregation of microalloying elements during thick slab processing may be difficult due to relatively slow cooling. This is due to the fact that slow cooling leads to near equilibrium conditions which allow the segregation tendency of microalloying elements to be developed. Kundu [4] concluded that of all the alloying elements Nb had the greatest segregation tendency. It was reported that there was a periodic variation in the Nb levels, with up to 10 times as much Nb in inter dendritic areas compared with the dendritic areas in the as-cast material, whereas no systematic variation in the Nb

level in the homogenised sample was observed using EDS (energy dispersive spectrometry). The segregation of microalloying elements would subsequently lead to a precipitate population that is not homogenous in the dendritic and inter dendritic regions in the as-cast condition. The development of an inhomogeneous precipitate population in the as-cast condition may affect the grain growth behaviour of the material during subsequent processing (e.g. during reheating). It was concluded that a bimodal grain size might start to form during the continuous casting stage of TMCR due to segregation of microalloying elements such as Nb and Ti [4, 17, 22]. It is necessary to study the formation of microstructure during reheating as this determines the uniformity of the material in terms of segregation because reheating would reduce the extent of segregation. Reheating is also used for determining the starting grain size distribution of a material [4]. The following section will therefore discuss the reheating process.

2.2.1 Reheating

Reheating is used to ensure that microalloying elements (particularly V and Nb) are in solution, so that precipitation can occur during (commonly Nb (C, N) precipitates) and after (commonly VC) rolling, and as such the preferred strength levels can be realised by way of grain size control and dispersion strengthening precipitates [4, 11, 12]. Dissolution of the precipitates and grain growth is reliant on the reheat time and temperature [23]. Dissolution temperatures for microalloyed steels may range from 1150 - 1250 ^{o}C depending on the precipitate volume fraction and size. Precipitate dissolution temperature is usually predicted using Thermo-Calc software [4] while precipitate dissolution time is dependent on secondary dendritic arm spacing (SDAS) [4].

Kundu [4] used Thermo-Calc software to predict the dissolution temperature for a 0.046 wt - % Nb steel (which was predicted to be 1225 ^{o}C). She measured the spacing between inter dendritic regions in the as-cast material to be about 200 - 250 μm, so that Nb atoms would need to be diffused over a distance of 100 - 125 μm to reach the dendrite centres in so doing approach a uniform composition. The dissolution distance of 100 - 125 μm was used in Equation 2.1 (which is based on Fick's second law for changing concentrations with time) in order to determine the dissolution time for a 0.046 wt - % Nb steel (which was calculated to be 2 - 3 days). It was reported that after a homogenisation treatment of the 0.046 wt - % Nb steel at 1225 ^{o}C for 4 days a unimodal grain size was obtained with an average grain size of 240 - 280 μm [4]. Grain growth kinetics are discussed in the following section.

$$X_d = (D_d\, t)^{1/2} \qquad (2.1)$$

Where X_d is the dissolution distance, D_d is the diffusivity of Nb in austenite (m^2 / s) and t is the precipitate dissolution time.

2.2.1.1 Grain growth during reheating

Grain growth during reheating occurs in order to reduce the total grain boundary energy, which is usually reflected through the reduction of total grain boundary area (due to increase in grain size) [24, 25, 26, 27]. The driving force for grain growth is considered in terms of grain boundary curvature; the shape of the grain boundary could either be concave or convex. The driving force for grain growth is also considered in terms of grain angles; grains are assumed to be in equilibrium when corner angles attain 108^{o} and edge angles attain 120^{o} in a 3-dimensional (3-D) array [26]. In a 2-D array grain corners are assumed to be in equilibrium when they attain a grain angle of 120^{o}. The flattening of curved interfaces and the change in grain boundary and edge angles towards their equilibrium values (120^{o} for 2-D arrays)

reduces the total grain boundary energy. It is well accepted that concave and large angle grains favour growth of the grain whereas grains with convex curvatures and less than equilibrium edge and corner angles tend to shrink. In addition to the driving force provided by grain angle and the curvature effect there maybe additional driving forces for grain growth such as differences in energy density of grains caused by or associated with elastic strains due to an applied stress or residual stresses [26].

Grain growth kinetics are influenced by temperature and holding time [27 - 30]. During reheating the average grain size increases with increased temperature and soaking time as shown in Figure 2.2 and 2.3 for a 300 M steel heat treated at a range of temperatures (850 to 1050 ^{o}C) using different soaking times ranging from 5 to 120 minutes [29]. Zhang *et al.* [29] used linear intercept method in order to measure the average austenite grain size. Linear intercept method involves estimation of the grain diameter by measuring the number of intersections of the circle with grain boundaries and taking into account the magnification of microstructure and the diameter of the circle [6, 18, 31].

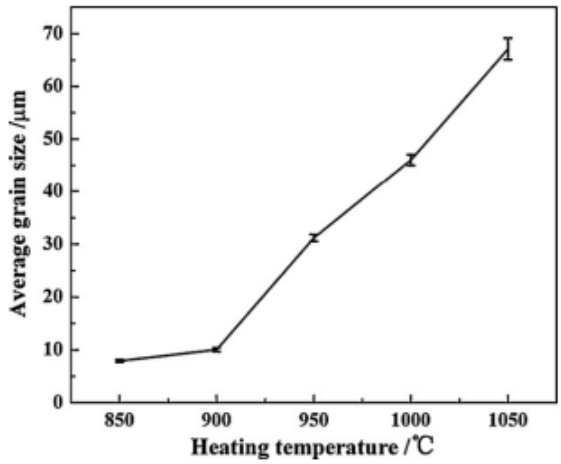

Figure 2.2: Effect of temperature on the reheated grain size [29].

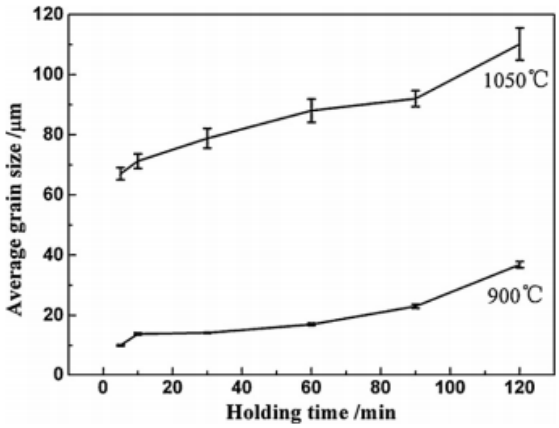

Figure 2.3: Effect of holding time on the reheated grain size [29].

Grain growth kinetics for steels are often modelled by Equation 2.2 (assuming steady state grain growth, that is, at constant temperature) [5, 16]. Empirical models in the form of Equation 2.2 are used for predicting classical isothermal grain growth in single phase alloys and show the dependency of grain diameter on time and temperature [25, 32]. Equation 2.2 was initially developed by Sellars [5] through equation fitting to C - Mn steels without microalloying elements [5] as well as microalloyed (Nb, V, Ti) C - Mn steels and ferritic steels [1, 5]. Most empirical models developed for different materials, for example austenitic steels [33], are based on Sellars model [5].

$$D^{ng} - D^{ng}_{o} = At^{mg} \exp(- Q_g / RT) \quad (2.2)$$

Where D_o is the initial grain size, R is the gas constant, T is the absolute temperature, D is the final grain size at time of t, mg and A are constants. The exponent ng is the grain-growth exponent (whose values typically range from 2 to 10). Although a grain-growth exponent of 10 gives a satisfactory fit to results obtained at short soaking times, it has been argued that it is higher than what is expected theoretically (a lower grain-growth exponent) [5]. Values ranging from 0.8 [33] to 1 [5] have been reported for mg and Q_g is the activation energy for

grain growth ($J.mol^{-1}$); some values for Q_g are given in Table 2.1. Table 2.1 highlights various parameters used in Equation 2.2 [5, 16, 30, 31, 33, 34].

Table 2.1: Summary of parameters used in predicting grain growth kinetics.

ng	mg	A	Q_g / kJ / mol	Grain size / µm	Steel composition	Ref.
10	1	5.3 *1032	400	46 - 126	C - Mn	34
10	1	1.66*1017 9.0*1015 3.77*1013	400	100 - 450	C - Mn	5
7		1.45*1027	400		C - Mn - V	16
10	1	2.6*1028	437	40 - 150	C - Mn - Ti	
4.5	1	4.1*1023	435	40-150	C - Mn - Nb	
4.3	1	2.04*1023	432	40-150	Nb - V -Ti	31
2.5	1	1.03*1016	398	10	0.044Nb	30
3.02	1	1.154*1013	236	10 - 80	AISI 4140 C - Mn	33

Zhao *et al.* [30] used a grain exponent of 2.5 (other parameters are given in Table 2.1) in order to predict the grain growth of a medium-carbon niobium bearing steel heated at different temperatures ranging from 950 - 1200 ^oC for an hour. It was shown that there was generally a good correlation between the measured and predicted, as shown in Figure 2.4. Figure 2.4 illustrates that the reheated grain size increases with heating temperature and that at lower temperatures (up to 1000 ^oC) the reheated grain size does not change significantly as the holding time increases. However, at higher temperatures the reheated grain size is a function of soaking time (larger grains are generated at longer soaking times).

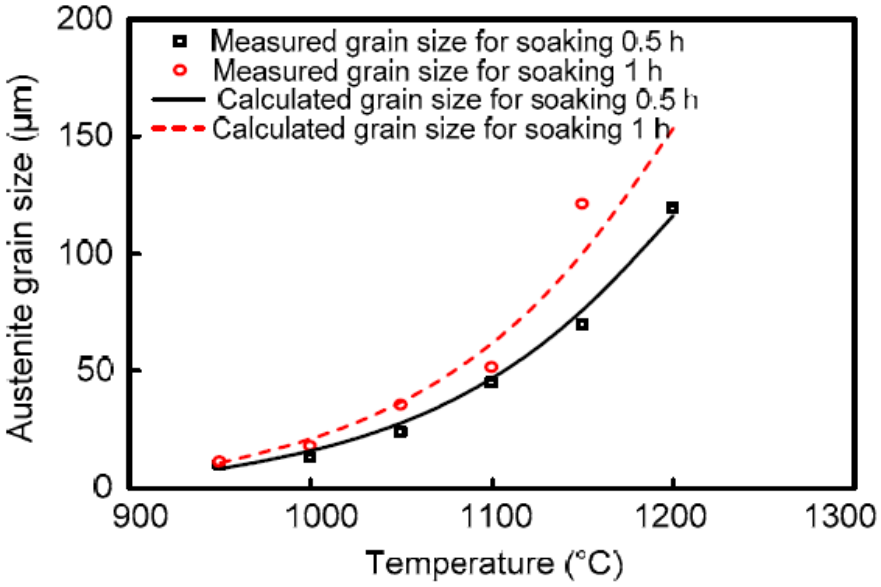

Figure 2.4: Comparison of measured average reheated grain size and predicted using Equation 2.2 (using ng = 2.5) at various heating temperatures for different soaking times [30].

Grain growth is influenced by the mobility / migration of high angle grain boundaries. The migration of grain boundaries occurs in response to a driving force pressure which arises from the grain boundary energy in the material. The moving boundary velocity (V) is generally represented by Equation 2.3 which has, in most cases, been found not to be valid for low angle boundaries as boundary mobility (M) is dependent on the driving pressure (P) for low angle boundaries [25, 26, 35].

$$V = MP \qquad (2.3)$$

Where boundary mobility is defined by the following equation:

$$M = M_o \exp(- Q_{bm} / RT) \qquad (2.4)$$

Where M_o is a constant.

Equation 2.4 predicts that boundary migration is dependent on temperature and activation energy for boundary migration (Q_{bm}) [35]. Huang *et al.* [35] carried out a combination of in - situ annealing (at 275 - 400 ^oC) and electron backscatter diffraction in the scanning electron

microscope (SEM) to determine the mobility of high angle grain boundaries in a deformed (0.5 - 0.7 strain) Al - Si alloy and found that boundary velocity was directly proportional to driving pressure. The mobility of grain boundaries is often inhibited by pinning of grain boundaries by undissolved precipitates or solute atoms in solution. The total pinning force (F_P (in N / m^2)) for an array of precipitates is given by the following equation [36]:

$$F_P = 4r\gamma N_s \quad (2.5)$$

Where N_s is the number of particles per unit area of boundary, γ is the interfacial energy per unit area of boundaries and r is the particle radius.

Solute drag by microalloying elements in steels may inhibit the mobility of grain boundaries at very high temperatures (above 1050 ^oC) and at strains lower than 0.2; however, solute drag is not as effective in reducing the rate of grain growth as is pinning of grain boundaries by undissolved precipitates at higher strains (i.e. strain > 0.2) and lower temperatures (below 1050 ^oC) [4, 28]. Solute drag consists of segregation of solute atoms to the grain boundaries or in certain cases their rejection from the grain boundaries. Migration of the grain boundary leads to the development of an asymmetric segregation profile. The formed profile causes a net force on the grain boundary, and as such opposing the migration of grain boundaries thereby slowing it down [4, 18, 28]. Precipitates tend to cause the Zener drag effect which occurs when the grain boundary intersects a particle causing a disappearance of a small area of the grain boundary thereby retarding grain growth [28, 26]. Zener equations [26] are used to describe the inhibition of grain growth precipitates pinning grain boundaries. The Zener equations describe the relationship between the maximum grain radius and the mean precipitate radius, as well as the volume fraction of the precipitates [26].

$$R = 4r_m / 3f \quad (2.6)$$

Where R is the maximum grain radius, r_m is the mean precipitate radius and f is the precipitate volume fraction.

Grain growth may either be normal or abnormal; normal grain growth results in having a unimodal grain size distribution (i.e. the grain size distribution is homogeneous). For log-normal distributions the ratio of mode grain size to largest grain size in the distribution is 1:3, and this does not change with time (Figure 2.5). During normal grain growth, the grain size distribution moves to larger sizes as a function of time and temperature [24, 26, 28, 37]. Any inhomogeneous distribution of microalloying elements (e.g. Nb and Ti) due to segregation may lead to bimodal grain structures developing during reheating. Figure 2.6 shows grain sizes obtained based on different reheat conditions in Nb-containing steels [38].

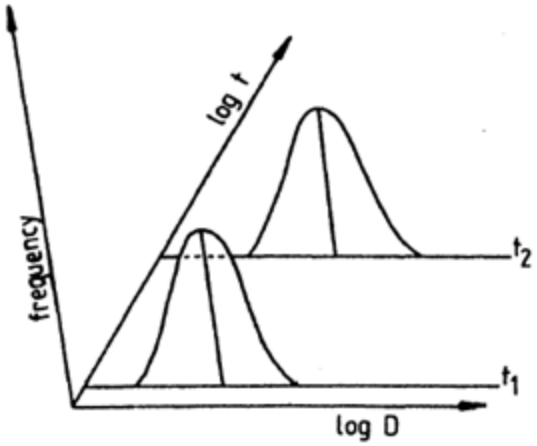

Figure 2.5: Changes in the grain size distribution with time for log-normal grain growth [27].

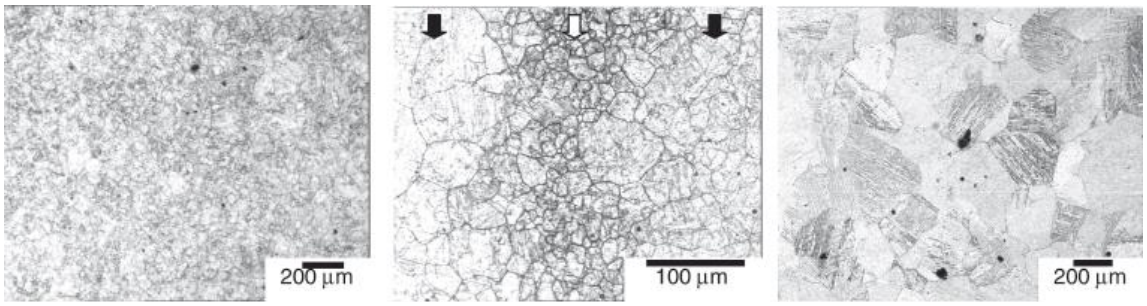

(a) (b) (c)

Figure 2.6: Prior austenite grain size for a 0.045 wt - % Nb steel reheated to (a) 1075 °C, (b) 1150 °C (fine grain regions are arrowed in white and coarse grain regions are arrowed in black) and (c) 1225 °C for one hour [38].

Kundu [4] reheated a 0.046 wt - % Nb steel to 1150 °C and 1225 °C for an hour and found that a unimodal grain size distribution was obtained at 1225 °C with an average grain size of 160 - 180 µm (Figure 2.7), whereas for the sample heat treated at 1150 °C a bimodal grain size distribution was achieved with average grain sizes of 40 - 60 µm and 200 - 220 µm in solute rich and solute depleted regions (Figure 2.8). This was due to the fact that reheating at 1225 °C led to complete dissolution, whereas reheating at 1150 °C led to growth in depleted regions (predicted dissolution temperature in depleted regions was about 1090 °C) and pinning in solute rich regions (pinned by Nb, Ti, V (C, N)). When partial dissolution of precipitates occurs, the pinning of precipitates becomes unstable, thereby leading to large grains with a size advantage growing abnormally. Abnormal grain growth results in a bimodal distribution which changes with time, as shown in Figure 2.9 [27, 39 - 43]. In Fe - 30 wt - % Ni steels abnormal grain growth may occur due to local differences in boundary mobility so that some grains grow whereas others do not.

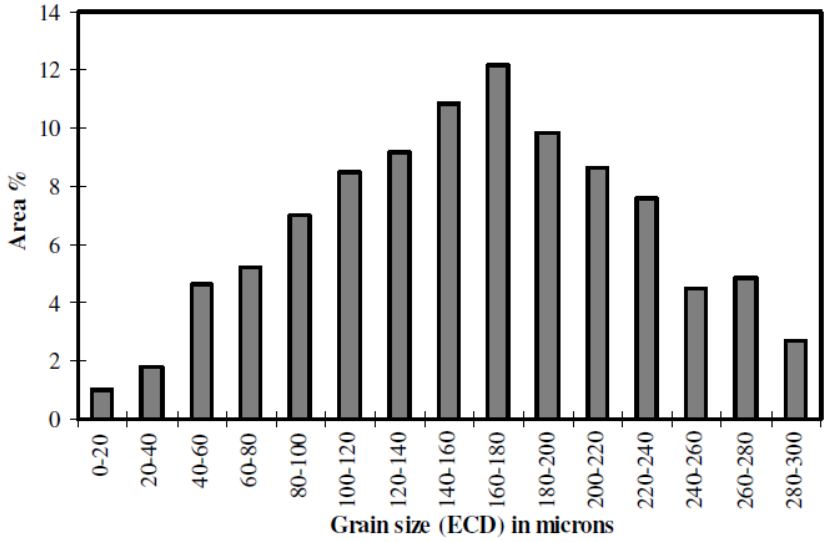

Figure 2.7: Grain size distributions for a segregated 0.046 wt - % Nb steel heat treated at 1225 ^{o}C for an hour [4].

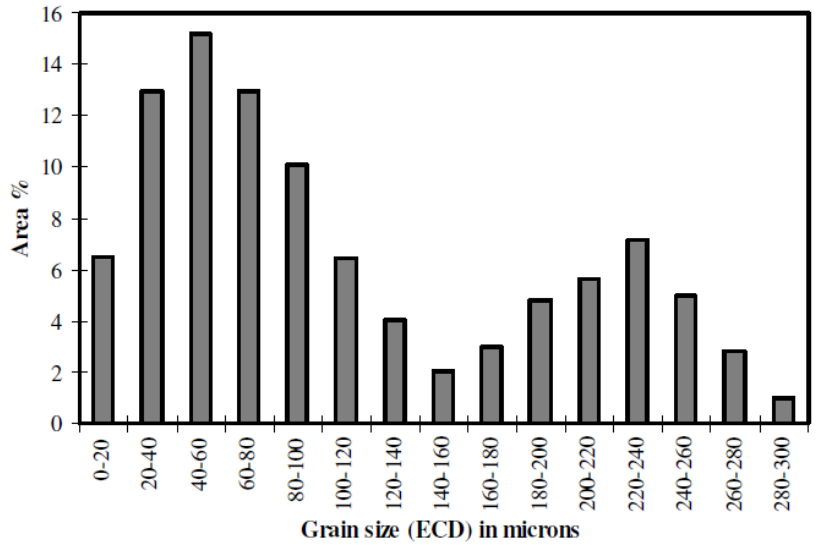

Figure 2.8: Grain size distributions for a segregated 0.046 wt - % Nb steel heat treated at 1150 ^{o}C for an hour [4].

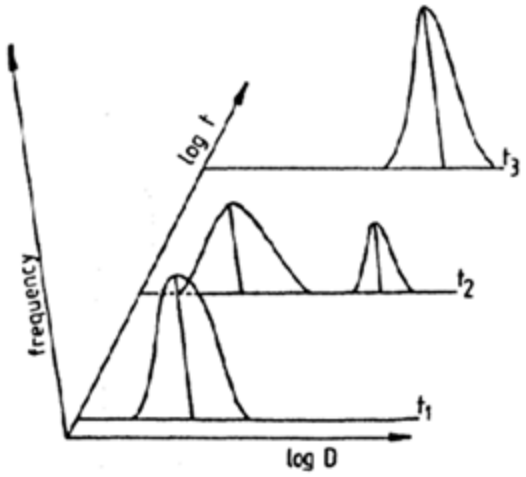

Figure 2.9: Changes in the grain size distribution with time for abnormal grain growth [27].

2.3 Microstructure development during hot deformation of microalloyed steels

Different metallurgical processes occur during and after hot working, such as recovery, recrystallisation and grain growth which influence the final microstructure of a material [18]. A schematic for key metallurgical processes taking place during and after deformation is shown in Figure 2.10 [18]. Different parameters such as strain rate, deformation temperature holding time, initial grain size and precipitates can influence recrystallisation kinetics [4, 6, 18, 34, 44 - 50].

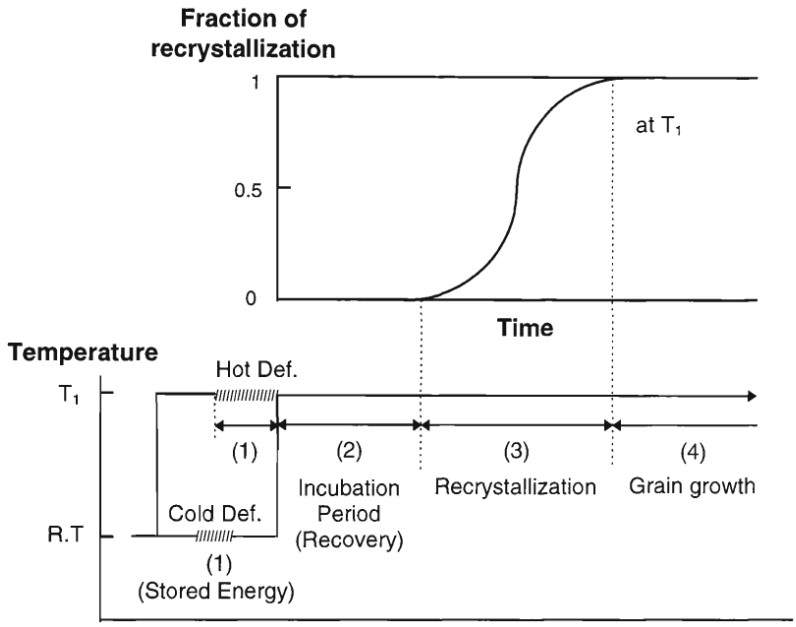

Figure 2.10: Schematic representation showing the key metallurgical processes taking place after deformation of a material [18].

2.3.1 Factors influencing recrystallisation

An increase in the amount of applied strain during deformation leads to an acceleration in recrystallisation kinetics as well as a decrease in the recrystallised grain size [4, 6, 18, 34, 44 - 47]. This is due to an increase in dislocation density, which is the driving force for recrystallisation and will be discussed in Section 2.3.3. In the experimental work of Sha *et al.* [6] the influence of strain was studied using a Nb - V - Ti steel with an initial grain size of 808 µm deformed at 1100 ^{o}C to 0.2 - 0.4 strain. It was reported that the material had refined by 74 %, 80 %, 87 % when deformed to 0.2, 0.3 and 0.4 strain respectively. Similarly, Abdollah-Zadeh [18] showed that the recrystallised grain size decreased with strain using Fe - 30Ni steel with an initial grain size of 310 µm deformed at 850 ^{o}C. It was shown that the recrystallised fraction increased with strain; at a strain of 0.25 no recrystallisation was

observed, while at a strain of 0.5, 8 % recrystallisation was observed after annealing the sample for 2 seconds [18].

A change in grain size will influence the available area for nucleation, thus affecting recrystallisation kinetics; finer grains have more available grain boundary area per unit volume compared to coarse grains. Finer grains will therefore provide a higher number density of nucleation sites thereby lowering recrystallisation start and finish times [4, 18, 28, 44, 48 - 52]. Li *et al.* [48] investigated a low carbon steel containing 0.055 wt - % Nb with initial grain sizes ranging from 12 - 71 μm deformed at 1000 ^{o}C. They observed that after a holding time of 1000 seconds the sample with an initial grain size of 12 μm had recrystallised completely while the sample with a larger initial grain size (71 μm) had softened fraction of 0.46 (the softened fraction was measured using the 2 % offset method) [48]. The recrystallised grain size decreases with a decrease in initial grain size due a higher number density of nucleation sites provided by finer grains [7, 8, 9, 53]. Equations for quantifying the recrystallised grain size will be discussed in Section 2.3.9.

There is conflict in the literature about whether strain rate has a strong influence on recrystallisation kinetics or not; some authors [47 - 50] claim that there is a weak dependency of recrystallisation kinetics on strain rate during hot deformation, while other researchers [46, 54] argue that strain rate has an effect on recrystallisation kinetics due to the differences in flow stress values (and consequently the amount of stored energy) realised after deformation [46, 54] and as such cannot be ignored. These researchers [46 - 54] have argued that the difference is flow stress values may be due to the fact that at higher strain rates, greater work hardening of the material, due to dislocation pileups, is observed which consequently leads to a higher stored energy as compared to lower strain rates. For example, Palmiere *et al.* [54]

deformed Fe - 30 wt - % Ni steel at 950 °C to a strain of 0.8 and varied the strain rate between 1 / s and 10 / s. Different flow curves were obtained from this work; at a strain rate of 1 / s a flow stress value of 150 MPa was obtained whereas for the sample deformed at a strain rate of 10 / s a flow stress of 270 MPa was obtained. On the other hand, Mannan *et al.* [46] and Laasraoui *et al.* [47] found that there was no significant difference in the recrystallised grain size and flow stress for a similar change in strain rate. For instance, Mannan *et al.* [46] observed that a grain size difference of 6 μm was obtained at lower temperatures (1000 °C) for the Ni - 30 wt - % Fe steel deformed to a strain of 0.2 at strain rates of 0.1 / s and 1 / s. A difference of 20 μm was observed at higher temperatures (1150 °C) when strain rate was varied from 0.1 to 1 / s, with the largest grain size being at a strain rate of 1 / s. The reasons for this difference were not given; however, this could have been due to grain growth as a result of higher activation energy for grain boundary mobility at such high temperatures (1150 °C). This could also be due to the fact that a higher stored energy (higher flow stress) would change the degree of refinement. It seems plausible from the above discussion to suggest that strain rate may not significantly influence recrystallisation kinetics or the recrystallised grain size, although Palmiere *et al.* [54] reported an increase of 130 MPa for the same change in strain rate which seems large enough and may alter recrystallisation kinetics.

The presence of precipitates in a sample and solute atoms in solution will lead to grain boundary pinning via Zener drag or solute drag and consequently slow down recrystallisation kinetics [18, 47] as discussed in Section 2.2.1.1. The influence of solute drag and precipitation on recrystallisation kinetics will be discussed in Section 2.3.6.2 and 2.3.8.2. Abdollah-Zadeh [18] compared the recrystallisation amounts (%) for the Fe - 30Ni - 0.02Nb steel and Fe - 30Ni steel deformed at 900 °C and strained to 0.5 and found that only 4 % recrystallisation was observed for the Nb-containing steel while 35 % recrystallisation was observed for the

niobium free steel after a holding time of 2 s. Some researchers suggest that solute drag and undissolved precipitates (> 1 μm) may influence the recrystallised grain size after deformation by slowing down the movement of grain boundaries, and by the occurrence of particle stimulated nucleation (PSN) of recrystallisation respectively [28, 55, 56]. PSN will be discussed in detail in Section 2.3.6.2. Quantification of recrystallisation kinetics and recrystallised grain size will be discussed in Section 2.3.8 and 2.3.9.

Table 2.2 and 2.3 gives a summary of some of the deformation process parameters investigated and reported in the literature for HSLA steels and model steels, such as Fe - 30Ni steels and Ni - 30Fe steels. [4 - 7, 34, 44, 45, 47, 57, 58]. Most of the deformation tests for HSLA steels have been carried out at high temperatures (800 - 1200 ^{o}C) with strains ranging from 0.1 - 2 and strain rates ranging from 0.0022 - 50 / s as shown in Table 2.2 [4 - 7, 34, 44, 45, 47, 57, 58]. It can also be seen from Table 2.3 that most of the deformations for model steels have been carried out at 800 - 1150 ^{o}C with strains ranging from 0.25 - 1.2 at strain rates of 0.01 - 10 / s [18, 46, 54, 59]. Deformations at room temperature have also being carried out, although in all the literature reviewed for this work no strain rate values have been reported [60 - 62].

Table 2.2: Summary of processing parameters for microalloyed steels.

Material / wt - %	$\dot{\varepsilon}$ / s	ε	Deformation temperature / °C	Softening mechanism	Deformation Method	Ref.
0.046 Nb steel	10	0.3	1075	Static	Plane strain compression	4
Nb - V -Ti microalloyed steel	3	0.2 - 0.4	1100	Static	Uniaxial compression	6
C - Mn - 0.06 Nb -0.0109 Mo steel	0.05	0.3	1000	Static	Uniaxial compression	15
0.051 Nb steel	1	0.25 - 0.37	1040 - 1095	Static	Plane strain compression	57
	0.22	0.3	850 - 1050	Static		
0.015 Nb steel	0.0022	0.3	850 - 950	Static	Tensile	7
	0.0022	0.3	1050	Dynamic		
Pure Copper	not given	0.18 - 0.38	Room temperature	Static	Tensile test then annealed	60
Pure Copper	not given	0.18 - 0.93	Room temperature	Static	Tensile test then annealed	61
0.026 Ti steel	0.0043 - 5.2	2	1050	Dynamic	Torsion	34
	0.173	1.4	849 - 1150	Dynamic		
C - Mn steel	not given	0.9	Room temperature	Static	Cold rolling	62
Nb microalloyed steel	1	0.1 - 0.5	1100	Static	Torsion	44
Low alloy and microalloyed steel	0.54 - 3.63	0.20 - 0.35	850 - 1150	Static	Torsion	45
	1	0.3	1100	Static		
0.035 Nb steel	5	0.93	1080	Dynamic	Torsion	58
	0.2	0.75	800 - 900	Static		
0.058 Nb - 0.02Ti steel			1000 - 1200	Dynamic	Uniaxial compression	47
	0.2	0.75	800	Static		
0.02Ti steel			900 - 1000	Dynamic	Uniaxial compression	47
	2	0.75	800	Static		
			900 - 1100	Dynamic		

Table 2.3: Summary of processing parameters for model steels.

Material	$\dot{\varepsilon}$ / s	ε	Deformation temperature / °C	Softening mechanism	Deformation Method	Ref.
Fe - 30Ni steel	10	0.8	950	Static	Plane strain compression	54
	1	0.8	950	Static		
Fe - 30Ni Fe - 30Ni-0.02Nb steel	0.7	0.25 - 0.9	850 - 1000	Static	Uniaxial compression tests	18
AISI 304 stainless steel	1	0.5, 1	700	Static	Plane strain compression	59
	1	0.5, 1	800 - 900	Dynamic		
Ni - 30Fe steel	1	0.5, 1	800 - 900	Static		
Ni - 30Fe - Nb / Ni - 30Fe steel	0.01-1	1.2	925	Static	Plane strain compression	46
			1000 - 1150	Dynamic		

2.3.2 Softening mechanisms

The main softening mechanism occurring during deformation processes is recovery, dynamic (DRX) or static recrystallisation (SRX). The most likely mechanism for nucleation of recrystallisation is assumed to be strain induced boundary migration (SIBM) of the grain boundaries discussed in detail in Section 2.3.6.1. Static recrystallisation will occur after deformation, depending on several deformation factors such as strain rate, strain (generally less than 0.5), deformation temperature and interpass time / holding time [46, 47]. SRX is said to be initiated at critical strains of 0.07 for temperature ranges of 900 - 1000 ^{o}C for C - Mn steels [4, 5, 26]. DRX (nucleation and growth of new grains during deformation) has generally been observed to occur at very low strain rates (e.g. 0.0022 / s) and very high strains. Initiation of dynamic recrystallisation may occur at critical strains of 0.5 - 0.6 in a temperature range of 900 - 1000 ^{o}C for microalloyed steels. DRX may also occur due to high deformation temperatures depending on the material [4, 10, 63]. Figure 2.11 and Figure 2.12 show typical flow curves for dynamically (flow curve exhibits regular oscillations in stress at a peak stress, followed by softening and finally a steady state flow at high strains) and statically recrystallised (flow curve exhibits dynamic recovery / work hardening behaviour of the material) materials respectively.

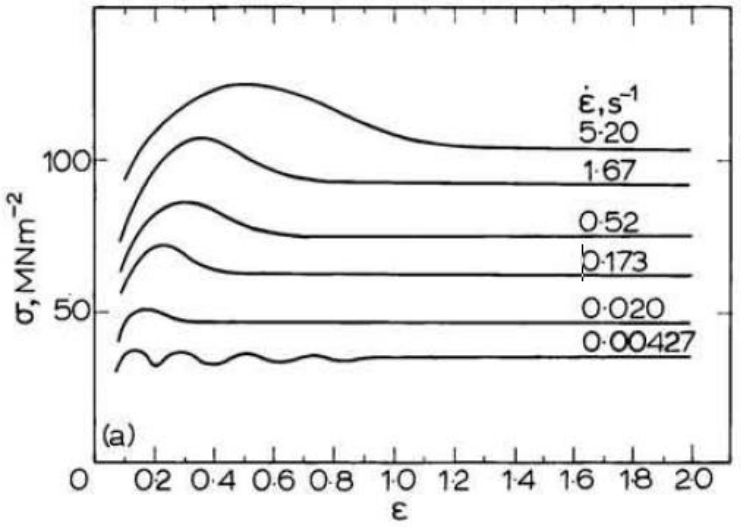

Figure 2.11: Typical flow curves exhibiting dynamic recrystallisation for a 0.37 wt - % C steel torsion deformed at 1050 °C at different strain rates [34].

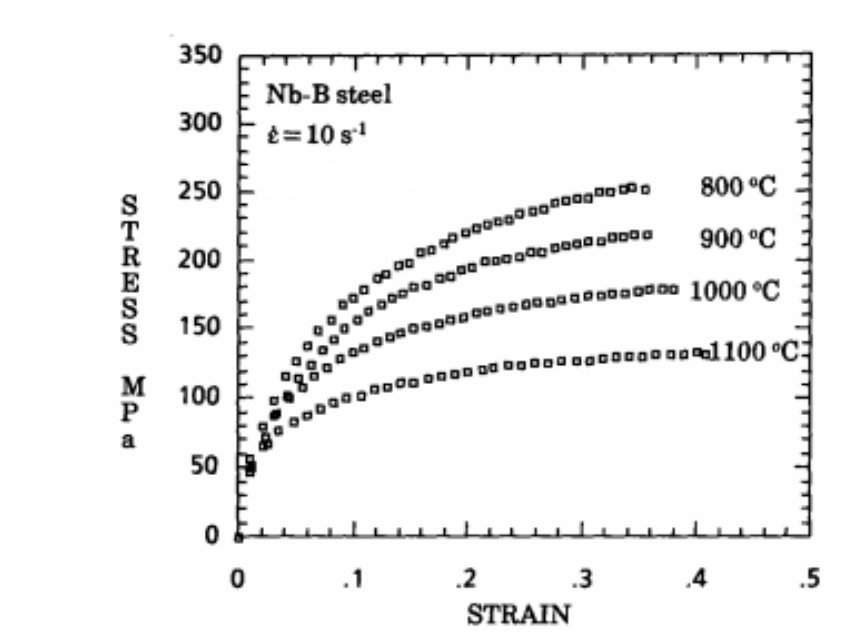

Figure 2.12: Typical flow curves for Nb - B microalloyed steel deformed at different temperatures to a strain of 0.4 at a strain rate of 10 / s exhibiting dynamic recovery / work hardening [47].

The type of material (i.e. whether the material has a high stacking fault energy or a low stacking fault energy) has an influence on the restoration mechanism. In materials with high stacking fault energy such as aluminium and its alloys dynamic recovery (DRV) balances work hardening thereby, realizing a plateau in stress-strain curves. DRV involves annihilation of individual or pairs of dislocations because of ease of climb, leading to the subsequent annihilation of dislocations of opposite sign. The DRV process also involves creation of cells and subgrains that act as sinks for mobile dislocations [32]. Hot deformed materials often contain a collection of equiaxed subgrains (with low misorientations across their boundaries) contained within elongated initial grains due to the continuous formation and annihilation of subgrains during DRV [32]. Annealing the sample that undergoes DRV after deformation leads to static recrystallisation occurring [32, 64]. For materials with low stacking fault energy, the kinetics of DRV are low under hot working conditions (because mobile dislocations are dissociated, making climb difficult, as earlier stated) and as such dynamic recrystallisation is initiated at a critical strain [32, 53, 64]. Dynamic recrystallisation occurs due to somewhat higher dislocation densities than in materials undergoing DRV, coupled with high mobility of grain boundaries at high temperatures. Stacking fault energy will be discussed in Section 2.3.5.

Lower deformation temperatures and microalloying elements in the material can delay the initiation of dynamic recrystallisation [46, 47]. At lower temperatures grain boundary mobility decreases due to less thermal activation and as such the initiation of DRX is delayed [64]. For instance, Laasraoui *et al.* [47] investigated the factors affecting dynamic recrystallisation by varying strain rate, deformation temperature and composition. It was observed that for the base material (0.02Ti - 0.0048N steel) dynamic recrystallisation was observed to occur at deformation temperatures of 900 - 1100 ^{o}C for strain rates of 0.2 / s and

2 / s, whereas when deformed at 800 °C the sample underwent static recrystallisation. It was concluded that the deformation temperature has an effect on the initiation of dynamic recrystallisation and that dynamic recrystallisation is more prevalent at higher deformation temperatures. The increase in flow stress with a reduction in deformation temperature and increase in strain in stress-strain curves has been reported to be due to the reduction in the rate of restoration processes and consequent increase in the strain hardening rate [47, 59, 64].

Grain boundaries may also be slowed down (by pinning of grain boundaries) by either precipitates or by solutes and thereby retarding the initiation of dynamic recrystallisation. For example, Laasraoui *et al.* [47] showed that precipitates retarded the initiation of dynamic recrystallisation because for a less microalloyed (0.02Ti - 0.0048N) steel deformed at temperatures of 900 - 1000 °C using a strain rate of 2 / s, dynamic recrystallisation had occurred, whereas for the highly microalloyed (0.020Ti - 0.055Nb - 0.0063N) steel only static recrystallisation occurred at a similar strain rate and deformation temperature. The delay in the initiation of dynamic recrystallisation was attributed to the retarding effect of Nb.

Table 2.2 and 2.3 shows literature deformation conditions and the type of softening that occurs for various materials [4, 6 - 7, 15, 44 - 47, 57 - 62]. It can be seen from Table 2.2 that HSLA steels deformed at temperatures ranging from 800 - 1150 °C to strains ranging from 0.1 - 0.4 at strain rates of 0.22 - 50 / s recrystallised statically [4, 6, 7, 15, 34, 44 - 47, 58 - 62]. However, for HSLA steels deformed to higher strains of 0.93 - 2 at 1080 °C and 1050 °C dynamic recrystallisation occurred due to high applied strains [34]. Dynamic recrystallisation has been observed to occur in HSLA steels deformed at 1050 °C to a 0.3 strain at low strain rates of 0.0022 / s [7]. Dynamic recrystallisation is also observed in Ni - 30Fe steels with and without Nb and in austentic stainless steels at temperatures of 800 - 1150 °C deformed to 1 -

1.2 strain at a strain rate of 0.01 - 1 / s [46, 59]. For Fe - 30Ni steel, with and without Nb materials, static recrystallisation is observed at deformation temperatures of 850 - 950 ^{o}C for strains ranging from 0.25 - 0.9 at strain rates of 1 - 10 / s [18, 54], Table 2.3. From Table 2.2 and 2.3 it can be seen that deformation is carried out either hot or cold (below recrystallisation temperature) [32]. The majority of research [3 - 10, 65] on recrystallisation kinetics has employed hot deformation in simulating industrial deformation as compared to cold deformation. Cold deformation has mainly found use in research on strip steels, in which cold deformation is followed by annealing at lower temperatures (up to 700 ^{o}C) [66]. Hot deformation (hot rolling, TMCR, etc.) is desired over cold deformation as it is easier to fabricate materials at higher temperatures [32].

It can be concluded that for microalloyed steels deformed via rolling and TMCR, static recrystallisation may be the main softening mechanism for strains up to 0.4 at temperature ranges of 800 - 1150 ^{o}C. For the model steels (e.g. Fe - 30Ni steel) static recrystallisation may occur even up to a strain of 0.9 at temperature ranges of 800 - 1000 ^{o}C. A combination of different factors may lead to initiation of dynamic recrystallisation, such as the material type, lower strain rate and a higher deformation temperature. The current work has employed cold deformation with a deformation rate of 2 mm / minute (0.0022 / s) and furnace recrystallisation; however, since most of the data available on recrystallisation kinetics are for hot deformed tests, equivalent hot strains have been determined using equivalence of stored energy; details of how hot and cold deformations have been compared will be discussed in Chapter 3. This work will only consider static recrystallisation (hot deformation strains below 0.5 with a strain rate of 1 / s) which will be discussed in detail in Section 2.3.6.

2.3.3 Driving force for recrystallisation

When a material is plastically deformed by either hot or cold working about, 1 - 15 % (stored energy) of the total plastic energy is stored in the form of dislocations and the rest is converted into heat [28, 67, 68]. The residual energy is stored in the form of statically stored dislocation (SSD) and geometrically necessary dislocations (GND) and is considered to be the driving force for recrystallisation [28]. GNDs form at grain boundaries due to the fact that the presence of grain boundaries leads to non-uniform deformation, which is necessary to maintain the material compatibility during plastic deformation [67, 68]. Both SSDs and GNDs depend on the strain (increase with strain) and material properties, such as stacking fault energy and grain size [28]. The relationship between stored energy and dislocations was investigated by [69, 70]. Stored energy has been reported to be directly proportional to dislocation density based on flow stress-stored energy and flow stress-dislocation density relationships, and by making an assumption that the dislocation distribution is not homogenous [69, 70]. Bailey [69] deformed a 99 wt - % Cu material in tension to strains in the range 0.01 - 0.3. He measured dislocation densities (ρ) using TEM and stored energies using isothermal calorimetry at temperatures of 170 ^{o}C and 190 ^{o}C. Flow stresses (τ) were taken as half of the tensile stress. Bailey [69] equation fitted data for flow stress and stored energy to establish the direct proportional relationships between stored energy and dislocation density and did the same to obtain the flow stress-dislocation density relationship. Dislocation densities were estimated to be accurate to 25 % based on the spread in the values obtained from examined micrographs [69].

$$\tau = 0.5\mu b^{*}\rho^{1/2} \quad (2.7)$$

$$E_S = \alpha (\tau^{2} / \mu) \quad (2.8)$$

Where α is a constant, μ is the shear modulus and b is the burgers vector. Combining Equation 2.7 and 2.8 gives a directly proportional relationship between stored energy and dislocation density ($E_S \alpha \rho$).

2.3.3.1 Measurement of stored energy

The most common method used to measure the total stored energy of deformation is either direct or indirect calorimetry, with typical heating rates ranging from 6 - 20 ^oC / minute, Table 2.4 [71 - 78]. Direct methods involve deforming the sample with a known applied force and then taking the difference between the value of the supplied energy and the heat of the sample determined by measuring the increase in sample temperature. The accuracy of this method has been reported to be about 10 % [79]. Indirect methods, such as differential scanning calorimetry (DSC), measure residual energy in deformed specimens in the form of heat release [28, 67]. The samples are usually annealed in the calorimeter either isothermally where tests are carried out at a constant temperature for a period of time or anisothermally where the heating rate is fixed through a range of selected temperatures. Two samples, one deformed and the other annealed (reference sample) with similar masses or just one (deformed sample) may be used when carrying out DSC tests. Two runs are usually performed on each sample in order to obtain a base line for quantitative measurement of stored energy [77, 79]. The stored energy is obtained by integration of the area under the power difference-temperature curve between peak onset and finish temperatures [77, 79], errors associated with using this technique have been reported to be about 5 %.

Table 2.4: Measured stored energy from literature.

Composition	ε	Initial grain size / μm	Stored energy / J / g	Deformation techniques	Technique / Method for measuring stored energy	Ref.
99.99% Cu	0.32 - 3.35	32, 60, 274	0.17 - 0.72	cold rolled	Indirect calorimetry DSC	47
99.99% Ni	0.1 - 3	50 - 15000	0.3 - 0.8	cold rolled	Indirect calorimetry DSC, 20 °C / minute	46
99.99% Cu	0.19 - 0.68	100	0.4 - 0.95	rapid adiabatic deformation between two pendulum hammers	Direct Calorimetry	49
99.99% Cu	0.1 - 0.47	30 - 150	0.01 - 0.5	Tension	Indirect calorimetry (anisothermal)	48
99.99% Cu	0.18 - 0.36	15	0.26 - 0.4	Tension	Indirect calorimetry (isothermal)	50
99.99% Cu	0.3	150 - 700	0.36 - 0.48	Compression	Indirect calorimetry (Calorimetry 6 °C / minute)	51
C - Mn - 0.08Ti	0.25 - 0.95	Not given	16.5 - 29.5	colled rolled	Indirect calorimetry (DSC, 10 °C / minute)	52
99.9% Tantulum	0.87	Not given	0.17	colled rolled	Indirect calorimetry (DSC, 20 °C / minute)	53

Values for stored energy ranging from 0.3 to 21 J / g for different initial grains and strains have been reported, as highlighted in Table 2.4 [72 - 78]. Researchers [73, 75, 78, 79] have reported that the errors are within 5 to 10 % of the measured values. It has been suggested that sources of errors in the measured stored energy values may arise from factors such as: sample preparation, sensitivity of the machine and the deformation method.

A typical curve obtained by annealing a pure copper specimen using the anisothermal method together with hardness and electrical resistivity results is shown in Figure 2.13 [68]. It has been revealed, through techniques such as metallographic examination, that the single plateau as illustrated in Figure 2.13 corresponds to recrystallisation. This is achieved by carrying out interrupted tests and directly examining the micrographs to establish whether recrystallisation has taken place or not [68]. Recrystallisation is accompanied by sudden changes in hardness, electrical resistivity and density of dislocations [80].

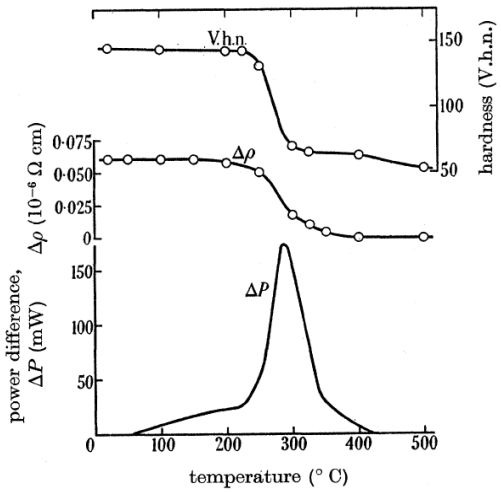

Figure 2.13: Typical anisothermal annealing curves (representing release of stored energy) at a heating rate of 6 ^{o}C / min, incremental electrical resistivity and hardness for electrolytic copper deformed in torsion to nd / l = 1.87 [68].

Researchers have reported that for certain materials two plateaux are observed [81] in anisothermal (DSC) curves (especially materials with high stacking fault energy values) e.g. in nickel alloys, where the first plateau represents recovery and the second recrystallisation. Deng *et al.* [78] carried out DSC tests at a heating rate of 20 ^{o}C / minute using tantalum deformed to a strain of 0.87 and obtained two plateaux (exothermic peaks) in the first run; the first plateau occurred from 770 ^{o}C to 900 ^{o}C (representing recovery; stored energy of 0.12 J / g) and the second from 1050 ^{o}C to 1150 ^{o}C (representing recrystallisation; stored energy of 0.05 J / g) as illustrated in Figure 2.14. It can be seen from Figure 2.14 that there were no exothermic peaks present in the second run, indicating that all the stored energy had been released. It was confirmed that the material had either recovered or fully recrystallised by carrying out metallography [78]. It must be noted here that although Deng *et al.* [78] shows a higher reduction in stored energy (70 %) due to recovery, most of the researchers have reported lower amounts of recovery (about 3 - 14 % of total stored energy) [28, 67, 69, 79].

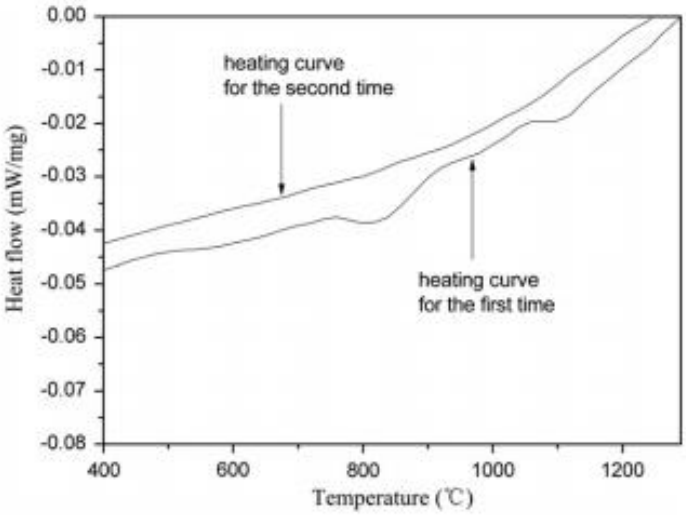

Figure 2.14: DSC curves for tantalum material deformed to a strain of 0.87 [78].

The driving force for recrystallisation is influenced by a number of parameters, such as the composition of the material, the initial grain size and process parameters such as plastic strain and deformation temperature [24, 28, 71 - 73]. Recovery processes taking place in some materials reduce the amount of stored energy [28, 32, 67, 68, 78]. Recovery will be discussed in Section 2.3.4, whereas the other factors influencing stored energy are discussed in the next section.

2.3.3.2 Factors influencing the driving force for recrystallisation

The influence of composition on the amount of the driving force for recrystallisation was investigated by Clarebrough *et al.* [79] who compared the stored energy values for a copper material containing 0.006 % impurities (arsenic, phosphorus etc.) obtained using calorimetry to those obtained by Taylor and Quinney [82] for a copper material with higher impurities (0.6 %) highlighted in Table 2.5. It was concluded that the values for stored energy obtained from Taylors and Quinney's [82] work were slightly higher than the ones obtained by Clarebrough *et al.* [79]. Later, Clarebrough *et al.* [83] investigated the influence of composition on the driving force for recrystallisation using copper (99.96 %) and nickel (99.96 %) materials deformed by torsion, and observed that the nickel based material had more driving force for recrystallisation (2.5 J / g) than the copper based material (1.3 J / g). This may have been due to differences in the shear modulus of the materials (48 GPa for copper and 128 GPa for nickel [28]). A difference in shear moduli means that the work hardening properties of the materials in question are different, and as such the amount of energy stored for recrystallisation is expected to be higher in the sample with a higher shear modulus as it work hardens more than the sample with a lower shear modulus.

Table 2.5: Driving force for recrystallisation for copper materials with different compositions deformed to different strains using torsion tests.

Degree of deformation / *nd / l	Driving force for recrystallisation / J / g	
	0.6% impurities [82]	0.006% impurities [79]
0.47	0.02	0.007
0.94	0.06	0.01
1.41	0.04	0.02

*nd / l is used to measure the degree of deformation for torsion tests where n is the number of turns, d is the diameter of the specimen and l is the length of the twisted portion of the specimen.

Undissolved particles in microalloyed materials may also lead to an increase in dislocation density and consequently an increase in stored energy, however this apparent increase in dislocation density for materials containing small (< 1 μm) non-deformable particles is only obtained for very small strains (< 0.05) than at larger strains which are usually of importance for recrystallisation [28]. The experimental work of Greenfield and Bever [84] investigated the effect of deformation temperature on the driving force for recrystallisation and concluded that variation in the temperature of deformation led to differences in flow stress, such that for similar strains the flow stress was higher in a sample deformed at a lower temperature (- 195 ^{o}C) compared to the sample deformed at room temperature due to great work hardening of the material at lower temperatures than at higher temperatures. This may be due to the fact that at

higher temperatures some of the dislocations may be annihilated, leading to a lower flow stress.

The driving force for recrystallisation is influenced by strain and initial grain size which consequently influences the dislocation density [28, 36, 67, 68, 85]. Driving force values for recrystallisation are given in Table 2.6 for different strains and materials [69, 79]. It can be seen from Table 2.6 that the driving force for recrystallisation increases with degree of deformation.

Table 2.6: Driving force for recrystallisation for samples deformed to different strains using torsion tests.

Material	**Degree of deformation / nd / l**	**Driving force for recrystallisation / J / g**	**Ref.**
99.985 Cu	0.47	0.007	79
	0.94	0.01	
	1.41	0.013	
	2.15	0.02	
	3.03	0.02	
99.6% Ni	0.94	0.5	79
	2.34	1.35	
99.99 % Cu	0.108	0.15	69
	0.175	0.23	
	0.3	0.31	
	0.4	0.40	

An increase in strain leads to an increase in stored energy due to a higher dislocation density. Likewise, a finer initial grain size leads to an increase in stored energy due to a larger grain boundary area per unit volume [4, 28, 67, 68, 85]. Baker *et al.* [71] and Madal *et al.* [72] investigated the effect of strain and initial grain size on stored energy using pure nickel and pure copper respectively; the results obtained are re-plotted in Figure 2.15.

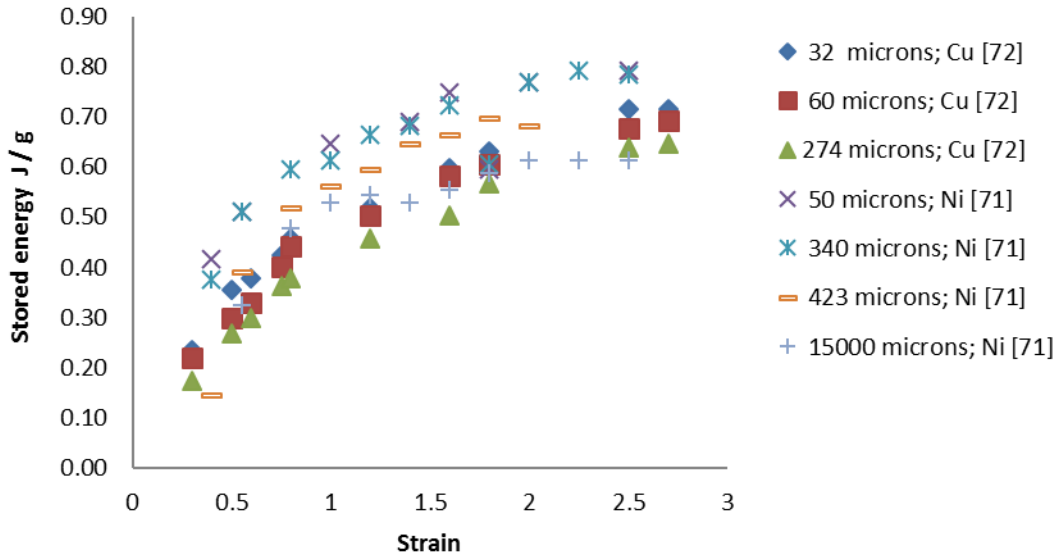

Figure 2.15: Effect of initial grain size and strain on the measured stored energy of deformation using cold rolled 99.99 wt - % Ni (with grain sizes of 50 µm, 340 µm, 423 µm and 15000 µm) [71] and 99.99 wt - % Cu (with grain sizes of 32 µm, 60 µm, and 274 µm) [72].

Figure 2.15 illustrates that the fine grain-sized material tends to have higher stored energy than coarse grain-sized material; for example, for copper material strained to 0.6; stored energies of 0.3 J / g, 0.33 J /g and 0.38 J / g were obtained for the samples with initial grain sizes of 274 µm, 60 µm and 32 µm respectively. The higher energy stored in smaller grains is because small grains have a larger grain boundary per unit volume thereby storing more energy as compared to coarse grains [72 - 74, 76]. However, at very high strains (above deformation strains of 2.5) there is no significant difference observed in the amount of stored energy in fine or coarse grain-sized materials [72 - 74, 76], since specimens with different initial grain sizes deformed to comparable strains (2 - 3) had stored energies with very little differences between them ranging from 0.64 - 0.72 J / g. It must be mentioned here that even though the rate of increase of the stored energy decreases, the smallest grain size still has

more stored energy. However, for all grain sizes examined, there is no significant difference in stored energy values observed at higher strains compared to the differences in stored energy observed at strains lower than 2.5, where materials with fine grains are seen to have higher stored energies than coarse grained materials. Similarly, Baker *et al.* [71] also showed that at a strain of 2.5 for the 50 and 340 μm samples a similar amount of stored energy (0.78 J / g) is observed. The reason for the gradual decrease and eventually no significant difference between the amount of stored energy measured in fine and coarse grains may be due to strain saturation; that is, annihilation of new dislocations takes place as they are generated, leading to a decrease in the rate of work hardening in both materials. The other reason for minimal differences observed in the measured stored energy for fine and coarse-grained materials may be that once geometrically necessary dislocations become saturated at higher strains, statically stored dislocations become the controlling factor [73].

Figure 2.15 also illustrates that below deformation strain of 2.5 for these materials, the initial grain size is inversely proportional to the amount of stored energy, whereas strain is directly proportional to the amount of stored energy. Generally, Figure 2.15 demonstrates the fact that strain has an influence on stored energy; the higher the strain the higher, the amount of energy stored due to an increase in dislocations [71, 78]. For instance, for the nickel based material [71] the following increase in stored energy with strain (0.4 - 2.5) is observed for the different grain sizes examined: 0.09 - 0.02 J / g for the 50 μm sample, 0.14 - 0.01 for the 340 μm sample, 0.25 - 0.03 J / g for the 423 μm and up to 0.15 J / g for the 15000 μm. Whereas for the copper based material [72] the following increase in stored energy with strain (0.3 - 2.7) was observed: up to 0.12 J / g for the 32 μm sample, up to 0.08 J / g for the 60 μm sample and 0.09 - 0.01 J / g for the 274 μm. It can be observed that the rate of increase in stored energy with strain decreases at higher strains, and is rapid at lower strains for both the copper and

nickel based material due to reasons discussed in previous paragraphs. It can be seen from Figure 2.15 that the values reported by Madal *et al.* [72] are consistently lower than those reported by Baker *et al.* [71] for all grain sizes examined, even though they both used similar DSC testing machines. The difference in the shear modulus of the materials may also lead to the differences in the amount of energy stored, as discussed in previous paragraphs [28].

The above discussion highlights the dependency of stored energy on initial grain size and plastic strain and other parameters. Depending on the amount of stored energy, recrystallisation kinetics may either be fast or slow; a finer initial grain size (higher grain boundary area per unit volume leading to a higher dislocation density) and a higher deformation strain (higher dislocation density) leads to faster recrystallisation kinetics and a greater degree of grain refinement [44, 45] as discussed in Section 2.3.1.

2.3.3.3 Calculation of stored energy

An estimation of the driving force for recrystallisation (F_R) can be made from the difference in dislocation density across the moving boundary as follows [85]:

$$F_R = (\mu b^2 \Delta\rho)/2 \qquad (2.9)$$

Where μ is the shear modulus ($4*10^4$ MN / m^2 for austenite [85]), and $\Delta\rho$ is the difference is dislocation density.

The density of dislocations present during deformation increases due to piling up of existing dislocations and the generation of new dislocations (the material work hardens) [28]. The equation for calculating the dislocation density (ρ^G) for geometrically necessary dislocations given by Ashby [86] shows a dependency of dislocation density on the initial grain size and shear strain and is given as follows:

$\rho^G = 4\,\gamma_1 / b\, C_G D_o$ (2.10)

Where γ_1 is the shear strain, D_o is the grain size and C_G is a constant.

Whereas Ashby [86] showed the dependency of dislocation density on shear strain and initial grain size, Keh [87] showed that dislocation density is dependent on the increase in dislocation density during work hardening. He estimated the increase in dislocation density from stress-strain curves using Equation 2.11:

$\Delta\sigma = 0.2\mu b\,(\Delta\rho)^{0.5}$ (2.11)

Where $\Delta\sigma$ is the increase in dislocation density during work hardening.

Bailey [69] investigated the influence of deformation strain (0.01 - 0.3 strain) on dislocation density using transmission electron microscopy (TEM) on 99.99 wt - % Cu foils with an initial grain size of 20 µm and proved that the dislocation density increased from 0.19 $*10^{10}$ m / m^3 to 5.7 $*10^{10}$ m / m^3 for strain of 0.01 and 0.3 respectively. Based on Equation 2.10 [86] researchers have proposed equations for calculating the total stored energy [60, 71] as a function of dislocation density. Kundu [4] employed Equation 2.12 and 2.13 [60] in order to determine the effect of grain size on the stored energy and found that the calculated stored energy was influenced by grain size and that the stored energy increased rapidly for finer grain sizes up to 100 µm and thereafter the rate reduced as shown Figure 2.16 [4].

$E_T = \alpha\mu b^2 (\rho^G + \rho^S)$; $\rho^G = 4\,\gamma_1 / b\, C_1 D_o$ (2.12)

$E_T = \alpha\mu b^2 (\rho^G + \rho^S) = (\alpha\, \mu b M_S \varepsilon / D_o)\,(1/\alpha_s + C_2)$ (2.13)

Where $\rho^G = C_2 M_S \varepsilon / b\, D_o$ and $\rho^S = M_S \varepsilon / \alpha_S b D_o$

Where α_s C_2, and M_S are constants.

These equations show that the stored energy of deformation has a dependency on applied strain and initial grain sizes. Equations 2.12 and 2.13 seem to suggest that dislocation density

is proportional to shear strain and that stored energy is proportion to dislocation density so that stored energy should be linear with strain and inversely proportional to the initial grain size. However experimental data from [71] and [72], shown in Figure 2.15 suggests that a power law relationship may exist between stored energy and strain. Comparison between measured and predicted values using Equation 2.12 is given in Table 2.7. It can be seen from Table 2.7 that experimental values are higher than predicted values. The difference between stored energy values obtained using Equations 2.12 and 2.13 and measured values may be because Equations 2.12 and 2.13 do not take into account strain saturation and therefore making the measured and predicted values not comparable. SFE may affect computed stored energy values through recovery and cell formation leading to discrepancies between stored energy values obtained using Equation 2.12 and 2.13 and those experimentally obtained [4].

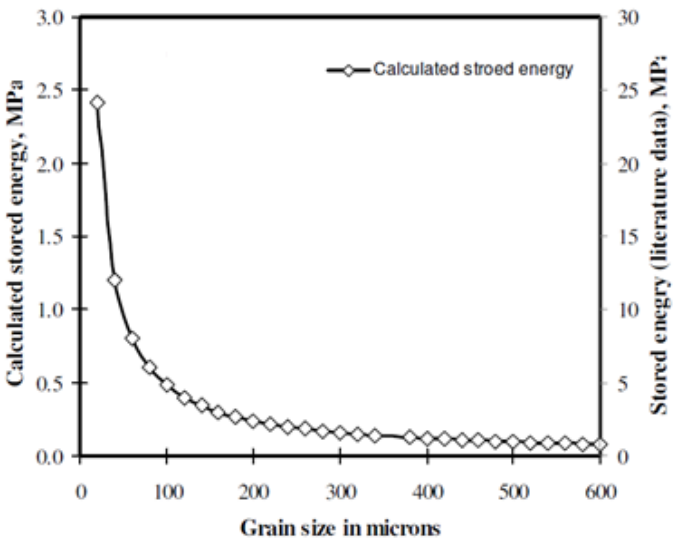

Figure 2.16: Effect of grain size on stored energy determined using Equation 2.12 [4].

Table 2.7: Predicted using Equation 2.12 with parameters for copper (density 8.96 g / cm^3, dislocation densities and measured stored energies using calorimetry ($5.7*10^5$ (0.3) and $2*10^5$ (0.17 strain) measured using TEM) [69].

Strain	Dislocation density / m / m^3	Predicted stored energy / J / g	Measured stored energy / J / g
0.17	$2*10^5$	0.0023	0.17
0.3	$5.7*10^5$	0.0062	0.34

The work done by deformation is often considered to be equal to the area under the stress-strain curve [28, 69] as such, it is possible to estimate the amount of energy stored in a material using stress-strain curves. In order to compare hot and cold deformation in this work, equivalent strains have been determined by assuming equivalence of stored energies using stress-strain curves. Deformation of samples at different deformation temperatures may lead to differences in stored energy as discussed in Section 2.3.3.2. For example, Vandermeer *et al.* [88] examined grain refinement in hot and cold deformed aluminium with similar initial grain sizes (100 μm). They cold deformed the specimen to a strain of 2, while a 2.3 strain was applied for the hot deformed sample. Vandermeer *et al.* [88] concluded that the recrystallised grain size was almost four times smaller (14 μm) for the cold deformed sample compared to the hot deformed sample (56 μm). This was due to the cold deformed sample having a higher flow stress and hence a higher stored energy due to work hardening of the material.

2.3.4 Recovery

The driving force for recrystallisation can be reduced by recovery processes as discussed in Section 2.3.3. Rearrangement and annihilation of dislocations, climb of dislocations and the absorption of dislocations into sub-boundaries and their growth leads to reduction in dislocation densities and subsequently stored energy which is the driving force for

recrystallisation by generally 3 -14 % [28, 32, 69, 78, 79, 83, 89 - 94]. Table 2.8 generally shows that the overall reduction in stored energy is small [28, 69, 83]. However, in certain instances the reduction in stored energy due to recovery has been shown to be higher than the amount of stored energy as shown in Table 2.8 [78, 83, 84].

Table 2.8: Measured stored energies using calorimetry.

Material	Degree of deformation / nd / l	Recovery / J / g	Stored energy / J / g	Recovery percentage	Ref.
99.99 % Cu	0.108	0.018	0.15	11.56	69
	0.175	0.013	0.23	5.27	
	0.3	0.016	0.31	5.05	
	0.4	0.013	0.40	3.12	
99.96 % Cu	1.87	0.2	-	14	83
99.96 % Ni	0.94	0.94	0.15	54	
	2.34	1.57	1.35	67	
82.6 Au -17.4Ag	not given	1.1	-	54	84

Recovery involves two main primary processes; rearrangement of dislocations of the same sign into low energy configurations (low grain boundaries) and annihilation of dislocations with opposite signs in the crystal structure. These processes are accomplished by means of glide, climb and cross slip of dislocations [28, 89]. Different sub-processes that may operate in a material (leading to recovery), that is, formation of cells, annihilation of dislocations within cells, formation of low-angle-subgrains and subgrain growth are shown in Figure 2.17 [1].

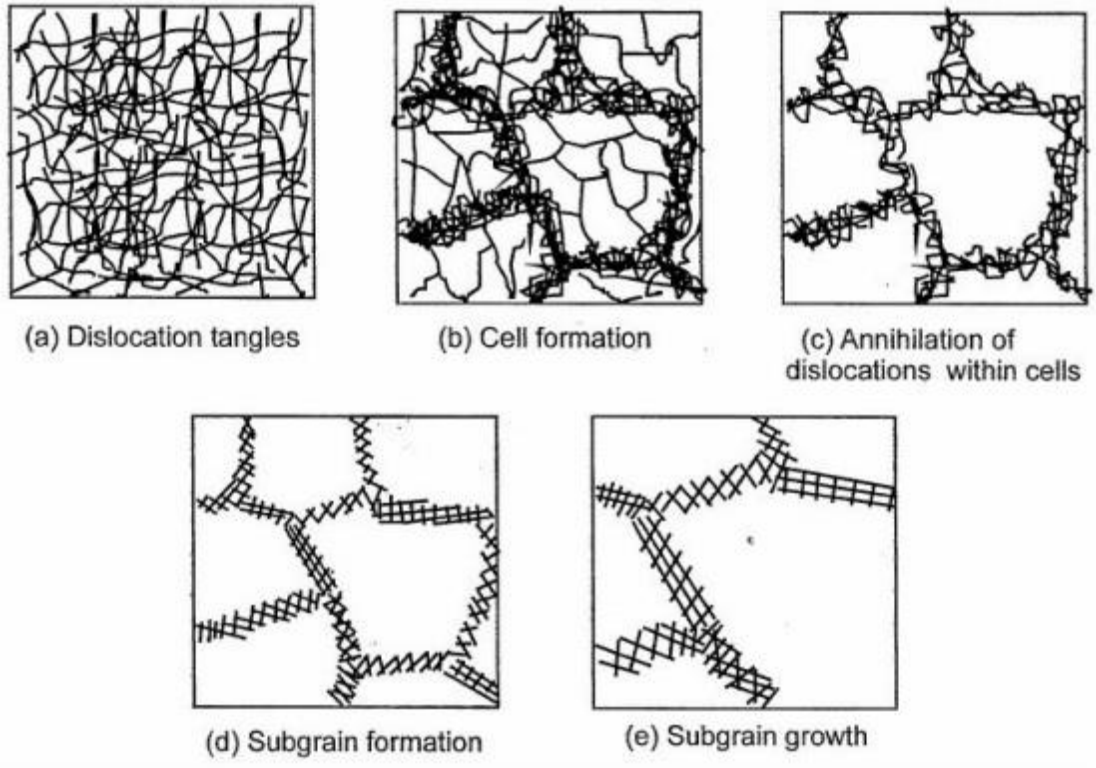

Figure 2.17: Stages in the recovery process [1].

2.3.4.1 Measurement of recovery

Recovery is often measured by changes in physical properties (resistivity) and mechanical properties (hardness, yield stress etc.) which are altered during deformation and may be partially restored via recovery. However, physical properties are sensitive to any slight phase transformation, which may occur on annealing. It is therefore challenging to relate quantitatively these changes to the microstructural changes which take place during recovery [28]. Recovery is therefore often measured by following changes in mechanical properties although the changes occur at a small scale and are subtle [28].

Recovery could be measured by differential scanning calorimetry (DSC), however since the amounts of stored energy involved for the kind of strains (> 0.5) employed in TMCR are very small, it is not an easy task [67]. Figure 2.18 exhibits a DSC curve (with two peaks) for pure

aluminium deformed to a 6.9 strain at - 196 ^{o}C; the broad peak at - 70 ^{o}C corresponds to recovery and the one at - 20 ^{o}C corresponds to recrystallisation [28, 95].

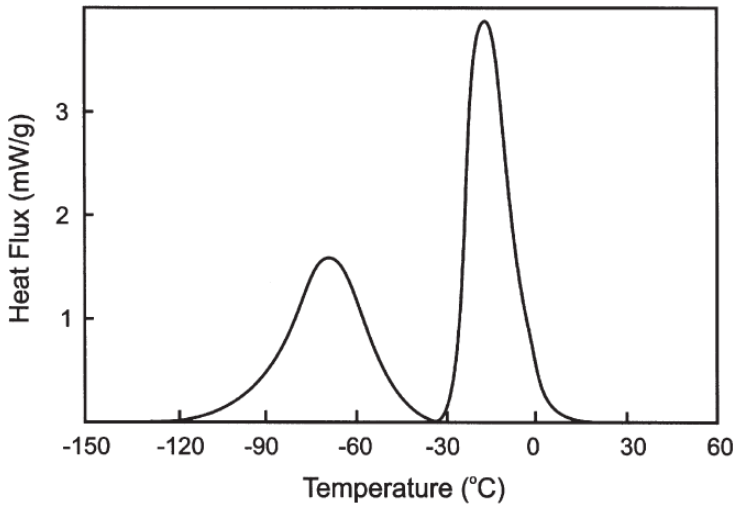

Figure 2.18: DSC curves showing occurrence of recovery for a 99.9 wt - % Al deformed to a strain of 6.91 at - 196 ^{o}C [28, 95].

Typical recovery values (ranging from 0.012 - 1.6 J / g) for different materials (copper, nickel and gold and silver) measured using calorimetry are given in Table 2.8. Indirect methods such as stress relaxation tests and double hit tests, which involve measuring the changes in the properties of the material such as stress, hardness, and electrical resistivity, can also be used to measure recovery [28]. A discussion of the different aspects of indirect and direct methods used for quantification of stored energy and fractional softening is given in Sections 2.3.3 and 2.3.7 respectively. To avoid interference from recrystallisation most tests are carried out below the temperature for no recrystallisation (T_{NR}) or for short holding times above T_{NR}. [1]. In cases where deformation is carried out above T_{NR}, difficulties in separating recovery from recrystallised amounts have arisen due to the fact that both processes are driven by stored energy. Pertuula *et al.* [51] and Barraclough *et al.* [96] argued that the first 0.2 fractional softening is solely due to recovery because when this was verified using metallography it was

found that recrystallisation had not yet occurred in the material as there was no presence of recrystallised grains, only deformed elongated grains were present in the microstructure. For example, Pertuula *et al.* [51] double compressed (DC) a stainless steel material at 1000 °C and analysed the softening data using 0.2 % offset stress method (discussed in Section 2.3.7.1) and metallography. A 0.2 softened fraction was obtained after a holding time of one second as demonstrated in Figure 2.19, however when this was verified using metallography there was no evidence of recrystallised grains; only deformed elongated grains were present in the microstructure. It was therefore concluded that the 0.2 softened fraction correlated to recovery. On the other hand, other researchers [48, 97] have argued that recovery may correlate to a softened fraction of 2 as they may be 'noise' in the data obtained at a softened fraction of 0.2 [48]. A discussion on different methods used for quantification of recrystallisation kinetics is given in Section 2.3.7.

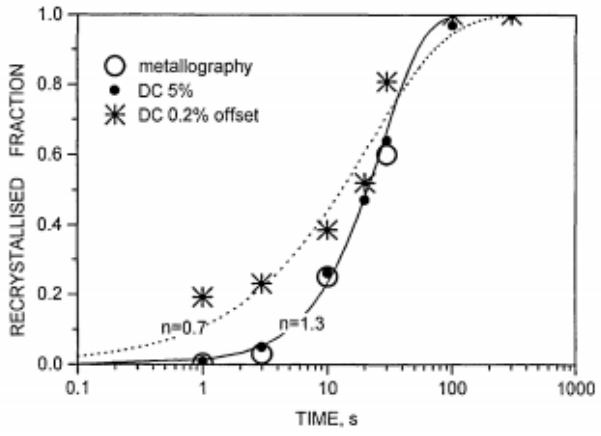

Figure 2.19: Fractional softening calculated using different methods (metallography and DHT (DC) for a 304 stainless steel deformed at 1000 °C [51].

2.3.4.2 Factors influencing recovery

It has been reported that recovery processes can often take place at low annealing temperatures (0.3 - 0.5 of the melting temperature) [28] and that it may occur at strains much lower than those required to initiate dynamic recrystallisation as sufficient stored energy to nucleate static recrystallisation is not available [28, 32]. For instance, recovery has been reported to occur at temperatures ranging from 200 - 500 ^{o}C for low carbon steels [28, 92, 98]. Researchers [28, 32, 67, 99] have shown that recovery processes would also occur at low strain rates and higher deformation temperatures due to higher driving forces for boundary mobility, and as such, cross-slips occur easily. It must be noted here that recovery will not lead to a fully softened material in the absence of static recrystallisation and as such some dislocation substructure is retained [32]. Researchers [28, 88, 90] have shown that recovery kinetics are influenced by anything that impedes movement of dislocations, such as temperature as already mentioned in the previous paragraph, applied strain, the material type (whether the material has a low, medium or high stacking fault energy), and as well as by solute drag and precipitation. An example of how applied strain influences recovery was given by Vicente Alvarez *et al.* [88]. It was reported that at a low pre-strain of 2.6 % complete recovery (i.e. yield stress was similar to the annealed sample before deformation) had occurred at annealing temperatures of 650 ^{o}C and 680 ^{o}C whereas at a pre-strain of 7 % partial recovery was achieved after 20 minutes of annealing. At annealing temperatures of 450 ^{o}C no change in the yield strength was observed after annealing the sample deformed to a 2.6 % strain for 20 minutes. They confirmed that recovery had occurred by using TEM, which revealed that stable structures characterised by low annihilation kinetics with no formation of cells within the grains were present.

The other factor that influences recovery is the SFE of a material. SFE influences the degree to which dislocations dissociate, and as such controls the rate of dislocation climb and cross slip, which are the mechanisms which usually affect the rate of recovery (discussed in Section 2.3.5) [28]. Recovery may occur in materials with a high stacking fault energy (e.g. aluminium and its alloys and iron in the ferrite phase field) due to ease of dislocation climb. It has been argued that in materials with low stacking fault energy (< ~80 mJ / m^2), e. g. copper, nickel, iron and steel in the austenitic phase field, little recovery may occur prior to recrystallisation due to difficulty in dislocation climb (due to a large distance between dissociated dislocation partials) [24, 28, 32]. By pinning dislocations, precipitates and solutes may also influence recovery, as solute / precipitate pinning will inhibit dynamic recovery leading to a high retained dislocation density which may promote recovery (subgrain formation) on subsequent annealing thereby reducing the dislocation density and hence the driving force for recrystallisation. Over time, equations for describing the rate of recovery kinetics have been proposed in the literature in terms of the rate of change in mechanical properties (such as hardness, yield stress), magnetic and electrical properties among others [28, 91, 92, 100 - 102].

2.3.5 The deformed structure

In most materials, the method of deformation is either slip or twinning [28]. The plastic deformation behaviour of a material is dependent on the value of the stacking fault energy [28, 32]. As stated in Section 2.3.4, the difficulty of cross-slip in materials (e. g. austenitic steels) with low values of stacking fault energy (< ~80 mJm^{-2}) reduces the ability of a material to change its shape during plastic deformation by slip alone and as such deformation occurs by twinning [28]. The volume of deformation twins has been observed to increase with

an increase in strain and strain rate and with a decrease in deformation temperature [28]. Figure 2.20 depicts fine deformation twins in rolled copper [28].

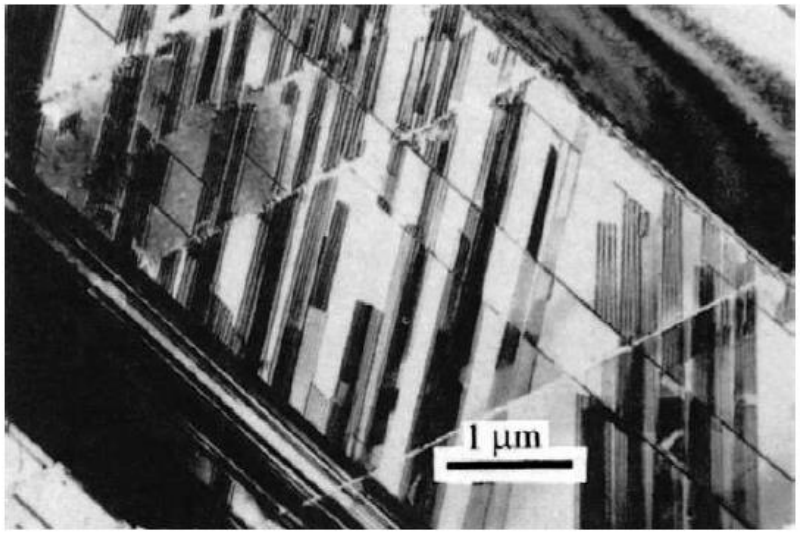

Figure 2.20: Fine deformation twins in rolled copper with 8.8 wt - % Si [28].

2.3.5.1 Methods for determining SFE

Various methods have been used to determine the stacking fault energy, however their reliability in determining SFE values is still under debate, and as such, values for SFE must be used as approximations only [59]. A detailed review of several methods that have been used in determining SFE and their reliability has been given by Campo *et al.* [103]. This review will briefly consider the weak beam method using TEM which involves direct observation of dissociated partials and thereby estimating the distance between dissociated dislocations. The stacking fault energy is calculated using anisotropic elasticity theory [59]. This method has been used often and has been found to be more reliable as it gives SFE values closer to reference values (measured using the weak beam method and a high-resolution electron microscopy [104 - 107]). SFE values for gold, silver, aluminium and copper have been verified by several researchers [28, 103] and as such it has been argued that they can be used

as reference values. The most reliable reference values have been said to be those determined for pure metals such as gold (~32 mJ / m^2) [104], silver (~16 mJ / m^2) and copper (~41 mJ / m^2) [105] (measured using the weak beam method) and aluminium (~150 mJ / m^2) [106] (measured using a high-resolution electron microscopy) [28, 103, 107]. Some SFE values determined using partial dissociation of dislocations for different materials are given in Table 2.9 [28, 59, 103, 108, 109].

2.3.5.2 Factors affecting SFE

Different material types have different SFE values (as shown in Table 2.9) which leads to materials having different deformation and restoration mechanisms as discussed in Section 2.3.1.

Table 2.9: Typical SFE values for some materials at room temperature.

Material	SFE Values / mJm^{-2}	Ref.
Ni - 30Fe steel	35 - 75	59, 108
Copper	41 - 78	28
Silver	16 - 22	28, 103
304 stainless steel	21 - 45	28
Fe - 18Cr - 30Ni steel	35 - 45	109
Ni	125 - 128	28, 103
70Fe - 30Ni steel	~20	59
C - Mn steel	~75	59

The difference in SFE for different materials as discussed in the introductory part of Section 2.3.5 is due to difficulty of cross-slip in some materials because of a large distance between dissociated partial dislocations, which reduces the ability of a material to change its shape during plastic deformation [28, 32]. SFE values are highly sensitive to the method of determination as discussed in Section 2.3.5.1 and they are dependent on the chemical composition of the material [59, 103, 109 - 113]. An example of the effect of chemical

composition on SFE is given by Dillamore *et al.* [110] who investigated the effect of composition on stacking fault energy using TEM. They varied the percentage of silver (from 0 to 100 wt - % Ag) in Pd - Ag alloys and found that SFE values varied slightly with composition, as shown in Figure 2.21. Similarly, Rhodes *et al.* [109] examined the effect of composition on SFE by varying the amount of Ni in a Fe - 18Cr - 30Ni steel deformed to a 3 % strain between 10 and 30 wt - % Ni. Rhodes *et al.* [109] concluded that generally the relationship between composition and alloying elements was complex and non-linear. It was concluded that alloying elements have an influence on SFE; however, they did not investigate whether the changes in SFE translated into any changes in the deformation and recrystallisation behaviour of the material.

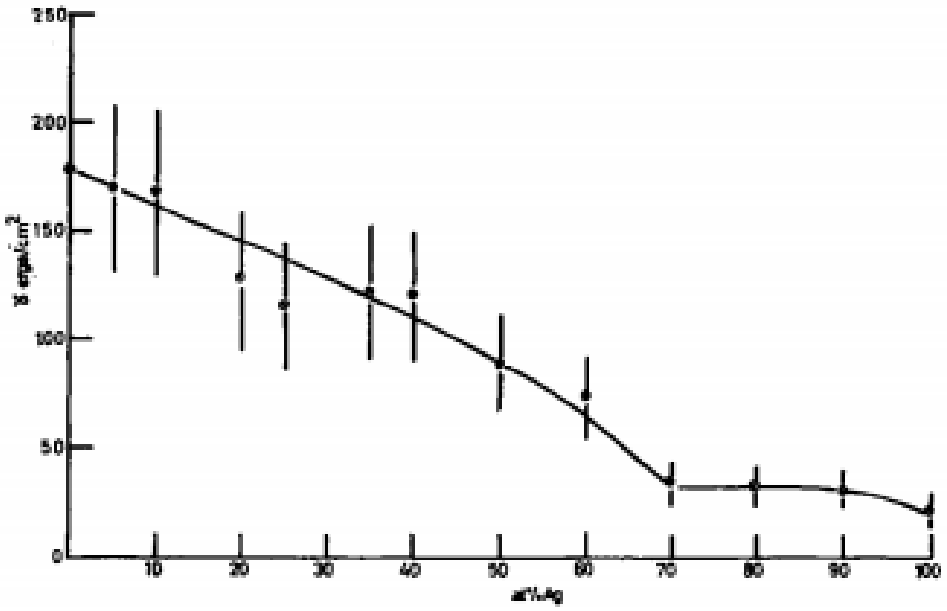

Figure 2.21: Stacking fault energy for Pd - Ag alloys as a function of composition [110].

It has also been reported that SFE increases with temperature which may be due to the fact that as the grain boundary mobility increases the distance between dissociated partial dislocations is reduced and consequently altering the deformation behaviour of materials [28,

114]. Lecroisey *et al.* [114] and Pontini *et al.* [115] investigated the dependency of SFE on the deformation temperature and reported that SFE values increase slightly with deformation temperature. Lecroisey *et al.* [114] used a 304 stainless steel in order to investigate the dependency of deformation temperature by varying temperature from - 196 to 67 ^{o}C and found that SFE slightly increased (by 0.01 mJ / m^2) with deformation temperature.

As discussed in the previous paragraphs, variation in SFE due to differences in amounts of alloying elements or deformation temperature will influence the deformation and recrystallisation behaviour of the material, that is, the material will either recrystallise statically (e.g. materials with high stacking faults) or dynamically (e.g. materials with low stacking faults) [29, 31, 39, 44]. Although the above discussion shows that alloying elements may influence SFE, there are no significant differences in SFE values observed, and as such the deformation behaviour might not change, however the rate of recrystallisation kinetics may be slowed down. It can therefore be concluded that variation in composition will have a stronger influence on SFE values than deformation temperature because a greater variation in SFE is observed when alloying elements are varied compared to variation in deformation temperature.

2.3.5.3 Structure of the deformed material

Extensive studies [28, 59, 93, 108, 116, 117] have been carried out to establish the structure of the deformed material using such methods as TEM, X-Ray diffraction, electron backscatter diffraction (EBSD) and scanning electron microscopy (SEM). The major features seen in a deformed microstructure are dislocations, dislocation cells (tangled equiaxed micron-sized volumes bounded by dislocation walls), subgrain (well-ordered low angle boundaries)

structures and deformation bands [28, 56, 93]; different features found in a deformed microstructure are given in [28].

As discussed in Section 2.3.3, during deformation work done in deforming a material is given off as heat and about 1 - 15 % is stored in form of dislocations [28, 67, 68]. It was stated in Section 2.3.3 that dislocation density is influenced by parameters such as applied strain and initial grain size. The higher the strain and finer the initial grain size the higher the dislocation density will be and consequently the higher the driving force for recrystallisation [28, 71, 72]. Applied plastic strain causes microstructure changes [28] such as elongation (increased total grain boundary area) of equiaxed grains in order to incorporate dislocations [25, 28, 59]. Grains become more pancaked and elongated with an increase in deformation strain and at low deformation temperatures [59]. Dislocations form and exist in the form of tangles, particularly after low strains for materials that do not form cells [28]. Dislocation cell structures form in materials with high to medium (> 80 mJm^{-2}) stacking fault energy (e.g. Al-, Ni- and Cu- based alloys) whereas in materials with low values of stacking fault energy (e.g. Ag - based alloys, austenitic steels and Fe - 30 wt - % Ni steel) dislocation cell structures do not form, but, instead, dislocation dissociate to form planar arrays of stacking faults on the slip planes.

Subgrain formation comes about due to annihilation of dislocations and rearrangement of others into low angle grain boundaries as earlier stated in Section 2.3.4 [28, 56, 89, 90, 93, 116, 118]. The driving force for subgrain growth arises from the energy stored in the subgrain boundaries [28]. Most subgrain boundaries have low mobility since most of the subgrains have only a small misorientation with their neighbours [56]. Subgrain formation and growth leads to a reduction in the dislocation density and consequently reduction in the driving force for recrystallisation. As the stored energy of a recovered substructure is still large, coarsening

of the substructure occurs, which further lowers the stored energy [28]. Typical average subgrain sizes of 0.5 - 6 μm have been reported in deformed materials as shown in Table 2.10 [56, 59, 90, 119, 120].

Table 2.10: Typical subgrain sizes and the angle of misorientations.

Material	Strain	Average misorientation / degrees	Average sugrain size / μm	Ref.
Polycrystalline Iron	0.7	2 - 6	0.5 - 1	117
Al	heavily deformed	-	1	56
	0.1 - 6	2 - 3	0.4 - 3.5	91
Al	0.2 - 0.3		2 - 3	119
Ni - 30wt - % Ni, 304 austenitic steel	0.5 - 1	1.1 - 2.6	0.46 - 6	59
99.99wt - % Ni and Al	0.1 - 3	0.5 - 4	-	94

Furu *et al.* [120] showed that for strains of 0.1 up to 6, subgrain sizes decreased from 3.5 μm to 0.4 μm. Similarly, Taylor *et al.* [59] observed subgrain sizes ranging from 0.46 - 6 μm when they examined Ni - 30 wt - % Fe steel and 304 austenitic stainless steel deformed to strains of 0.5 and 1 using EBSD. They reported that for all temperatures investigated (700 - 900 ^{o}C) the subgrain size decreased initially with strain and thereafter remained constant at strains greater than 0.5 [59, 121]. Average subgrain sizes have been reported to decrease with strain and then remain constant for different materials when the subgrain size is plotted against strain [56, 59, 90, 116, 119, 120]. This might be because as strain increases, the driving force for subgrain growth initially increases and then becomes constant as high angle boundaries are formed [28]. Typical average misorientation across the subgrain boundaries have been reported to be between 0.5 - 6^{o} for materials such as aluminium, austentic steel, Ni - 30 wt - % Fe steel and polycrystalline iron for strains ranging from 0.1 - 6 as shown in Table 2.10 [40, 59, 90, 93, 116]. The experimental work of Hansen *et al.* [93] showed that for pure

nickel and aluminium materials the angle of misorientation increased from 0.5 - 4^{o} for strains ranging from 0.1 - 3. On the other hand, Taylor *et al.* [59] varied deformation temperature (700 - 900 ^{o}C) and strain (0.5 - 1) for the Ni - 30 wt - % Fe steel and 304 austenitic stainless steel and observed average misorientations of 1.4 - 2.6^{o} using EBSD. It was concluded that misorientations were greater at lower deformation temperatures (700 ^{o}C) than at higher temperatures (900 ^{o}C). This may have been due to higher grain boundary mobility at higher temperatures, which would lead to annihilation and rearrangement of dislocation thereby reducing the dislocation density [28].

The differences in the subgrain misorientations in different materials such as in the polycrystalline iron (high SFE) and the austenitic steel (lower SFE) might be due to occurrence of phase transformation. Materials with high SFEs are expected to have lower misorientations across subgrain boundaries due to continuous formation and annihilation of subgrains during deformation compared to materials with low SFEs where greater misorientations occur due to higher dislocation densities [28, 32]. Grain boundary migration will occur due to greater boundary misorientations (10 - 15^{o}), leading to nucleation of recrystallised grains and eventually formation of new strain free grains [25, 28, 56, 122, 123]. The variation in the values obtained for the subgrain size and average misorientations has been reported to be due to differences in orientation of the grains, in which the substructure had formed [59, 121]. During deformation, the orientation of grains changes relative to the direction of the applied force thereby grains acquiring a preferred orientation or texture [28, 59]. Several factors influence the development of texture, such as strain, strain rate and deformation temperature; more details on texture are given in [28, 59].

As discussed in the previous paragraphs, different factors may affect the stacking fault energy of a material, such as composition, deformation temperature, method of measurement and

strain. No definite values for SFE for Fe - 30 wt - % Ni steel have been reported, although Taylor *et al.* [59] suggested that the SFE value for Fe - 30 wt - % Ni steel may approximately be about 20 mJ / m^2 whereas Rhodes *et al.* [109] suggested a value of 45 mJ / m^2 for a model steel containing 30 wt - % Ni. It can be concluded that the model steel (Fe - 30 wt - % Ni) used in this work may have a low stacking fault energy and would deform via twinning. This is based on the SFE values proposed in literature [59, 109] as well as the microstructure observed by Abdollah-Zadeh [18] (austenitic microstructure) during annealing (annealing twins) and after deformation (deformation twins) of Fe - 30 wt - % Ni with and without Nb. The current work has not focused on texture, and as such a detailed discussion of texture has not been given but for more details the reader can refer to [28].

2.3.6 Static recrystallisation

Static recrystallisation is a thermally activated process and involves the migration of high angle grain boundaries (angle of misorientation greater than 10 to 15^o) [24, 28, 56]. The migration is driven by the stored energy of deformation, which has been discussed in Section 2.3.3. The following sections will discuss nucleation and quantification of recrystallisation as well as the recrystallised grain size.

2.3.6.1 Nucleation of recrystallisation

Several studies have been carried out to establish the nucleation mechanisms for recrystallisation. Turnbull and Fisher [24, 124] first proposed what is now known as the classical nucleation theory which was extended to nucleation in recrystallisation processes by Burke and Turnbull [125]. The theory stipulated that nucleation takes place by random atomic fluctuations leading to the formation of small crystallites separated by high angle boundaries [24, 124, 125]. However, a number of researchers [126 - 128] concluded that the theory was not practical because the driving force available for recrystallisation was small and also to

create high angle boundaries a high interfacial energy (typically 0.625 J / m^2) is required [28]. Therefore, alternative nucleation mechanisms were proposed such as subgrain growth [129], and strain induced grain boundary migration (SIBM) [130].

The subgrain growth model reported by Cahn [129] involves the evolution of a small region of high strain gradients and high local misorientations into a small strain-free cell through dislocation annihilation thus becoming more misoriented with respect to its neighbours. The subgrain continues to grow and gradually loses its subgrain nature and becomes a conventional grain. An illustration of subgrain growth is shown in Figure 2.22 [28].

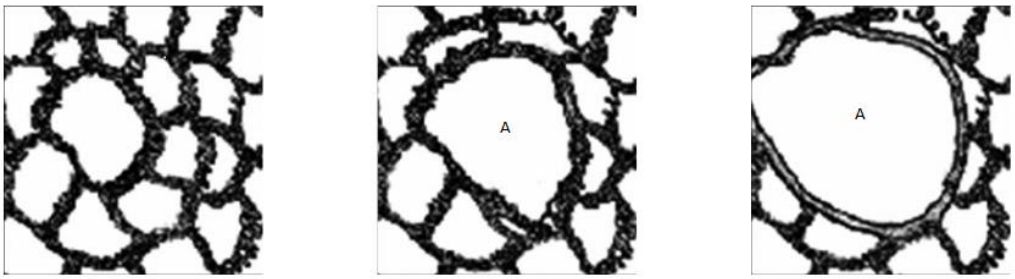

(a) **(b)** **(c)**

Figure 2.22: Schematic representation of the nucleation of a recrystallised grain based on the subgrain growth model (a) Initial substructure (b) Larger subgrain (denoted A) growth over smaller ones and (c) Defect free area associated to a high angle boundary that is being formed [28].

In the SIBM model, originally developed for low strains by Beck and Sperry [130] and extended by Bailey and Hirsch [122], where the driving force for SIBM was assumed to be the difference in stored energy (non-uniformity in dislocation density) in adjacent subgrains such that a subgrain with low stored energy dislocation density would bulge into a subgrain of high stored energy. The nuclei for recrystallisation have been reported to form in regions of

large strain gradients, such as twin boundaries, grain boundaries, and the surface of the material, phase interfaces and deformation bands [122, 123]. A higher strain gradient between grains leads to formation of a higher number of nuclei [123]. Studies on stored energy [24, 70, 71, 131] suggest that they may be a power law relationship between stored energy (strain gradient) and strain as discussed in Section 2.3.3. Nucleation rate has been reported to be influenced by the driving force, volumetric free energy, which is related to the applied strain; an increase in applied strain leads to an increase in the nucleation rate and as such, strain is directly proportional to nucleation rate. Therefore, it can be presumed that a power law relationship may exist between strain gradient and nucleation rate [24, 131]. Furthermore, Beck and Sperry [130] examined deformed and annealed aluminium and proposed that a subgrain of one grain adjacent to a pre-existing high angle grain boundary bulges by migration into the neighbouring grain with high stored energy. Later, Bellier and Doherty [133] examined partially recrystallised aluminium deformed to a strain of 0.2 and supported Beck and Sperry [130, 132] that nucleation was by SIBM of pre-existing grain boundaries. Most recently, Paggi *et al.* [134] used electron backscatter diffraction (EBSD) to also investigate the prevalent nucleation mechanism operating in AISI 304L stainless steel deformed at 1100 ^{o}C to strains ranging from 0.15 - 0.25 at a strain rate of 0.01 / s. It was concluded in this work that new grains nucleate by SIBM of pre-existing grain boundaries, confirming the proposition by Beck and Sperry [130]. Of the two nucleation mechanisms presented, SIBM, shown in Figure 2.23 seems to be the most commonly used for rolling [1, 4, 18, 134].

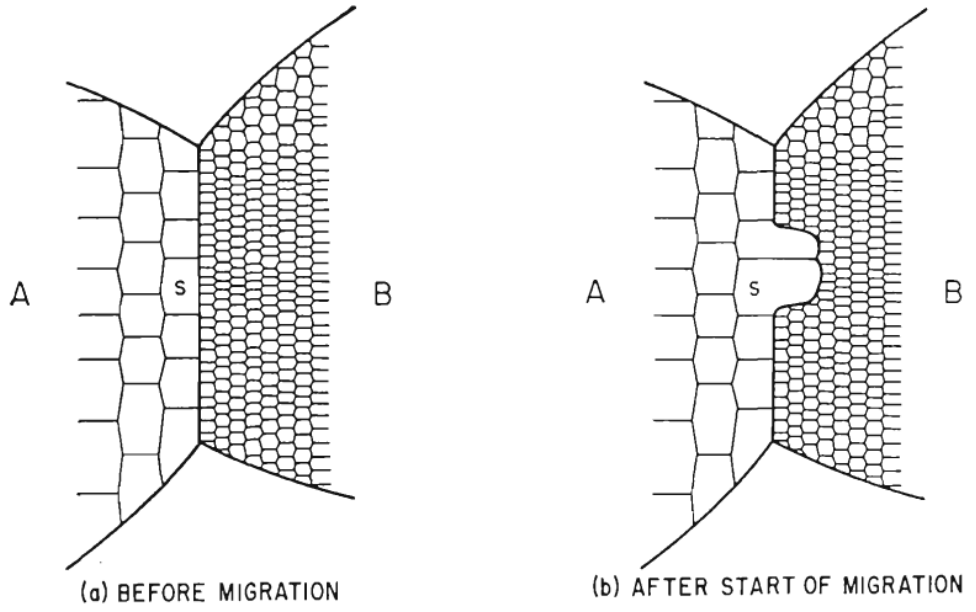

Figure 2.23: Schematic representation of strain induced grain boundary migration [18].

2.3.6.2 Grain growth after nucleation of the recrystallised grains

The reasons for grain growth after nucleation of the recrystallised grains and after recrystallisation are similar to those for grain growth during reheating. As discussed in Section 2.2.1.1, grain growth occurs to reduce the total grain boundary energy which is usually reflected through the reduction of total grain boundary area [24 - 27]. After nucleation grain growth occurs at the expense of the deformed structure, while after recrystallisation grain growth occurs by large grains growing at the expense of smaller ones thereby maintaining the material volume [26, 28]. Since grain growth during reheating (discussed in Section 2.2.1.1) and after recrystallisation occur in a similar manner, the following paragraphs will therefore focus on factors that influence grain growth after nucleation of recrystallised grains, such as solute drag and undissolved precipitates present in the material [18, 28, 47, 55, 135]. Strain induced precipitation influences grain growth as well, however it will be discussed in Section 2.3.8.2. The influence of solute drag and precipitation on the grain growth of nucleated recrystallised grains leads to retardation of recrystallisation through grain

boundary pinning, as briefly discussed in Section 2.3 [18, 28, 44, 47, 135]. The retarding force (P_r) depends on the volume fraction of particles (f), specific boundary surface energy (σ_B) and the radius of the particle (r) [136].

$$P_r = -3f\sigma_B / 2r \qquad (2.14)$$

The greatest retardation of recrystallisation by solute drag is observed in Nb-containing steels, as compared to other alloying elements such as V, Mo and Ti at a deformation temperature above dissolution temperatures [4, 135, 137, 138]. The difference between Nb and other alloying elements effectiveness in retarding recrystallisation has been attributed to atomic size difference (e.g. 15 % Nb and 6 % V) at an equal atom fraction in solution between solute and solvent [137]. In the experimental work carried out by Kundu [4] it was reported that solute drag is more effective in Nb and V microalloyed steels at temperatures above 1050 ^oC (i.e. above the dissolution temperature of the 0.0046 wt - % Nb and at low deformation strain (i.e. strain < 0.2) [4]. Precipitate pinning was reported to be higher at a higher strain range (i.e. strain > 0.2) and temperatures lower than 1050 ^oC.

The influence of solute drag on recrystallisation kinetics was investigated by Andrade *et al.* [135] using 4 different steels (plain carbon, 0.3Mo, 0.035Nb and 0.115V) deformed at 900 - 1000 ^oC to a strain of 0.25. They showed that at a deformation temperature of 1000 ^oC, recrystallisation had completed in 5 s for both the plain carbon and vanadium steel while for the molybdenum steel recrystallisation completed in 50 s. Recrystallisation took longer to complete in the Nb-containing steel (150 s) at a deformation temperature of 1000 ^oC. Therefore, it was concluded that the progress of recrystallisation was faster in the plain carbon steel than in the Nb-containing steel. They reported that retardation of recrystallisation was due to solute drag at a deformation temperature of 1000 ^oC because it was assumed that all the

alloying elements were in solution. In contrast, Irvine *et al.* [139] found little or no effect of solute drag on recrystallisation kinetics when they examined a 0.0150 wt - % V and 0.03 wt - % Ti steel. It has been reported that solute atoms only have a greater effect on the growth process rather than recrystallisation nucleation [1, 5, 6, 140 - 143] as the stored energy for recrystallisation nucleation is not affected. In contrast to reports that solute drag has no effect on recrystallisation nucleation, Miao *et al.* [55] claimed that for steels with very high Nb content (0.1 wt - % Nb) the slow growth rate of the recrystallised grain size due to solute drag and / or strain induced precipitation can lead to a finer recrystallised grain size after deformation as compared to steels with low Nb contents (0.06 wt - % Nb and 0.012 wt - % Nb). Nb - containing steels were deformed at temperatures ranging from 850 - 1050 ^{o}C to a strain of 0.25 at a strain rate of 1 / s. They argued that solute drag, depending on the amount of Nb in solution, might decrease the efficiency of both static and dynamic recovery and thereby maintain a higher driving force for recrystallisation, which would subsequently lead to greater refinement of the recrystallised grain size. They also stated that strain induced precipitates, depending on the volume fraction and precipitate size (particle sizes < 50 nm at 950 ^{o}C were observed using TEM), can pin segments of the dislocation network thereby slowing down the mobility of dislocations and subsequently leading to refinement of the recrystallised grain size. It was concluded that there is no effect of solute drag on the recrystallised grain size for samples with a low Nb content (0.012 wt - % Nb and 0.063 wt - % Nb) due to these materials having a lower amount of Nb in solution [55]. They however did not provide grain size distributions nor any average grain size data to verify their claims that a finer recrystallised grain size was obtained they only showed micrographs. The micrographs clearly showed that there was more grain refinement in the high Nb steel (0.1 wt -% Nb) than in the low Nb steel (0.063 wt - % Nb).

During recrystallisation the growth of the nucleated grains may be influenced by undissolved precipitates. Precipitates are retained at high temperatures (1100 - 1300 ^{o}C) due to increase in size, and as such they take longer to dissolve. Undissolved particles after reheating due to heat treatments carried out below the dissolution temperature of precipitates can slow down grain growth if the volume fraction and particle size meets the critical conditions (< 0.5 μm) for pinning of grain boundaries [28, 144, 145]. A low volume fraction of precipitates has little effect on static recrystallisation (63, 146]. Andrade *et al.* [93] reported the presence of NbC with particle size of 0.2 μm using transmission and scanning microscopy at a deformation temperature of 900 ^{o}C. They argued that the precipitates were too small to act as nucleation sites [135]. Undissolved particles may either deform or not depending on whether the particle is strong enough to withstand a shear stress exerted by an Orowan loop that forms around the particle. An Orowan loop is what remains after dislocations bow around particles. The undeformed particle leads to the formation of an extra dislocation in the form of an Orowan loop at the particle, unless the particle deforms either before or after the Orowan configuration is reached, in which case no extra dislocations are formed at the particle [28]. The stress on a particle from a single Orowan loop is given by the following equation:

$$\tau_S = \mu b / 2r \qquad (2.15)$$

Where τ_S is the applied stress and r is the particle radius.

As deformation continues more Orowan loops are formed leading to local strain incompatibility between the deforming matrix and the non-deformable particles. The strain gradient in the surrounding area of the non-deforming particle forms a region of high dislocation density and large misorientations and as such a particle deformation zone is formed [28, 86, 88, 147 - 149]. Upon annealing, particle stimulated nucleation (PSN) of

recrystallisation in the deformation zone may occur depending on the size of the particle and strain (particles greater than 1 μm and at high strains) [28, 56, 88, 147 - 149]. The particle deformation zones will act as a source of particle stimulated nucleation of recrystallisation due to strong strain gradients, higher dislocation densities and significant orientation gradients present in the area near the non-deformable particle. Occurrence of PSN may influence recrystallisation kinetics due to an increase in stored energy (increased dislocation density) [28, 56, 88]. As discussed in Section 2.3.3 the apparent increase in dislocation density for materials containing small (< 1 μm) non-deformable particles is only obtained for lower strains (< 0.05) than at higher strains, which are usually of importance for recrystallisation [28].

2.3.7 Quantification of recrystallisation kinetics

Different methods have been used in assessing and quantifying recrystallisation kinetics. Direct observation methods such as EBSD [151] and optical microscopy [150] of deformed and quenched specimens are used in order to measure the prior austenite grain size [15], as well as indirect observation methods which are based on assessment of how the material softens such as stress relaxation (SRT) and double hit tests (DHT) [15, 140, 152]. The indirect observation methods enable the progress of softening to be determined as a function of temperature in a given time interval after or in between deformation passes [153, 154]. Several deformation methods on various types of equipment, such as a high speed press [48, 135], uniaxial compression [155, 156] or plane strain compression [157], or Gleeble thermo-mechanical simulator, can be employed to carry out isothermal deformation tests [52, 158]. Comparisons between the various methods and techniques have been carried out by different researchers [159 - 161]. Several researchers have compared the recrystallised fractions obtained after a double deformation test and that obtained after a stress relaxation test [52,

154, 158]. Some researchers [52, 158] find good agreement between the fractions obtained from SRT and DHT whereas others [162] have argued that in a stress relaxation test recrystallisation is accelerated and as such significant discrepancies are observed. It is however difficult to establish the reasons for the observed discrepancies between various methods because different researchers use different analysis techniques and equipment to obtain their data [2]. A comparison was performed [15] for a single alloy using DHT and SRT, using different types of equipment and different analysis techniques. Later, the comparison was extended to multi-deformation tests [153]. It was concluded that the computed recrystallised fraction is not affected by the type of equipment used but that differences arise due to different methods used to determine fractional softening when double deformation is employed [15]. The use of different equipment was found to have an influence on the recrystallised fraction when stress relaxation was used, this was said to be due to precise setup and control of the deformation system and temperature that is required. Although plane strain deformation tests were not studied in [15] and [153] they are also often used in determining the amounts recrystallised [3, 4, 54, 57, 163].

2.3.7.1 Double deformation

Double deformation tests are used to study the progress of recrystallisation which is measured from interrupted mechanical tests [15, 18, 153, 164]. The test involves a reheating cycle, cooling to the deformation temperature; the first deformation applied and holding the material for a given period of time before a second deformation is applied with the same strain and strain rate as the first deformation [15, 48, 153]. A typical double hit compression test is shown in Figure 2.24 [15]. Direct observation of the stress-strain curves generated after the first and second deformations gives an indication as to whether recrystallisation is complete or not, for example, if full softening occurs the second flow curve would be identical to the first

flow curve (stress-strain curve obtained after a 500 second hold as shown in Figure 2.25), however, if the holding time is not sufficent for any softening to occur the second flow curve (multi-stage flow curves) will appear as an extrapolation of the first flow curve (stress-strain curve obtained after a 0.5 second hold shown in Figure 2.25) [143 - 153].

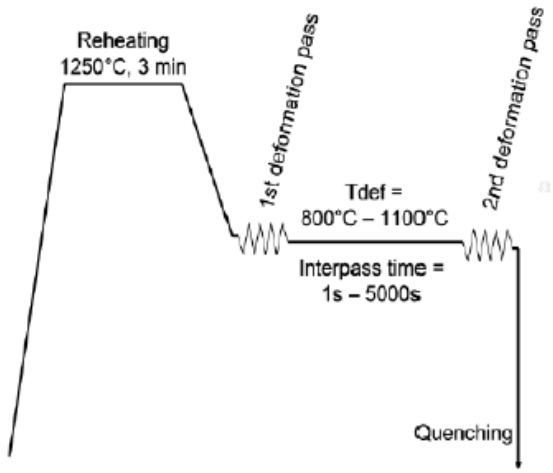

Figure 2.24: A schematic representation of a double hit compression test (DHT) route [15].

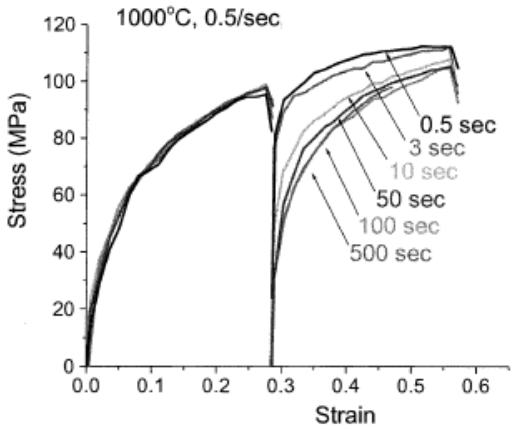

Figure 2.25: Typical flow stress-strain curves obtained from interrupted double deformation tests on a 0.045 wt - % Nb steel with holding times ranging from 0.5 to 500 s [143].

Table 2.11 highlights different methods that have been used in literature to quantify the amount of softening between a fully softened and non softened material such as the 0.2 % offset stress method [48], 2 % offset stress method [48], back extrapolation [135] and mean flow stress method [47]. Other methods used in the literature are the 5 % true strain [52] and the method based on correcting the 0.2 % offset stress by 20 % [165]. Stress-strain curves demonstrating the way the different methods are applied and how different parameters are obtained for the different methods are shown in Table 2.12. The softened fraction (FS) is conventially determined using Equation 2.16. Comparison between the different methods has been carried out by a number of researcher [15, 47, 48, 96, 135, 165]. From these studies it has been concluded that different methods have different effects on the determined softened fractions. The following paragraphs will discuss the accuracy of the different methods in determining the softened fraction.

$$FS = \frac{\sigma_m - \sigma_2}{\sigma_m - \sigma_1} \qquad (2.16)$$

Where σ_m is the maximum stress of the first deformation stress, σ_1 and σ_2 are stresses in the first and second deformation respectively. The value for σ_m, σ_1 and σ_2 depends on the method used to quantify fractional softening [1, 165].

Table 2.11: Methods used for quantifying recrystallisation kinetics in literature.

ε	Grain size / µm	T_{def} / ℃	Strain rate / s^{-1}	Steel composition / wt - %	Softening method	Measurement of softened fraction	Ref
0.1- 0.6	23 - 1073	1100 - 1150	1	0.035 Nb 0.034Nb-0.067Ti	Single/Double hit	2% offset/Direct observation	44
0.20 - 0.35	122	1050 - 1100	3.63	C - Mn - 0.042 Nb	Double hit	Back extrapolation	49
0.3 - 0.058	Not given	1000	Not given	Ti - V	Single hit	Direct observation	141
0.34	Not given	900-1100	0.05 - 5	AISI 304stainless	Double hit	0.2% offset	142
0.2	100	1000	0.5	0.045 Nb	Double hit	Mean flow stress	143
0.2	15 - 196	950	1	C- Mn	Double hit	0.2% offset	50
0.2	12 - 83	1000	0.2	C - Mn - 0055Nb	Double hit	0.2 & 2% offset	48
0.12, 0.25, 0.5	17 - 40	1000 - 1200	0.2 - 2	C - Mn, Cu - Nb - B steel	Direct observation	Mean flow stress	47

Table 2.12: Different methods used in calculating the softened fraction from double deformation tests [1].

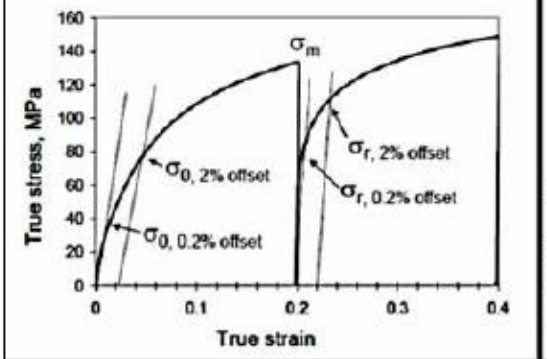	**Offset Method (0.2 % and 2 %)** $FS = \frac{\sigma_m - \sigma_{r,offset}}{\sigma_m - \sigma_{0,offset}}$ σ_m = maximum stress of first deformation $\sigma_{0,offset}$, $\sigma_{r,offset}$ = stresses at a plastic strain of 0.2 % or 2 % for the first and second deformation, respectively.
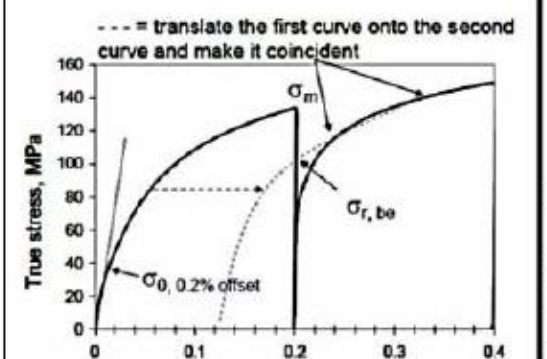	**Back Extrapolation Method** $FS = \frac{\sigma_m - \sigma_{r,be}}{\sigma_m - \sigma_{0,0.2\%offset}}$ σ_m = maximum stress of first deformation $\sigma_{0,\ 0.2\%\ offset}$ = stress of first deformation at 0.2 % plastic strain $\sigma_{r,\ be}$ = stress value at the intersection of the translated first curve with the unloading line.
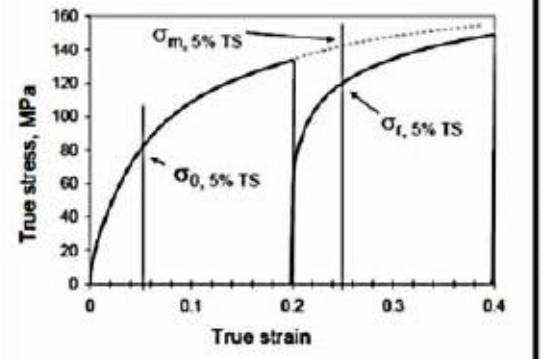	**5 % True Strain Method** $FS = \frac{\sigma_{m,5\%TS} - \sigma_{r,5\%TS}}{\sigma_{m,5\%TS} - \sigma_{0,5\%TS}}$ $\sigma_{m,\ 5\%\ TS}$ = flow stress at 5 % true strain of a hypothetical second curve corresponding to zero softening. $\sigma_{0,\ 5\%\ TS}$, $\sigma_{r,\ 5\%\ TS}$ = stress at 5 % true strain, first and second deformation, respectively.
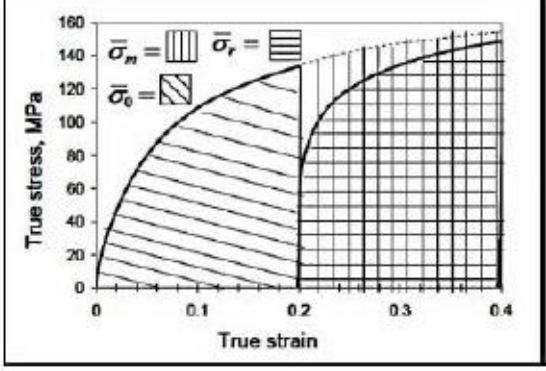	**Mean Flow Stress Method** $FS = \frac{\bar{\sigma}_m - \bar{\sigma}_r}{\bar{\sigma}_m - \bar{\sigma}_0}$ $\bar{\sigma}_0$, $\bar{\sigma}_r$ = area under the stress strain curve of the first and second deformation, respectively. $\bar{\sigma}_m$ = area under a hypothetical second curve corresponding to zero softening.

The 0.2 % and 2 % offset methods involve the use of stress values obtained at a plastic strain of 0.2 % and 2 % (for the first and second deformation) as inputs into Equation 2.16. respectively. The suitablity of the offset methods (0.2 % and 2 %) in determining the softened amount has been investigated by a number of researchers [15, 44, 47, 48, 96, 135, 165]. Many have argued that the 0.2 % offset method gives higher softened amounts than recrystallised amounts and they attribute this to the occurrence of recovery. A fractional recovery of 18 - 20 % has been observed when the 0.2 % offset method is employed [15, 47, 96, 135, 165]. Difficulties in accurately determining the 0.2 % offset stress may lead to a higher degree of uncertainty in the softened fraction determined using the 0.2 % offset method making it to be unreliable [15]. Some researchers have recommended [15, 44, 48, 165] the 2 % offset method, arguing that it excludes recovery better than the 0.2 % offset method. The experimental work of Li *et al.* [48] investigated three different methods used in determining the softening percent, that is, the 0.2 % offset method, 2 % offset method and the mean flow stress method using a 0.055 Nb steel. Li *et al.* [48] argued that in order to avoid the 'noise' that appears in the early stages of stress-strain curves obtained at high temperatures (950 ^{o}C and above) a 2 % offset be used instead of the 0.2 %. The suitability of these methods in determining the softened amounts was determined by comparing the amount of softening obtained at a given holding time using the 0.2 % offset method, 2 % offset method and the mean flow stress, as shown in Figure 2.26 [48]. It was observed that the softened amounts measured by 2 % were lower than that determined using 0.2 % offset stress and the mean flow stress methods particularly at shorter holding times. At longer holding times the method of measuring the softening amount did not seem to have an influence on the measured softened amount as there was little or no difference in the amounts obtained, Figure 2.26 [48]. It was concluded that the higher amounts obtained at shorter holding times when the mean flow stress method and 0.2

% offset method were used was due to recovery, however they did not validate their results by carrying out metallography to confirm whether the 0.2 fractional softening was due to recovery or recrystallisaton.

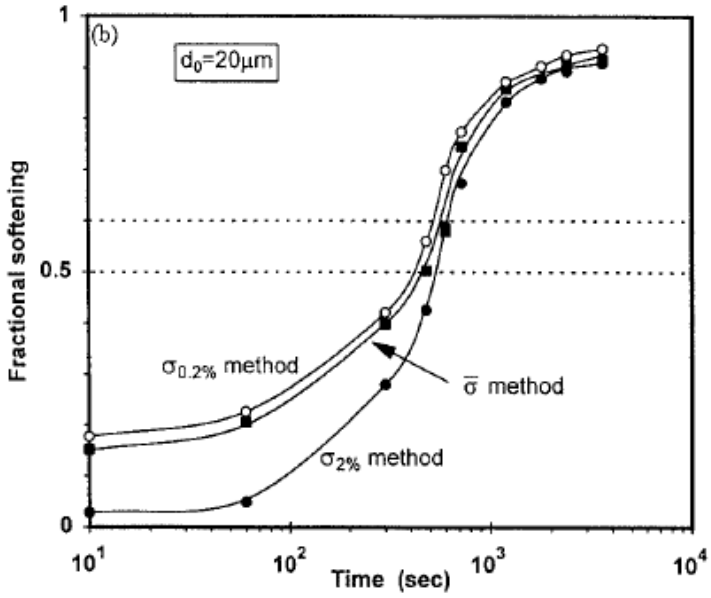

Figure 2.26: Plots of fractional softening vs. time as measured by three different methods (0.2 % and 2 % offset stress and mean flow stress) for a 0.055 wt - % Nb steel with an initial grain size (D_o) of 20 μm [48].

The accuracy of the 2 % offset stress method in predicting recrystallised fractions was also supported by Fernandez *et al.* [165] who examined six different methods (0.2 % offset stress, 2 % offset stress, 5 % true strain, mean flow stress, back extrapolation and the method based on correcting the 0.2 % offset stress by 20 %). Fernandez *et al.* [165] reported that a reasonably linear relationship existed between the softened fractions and recrystallised fractions for some of the methods examined (i.e. the 2 % offset, the 5 % true strain and mean flow stress). The relationship between softened amounts and recrystallised amounts was established by comparing determined softened fractions using the different methods studied to metallographically measured recrystallised fractions. It was reported that the amount of

recovery attributed to individual methods decreased from 18 % for the 0.2 % offset method to 10 % for the other methods investigated. However, it was reported that even though the recrystallised fractions obtained using the 2 % offset, the 5 % true strain and mean flow stress methods showed similar times for complete recrystallisation (200 s) the differences in the methods were evident at shorter holding times. Fernandez *et al.* [165] concluded that the 2 % offset stress and back extrapolation methods were suitable for use in determining the softened amount. However, concerning the back extrapolation method it was observed that the linear relationship was no longer followed as recrystallisation proceeded, leading to underestimation of the recrystallised fraction.

However, Andrade *et al.* [135] argued that back extrapolation predicted lower softened amounts than the offset method when they deformed three different materials (C - Mn steel, C - Mn - 0.0115V and C - Mn - 0.035 Nb). The softened amount attributed to recovery was reported to be 10 % using back extrapolation while it was 20 % for the 0.2 %. They estimated the onset of static recrystallisation from the intersection of two straight lines, each line extrapolated from recovery and recrystallisation regions (from the plot of fractional softening vs. holding time). Andrade *et al.* [135] reported that they did not use optical metallography to confirm or establish the onset of recrystallisation due to difficulties in observing the microstructure after deformation as austenite is unstable at lower temperatures (phase transformation). They claimed that the difference in the softened fractions obtained using back extrapolation and the 0.2 % offset method was associated with a transient (denoted AE in Figure 2.27) behaviour observed in the flowcurve for the second compression. It was reported that the transient occurred because of the decrease in dislocation density due to recovery. Therefore in order to regenerate the dislocations 'lost' due to recovery upon unloading an increament of strain was applied on reloading. This lowered stress leads to the

occurrence of a short transient. The reloading stress given by the back extrapolation was reported to be slightly larger than the actual one (leading to lower amounts of softened fraction). The back extrapolation method involves determination of the stress value in the first curve using the 0.2 % offset method as shown in Table 2.12 [1]. The stress value for the reloading stress corresponds to the intersection of the reloading line with the line obtained by superimposing the first deformation curve on the second deformation curve as shown in Table 2.12 [1, 135].

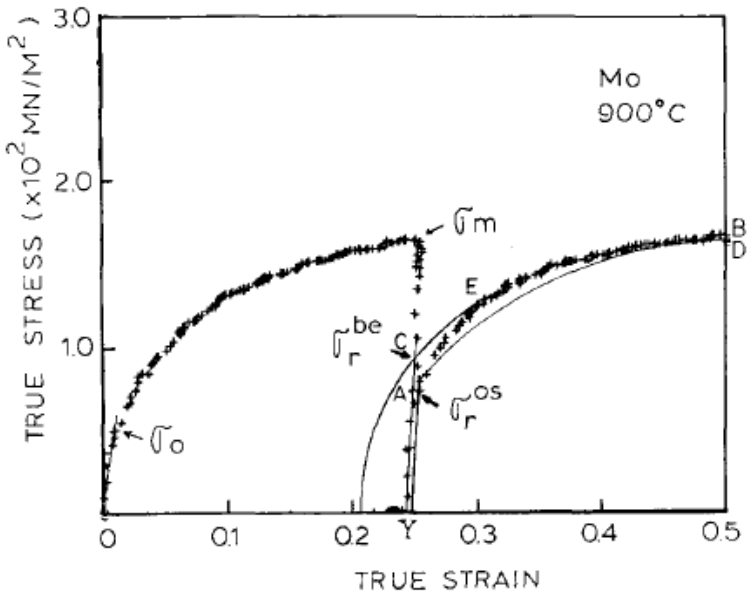

Figure 2.27: Determination of the reloading flow stress by back extrapolation and the 0.2 % offset stress method for a C - Mn - 0.29 Mo steel deformed at 900 ^{o}C [135].

The mean flow stress method on the other hand, involves the use of mean flow stresses obtained from the first and second deformations and the maximum stress of the first deformation curve. The maximum stress of the first deformation is evaluated from the extrapolated curve for the first deformation which corresponds to zero softening as shown in Table 2.12 [1, 15, 165]. The accuracy of the mean flow stress method in calculating the recrystallised fraction was examined by Fernandez *et al.* [165] and Vervenynckt *et al.* [15] by

comparing it to the 0.2 % offset stress, 2 % offset stress, the 5 % true strain and back extrapolation. For instance, Vervenynckt *et al.* [15] reported that the mean flow stress method gave recrystallised fractions which were 10 % higher than the 5 % true strain and 2 % offset stress method at longer holding times, however, the difference with the 2 % offset stress method became smaller at shorter holding times. On the other hand, Laasraoui *et al.* [47] used the mean flow stress method to determine the softened amounts of a low carbon steel using compression testing and reported that the effect of recovery was minimised when the mean flow stress method was used as compared to the 0.2 % offset stress method and back extrapolation methods. The differences in the results obtained by Laasraoui *et al.* [47] and those presented by Vervenynckt *et al.* [15] and Fernandez *et al.* [165] in terms of back extrapolation could be due to different deformation methods and equipment used [15].

The 5 % true strain method involves determination of stress values at 5 % true strain for the first and second deformations which are used in Equation 2.16. The maximum stress for the first deformation is determined from an hypothetical curve (which is an extrapolation of the first deformation curve) corresponding to zero softening as show in Table 2.12 [1]. The accuracy of the 5 % true strain in determining the recrystallised fraction has been investigated by a number of researchers [15, 52, 165]. From these studies it was concluded that the 5% true strain method does exclude recovery, however it is difficult to obtain the value of the stress of the work hardened material as this depends on the extrapolated hypothetical curve. Later, Vervenynck *et al.* [15] re-examined the accuracy of the different methods (the 0.2 % offset stress, 2 % offset stress, the 5 % true strain and mean flow stress, back extrapolation) and concluded that the softened fractions obtained using 5 % true strain, and 2 % offset stress methods were similar over the entire interval examined as shown in Figure 2.28. Of the two

methods the 2 % offset method was said to be suitable for analysing recrystallised fractions from double deformation tests. The back extrapolation method was not recommended because the stress value after the first deformation was determined using the 0.2 % offset method, and hence introducing uncertainities in the calculated fractions.

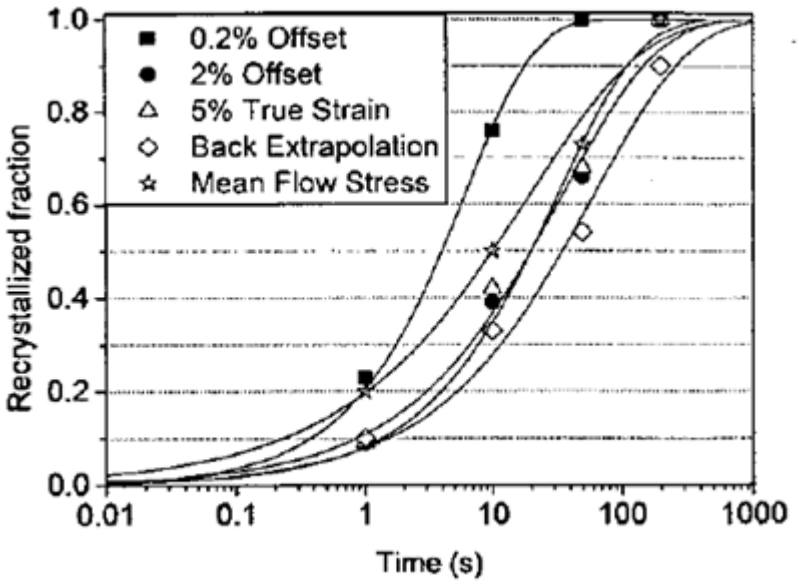

Figure 2.28: Comparison between the various analysing methods for computing the recrystallised fraction from DHT using a Nb - Mo alloy deformed with the dilatometer at 1000 ^{o}C [15].

From the above discussion it can be concluded that there is no standardised method for analysing the softening data when interrupted deformation tests are carried out, the method that tends to limit the effect of recovey on the fractional softening is usually employed. It can also be concluded that the 2 % offset method gives reduced recovery effects followed by the 5 % true strain method, the mean flow stress, back extrapolation and finally the 0.2 % offset stress method. The softened fraction determined from stress-strain curves is assumed to be appoximately equal to the recrystallised fraction of the sample. The disadvantage of using

double hit compression tests is that they require a new sample, which undergoes the same thermo-mechanical treatment for every data point making the process long and tedious [15].

2.3.7.2 Stress relaxation

Measurement of complete softening kinetics using a single sample can be achieved through stress relaxation tests. This technique involves a heating cycle to the deformation temperature and thereafter deformation is applied. After deformation the sample is held at the deformation temperature for a specified amount of time [2, 15, 52]. A uniform strain across the sample being deformed can be attained by minimising friction between the specimen ends and the anvils. This can be achieved through use of a very low friction material (lubricants) such as PTFE (polytetrafluoroethylene) tape and graphite foil on the faces of the platens, however, lubrication is a challenge at elevated temperatures [32]. Friction leads to an increase in pressure at the anvil / specimen interface which consequently causes the measured flow stress to be higher than the material flow stress [32, 166]. The increase in stress may influence the value of stress recorded (applied load) and consequently the recrystallised fraction. The amount of recrystallisation is determined from plots of stress against log (relaxation time) which are obtained after the prestrain [1, 52, 167, 168]. A typical stress-strain curve is given in Figure 2.29 showing a decreasing stress which corresponds to softening behaviour associated with microstructural events in the material such as creep and recovery (the first linear decrease denoted by A), recrystallisation (second stage showing a rapid decrease in stress, between A and B portions) and creep and grain growth (the second linear curve denoted by B) [15].

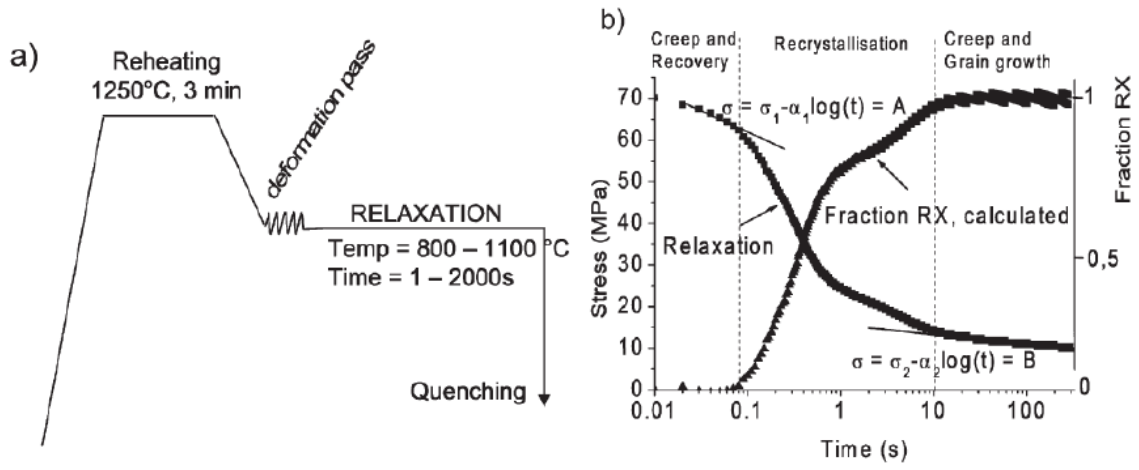

Figure 2.29: A typical stress relaxation test (a) Typical route for a stress relaxation test and (b) Typical results obtained from stress relaxation testing [15].

The second stage of the flow curve can be expressed in terms of the relative fractions of recrystallisation using a rule of mixtures approach [97]. In order to apply the rule of mixtures two assumptions are made; the first being that a partially recrystallised material consists of both deformed and fully softened regions and the second being that static recovery and recrystallisation can be separated. The three different stages are represented by the following equations [97]:

Stage 1 (A): $\sigma_{FS} = \sigma_{01} - \alpha_1 \log t$ (2.17)

Stage 2 (Between A and B): $\sigma_{FS} = (1 - X)(\sigma_{01} - \alpha_1 \log t) + X(\sigma_{03} - \alpha_3 \log t)$ (2.18)

Stage 3 (B): $\sigma_{FS} = \sigma_{03} - \alpha_3 \log t$ (2.19)

Where σ_{FS} is the stress in MPa, α_1 is the slope of the first curve (stage 1), α_3 is the slope of the third curve (stage 3), t is the relaxation time in seconds, σ_{01} and σ_{03} is the instantaneous stress value and X represents the recrystallised fraction, in Figure 2.29, σ_{01} and σ_{03} are represented by σ_1 and σ_2 respectively. The recrystallised fraction from stress relaxation can be determined by the following equation [97]:

$$X = \frac{\sigma_A - \sigma}{\sigma_A - \sigma_B} \quad (2.20)$$

Where σ_A is the stress for the first stage , σ is the stress for the second stage and σ_B is the stress for third stage. Using Equation 2.17 and 2.19 as inputs into Equation 2.20 the recrystallised fraction at a given time can be calculated by the following equation:

$$X = \frac{\{[\sigma_{01} - \alpha_1 \log(t)] - \sigma\}}{\{(\sigma_{01} - \sigma_{03}) - (\alpha_1 - \alpha_3)\log(t)\}} \quad (2.21)$$

The starting and finishing time for recrystallisation can be determined from the relaxation curves and it corresponds to the deviation of the straight lines from the record curve [1, 15]. Karjalainen [97] investigated the softening kinetics in a C - Mn steel with an initial grain size of 65 - 85 μm and a 0.041 Nb steel with an initial grain size of 50 μm using stress relaxation. He deformed the samples at 850 - 1000 ^oC using uniaxial compression on a Gleeble 1500 thermo-mechanical simulator, to strains of 0.02 - 3.6 at strain rates ranging from 0.01 - 2.4 / s. The obtained stress relaxation curve after deformation is shown in Figure 2.30 exhibiting the three different stages described above. Using stress relaxation curves for a C - Mn steel sample reheated at 1000 ^oC and deformed at 800 ^oC and 900 ^oC to a 0.36 strain at a strain rate of 0.01 / s, softened amounts were calculated and plots of the softened amount (X) versus log (t) made, Figure 2.31. The obtained sigmoidal curve corresponded to the Avrami type relationship observed by other researchers for plots of the recrystallised fraction against time [16, 45]. Figure 2.31 shows that recrystallisation is faster in the sample deformed at 900 ^oC than in the sample deformed at 800 ^oC which shows that recrystallisation kinetics are influenced by the deformation temperature, as discussed in Section 2.3.1. Avrami type equations / expressions are given in Section 2.3.8.1. The softening behaviour can be influenced by parameters such as precipitation and solute drag [28]. Precipitates and solute

atoms in solution may pin grain boundaries and thereby retard recrystallisation due to retardation of grain boundary migration [18, 28]. Depending on the volume fraction and precipitate size of the precipitates and solute atoms, recrystallisation kinetics will be significantly retarded as discussed in Section 2.3.1 [28, 47, 48, 97].

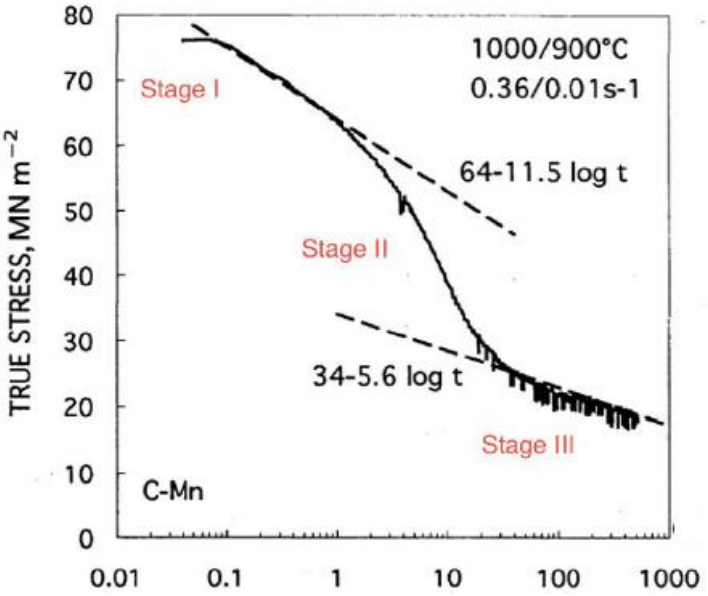

Figure 2.30: A stress relaxation curve for a C - Mn steel deformed to a strain of 0.36 [97].

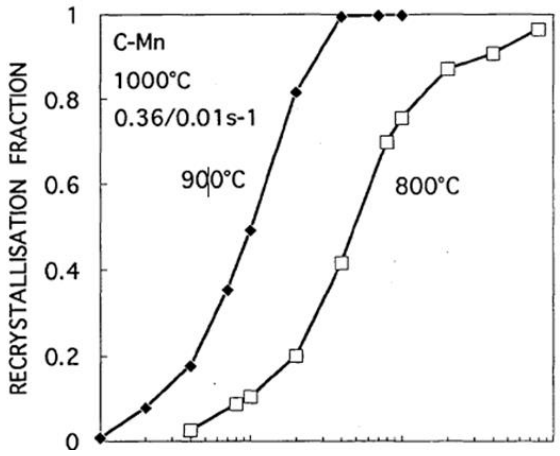

Figure 2.31: Softening fractions measured during stress relaxation in a C - Mn steel [97].

One disadvantage of stress relaxation testing is that complicated stress relaxation curves are obtained for Nb-microalloyed steels which makes it difficult to separate recovery and recrystallisation. However, Karjalainen [97] proposed that the use of the stress relaxation data from a sample subjected to a low strain (0.02) would help in separating recovery and recrystallisation by using the low strain curves to determine the instantaneous stress for stage 3 in a given, stress relaxation curve and thereby determining the amount softened using Equation 2.21, this is demonstrated in Figure 2.32 for a 0.041Nb steel deformed at 950 ^{o}C to a strain of 0.36 at a strain rate of 0.12 / s. From Figure 2.32 the recrystallised fraction is determined by in putting into Equation 2.21 values for the fitted equations to the first stage of the sample deformed to a 0.36 (83 - 16.5 log t) and taking the values from the equation fitted to the sample deformed to a low strain of 0.02 (32 - 7.4 log t) instead of values obtained from stage 3 of the 0.36 strained sample. The degree of recrystallisation can be determined using stress relaxation methods; however, for predicting grain size development, more accurate measurements such as direct observation methods (metallographic techniques) are required [97].

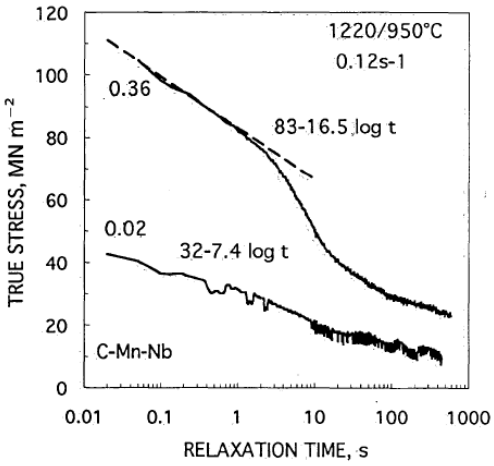

Figure 2.32: Use of low strain curves in determining the stress corresponding to stage III in a typical stress relaxation curve for C - Mn - 0.041 wt - % Nb [97].

Values from hardness testing have been used in literature to determine softened fractions [60, 61, 169]. Kazeminezhad *et al.* [60] and Saidi *et al.* [61] carried out cold deformation tests on pure copper by performing micro hardness tests on annealed samples with different annealing times and thereafter generating a plot of hardness values versus annealing time, the resulting plot was an Avrami type curve similar to what is observed when the recrystallised fraction is plotted against holding time [16, 45]. It was reported that full softening was achieved if the hardness values for an annealed sample and a deformed and annealed sample (with a similar grain size) were relatively similar, which would indicate that there was no residual strain in the deformed sample after recrystallisation [60, 61, 169]. They however did not compare their obtained data from hardness testing to any of the other techniques (such as the offset, mean flow stress, back extrapolation and metallographic methods [47, 48, 165]) used to determine softening fractions to establish how accurate measurements from hardness tests were in determining the softened fraction. Although, hardness measurements cannot be used to accurately determine the fraction recrystallised as they do not distinguish recovery; they can however be used to indicate whether softening has occurred or not.

The differences in the methods used to analyse the softening data and in turn the recrystallised fraction may lead to variation in the values of the derived constants for empirical and semi-empirical equations proposed by different researchers for predicting recrystallisation kinetics [5, 14, 16, 44, 45, 170]. In the current study stress relaxation tests have been carried out in order to help make comparisons of the predicted recrystallisation times using Dutta-Sellars equations (discussed in Section 2.3.8) [170] with those obtained using the Gleeble 3500 thermomechanical simulator, whereas double hit tests were carried out in order to generate a finer grain size. Hardness testing using a Vickers hardness testing machine has been carried

out in this work to determine whether samples had fully softened or not, and hence ensure that there was no residual strain in the recrystallisation annealed samples (fully softened).

2.3.8 Review of Dutta-Sellars equations

2.3.8.1 Modelling fraction recrystallised

As earlier pointed out in Section 2.3.1, recrystallisation is influenced by parameters such as strain, strain rate, initial grain size, and deformation temperature. In order to describe the evolution of microstructure after hot deformation empirical or semi - empirical equations have been developed over several decades [5]; an overview of equations used in the prediction of different types of steels is provided in [4, 48]. These equations were initially proposed by Sellars [5] by fitting them to several sets of data from different researchers and were valid for C - Mn steel, low carbon and HSLA steels with Nb contents of 0.03 - 0.046 wt - % for grain sizes ranging from 100 - 450 μm and strains of 0.3 to determine appropriate values of the constants in the model as briefly mentioned in Section 2.3.7. The fraction recrystallised at a given time (rate of static recrystallisation) is represented by the following Avrami expression [5, 14, 16]:

$$X = 1 - \exp\left(-0.693 * \left(\frac{t}{t_{0.5}}\right)^{n}\right) \qquad (2.22)$$

Where X is the recrystallised fraction, t is specified time for recrystallisation, the time for 50 % of recrystallisation, $t_{0.5}$ and n the Avrami exponent which Sellars [5] proposed to be equal to 2. The Avrami exponent (n) represents nucleation and growth rate [28]. An avrami exponent of 2 would indicate that nucleation and growth of recrystallised regions is heterogeneous due to differences in kinetics for individual grains within a material. For example, smaller grains may have faster recrystallisation kinetics than larger grains due to a higher stored energy in smaller grains leading to different nucleation and growth rates [171].

Typical values for n have been proposed to be between 1 and 2 for materials deformed to strains less than the critical strain for dynamic recrystallisation ($\varepsilon_c < 0.5$) as shown in Table 2.13 [5, 16, 44, 49, 97, 141 - 142].

Table 2.13: Typical values used for the Avrami constant in Equation 2.22.

Avrami constant (n)	**Material**	**Ref.**
1.02	AISI304 stainless steel	142
2	C - Mn steel C - Mn - 0.03 - 0.046 wt% Nb	5
2	Ti - V steel	141
1	0.013 - 0.03 wt% Nb steel	16
0.9	C - Mn steel	164
28.33exp (-36,000/RT) (0.62 - 1.50)	0.007 - 0.093 Nb	45
1	0.034 Nb 0.008N 0.035 Nb 0.0043 N	44
27.35 exp (- 40000/RT) (0.6 - 0.8)	C - Mn - 0.42 Nb	49
1.3	C - Mn, C - Mn- 0.041Nb	97

For microalloyed steels the Avrami exponent values of 1 and 2 are valid for deformation carried out above the static recrystallisation critical temperature (SRCT), that is, the temperature at which precipitation of particles such as Nb (C, N) starts under isothermal conditions. For instance Cho *et al.* [142] carried out deformation tests on a stainless steel sample at temperatures of 900 - 1100 ^{o}C to strains of 0.34 - 0.68 at strain rates of 0.05 - 5 / s. They plotted Ln (time) vs Ln (Ln (1/ (1 - X)) in order to determine the value of n. They found

that the value of n (1.018) was constant for different deformation conditions such as deformation temperature, strain and strain rate as illustrated in Figure 2.33. In contrast, Luo *et al.* [172] found that the avrami exponent value (that is, for the overall recrystallisation kinetics) varied with local strain heterogeneity when they analytically considered the entire recrystallisation process. It was concluded that average avrami exponent values varied from 1 to 2 over the entire recrystallisation process. They associated the lower value of n to a higher heterogeneity in the local strain. Values observed by Luo *et al.* [172] and Cho *et al.* [142] are in good agreement with the experimental observations on static recrystallisation after deformation for different materials. Avrami exponents of 3 and 4 have been proposed when site saturation is assumed [28].

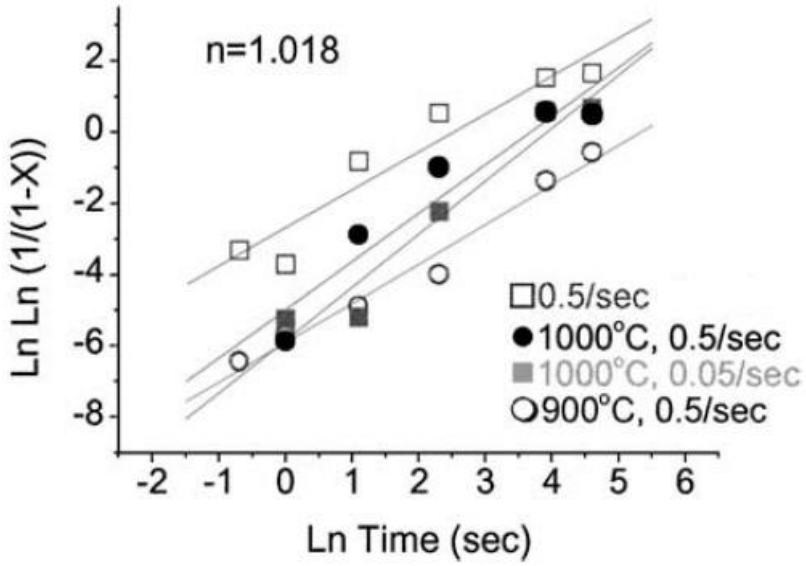

Figure 2.33: Determination of n (Avrami constant) using different deformation conditions for a AISI 304 steel [142].

The parameter $t_{0.5}$, which is the time corresponding to 50 % recrystallisation by volume is influenced by initial grain size, strain, temperature, and microalloying elements [14, 45]. The presence of microalloying elements in the material either as solutes (Nb, V, Ti, Cr etc.) or

precipitates (Nb, Ti (C, N)) will retard recrystallisation [14, 45]. It has been shown that $t_{0.5}$ decreases as the deformation temperature and strain is increased due to a higher driving force for recrystallisation and lower activation energy respectively. Smaller initial grain sizes give faster recrystallisation kinetics as compared to coarse grains, due to the fact that for small grains there is more available grain boundary area per unit volume, which provides a higher density of nucleation sites [49, 50, 143]. Sun *et al.* [50] investigated the influence of initial grain size and deformation temperature on the recrystallisation kinetics ($t_{0.5}$). They deformed a 0.17 wt - % C - Mn steel with an initial grain size of 196 μm at 950 °C to a strain of 0.2 at strain rate of 1 / s, and varied the initial grain size from 15 - 196 μm. They showed that 50 % recrystallisation occurred after 1 second for the sample with an initial grain size of 15 μm, whereas it took 30 seconds for the sample with an initial grain size of 196 μm to reach 50 % recrystallisation as illustrated in Figure 2.34 a. They also studied the influence of deformation temperature using a 0 .17 wt - % C - Mn steel with an initial grain size of 196 μm deformed to a strain of 0.2 at a strain rate of 1 / s by varying deformation temperatures from 900 - 1100 °C. They reported that at a higher temperature of 1100 °C, 50 % recrystallisation occurred after a second, whereas it took about 100 seconds for the same sample to attain 50 % recrystallisation at 900 °C, Figure 2.34 b.

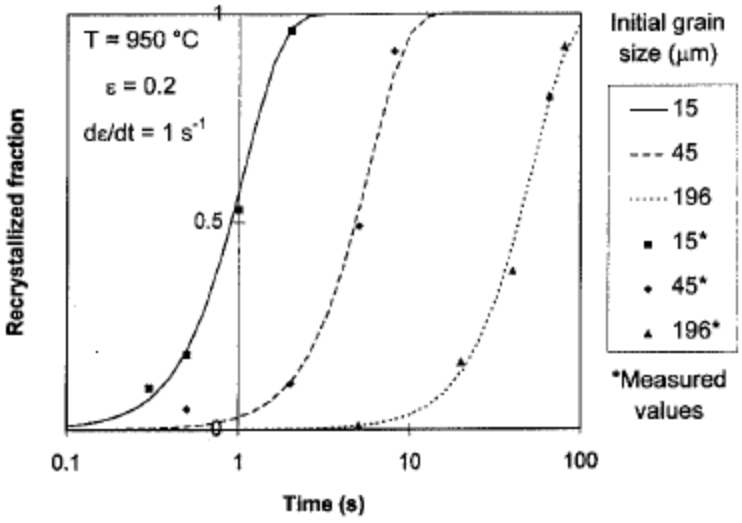

(a)

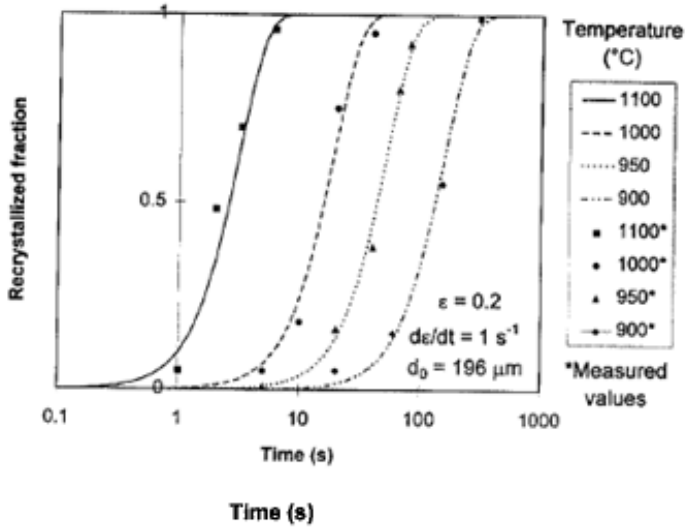

(b)

Figure 2.34: Influence of deformation parameters on recrystallisation kinetics for a 0.17 wt - % C - Mn steel deformed to a strain of 0.2 at a strain rate of 1 / s. (a) Effect of initial grain size and (b) Effect of deformation temperature [50].

The effect of strain on recrystallisation kinetics ($t_{0.5}$) was studied by Fernandez *et al.* [44] using a Nb - Ti steel with an initial grain size of 109 μm. The Nb - Ti steel was deformed at 1100 ^{o}C at a strain rate of 1 / s. They varied the strain from 0.1 to 0.3 and found that, for the

sample strained to 0.1, 50 % recrystallisation occurred after about 100 seconds, whereas for the sample strained to 0.3 it only took about a minute for 50 % recrystallisation to occur, Figure 2.35.

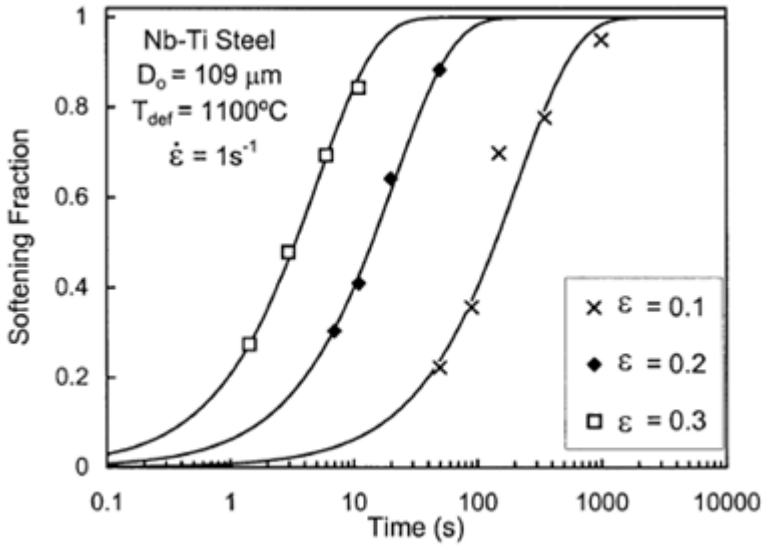

Figure 2.35: Influence of strain on recrystallisation kinetics [44].

The relationship for $t_{0.5}$ is generally expressed as follows [5, 14, 16, 142]:

$$t_{0.5} = A_1 D_o^m \varepsilon^{-p} \dot{\varepsilon}^{-q} \exp(Q_{rex} / RT) \quad (2.23)$$

Where $\dot{\varepsilon}$ is strain rate, A_1, m, p and q are constants, R is the gas constant (8.314 J / K mol), D_o is the initial grain size and Q_{rex} is the activation energy for static recrystallisation.

The constants and activation energy are obtained by fitting to experimental data, however, in the case of the original Dutta-Sellars equation [5, 170] the constants and other parameters were obtained by fitting to data from different researchers. Typical values for the constants and other parameters used in Equation 2.23 are given in Table 2.14 [2, 5, 48 - 50, 141 - 143]. From Table 2.14 it can be seen that the initial grain size exponent varies from 0.81 - 2 for HSLA steels (0.03 - 0.055 wt - % Nb) and austenitic steels for deformation temperatures

ranging from 900 - 1150 ^{o}C, deformed to 0.1 - 0.68 strain and initial grain sizes ranging from 15 - 1073 μm. Initial grain size exponents up to 1 are observed for austenitic and C - Mn steels, whereas for microalloyed steels a value of 2 is generally proposed. A higher initial grain size exponent will lead to slower recrystallisation kinetics, whereas a lower one will lead to faster recrystallisation kinetics. For the various steels and deformation conditions strain exponent values range from 0.67 - 4, as given in Table 2.14 [5, 44, 50, 141 - 143]. In the literature, the value for q (strain rate exponent) has been reported to be zero in most cases; that is the effect of strain rate has been ignored, as mentioned in Section 2.3.1 [48 - 50]. For instance, Li *et al.* [48] ignored the influence of strain rate on $t_{0.5}$ due to a weaker dependency of $t_{0.5}$ on strain rate as compared to the influence of the initial grain sizes exponent of 1.7 on $t_{0.5}$. The weaker dependency of $t_{0.5}$ on strain rate was also observed by Sun *et al.* [50] when they examined a plain C - Mn steel deformed at 950 ^{o}C to strains of 0.20 at a strain rate of 1 / s. The lower values observed for q (0.3 - 0.53), as shown in Table 2.14, would suggest that strain rate indeed has little influence on recrystallisation kinetics as compared to other parameters such as strain exponent (0.6 - 4) and initial grain size exponent (0.8 - 2) therefore being ignored in Equation 2.23 by some researchers [5, 44, 48 - 50, 141 - 143]. The variation in the values for the constants has been attributed to differences in composition and initial grain size; a smaller value of q may be obtained for samples with smaller initial grain sizes compared to materials with coarse initial grain sizes [5, 48]. Similarly, large amounts of alloying elements such as Ti and Nb present in a material might lead to a smaller value of q [4, 44, 48].

Table 2.14: Summary of different parameters used in predicting $t_{0.5}$, softening methods and techniques used to determine fractional softening (FS).

Parameters	[44]	[49]	[141]	[142]	[143]	[5]	[50]	[48]
A	$9.92*10^{-11}$	$3.94*10^{-13}$	$5*10^{-18}$	$2*10^{-10}$	$1.9*10^{-18}$	$6.75*10^{-20}$	$5.22*10^{-13}$	-
m	1	1	2	0.81	2	2	1	1.7
p	$5.6\ D_o^{-0.15}$	1.96	3.5	1.56	2.8	4	0.67	-
q	-0.53	0.44	-	-	0.41	-	0.3	-
ε	0.1- 0.6	0.20 - 0.35	0.3 - 0.058	0.34, 0.68	0.2	$\varepsilon_p > 0.8$	0.2	0.2
$\dot{\varepsilon}$ / s^{-1}	1	3.63	-	0.05 - 5	0.5	-	1	0.2
Q_{rex} / kJ / mol	180	262	280	197	324	300	248	-
Grain size / µm	23 - 1073	122	-	Not given	100	100 - 450	15 - 196	12 - 83
T_{def} / °C	1100 - 1150	1050 - 1100	1000	900 - 1100	1000	900 - 1100	950	1000
Steel composition	0.034Nb - 0.067Ti	C - Mn - 0.042Nb	Ti - V	304 stainless	0.045Nb	C - Mn - 0.03 - 0.046Nb	C - Mn	C - Mn - 0.055Nb
Softening method	Single / Double hit	Double hit	Single hit	Double hit	Double hit	-	Double hit	-
FS Measurement	2 % offset stress / direct observation	Back extrapolation	Direct observation	0.2 % offset stress	Mean flow stress	-	0.2 % offset stress	0.2 % & 2 % offset stress

The activation energy used in Equation 2.23 is a fitted parameter and is determined from plots of $t_{0.5}$ against the inverse of temperature; the slope (Q / R) gives the value of the activation energy. A number of researchers have reported different values for the activation energy for recrystallisation; some of the values are given in Table 2.14 [5, 44, 48 - 50, 141 - 143]. Medina *et al.* [173] investigated 11 steels and found that the activation energy for static recrystallisation was highly sensitive to the chemical composition, and also reported that the highest value for activation energy was observed in Nb microalloyed steels (276 kJ / mol) and as such recrystallisation was retarded due to slowing down of recrystallisation kinetics by Nb as compared to C - Mn, C - Mn - Mo and C - Mn - Ti steels; the lowest value for activation was observed in the plain carbon steel (92 kJ / mol) which led to faster recrystallisation kinetics. Similarly, Medina *et al.* [49] reported that Nb (0.042 wt - %) had the highest retarding effect on static recrystallisation leading to higher activation energy of 262 kJ / mol followed by Ti (0.075 wt - %) with activation energy of 227 kJ / mol. The vanadium steel (0.095 wt - %) was observed to have the least value for activation energy (198 kJ / mol). Therefore, it can be concluded that the values reported for activation energy change Q_{rex} in a direction that is consistent with the action of the different alloying elements. Scatter in the value of the activation energy for steels with almost similar compositions was observed. Activation energy has an influence on recrystallisation kinetics, such that the higher the activation energy (recrystallisation barrier) the longer it takes to fully recrystallise the sample.

The models proposed by different researchers for predicting recrystallisation kinetics have been shown to have good agreement with measured values when applied to materials with similar deformation conditions as those that they were developed for. However, when applied to materials with deformation conditions other than those for which they were developed, significant errors may occur [4, 44, 45]. For example, Fernandez *et al.* [44] validated their

model for predicting recrystallisation kinetics developed from examining Nb, Ti and Nb - Ti steels with a wide range of grain sizes (20 - 1000 μm) by comparing the calculated $t_{0.5}$ to the measured $t_{0.5}$ from a specific experimental set of data generated. They reported a good correlation between the calculated and predicted $t_{0.5}$ values as illustrated in Figure 2.36. However, applying the original Dutta-Sellars equations [5, 170] to the data generated by Fernandez *et al.* [44] predicted shorter times for $t_{0.5}$ (0.0007 s) as compared to the measured $t_{0.5}$ (20 s) for the 0.035Nb steel with an initial grain size of 806 μm deformed at 1100 ^{o}C to a 0.2 strain at a strain rate of 1 / s. Dutta-Sellars [170] developed equations for predicting the recrystallisation start time (R_s) and recrystallisation finish time (R_f) in addition to $t_{0.5}$, details of which are given in Section 2.3.8.2.

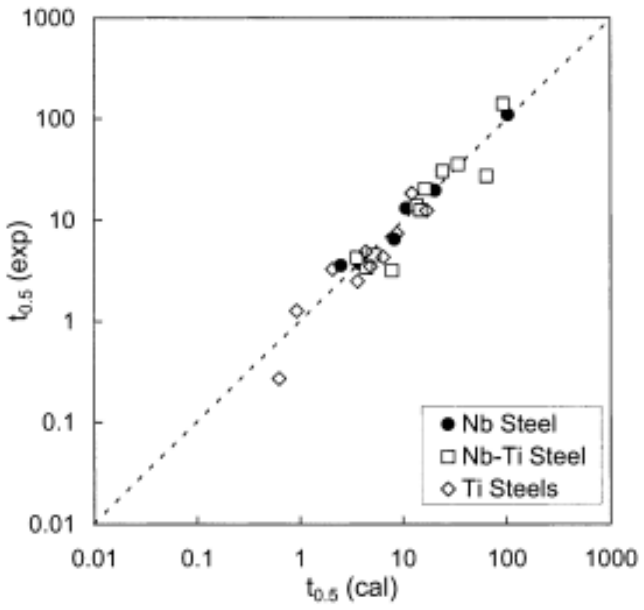

Figure 2.36: Comparison between the $t_{0.5}$ experimental data and the predictions made using the equation for $t_{0.5}$ proposed by Medina *et al.* [45] for Nb, Ti and Nb - Ti microalloyed steels.

2.3.8.2 Predicting recrystallisation start (R_s) and recrystallisation finish time (R_f)

Dutta and Sellars [170] proposed a model which has often been used to predict static recrystallisation in Nb microalloyed steels. As discussed in Section 2.3.8, the equations were developed by considering the thermodynamics of the material and classical nucleation theory and thereafter, equation fitting data obtained from different researchers for grain sizes ranging from 100 - 450 µm and strains of 0.3 to determine appropriate values of the constants in the model. These equations are valid for C - Mn steels with Nb contents of 0.03 - 0.046 wt - %. The semi-empirically fitted equations are given by [170]:

$$R_s = 6.75 \times 10^{-20} D_o^2 \varepsilon^{-4} \exp\left(\frac{300{,}000}{RT}\right) \times \exp\left(\left(\frac{2.75x10^5}{T} - 185\right)\right) [Nb] \quad (2.24)$$

$$P_s = C_3 [Nb]^{-1} \varepsilon^{-1} Z^{-0.5} \times \exp\left(\frac{270{,}000}{RT}\right) \times \exp\left(\frac{B}{T^3 (lnK_S)^2}\right) \quad (2.25)$$

Where P_s (5 % precipitation of the microalloying element in solution) is the strain induced Nb (C, N) precipitation start time, R_f (85 % recrystallisation) is the recrystallisation finish time and R_s (5 % recrystallisation) is the recrystallisation start time. D_o (in µm) is the average grain size after reheating, T (in Kelvin) is the temperature where recrystallisation and precipitation is taking place, [Nb] is the amount of Nb (wt - %) in solution, ε is the applied strain. K_s is the supersaturation ratio following the solubility product (Equation 2.26) [164] and Z is the Zener-Holloman parameter, which is related to $\dot{\varepsilon}$ and deformation temperature (T_{def}) given by Equation 2.27; B and C_3 are constants [5, 170].

$$K_s = [Nb][C+12N/14]/10^{2.26-6770/T} \quad (2.26)$$

$$Z = \dot{\varepsilon} \exp\left(\frac{Q_{def}}{RT_{def}}\right) \quad (2.27)$$

Where Q_{def} is the activation energy for deformation.

The accuracy of any fit will depend on determining the 5 and 85 % recrystallisation fractions. R_f is predicted from the following Avrami equation [4, 5, 170].

$$0.85 = 1- \exp [(\text{In } (0.95)(\frac{R_f}{R_s})^2] \quad (2.28)$$

The parameters proposed in Equation 2.24, such as a strain exponent of - 4, D_o exponent of 2 and activation energy of 300 kJ / mol, were found not to be appropriate for use in predicting the recrystallisation finishing times as they predicted faster recrystallisation kinetics. For instance, a strain exponent of - 4 which relates to the driving force for recrystallisation may be on the higher side, leading to accelerated recrystallisation kinetics. An example of how recrystallisation kinetics are accelerated when Equation 2.24 is employed was given by Kundu [4] who investigated a 0.046 wt - % Nb steel with an initial grain size of 280 µm deformed to a strain of 0.3 at 1075 ^oC. It was concluded that Dutta-Sellars equations [170] predicted the recrystallised amount (area percent) to be 95 % compared to the measured recrystallised amount of 72 % [4]. She reported that partial recrystallisation occurred when the mode grain size was employed in the Dutta-Sellars equations [170] for the examined steel and deformation conditions given above [4].

In order to compare the measured and the predicted recrystallised amounts, data available in the literature covering a wide range of grain sizes (20 - 806 µm) was used [4]. Kundu [4] reported that the equations are only accurate for some deformation conditions (T_{def}: 900 - 1100 ^oC, ε: 0.1- 0.5, initial grain size: 100 - 450 µm,) and compositions (for overall range in composition, wt - %: 0.06 - 0.17C, 0.03 - 0.084 Nb, 0.005 - 0.015N, when using a wide range of values for constants: B ($1x10^{10}$ to $6x10^{10}K^3$) and C_3 (3×10^6 to $2.5x10^{-5}$) [3 - 5, 9, 12] as shown in Figure 2.37. Further, Kundu [4] examined the validity of the Dutta-Sellars equation in predicting the recrystallised amounts using data from other researchers for steels with

larger austenite grain sizes (> 450 μm) and a greater range of Nb contents than those used to develop the original equation as shown in Figure 2.38. It can be seen that discrepancies do occur when the Dutta-Sellars equation is applied to conditions outside those for which it was developed; the recrystallised amounts were seen to be over predicted. The variations observed in the predicted amount of recrystallisation may be due to a number of factors, such as differences in the deformation conditions employed, compositions, or may even be due to inaccuracies in the method of measurement used to determine the recrystallised fractions.

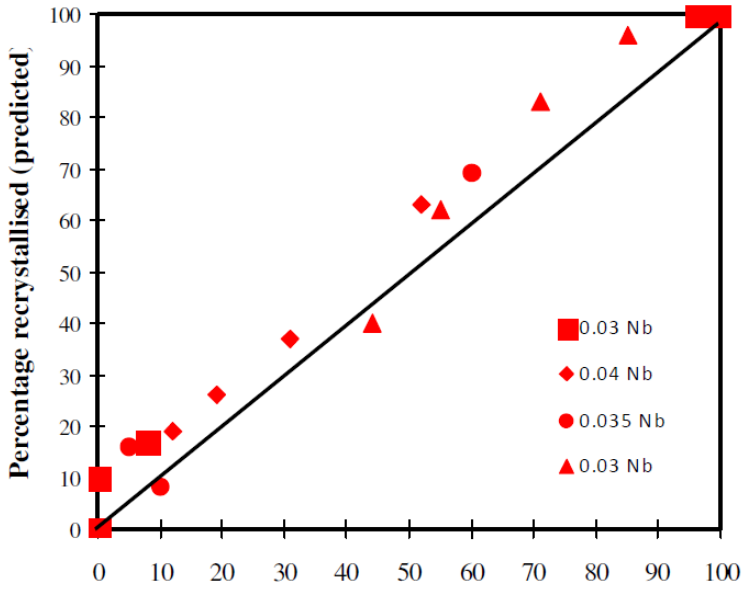

Figure 2.37: Comparison of predicted recrystallised amounts (%) with measured recrystallised amounts (%) for samples deformed to a 0.3 strain (from literature) [4].

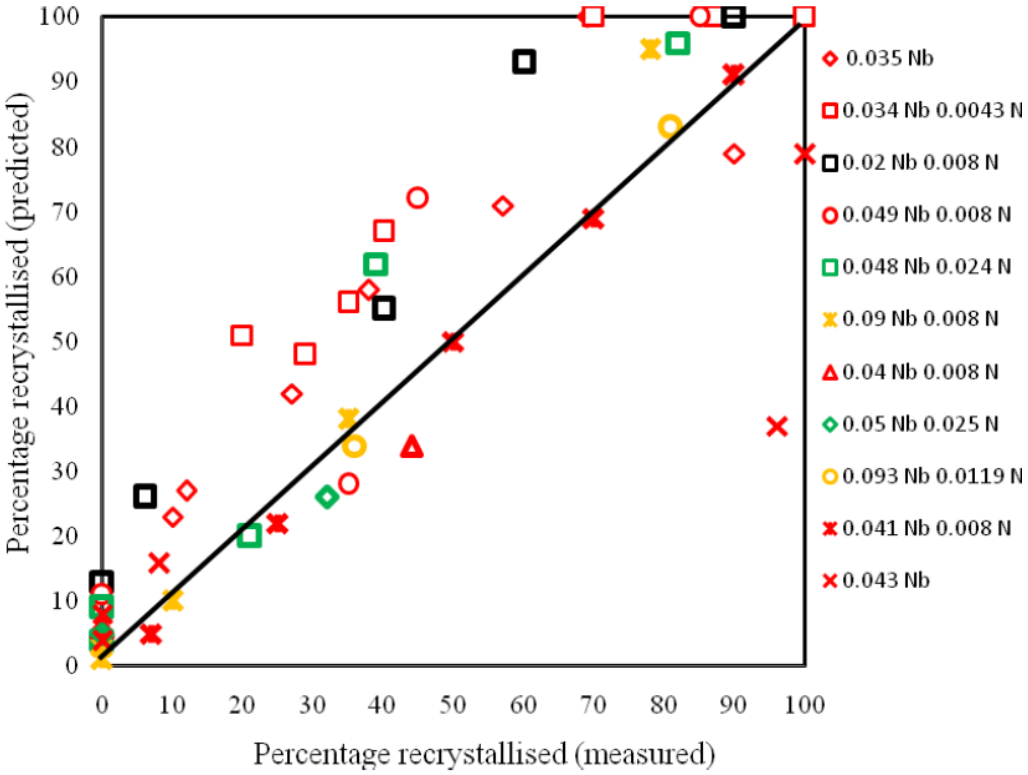

Figure 2.38: Comparison of predicted recrystallised amounts (%) using Dutta - Sellars equations [170] with measured recrystallised amounts (%) for samples deformed to a 0.3 strain (from literature) [4].

The Dutta-Sellars equations (2.24, 2.25, 2.26, 2.27 and 2.28) are employed in the prediction of recrystallisation-precipitation-temperature-time (RPTT) curves. RPTT curves are used in designing TMCR schedules so that the development of microstructure is controlled. Predicted RPTT curves for a 0.046Nb steel ($\dot{\varepsilon}$: 10 s^{-1}; ε: 0.3; D_o: 60 μm) [4], illustrated in Figure 2.39, comprise P_s, R_s, and R_f curves and are used to select deformation temperatures, that is, temperatures at which either no recrystallisation or partial recrystallisation or full recrystallisation is expected to occur. If the holding time (10 seconds hold is often used commercially) and temperature is known, prediction of the recrystallised fraction can be done [164]. Figure 2.39 highlights the fact that, if deformation is performed above 1050 °C full recrystallisation may be achieved, while deformations performed between 890 °C and 980 °C

may lead to partial recrystallisation, and no recrystallisation will occur below deformation temperatures of 850 °C. A change in the initial austenite grain size used to predict the RPTT curves results in a shift in the R_f and R_s curves because the prior austenite grain size influences the rate of recrystallisation. For example, if a finer prior austenite grain size is used, there would be an increase in the amount of grain boundary per unit area resulting in more available area for nucleation and as such increasing the nucleation rate and consequently the recrystallisation rate, as discussed in Section 2.3.1 [4, 52].

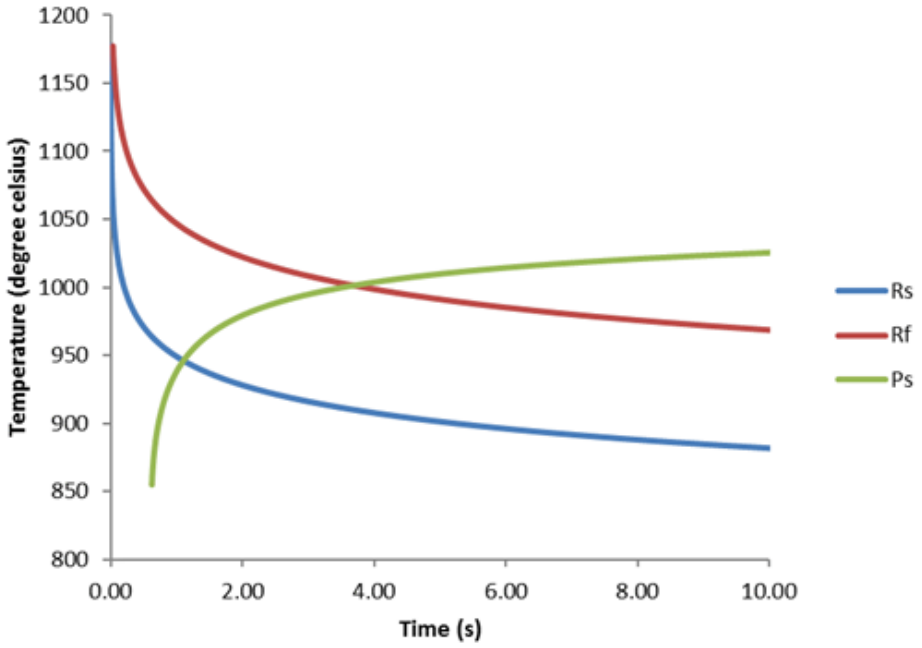

Figure 2.39: Predicted Dutta-Sellars recrystallisation-precipitation-temperature-time (RPTT) curves for a 0.046 wt -% Nb steel (ε: 0.3; έ: 10 s^{-1}; D_o: 60 μm) [4]. R_s is the recrystallisation start time, R_f is the recrystallisation finish time and P_s is the strain induced precipitation start time [4].

Most of the work done on microalloyed steels have found that strain induced precipitation slows down recrystallisation kinetics [5, 44, 45, 49, 55, 174]. Retardation in static recrystallisation may take place when deformation tests are carried out so that precipitation

precedes recrystallisation due to the Zener drag effect caused by strain induced precipitates of (Nb (C, N), TiN) etc. For Nb microalloyed steels Nb (C, N) precipitates of particle size 4 -10 nm have been reported [46, 85, 145, 177 - 182]. Strain induced precipitates with small particle sizes, larger volume fraction and uniformly dispersed leads to pinning of grain boundaries and therefore slowing down recrystallisation kinetics [4, 18, 28, 44, 45, 49]. Precipitation is predicted to retard or halt recrystallisation when the P_s (5 % precipitation) line in Figure 2.39 intersects the R_s line because once strain induced precipitation has started, activation energy increases as a consequence of the rise in recrystallisation inhibition energy. Strain application during deformation leads to an increase in dislocation densities, which in turn leads to faster precipitation [5, 28, 174].

Grain boundaries are preferred precipitate nucleation sites, and as such a pinning force is exerted on moving grain boundaries, thereby increasing the recrystallisation inhibition energy, making it difficult for austenite to recrystallise [28]. Recrystallisation will be retarded or halted if the Zener pining force on the grain boundaries is higher than the driving force for recrystallisation [4, 5, 28, 49, 174]. Halting of recrystallisation (permanent plateau in fraction recrystallised versus time plots) by strain induced precipitates will occur if recovery plays a part due to a reduction in the driving force for recrystallisation so that the final recrystallised fraction is lower than 1 [28, 49, 174]. However, if coarsening of the precipitates takes place (at constant volume fraction) after a particular holding time, the Zener force is reduced to levels where recrystallisation can proceed until a recrystallised fraction of 1 is reached (this is represented by a temporal plateau in fraction recrystallised versus time plots) [49]. Medina *et al.* [49] deformed a 0.042 wt - % Nb steel to a strain of 0.2 and observed that recrystallisation kinetics were slowed down due to the strain induced precipitates (presence of a plateau in the curves in Figure 2.40) for deformation temperatures below 1000 ^{o}C. The presence of a plateau

in the curve (plot of fraction recrystallised versus time) for the Nb-containing sample shows that temporary retardation of recrystallisation (between 20 s to about 100 s) occurred with the volume fraction increasing with continued holding due to the decrease in Zener pinning force due to coarsening of precipitates after completion of precipitation.

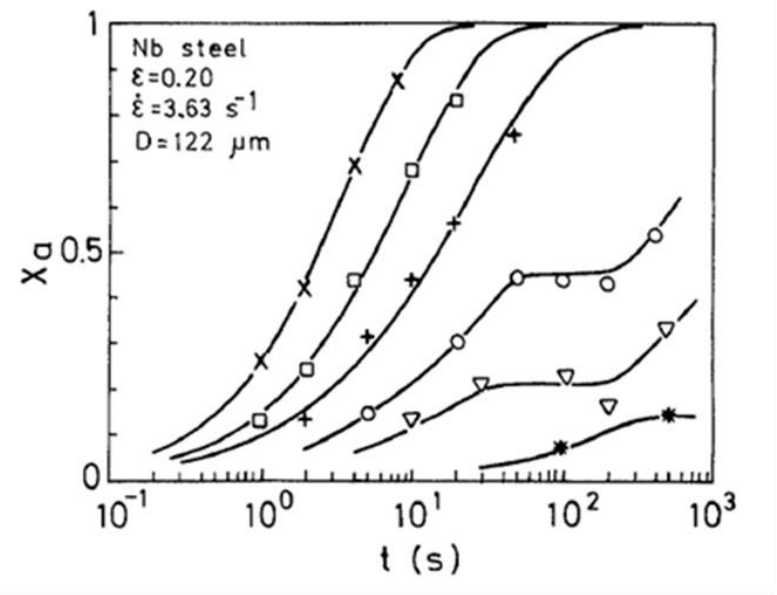

x =1150 °C; □ = 1100 °C; + = 1050 °C; ○ = 1000 °C; ∇ = 975 °C * = 950 °C

Figure 2.40: Recrystallisation volume fraction (X_a) versus holding time for a 0.042 wt - % Nb steel with an initial grain size (D) of 122 μm deformed at different temperatures (950 - 1150 °C) to a strain (ε) of 0.20 at a strain rate (ε̇) of 3.63 / s [49].

However, Kundu [4] investigated steel containing 0.046 wt - % Nb and reported that there was no effect of precipitation on recrystallisation at a strain of 0.3 and deformation temperature of 990 °C (where precipitation was predicted to precede recrystallisation). The effect of precipitation was investigated by comparing the predicted recrystallised amounts to that measured. She found that the predicted amount (8 % using the individual grain size class approach) was lower than what was measured (10 %); this confirmed the fact that even

though precipitates were present in the sample (confirmed using TEM), recrystallisation was not retarded at a deformation temperature of 990 ^{o}C. Kundu [4] reported a volume fraction of 0.00008 (which was 25 % of the equilibrium amount of precipitates at 990 ^{o}C) with an average particle size of about 3.9 nm. They observed no change in the particle size and concluded that progression of recrystallisation was not due to coarsening of the particles and as such there was no effect of strain induced precipitation at 990 ^{o}C. As discussed in the previous paragraphs, strain induced precipitates no longer retard recrystallisation when they exceed a critical size (> 0.5 μm side length) as they are too coarse to pin grain boundaries; in which case, they then can sometimes act as nucleation sites for recrystallisation and thereby increase the rate of recrystallisation [145, 175, 176]. The conflicting trends shown by Medina *et al.* [49] and Kundu [4] may be due to differences in volume fractions and particle sizes, although Medina *et al.* [49] did not give the volume fraction and particle size. As discussed in Section 2.3.6.2 solute drag can also slow down mobility of grain boundaries, which consequently retards recrystallisation, however precipitates are generally more effective in pinning grain boundaries than solute atoms [4, 18, 28. 55].

Based on the Dutta-Sellars approach [170] models for the recrystallisation-precipitation interaction in Nb microalloyed steels have also been developed for a wider range of compositions and strains [44, 45] and have been summarised in [4]. The study by Kundu [4] concluded that a large number of equations developed by several researchers for quantifying the amount of recrystallisation had a similar structure to that of the original Dutta-Sellars equation [44, 45]. Kundu [4] examined the validity of the original and modified Dutta-Sellars equations [44, 45] in quantifying the amount of recrystallisation for a 0.046 wt - % Nb steel in a homogenised condition deformed to a strain of 0.3 with an initial grain size of 280 μm by comparing the measured percentage recrystallised to the predicted amount using the original

and modified Dutta-Sellars equations [5, 44, 45]. It can be seen from Figure 2.41 that the original Dutta-Sellars equation over predicts (10 % measured using root mean square (RMS) error approach) the experimentally measured amount of recrystallisation. She showed that the recrystallised amount is over predicted by using equations developed by Fernandez *et al.* [44] (18 %) and under predicted (21.5 %) by those from Medina *et al.* [45], as illustrated by Figure 2.42.

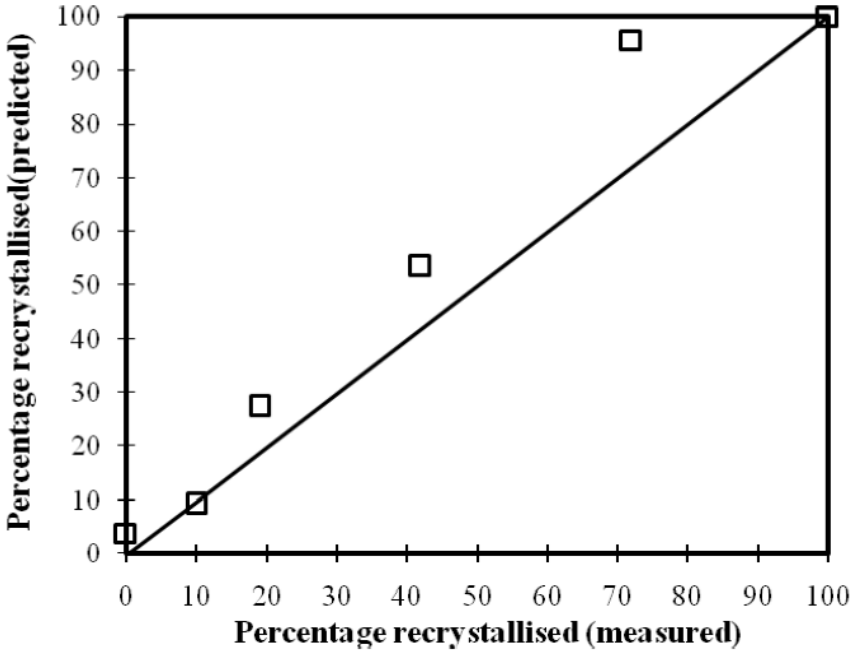

Figure 2.41: Comparison of predicted recrystallised amounts (%) using the original Dutta-Sellars equation [170] with measured recrystallised amounts (%) for a 0.046 wt - % Nb steel with an initial mode grain size of 280μm deformed to a 0.3 strain [4].

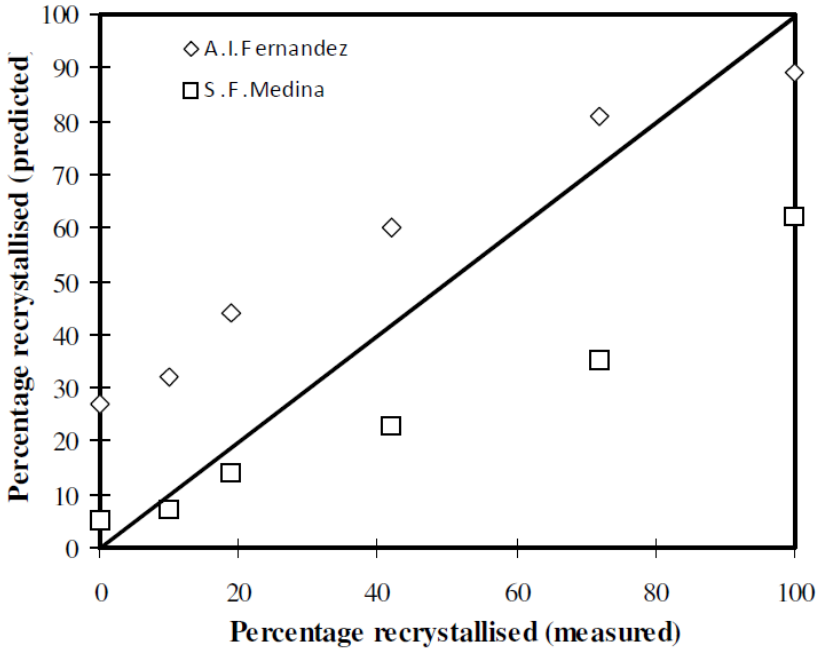

Figure 2.42: Comparison of predicted recrystallised amounts (%) using equations proposed by Fernandez *et al.* [44] and Medina *et al.* [45] with measured recrystallised amounts (%) for a 0.046 wt - % Nb steel with an initial grain size of 280 μm deformed to a 0.3 strain [4].

Kundu [4] proposed an approach for predicting R_f and the recrystallised amounts which involved halving individual grain size classes in a grain size distribution (which has been described in full elsewhere [3, 4]) as inputs into the Dutta-Sellars equation, instead of just using the mode grain size. It was concluded that the use of the individual grain size class approach in cooperation with the Dutta-Sellars [170] equations for predicting R_f in order to achieve complete recrystallisation and the amount of recrystallisation using the individual grain size class gave a much better fit, as compared to when a mode grain size was used as an input (over predicted the recrystallised amounts in the Nb-containing steel after deformation to a strain of 0.3), Figure 2.43 [4]. She further examined the validity of the individual grain size class approach by applying it to data available in literature, as shown in Figure 2.44 [4]. Less scatter in the predicted results was observed when the individual grain size class

approach in cooperation with the Dutta-Sellars equations was used instead of just using the mode grain size with the Dutta-Sellars equations [170]. It was concluded that the results obtained from models developed through equation fitting to data for a high strain range or larger amounts of Nb did not agree well if data other than those used to develop the model were used [4].

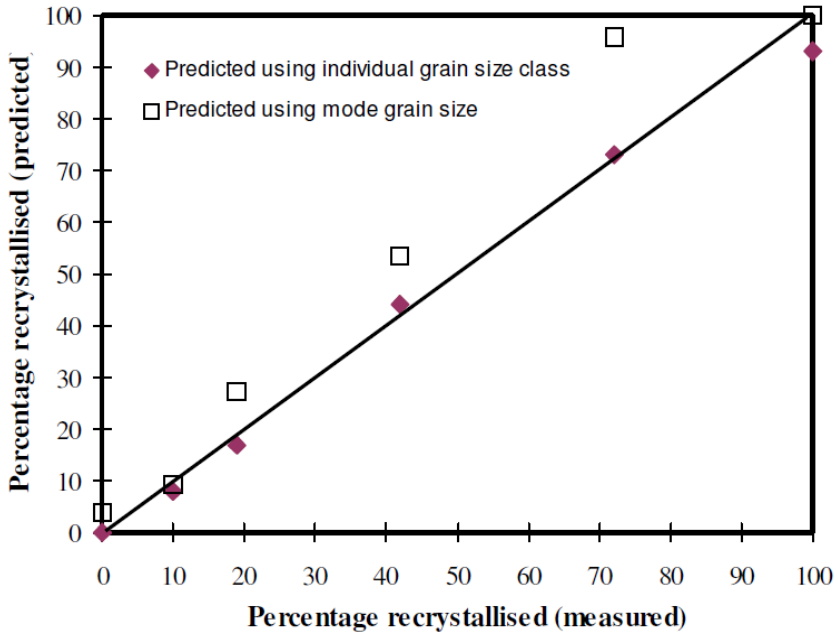

Figure 2.43: Comparison of predicted % recrystallised amount with that measured at a 0.3 strain using a 0.046 wt - % Nb steel with an initial grain size of 280 µm using the entire reheated grain size distribution (individual grain size class) and the mode grain size [4].

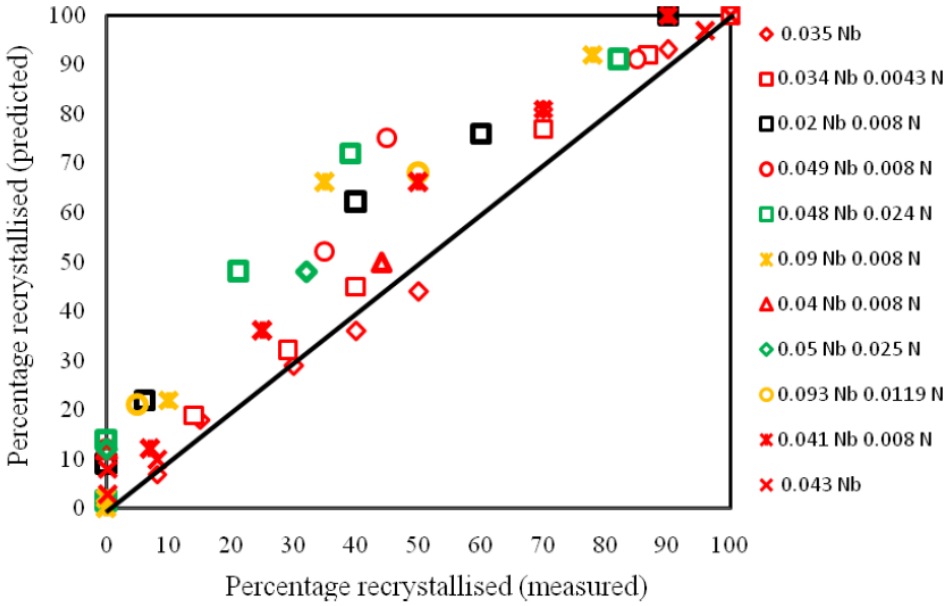

Figure 2.44: Comparison of the predicted % recrystallised with the measured amount (%) at a strain of 0.3 for the literature data using individual grain size class [4].

2.3.9 Recrystallised grain size

It has already been stated in Section 2.3.1 that the recrystallised grain size is influenced by the applied strain and initial grain size [3 - 9, 16, 18, 28, 34, 44]. It has been shown that as strain is increased and the initial grain size decreased, a finer recrystallised mode grain size is obtained [5 - 8]. Equations of the form given in Equation 2.29 have been proposed for predicting the mode recrystallised grain size by equation fitting to experimental data [6, 185] and, in the case of Sellars [5], to data obtained from different researchers. They are valid for strains below the critical strain for dynamic recrystallisation (> 0.5 strain). A detailed discussion of Equation 2.29 in terms of parameters used and its limitations is given in Section 2.4.

$$D_{rex} = D'D_o^{x}\varepsilon^{-y} \qquad (2.29)$$

Where D_{rex} is the static recrystallised mode grain size, D_o is the initial mode grain size, ε is the applied strain and *D'*, x and y are constants. A summary of parameters used in the Sellars equation for predicting the recrystallised mode grain size is given in Table 2.15 [5].

2.3.9.1 Effect of strain and initial grain size on recrystallised mode grain size

Figure 2.45 shows the effect of initial grain size on the recrystallised grain size; the smaller the initial grain size the smaller the recrystallised grain size [6, 7, 8, 9]. This effect has been reported to be because of finer grains having more available grain boundary area per unit volume, which leads to a higher number density of nucleation sites as discussed in Section 2.3.1 [28, 72 - 74, 76]. The details of the deformation method, deformation parameters and compositions used in obtaining the recrystallised grain size are given in Table 2.16.

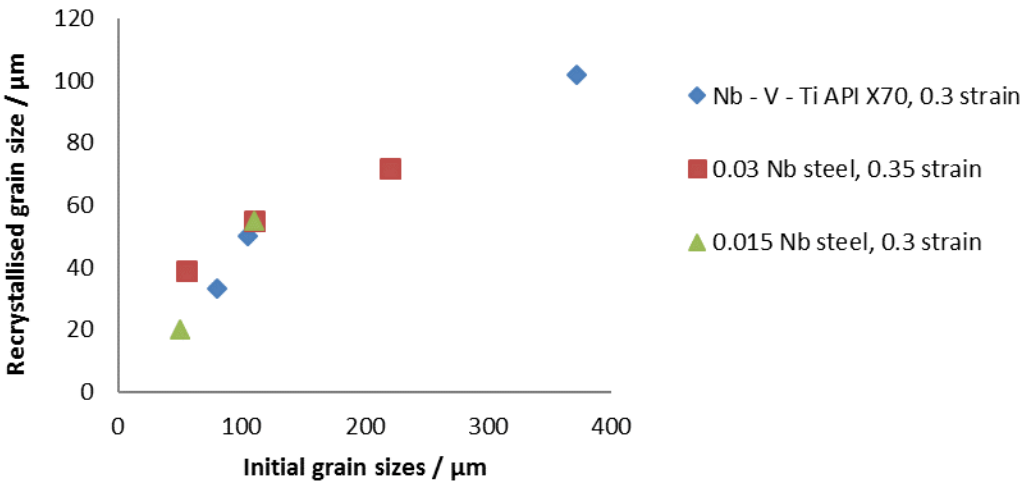

Figure 2.45: Effect of initial grain size on the recrystallised grain size; graph plotted using literature data (Table 2.15) [6, 7, 9].

Table 2.15: Summary of parameters used in Equation 2.29 [5] for predicting the recrystallised mode grain size.

T_{Def} / °C	Strain	Initial grain size / µm	D_{rex} / µm	D' value observed / $\mu m^{0.33}$	Strain exponent, y	Grain size exponent, x	Nb content / wt - %	Ref.
850	0.1 - 1.3	Not given	40 - 12	1.86	0.67	0.67	0.015	7
900	0.55 - 1	250	70 - 30	0.83	1	0.67	-	10
900 - 1000	0.17 - 0.3	56-44	48 - 14	0.35	1	0.67	-	8
900	1 - 1.6	250	25 - 14	0.66	0.67	0.67	0.04	10
850	0.26 - 1.5	220-55	110 - 20	1.1	0.67	0.67	0.04	9

Table 2.16: Summary of deformation methods, deformation parameters and compositions used to obtain the recrystallised grain size.

Parameters	[6]	[7]	[8]	[9]	[18]
Strain	0.2 - 0.4	0.07 - 1.3	0.17 - 0.3	0.2 - 0.9	0.25 - 0.9
D_o / µm	80 - 808	50, 110	44, 56	50 - 220	310
Temperature / °C	1100	850	900 - 1000	1000 - 1200	850
Steel composition	Nb - V - Ti API X70	0.015 Nb	0.045 - 0.047Nb	0.03Nb	Fe - 30Ni - 0.02Nb, Fe - 30Ni
Experimental method	Uniaxial compression using Gleeble 3800	Tension using Instron machine	Hot rolling mill	Hot rolling mill	Uniaxial compression by Servo hydraulic machine
Strain rate / s^{-1}	3	0.22	Not given	14	0.7

Sellars [5] empirically fitted equations to experimental data from several researchers and suggested that the following relationship existed between the recrystallised grain size and the initial grain size:

$$D_{rex} \alpha D^{x}_{o} \quad (2.30)$$

The values for the initial grain size exponent x are obtained by plotting D_{rex} vs. log [D_o] [5]. The value of x has been reported to be between 0.56 - 0.67 [5, 6, 183]. There is not much significant difference in the values of the initial grain size exponent (x) proposed for different deformation conditions and compositions.

A number of researchers [5 - 7, 10, 18, 141 - 143] have demonstrated that the recrystallised mode grain size decreases with increased strain as illustrated in Figure 2.46. This effect may be due to the fact that dislocation density (high stored energy), which is the driving force for recrystallisation, increases with strain [71, 72]. From Figure 2.46 the rate of grain refinement for the C - Mn steel with an initial mode grain size of 250 μm decreases with an increase in strain and also despite the samples having different initial grain sizes as strain increase the recrystallised grain size seems to converge, this may be due to saturation of nucleation sites. The effect of strain on the recrystallised grain size was studied by Weiss *et al.* [7] by examining a 0.015 wt - % Nb - Ti microalloyed steel with an initial mode grain size of 110 μm. They varied strain from 0.07 to 1.3 and found that as the strain increased the recrystallised mode grain size decreased. They also observed that after a strain of 1.0 (critical strain) the specimen could not be refined further and suggested that this could be due to saturation of nucleation sites [7].

Recently, the decrease in recrystallised grain size with strain has been reported by Dong *et al.* [53] using a SA508 III steel deformed at 950 ^{o}C to a range of strains (0.15 - 0.25) at a strain

rate of 0.1 s^{-1}. The empirically fitted equation proposed by Sellars [5] suggests that the following relationship between the obtained recrystallised grain size and applied strain exists:

$$D_{rex} \alpha \varepsilon^{-y} \quad (2.31)$$

The values for the strain exponent y are obtained by plotting D_{rex} vs. log [ε] [5]. The reported values for Nb-containing steels are between 0.67 - 1 [5, 6, 57] and 1 [5] for non-Nb containing steels (C - Mn steels) and are valid for strains below the critical strain for dynamic recrystallisation [5].

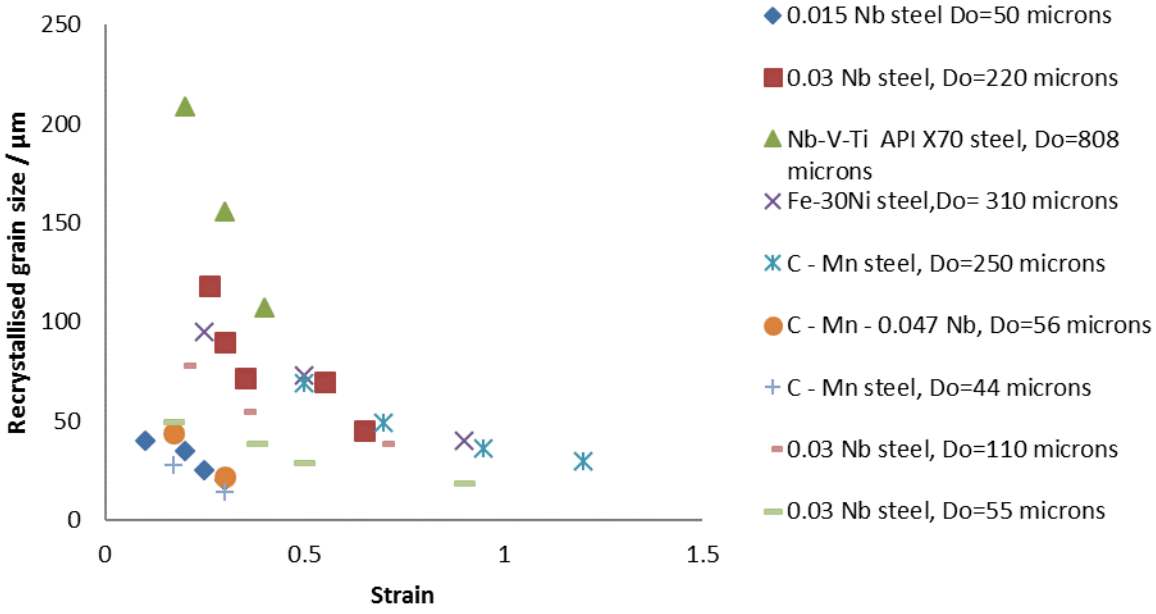

Figure 2.46: Effect of strain on the recrystallised grain size; graph plotted using literature data (Table 2.15) [6, 7, 9, 10] and data from [18].

Most studies have thus far only focused on the influence of strain on the recrystallised mode grain size and not the entire recrystallised grain size distribution. Uranga *et al.* [58] proposed a mathematical model based on mean grain size values and constant deformation parameters such as strain per pass, strain rate and temperature for predicting recrystallised and unrecrystallised grain size distributions after each deformation pass. They used a 3-dimensional initial grain size distribution as input into the computer model. They built

recrystallised grain size distribution by dividing the initial grain size distribution into 10 - 15 intervals (to enable computer simulation). In order to predict the recrystallised grain size distribution they assumed that the recrystallised grain size distribution was log-normal and that the ratio of the coarsest to mode / mean grain size was 3:1. The log-normal distributions for each interval were built using the calculated mean value (D_{mean}) using Equation 2.32 (developed based on the assumption that the theory of site saturation holds, (which means that no shape changes occur), the distribution of recrystallising grains remain stable during recrystallisation and no grain coarsening occurs). Equation 2.32 describes the evolution of the mean recrystallised grain size, (D_{mean}) with time and the recrystallised fraction (X) determined using Equation 2.22 [5] (given in Section 2.3.8) with an Avrami exponent of 1 [44]. The overall recrystallised grain size for each pass was obtained by the composition of all the resultant log-normal grain size distributions of all the intervals in the initial grain size distribution, each weighted by its corresponding initial volume fraction. The results obtained at each interpass were considered as input for the next deformation pass. The model was validated at a strain of 0.3 at a strain rate of 1 / s using a thin slab direct rolled (TSDR) 0.035 wt - % Nb steel held for 100 s. A discrepancy of 4 % RMS error was observed between the predicted and measured recrystallised fractions. The model is valid for highly alloyed as-cast materials (with large initial grain sizes of about 800 μm).

$$D_{mean} = D_{rex} X^{1/3} \qquad (2.32)$$

Where D_{rex} is the final recrystallised grain size determined using Equation 2.33. Equation 2.33 was developed by equation fitting to experimental data obtained from deforming a 0.035 Nb microalloyed steel (with initial grain sizes ranging from 129 - 806 μm) at temperatures ranging from 700 - 1180 ^{o}C to strains of 0.1 to 0.4 [183]. The exponents in Equation 2.33

indicate that there is a larger effect of initial grain size than strain on the recrystallised grain size.

$$D_{rex} = 1.4D_o^{0.56}\varepsilon^{-1} \quad (2.33)$$

For fully recrystallised samples considered in the current study, X in Equation 2.32 would be equal to 1 and as such $D_{mean} = D_{rex}$, thus Equation 2.33 would be used for predicting the recrystallised grain size. However, the accuracy of Equation 2.33 [183] in determining recrystallised grain size distributions for the Fe - 30 wt - % Ni steel will not be assessed in the current study. This is due to the fact that errors may occur if Equation 2.32 is used to predict grain size distributions for the Nb free steel, as the equation was developed and validated using a Nb-containing steel (supersaturated).

Recently, Pereda *et al.* [186] improved the model proposed by Uranga *et al.* [58] to incorporate solubility tools to predict the amount of Nb in solution after deformation. They derived equations for solubility by regression data of the solubility curves calculated using Thermo-Calc software. They have also created a MicroSim software for predicting the recrystallised grain size distribution [186]. Inputs to the MicroSim model are: chemical composition, initial austenite grain size distribution and mill input parameters, and the outputs are the recrystallised fraction, non-recrystallised fraction, mean austenite grain size and maximum austenite grain size. The accuracy of the mathematical model proposed by Uranga *et al.* [58] in predicting the recrystallised grain size distributions will not be assessed fully in this work as the data available in their articles is not sufficient to allow for prediction of the recrystallised grain size distributions. This work will only assess the limits and validity of the individual grain size class approach [4] and equations proposed by Sellars [5] in predicting a full grain size distribution using Fe - 30 wt - % Ni steel.

2.4 Literature equations and approaches for predicting the recrystallised grain size

A number of equations and approaches have been proposed for predicting the recrystallised grain size, most of which are of the form given in Equation 2.29, differing only in the values of the constants involved [4 - 6, 16, 183, 184]. The different equations proposed by different researchers for predicting the recrystallised grain size are given in Table 2.17 [5 - 6, 16, 53, 183, 184]. The parameters proposed by Sellars [5] for C - Mn steels and Nb-bearing steels are given in Table 2.15 [5, 7 - 10].

Several values for *D'* have been observed for C - Mn steels, such as 0.35 [8], 0.83 $\mu m^{0.33}$ [10] and for Nb-bearing steels 0.66 [10], 1.1 [9] and 1.86 $\mu m^{0.33}$ [7]. Sellars [5] suggested that the spread in the values may be due to differences in composition. A lower *D'* value would lead to a smaller predicted recrystallised grain size, while a higher *D'* value would lead to a larger predicted recrystallised grain size. This might be due to differences in nucleation behaviour for steels with varying compositions, despite having similar initial grain sizes, strains and exponents. For example, if a material undergoes recovery, a large recrystallised grain size may be obtained due to reduction in the driving force for recrystallisation leading to a higher fitted *D'* value. The strains studied in developing these equations ranged from 0.1 to 1.6 at deformation temperatures of 900 ^{o}C to 1150 ^{o}C. Sellars [5] showed that the relationships based on Equation 2.29 are no longer followed for strains above a certain critical value, defined by $\varepsilon^* = 0.57 \times (D_o)^{0.17} \times \varepsilon_p$, where ε_p is the peak strain above which no further grain refinement occurs if additional strain is applied due to saturation of nucleation sites [5]. The peak strain is determined from stress-strain curves and corresponds to the peak flow stress [5]. Whilst it has been suggested that the constant *D'* depends on the composition of the material, no relationship between the composition of the material and *D'* has been proposed.

Table 2.17: Equations for predicting the recrystallised mode grain size.

Parameters	[6]	[5]	[53]	[16]	[184]	[183]
Do / µm	80 - 808	12 - 250	75 - 235	40 - 150	90	129 - 806
ε	0.2, 0.3, 0.4	0.1 - 1.2	0.15, 0.2, 0.25	0.3 - 2.4	0.4	0.1 - 0.4
T_{def} / °C	1000	850 - 1150	950 - 1250	850 - 1050	1000 - 1200	700 - 1180
$\dot{\varepsilon}$ / s^{-1}	3	Not given	0.01 - 1	Not given	0.05 - 5	1
Steel composition	Nb - V - Ti API X70	C - Mn and Nb microalloyed steel	C - Mn - V - Al	Microalloyed forging	AISI 316 stainless and C - Mn - Ti	0.035 Nb
Method	Uni-axial compression using a Gleeble 3500	Data collected from several researchers	Uniaxial compression using a Gleeble 1500D	Data collected from several researchers	Torsion	Torsion
Proposed equation	$D_{rex} = 0.88*D_o^{0.59} \varepsilon^{-0.98}$	$D_{rex} = D' D_o^{0.67} \varepsilon^{-0.67}$ D' = 0.66, 1.1, 1.86 for Nb steels $T_{def} > 950$ °C $D_{rex} = D' D_o^{0.67} \varepsilon^{-1}$ D' = 0.35, 0.5, 0.83, for C - Mn steels $\varepsilon < \varepsilon c$	For C - Mn - V- Al steel $D_{rex} = 233.8*D_o^{0.129} \varepsilon^{-0.488} \dot{\varepsilon}^{-0.016} \exp(-30852/RT)$	For 38MnV56(Ti) steel $D_{rex} = 4.3+195.78 *D_o^{0.15} \varepsilon^{-0.57}$ $\exp(-350000/RT)^{-0.11}$ For C - Mn steel $D_{rex} = 5*(SV\varepsilon)^{-0.6}$ $SV = 24/\pi Do (0.491\exp(\varepsilon) + 0.155 \exp(-\varepsilon) + 0.1433 \exp(-3\varepsilon)$	For AISI 316 stainless steel $D_{rex} = 0.57 D_o (t_{0.5})^{0.042}$ For medium C - Mn - Ti steel $D_{rex} = 82.96 (t_{0.5})^{0.01}$ $t_{0.5} = 3.72*10^{-8} D_o \varepsilon^{-2.2} \dot{\varepsilon}^{-0.66} \exp[(172000/RT)]$ $\varepsilon < \varepsilon c$	$D_{rex} = 1.4 D_o^{0.56} \varepsilon^{-1}$ $\varepsilon < \varepsilon c$

Recently, Sha *et al.* [6] derived an equation for the statically recrystallised grain size from experimental data obtained from examining API - X70 steel with Nb, V and Ti with initial grain sizes ranging from 107 to 808 μm. They developed the model by equation fitting to experimental results. The parameters for the equations were determined to be; *D'*= 0.88 $\mu m^{0.41}$, x = 0.59 and y = 0.98. The parameters obtained are within the range proposed in other models for predicting the recrystallised mode grain size [5]. There are no specific trends observed for *D'* values for different materials from published data. However higher strain exponents are observed for steels without Nb than for Nb-containing steels. The initial grain size exponent does not seem to vary significantly with composition.

Kundu [4] examined the accuracy of Equation 2.29 using different *D'* values (0.66, 1.1 and 1.86 $\mu m^{0.33}$) proposed in literature [5] and found that whilst the mode grain size was well predicted, there were errors between the measured and the predicted recrystallised grain size distributions when Equation 2.29 was used to predict full grain size distributions. For example, when a *D'* value of 1.1 $\mu m^{0.33}$ was used in predicting the recrystallised grain size distribution for a 0.046 wt - % Nb steel with an initial mode grain size of 240 - 280 μm deformed to a 0.3 strain the larger recrystallised grain size classes in the distribution were over predicted with a root mean square (RMS) error of 15.22 % while the finer grain size classes were under predicted with a RMS error of 5.77 % as shown in Figure 2.47. However, the *D'* value of 1.1 $\mu m^{0.33}$ gave correct prediction of the mode grain size. Furthermore, even though correct predictions of the recrystallised mode grain size using different *D'* values with a D_o exponent of 0.67 and strain exponent of 1 are achieved when Equation 2.29 is used for steels with and without Nb, the use of 0.67 or any number below 1 as the D_o exponent value would mean that the units for *D'* vary depending on the value of the exponent used leading to dimensional inaccuracy in Equation 2.29. In order to minimise the errors observed, an

individual grain size class approach, discussed in detail elsewhere [3, 4, 22] was proposed which reduced the differences between the predicted and experimental larger grain size classes in the distribution, Figure 2.48. The larger grains were now over predicted by a RMS error of 2.37 % (compared to 15.22 %) and the finer grain sizes were still under predicted, by a RMS error of 5.38 % (compared to 5.77 %). Kundu [4] showed that this approach could be used to predict the full grain size distribution for steels with an initial mode grain size of 240 - 280 µm and Nb content of 0.046 wt - % hot deformed to a strain of 0.3. However, the proposed approach did not consider different strain levels (only a strain of 0.3 was investigated) or a range of initial grain sizes. Errors may arise when the individual grain size class approach is used to predict the recrystallised grain size distribution for different ranges of grain size and strain other than those mentioned above since finer initial grain sizes will require a higher strain in order to recrystallise to a smaller size due to GNDs. In addition, errors will arise as the approach does not take into account the effect of high strain values on nucleation site density.

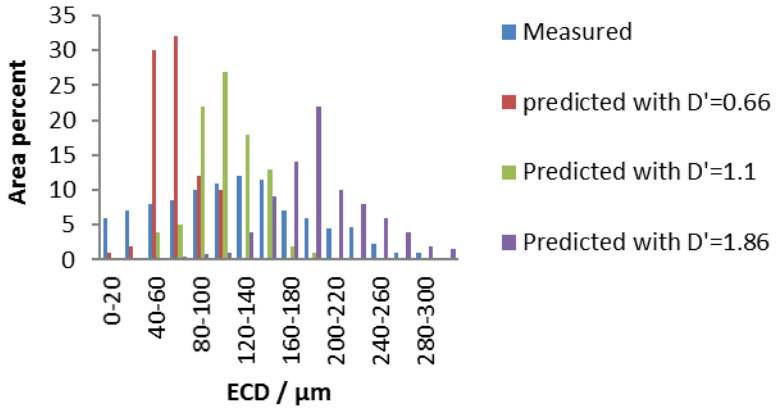

Figure 2.47: Prediction of the recrystallised grain size distribution for a 0.046 wt - % Nb steel with an initial mode grain size of 240 - 280 µm deformed to a 0.3 strain using different *D'* values from the literature [4].

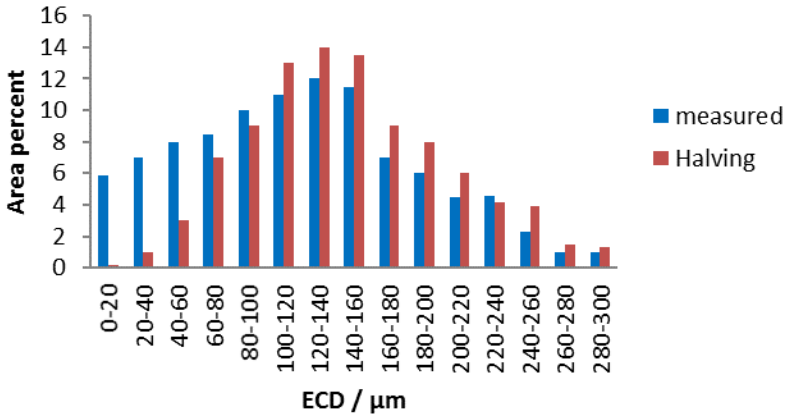

Figure 2.48: Prediction of the recrystallised grain size distribution for a 0.046 wt - % Nb steel with an initial mode grain size of 240 - 280 µm deformed to a 0.3 strain using the individual grain size class approach [4].

Toughness has a greater dependency on the large grains in the grain size distribution than the mode / average grain sizes, which mostly determine the strength of steel. Wu *et al.* [187] investigated the effect of duplex grain distributions (mixed coarse and fine grain sizes) on mechanical properties such as toughness and strength by carrying out micro hardness tests using two commercial steels. They measured hardness values for each grain size region and reported that the fine grain areas had significantly higher micro hardness values (high strength) than the coarse grain areas and they also carried out tensile and blunt-notch slow bend tests in order to measure the local fracture stress (toughness) and found that there was local variation in the fracture stress which was attributed to the coarse grain size distribution in the steel. It is therefore important to predict the entire grain size distribution in order to achieve uniformity in mechanical properties. However, not many models have been put forward for predicting the recrystallised grain size distribution for a wide range of deformation conditions and compositions. The current work will attempt to develop an approach that can predict recrystallised grain size distributions.

2.5 Comparison of recrystallisation of Fe - Ni model steel alloys with low carbon steels, C - Mn and HSLA steel

While many researchers [16, 44, 45, 58, 141, 142] have been able to study the microstructural evolution during hot deformation, the research has been hampered due to phase transformations taking place in low carbon steels at certain temperatures, and as such, direct observation of the microstructure is often difficult, and therefore investigation of recrystallisation kinetics is a challenge. This has led to use of model steels such as Fe - 30 wt - % Ni [54, 65, 168, 188] and Ni - 30 wt - % Fe steels [59] which are austenitic at room temperature as well as at elevated temperatures. Palmiere *et al.* [54] carried out double deformation tests (net strain of 0.5 to 0.9) using Fe - 30 wt - % Ni steel with an initial grain size of 370 μm to model the deformation of austenite microstructure during hot deformation of C - Mn steels and concluded that the flow curve characteristics observed for Fe - 30 wt - % Ni steel were similar (at 950 ^{o}C, 0.9 strain and strain rate of 10 / s flow curves for Fe - 30 wt - % Ni and C - Mn steel, the curves show that the samples are work hardened) to that of a conventional austenite stainless steel even though the flow stress values were not the same. Later, Almaguer *et al.* [168] made a comparison of static recrystallisation kinetics for Fe - 30 wt - % Ni alloy with that of a plain carbon steel. They investigated the progress of recrystallisation in the Fe - 30 wt - % Ni steel using stress relaxation and metallography examination at a deformation temperature of 950 ^{o}C over a range of strains (0.05 - 1.5). It was concluded that Fe - 30 wt - % Ni alloy exhibits similar flow characteristics to the conventional C - Mn steel. It was suggested that the differences in behaviour between the model steel and commercial steels were due to the difference in methods used for measuring the degree of recrystallisation [168]. Fe - 30 wt - % Ni steel has therefore been used in the current work because it has been shown to be a good

material to simulate recrystallisation behaviour during the hot deformation of low carbon steels.

2.6 Summary

The chapter discussed the key metallurgical processes during and after deformation, such as recovery, recrystallisation and grain growth. Recrystallisation kinetics and methods used to quantify recrystallisation are discussed. Recrystallisation kinetics are influenced by deformation parameters such as strain, deformation temperature, strain rate and initial grain size. The variations in the constants used in several equations may be as a result of using different quantification methods (difficulties in separating recovery and recrystallisation). Equations used to predict the mode grain size are discussed, as well as approaches used to model the recrystallised grain size distribution. The equations from the literature such as those proposed by Sellars, do predict the recrystallised mode grain size well however not many approaches and equations have been proposed for modelling the recrystallised grain size distributions.

2.7 Objectives of the present work

The aim of this work is to investigate the effects of prior austenite grain size and strain on recrystallisation of a model Nb - free (Fe - 30 wt - % Ni) steel and a Nb-containing model steel. The specific aims are:

1. To investigate the effect of strain and initial grain size on the recrystallised grain size distribution using data obtained experimentally.
2. To examine the validity of the individual grain size class approach in combination with the Dutta-Sellars equations for a range of strains and initial grain sizes.
3. To model the grain size distribution based on equations using the constant *D*'.

4. To predict and verify the full recrystallised grain size distribution after deformation for a range of steel grades, initial grain sizes and applied strain.

CHAPTER – 3

Materials and Experimental Procedures

This chapter describes the different experimental procedures undertaken and materials used in the current work. Experiments were carried out to enhance understanding of the influence of process parameters (such as strain and grain size) on recrystallisation and as such improve modelling (prediction) capabilities of grain size distributions after deformation.

3.1 Materials

Two laboratory cast and hot rolled (70 % reduction) Fe - 30 wt - % Ni steels (one with, 0.044 wt - %, and one without Nb), and one commercial high strength strip steel were supplied by Tata Steel Europe for this study. Investigations were carried out on the Fe - 30 wt - % Ni steels because it can be used to represent low alloy steels as it retains the austenitic microstructure upon cooling or heating which makes direct observation of the grain size distributions after deformation easier, whereas low alloy steels undergo a transformation from austenite to ferrite on cooling from hot deformation temperatures [54, 65, 168, 188] as discussed in Section 2.5. Data from other recrystallisation studies using a Nb microalloyed commercial steel (HSLA steel) deformed at 1075 ^{o}C in a Gleeble 3500 thermo-mechanical simulator [3, 4] and a high alloy (9Cr) forging steel (deformed at 1200 ^{o}C in a Gleeble 3500 thermo-mechanical simulator) [189] were also used. The chemical compositions of the different steel grades studied are given in Table 3.1.

Table 3.1: Chemical compositions for the different steel grades, all wt - %.

Material	C	Si	Mn	P	S	Cr	Mo	Ni	Cu	Sn	Al
Fe - 30Ni	**0.061**	**0.24**	**0.52**	**<.001**	**0.009**	**0.01**	**<.005**	**29.95**	**<.005**	**<.001**	**0.002**
Fe - 30Ni - Nb	**0.061**	**0.24**	**0.53**	**0.001**	**0.01**	**0.01**	**<.005**	**30.01**	**<.005**	**<.0.001**	**0.006**
Nb microalloyed HSLA steel [3, 4]	**0.1**	**0.31**	**1.42**	**0.017**	**0.005**	**-**	**-**	**0.32**	**-**	**-**	**0.046**
9Cr forging steel [189]	**0.12 - 0.15**	**0.15**	**0.3 - 0.4**	**-**	**-**	**9-9.60**	**1.4 - 1.6**	**-**	**-**	**-**	**-**
Strip steel	**0.066**	**0.107**	**1.56**	**0.01**	**0.003**	**0.499**	**0.239**	**0.024**	**0.012**	**0.001**	**0.075**

Material	Co	N	Nb	Pb	Ti	V	W	B	Fe
Fe - 30Ni	**0.021**	**<.001**	**-**	**0.05**	**0.001**	**<.001**	**<.001**	**-**	**Balance**
Fe - 30Ni - Nb	**0.002**	**<.001**	**0.044**	**0.05**	**0.002**	**<.001**	**0.002**	**-**	**Balance**
Nb micro alloyed HSLA steel [3, 4]	**-**	**0.008**	**0.045**	**-**	**0.002**	**0.052**	**-**	**-**	**Balance**
9Cr forging steel [189]	**1.15 - 1.35**	**0.01 - 0.04**	**0.03 - 0.07**	**-**	**-**	**0.15 - 0.25**	**-**	**0.005 - 0.010**	**Balance**
Strip steel	**-**	**0.005**	**0.04**	**-**	**0.002**	**0.051**	**-**	**0.002**	**Balance**

3.2 Thermodynamic Predictions

In order to determine reheating temperatures for the Fe - 30Ni - Nb steel, Thermo-Calc software (Version 4.0 TC - Fe7 database) from the Royal Institute of Technology, Stockholm, Sweden was used in Word mode to determine the dissolution temperatures for any microalloying element carbo-nitride precipitates (i.e. Nb (C, N)) that form. The Thermo-Calc software was also used to predict the melting temperature of Fe - 30 wt - % Ni steel in order to determine appropriate temperatures, to avoid melting, for heat treatment tests used for generating different initial grain sizes.

3.3 Heat Treatments

In order to establish the procedure for predicting the grain size distribution after recrystallisation a model alloy (Fe - 30 wt - % Ni) was examined. 10 mm diameter by 15 mm height cylindrical samples were electro-discharge machined (EDM) from the 25 mm thick plate perpendicular to the rolling direction. In order to monitor how quickly the sample heated up to the test temperature, and hence ensure the samples were soaked at the desired annealing temperature for the specified time, trial heat treatments were carried out using a Fe - 30 wt - % Ni sample with a 2 mm diameter by 7.5 mm hole drilled in the centre with thermocouples inserted to determine the time to reach the desired temperature. Several trial heat treatments were carried out at temperatures ranging from 1000 ^{o}C to 1300 ^{o}C using different soaking times (5 minutes to 2 hours) in order to determine appropriate temperatures and soaking times to give different uniform starting grain size distributions. The heat treatments used are summarised in Table 3.2; from these trials heat treatments of 1200 °C for 15 minutes and 1300 °C for 5 minutes were selected to generate different initial coarse uniform grain size distributions. In order to generate a finer uniform initial grain size, some specimens were heat treated at 1200 °C for 15 minutes, deformed

to a 0.3 strain at a deformation rate of 2 mm / minute and then furnace recrystallised at 850 °C for 16 minutes. The time required to achieve complete recrystallisation was determined using predictions (Dutta-Sellars model), described in Section 2.3.8.

Table 3.2: Heat treatment schedules for generating different initial grain sizes for the Fe - 30 wt - % Ni steel and the type of distributions obtained. and the type of distributions obtained

Temperature / °C	Soaking time / minute	Type of distribution
1000	30	Uniform distribution
1050	30	Uniform distribution
1100	30	Uniform distribution
1150	15	Uniform distribution
1200	15	Uniform distribution*
	30	Non-uniform distribution
	120	Non-uniform distribution
1250	20	Non-uniform distribution
	60	Non-uniform distribution
1300	5	uniform distribution*
	10	Non-uniform distribution
	15	Non-uniform distribution

**Selected heat treatments*

In order to verify the procedure for predicting the recrystallised grain size distribution, the model steel containing Nb (Fe - 30 wt - % Ni - 0.044 wt - % Nb), and a high strength strip steel were heat treated to generate different starting grain sizes. For the Fe - 30 wt - % Ni - 0.044 wt - % Nb steel 10 mm diameter by 15 mm height cylindrical samples were EDM prepared from a 25 mm thick plate perpendicular to the rolling direction. Specimens were annealed in a furnace (1150 °C for 4 hours) in order to generate an initial uniform coarse grain size distribution. Heat treatment temperatures and time for the Fe - 30 wt - % Ni - 0.044 wt - % Nb steel are those established in other projects [190]. For generation of a

finer initial grain size, some specimens were heat treated at 1150 °C for 4 hours, deformed to a 0.15 strain at a deformation rate of 2 mm / minute and then furnace recrystallised at 950 °C for 34 minutes in order to achieve complete recrystallisation. For the strip steel the cylindrical samples were EDM machined from the 12 mm thick plate perpendicular to the rolling direction. Specimens were annealed in a furnace (1200 °C for 5 minutes) in order to generate an initial coarse uniform grain size distribution. The heat treatment temperature and time to achieve the desired grain structure for the high strength strip steel are those established in another project [191]. In order to reveal prior austenite grain boundaries in the strip steel after deformation and quenching the samples were tempered for 6 hours at 550 ^{o}C before etching, as this was found to more clearly identify the boundaries than etching the as-quenched sample.

3.4 Cold and Hot Deformation

For the Fe - 30 wt - % Ni steels (one with 0.044 wt - % Nb and the other without) room temperature deformation (uniaxial compression) tests were carried out using a Zwick Z100 Universal Mechanical Tester at a deformation rate of 2 mm / minute. For the Fe - 30 wt - % Ni steel room temperature strains of 0.08, 0.12, 0.17, 0.22 and 0.30 were applied, whereas, for the Fe - 30 wt - % Ni - 0.044 wt - % Nb steel only strains of 0.08, 0.17 and 0.30 were applied. The tests were repeated two times for the same set of conditions. High temperature deformation tests were carried out on a Gleeble 3500 thermo-mechanical simulator at a deformation rate of 1 mm / s, at 850 - 950 °C for the Fe - 30 wt - % Ni steels and 1200 °C for the strip steel, for a range of hot strains (0.15, 0.3 and 0.45). It must be noted here that in the initial stages of this project a 0.044 wt - % Nb commercial steel was hot deformed using the Gleeble 3500 thermo-mechanical simulator (results from these tests will not be reported in the current work). Investigations on the 0.044 wt - % Nb

commercial steel could not be continued because the Gleeble was unavailable for a significant time period and as such a different material (Fe - 30 wt - % Ni steel) was examined using room temperature deformation. The Fe - 30 wt - % Ni steels retain an austenitic structure at low temperatures, such that room temperature deformation of the austenitic state, mimicking what is seen at high deformation temperatures is possible as discussed in Section 2.5. This allowed for a greater number of trials during the research project as the Gleeble 3500 was unavailable for a substantial period. In addition, room temperature deformation using the Zwick gave higher control of the strains introduced and a higher throughput as compared to using the Gleeble. The lower deformation rate used at room temperature is due to limitations in the Zwick machine operation; however, this is not expected to affect the results as recovery and creep, dominant mechanisms at slow strain rates and high temperatures [32], are not expected at room temperature (RT) in this material. Deformation conditions for all steels used in this work are given in Table 3.3.

Table 3.3: Deformation conditions for steels studied.

Material	**Deformation temp. / ^{o}C**	**Strain**	**Deformation mode**
Fe - 30Ni	Room temp.	0.15, 0.22, 0.3, 0.45, 0.7* (applied to all mode grain sizes)	Uniaxial compression
Fe - 30Ni - Nb	Room temp.	0.15, 0.3, 0.7*	Uniaxial compression
Nb microalloyed HSLA steel [3, 4]	1075	0.3	Plane strain
9Cr forging steel [189]	1200	0.15, 0.3, 0.45 0.3	Uniaxial compression
Strip steel	1200	0.15, 0.3, 0.45	Uniaxial compression

**Equivalent hot strains at 850 ^{o}C*

Flow stress is governed by a number of dislocations gliding through the material at any given time. Studies have shown that there is a difference in flow stresses when a sample is deformed cold or hot [32, 192, 193]. When a sample is deformed hot a much lower flow stress is realised due to the fact that at high temperatures dislocations become more mobile (they glide through the material). As strain is increased more dislocations move through the material leading to annihilation of some dislocations thereby reducing the number of mobile dislocations and as such the material is softened (lowering the flow stress) [32, 192, 193]. However, when a sample is cold worked the dislocations pile up and develop into networks, leading to work hardening of the sample, and hence a much higher flow stress is realised. Therefore, if two samples with the same initial grain size are subjected to the same strain, but at different deformation temperatures, the sample deformed at a lower temperature would have a higher stored energy compared to the one deformed at a higher temperature, making the two tests non-comparable in terms of recrystallisation [193]. Hence, in order to determine what strain would give the same stored energy when a sample is deformed cold or hot, stored energies can be equated (area under the flow stress curve excluding elastic work) as shown in Figure 3.1; it can be seen from Figure 3.1 that a cold strain of 0.17 would be equivalent to a hot (850 °C) strain of 0.3. The equivalent hot (850 °C) deformation strains to the cold strain values (0.08, 0.12, 0.17, 0.22, 0.3) used were determined to be 0.15, 0.22, 0.30, 0.45 and 0.70 respectively using an equivalence of stored energy from the flow stress curves at room temperature and 850 °C as shown in Figure 3.1. All strains are given in the results and discussion chapters as the equivalent hot (850 °C) strains (unless otherwise stated) to allow comparisons to be made with the literature results from hot deformation.

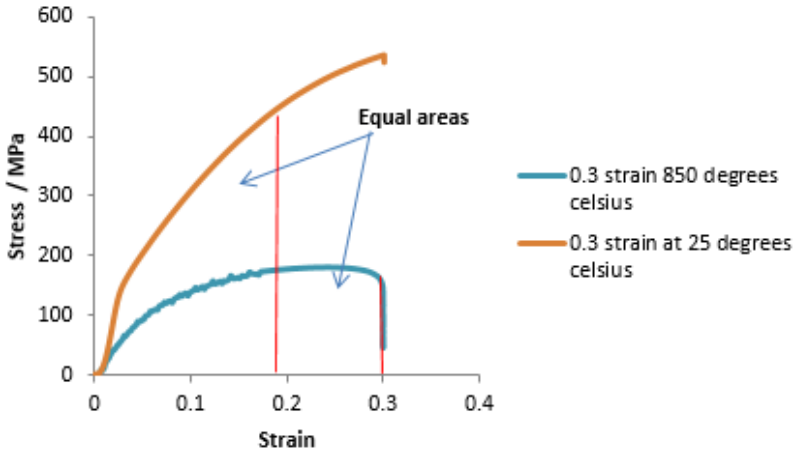

Figure 3.1: Stress-strain curve for the Fe - 30 wt - % Ni steel deformed to a strain of 0.3 at 850 °C and at room temperature.

In this work, the room temperature deformation gave a more uniform strain across the specimen than when it was hot deformed using uniaxial compression in a Gleeble thermo-mechanical simulator (resulting from friction between the anvils and the sample). A more uniform strain across the sample can be achieved by minimising friction between the specimen ends and the anvils through use of a very low friction material (lubricants) such as PTFE (polytetrafluoroethylene) tape and graphite foil on the faces of the platens, however, lubrication is a challenge at elevated temperatures. In this work, two pieces of PTFE tape and oil were used as lubricates. Non-uniformity of strain can also be minimised by ensuring the sample has a good aspect (height to diameter) ratio [32]. Karhausen *et al.* [194] suggested that aspect ratios of 1.2 - 2 would lead to uniformity of strain and as such minimise barrelling. Non-uniform strain occurring during compression with friction results in barrelling and hence formation of three zones of deformation with higher local strains in the central region of the hot deformed samples, Figure 3.2. The amount of barrelling in the samples after room temperature and hot deformation was measured using vernier callipers (to measure central diameters of the deformed samples and compare them to the predicted

diameters). Prediction of diameters after deformation was carried out by assuming constant volumes before and after deformation.

(a)

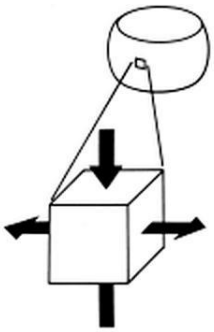

(b)

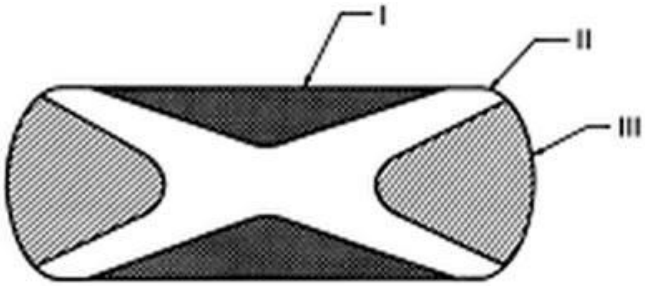

(c)

Figure 3.2: (a) Compression test samples: (left) undeformed sample; (centre) sample compressed with friction; (right) sample compressed without friction [32] (b) A schematic illustration of circumferential stress created by the barrelling effect and applied axial stress (c) Distribution of strain along the longitudinal section; I: Anvil-sample contacting region remains stationary with lowest local strain; II: the Central region has the highest strain; III: Outer surface region has moderate strain [32, 193].

3.5 Recrystallisation Furnace Heat Treatments

Table 3.4 shows all the furnace recrystallisation soaking times used in order to achieve complete static recrystallisation.

Table 3.4: Recrystallisation heat treatment schedule to achieve full recrystallisation for the Fe - 30Ni steel.

Initial grain size / μm	Strain	Holding time / s	Predicted R_f in seconds using Dutta - Sellars equations
50 - 60	0.15	720	19
	0.22	600	57
	0.3	480	17
	0.45	300	3
	0.7	240	0.6
110 - 120	0.15	480	76
	0.22	1080	227
	0.3	960	63
	0.45	600	13
	0.7	240	2.3
160 - 180	0.15	1800	171
	0.22	420	37
	0.3	1680	148
	0.45	600	30
	0.7	300	5

Recrystallisation-precipitation-temperature-time (RPTT) curves, based on the original Dutta-Sellars model [170], were used to predict the recrystallisation finish times by considering the entire initial grain size distribution instead of just the mode / average grain size, as described in [3, 4, 170] and discussed in Section 2.3.8. Cold deformed samples were heat treated (air furnace) to times greater than the predicted recrystallisation finishing times at 850 °C or 950 °C to ensure complete recrystallisation. At lower temperatures recrystallisation kinetics are slower than at higher temperatures [5, 170] and so for

convenience lower temperatures (less than 1000 °C) were chosen that gave reasonable recrystallisation finish times (above and including 2 minutes), for example furnace recrystallisation was carried out at 850 - 950 °C where the predicted recrystallisation times (for samples with an initial mode grain size of 160 - 180 µm) are in the range 300 - 1800 seconds for samples deformed to a strain of 0.7 and 0.15 respectively as compared to if recrystallisation furnace heat treatments were carried out at 1050 °C were the predicted recrystallisation finish times would be in the range 0.28 - 48 seconds respectively. Figure 3.3 shows the recrystallisation-precipitation-temperature-time curves for the specimen with an initial mode grain size of 160 - 180 µm deformed to a strain of 0.15.

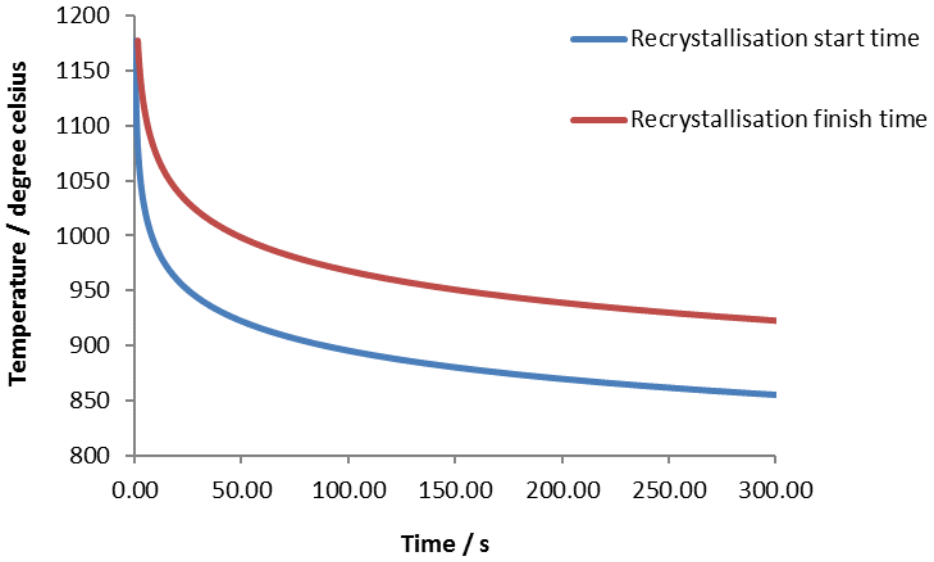

Figure 3.3: Predicted Dutta-Sellars recrystallisation-precipitation-temperature-time curves for Fe - 30 wt - % Ni (Nb-free steel) (ε: 0.15; D_o: 160 - 180 µm) showing recrystallisation start (R_s) and finish (R_f) times [170].

3.6 Microstructural Characterisation

3.6.1 Sample Preparation

For optical metallography, specimens were cut in the mid-section using a Struers Accutom 5 precision cutting machine, then were ground and polished to a 1 micron finish. The polished Fe - 30 wt - % Ni with and without Nb steels were etched using Kalling's reagent and the tempered high strength strip steel was etched using 2 % Nital.

3.6.2 Image Analysis

The equivalent circle diameter (ECD) values of 700 to 1000 austenite grains were measured for the laboratory cast and rolled, heat treated and furnace recrystallised heat treated samples using a Zeiss AKIOSKOP 2 Mat Met microscope fitted with a Sony CCD camera; Excel and ImageJ software were used in order to generate grain size distributions. The advantage of using ImageJ to measure austenite grain sizes is that the grain sizes are directly measured (from the central regions of the etched sample, avoiding the edges) and therefore more accurate assessment of the recrystallised grain size distribution (and development of appropriate grain size prediction equations) can be made [4]. The other advantage of using the ImageJ software to measure austenite grain sizes is that it is easy to use. No stereological grain size correction was done due to the fact that grains are equiaxed, since the current work ensured that complete recrystallisation was achieved. The equations developed by Sellars [5] for predicting the recrystallised grain size after deformation were developed for 2-dimensional grain sizes and therefore, consideration of 2-dimensional grain size is appropriate for use in modifying the existing equations to account for grain size distributions.

Quantification of errors between the measured and predicted grain size distributions has often been achieved by applying the RMS (root mean square) error approach [3, 4].

Computation of the RMS error value involves taking squares of the difference between the measured and the predicted area percent of a given grain size class, and thereafter adding them up and dividing the summed value by the total number of grain size classes (which is the number of bins for the widest grain size distribution) in a given distribution and lastly taking square roots. RMS error values are area percentage values. The area percent values are determined by multiplying the area of each grain size class by the number of grains measured for that particular grain size class, which gives the total area (in that class), thereafter adding up all the total areas calculated for all the classes in the distribution and dividing the total area for each given grain size class by the aggregated value. The accuracy of the RMS error approach in quantifying errors was examined in the current work. It was found that the approach is dependent on the number of bins being considered (it is scale dependent) such that when a different grain size bin is used a different RMS error is computed, for example, when bins of 10s or 20s are used, for the same measured and predicted grain size distribution with equal number of grain size bins (example distributions are given in Figure 3.4) different RMS values are computed as shown in Table 3.5. It can be seen from Table 3.5 that the value for the RMS error differs by 40 % if different bin size classes are used (e.g. bin class sizes of 10s or 20s). The discrepancies in the value of RMS error increases when non-matching distributions are considered (example distributions are given in Figure 3.5). The normalised root mean square (NRMS) error approach has therefore been considered for use in quantifying errors instead of RMS (which was used by Kundu [4]).

The NRMS error approach involves dividing the RMS (root mean square) error value by the mean of the total measured or predicted area percent for a particular distribution. The mean value is determined by dividing the total area percent (100 %) for either predicted or

measured grain size distribution by the number of bins for the widest distribution (that is whichever the widest distribution is whether it is the predicted or measured grain size distribution). The reasons for using the number of bins for the widest grain size in the computation of errors (using the NRMS error approach) are discussed in detail in appendix A.

Table 3.5: RMS and NRMS error values for different bin sizes for matching distributions (in terms of number of grain size classes in a distribution). Bin size is in microns.

RMS		NRMS	
Bins of 10	Bins of 20	Bins of 10	Bins of 20
10.3	18	0.92	0.90

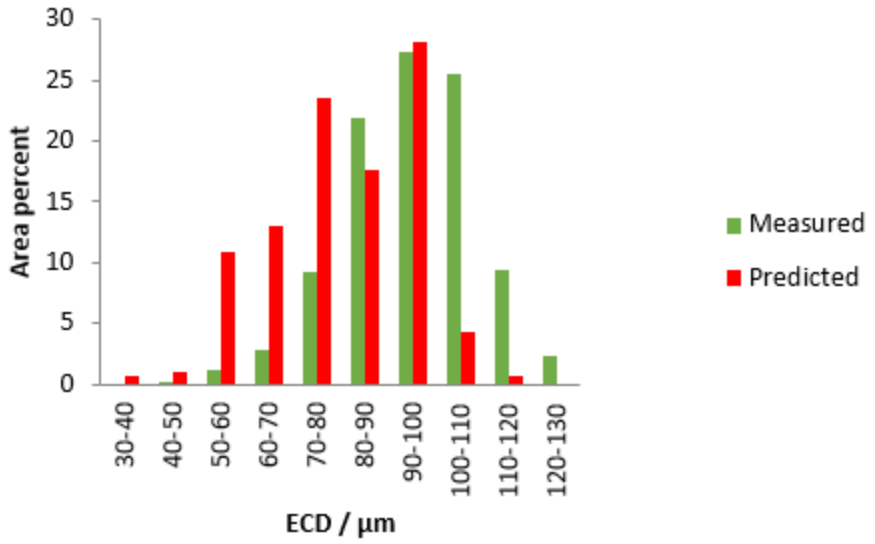

Figure 3.4: Matching distributions in terms of number of grain size bins for the predicted and measured distributions.

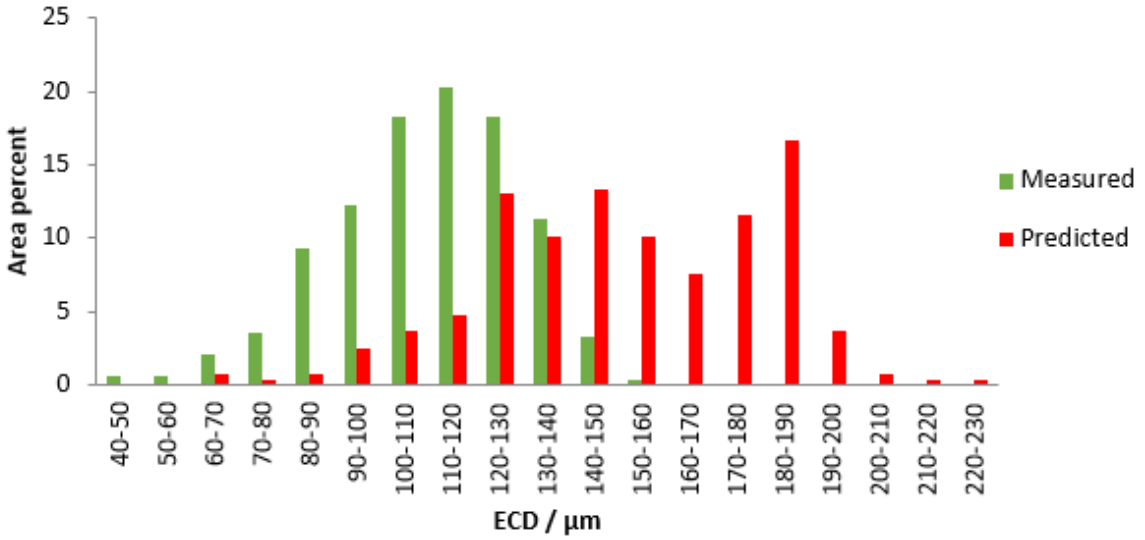

Figure 3.5: Non-matching distributions in terms of number of grain size bins for the predicted and measured distribution.

3.7 Hardness Testing

The specimens were machined as described in Section 3.6.1, mounted in Bakelite and ground using 1200 grade SiC paper. Hardness measurements using a 5030 SKV Vickers hardness testing machine, with a load of 20 kg were carried out to ensure full softening by recrystallisation had occurred for all furnace recrystallisation heat treatments. Ten hardness values were measured across the specimen in each condition.

3.8 Differential Scanning Calorimetry (DSC)

In order to measure the stored energy after deformation differential scanning calorimetry (DSC), using a Netzsch DSC 404, was carried out using cold deformed Fe - 30 wt - % Ni steel with three different initial grain sizes (50 - 60 µm, 110 - 120 µm and 160 - 180 µm). This was done in order to study the influence of initial grain size distributions on the stored energy of deformation.

3 mm diameter by 1 mm thickness machined (using EDM) specimens from samples deformed to 0.7 equivalent hot strain (0.3 cold strain) were used with a mass of about 50

mg each. A specimen machined from a sample annealed at 1300 °C for 5 minutes (160 - 180 µm mode grain size) was also investigated to determine whether any stored energy was introduced from sample preparation; this could then be taken into account to determine the net stored energy in the cold deformed samples. The specimen was placed in a standard alumina DSC crucible adjacent to the empty reference crucible. Specimens were heated up to 1000 °C at a heating rate of 10 °C / minute. Two runs were performed on every sample. The tests were repeated three times for the same set of conditions. At the end of the test run 1 and run 2, curves (plot of heat flow versus temperature) were subtracted and the curve obtained was integrated in order to determine the area under the curve (stored energy in J / g) using Proteus DSC analysis software, a schematic of DSC curves for run 1, run 2 and the subtracted curve for a high Mg aluminium alloy (AA5083) is shown in Figure 3.6 [195]. The actual stored energy was determined by subtracting the net energy release for the annealed sample (stored energy due to sample preparation) from the net energy release obtained for a given deformed (0.7 equivalent hot strain) sample.

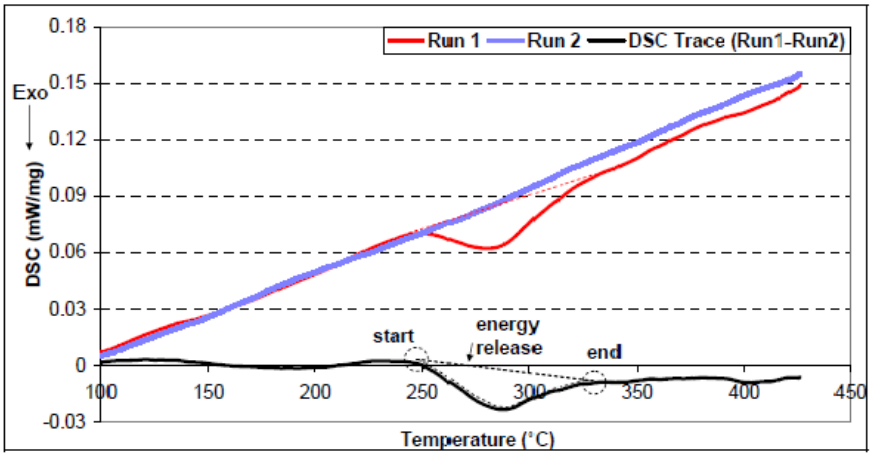

Figure 3.6: Schematic of DSC traces for a high Mg aluminium alloy; run 1, run 2 and the DSC trace for the difference between run 1 and run 2 which is used to determine the amount of energy stored during deformation [195].

To verify and ensure 100 % recrystallisation had been reached, samples (with initial mode grain size of 160 - 180 μm) were deformed to 0.7 equivalent hot strain and then were heated in the DSC machine between 50 ^{o}C to 400 ^{o}C and 850 ^{o}C at a heating rate of 10 ^{o}C / minute and thereafter micro hardness tests were carried out on polished samples using an automated micro hardness machine (Struers DuraScan) controlled by ECOS workflow software. Using the software, the required applied load (300 g) and objective lens were selected before the number of indents or the pattern of indents was chosen. Indents were at least 3 indent spacings away from the next nearest indent for the measurement to remain valid. The hardness values obtained for the deformed samples were compared to the hardness values for the annealed (1300 ^{o}C for 5 minutes) sample.

CHAPTER – 4

Effect of strain and initial grain size distributions

This chapter describes the grain size distributions that develop after heat treatments and deformation, and the influence that strain and initial grain size have on the recrystallised grain size, in the Fe - 30Ni steel. The chapter also discusses the accuracy of literature equations / approaches in predicting recrystallised grain size distributions.

4.1 Heat treatment

4.1.1 As-received grain structure

A representative micrograph and grain size distribution for a sample of as received (laboratory cast and hot rolled to 70 % reduction) Fe - 30 wt - % Ni steel is shown in Figure 4.1 and 4.2 respectively. The material has an initial mode grain size of 50 - 60 μm (as-received condition) with a maximum grain size of 130 μm.

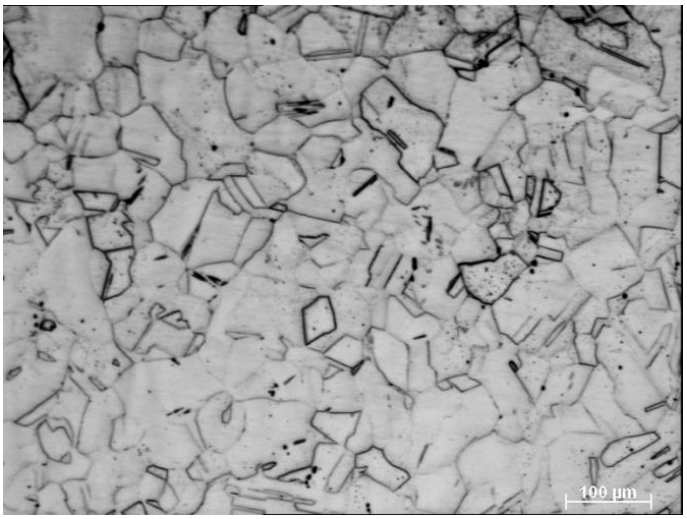

Figure 4.1: Representative micrograph for a laboratory cast and rolled (70 % reduction) Fe - 30 wt - % Ni sample.

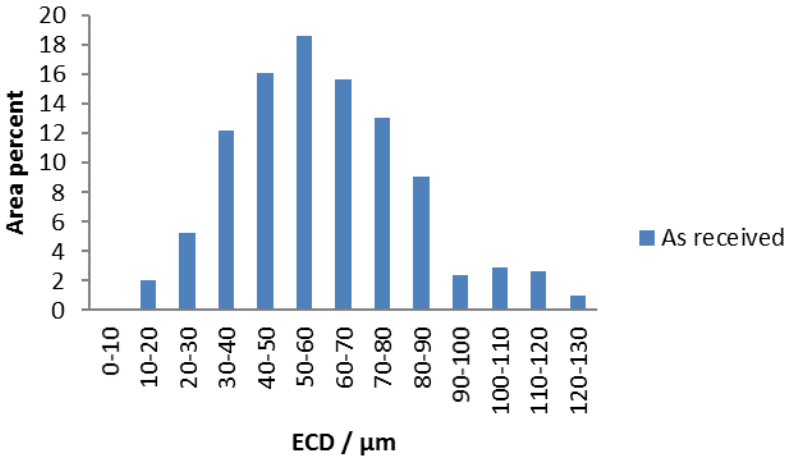

Figure 4.2: Grain size distribution for the laboratory cast and rolled (70 % reduction) Fe - 30 wt - % Ni sample.

4.1.2 Thermodynamic Predictions

In order to determine the maximum reheating temperature for the Fe - 30 wt - % Ni steel, Thermo-Calc software (Version 4.0 TC - Fe7 database) was used in Word mode to predict the melting temperature range. The melting range temperature for the alloy was predicted to be between 1380 ^{o}C (solidus) to 1460 ^{o}C (liquidus). A small amount (volume fraction of < 1 x 10^{-5}) of TiN is predicted to be present up to temperatures of 1140 ^{o}C, therefore TiN may provide some grain boundary pinning up to 1140 ^{o}C. However, given the predicted volume fraction, TiN particles with an assumed (based on literature reports for TiN forming after solidification [196]) size (side length) of about 50 - 100 nm would have number densities of about 318 / mm^2 to 1274 / mm^2. The pinning force is estimated to be about $3.18*10^{-11}$ N / m^2 to $2.5*10^{-10}$ N / m^2, calculated using the Zener equation (Equation 2.5), with an interfacial energy of 0.5 J / m^2 [197]. The limiting grain size (diameter) for these pinning forces is calculated to be approximately 6 mm to 14 mm using Equation 2.6 [26], suggesting that grain growth is unlikely to be inhibited. V (C, N) precipitates are not predicted (by the Thermo-Calc software) to be present in the Fe - 30 wt - % Ni steel, which may be due to the fact that the

steel only contains a small amount of vanadium (> 0.01 wt - %). V (C, N) precipitates if present may retard grain growth [4]. Thermodynamic predictions indicate that the steel will be austenitic from room temperature up to the liquidus temperature.

4.1.3 Generating different initial grain sizes

Table 4.1 gives the grain sizes developed (mode and maximum grain size in a given distribution); soaking times are given in Table 3.2 (Section 3.3, Chapter 3). Typical micrographs and reheated grain size distributions for unimodal and bimodal grain sizes are shown in Figures 4.3 and 4.4 respectively.

Table 4.1: Generated initial grain sizes for Fe - 30 wt - % Ni steel after different heat treatments.

Temperature / °C	Mode grain size / µm	Maximum grain size / µm
1000	40 - 50	130 - 140
1050	50 - 60	130 - 140
1100	60 - 70	240 - 260
1150	80 - 90	230 - 240
1200	110 - 120*	230 - 240
	110 -120	300 - 320
	120 - 140	440 - 460
1250	120 - 140	300 - 320
	160 - 180	680 - 700
1300	160 - 180*	460 - 480
	200 - 220	540 - 560
	260 - 280	580 - 600

**Selected heat treatments*

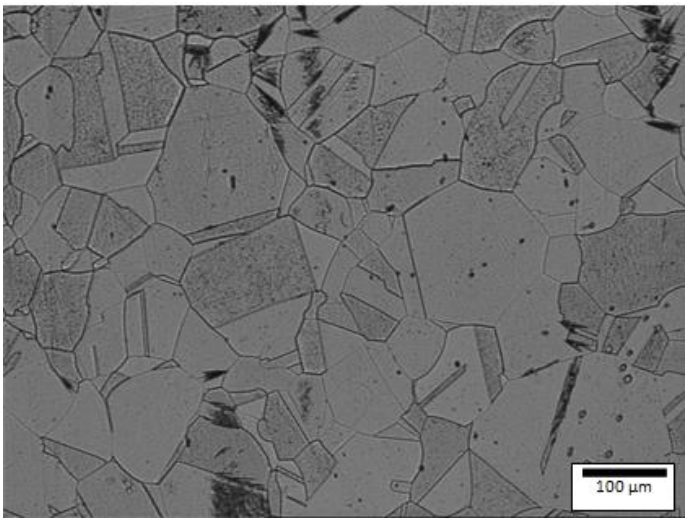

(a)

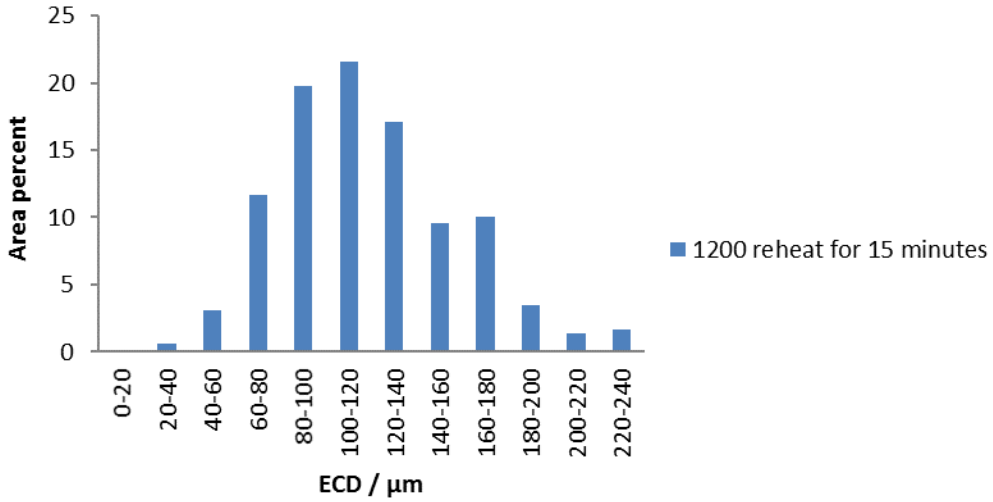

(b)

Figure 4.3: Heat treated Fe - 30 wt - % Ni sample to 1200 °C for 15 minutes (a) Micrograph (b) Unimodal grain size distribution.

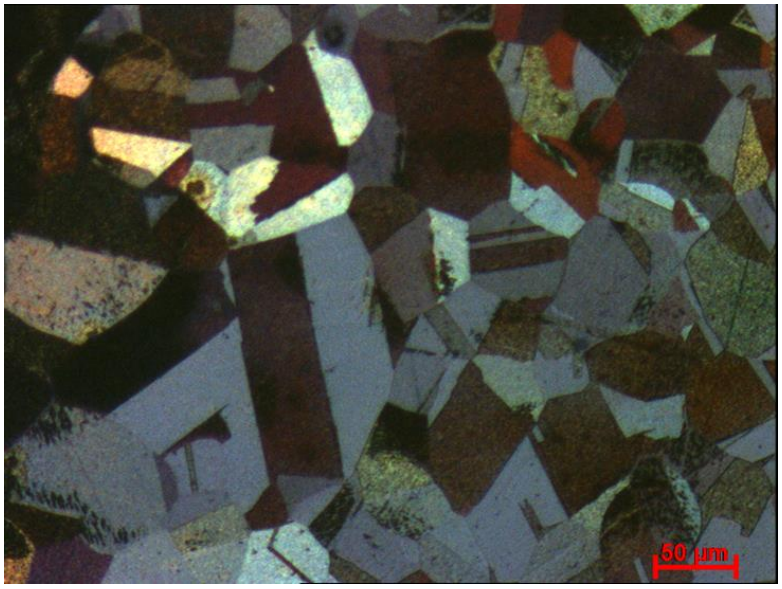

(a)

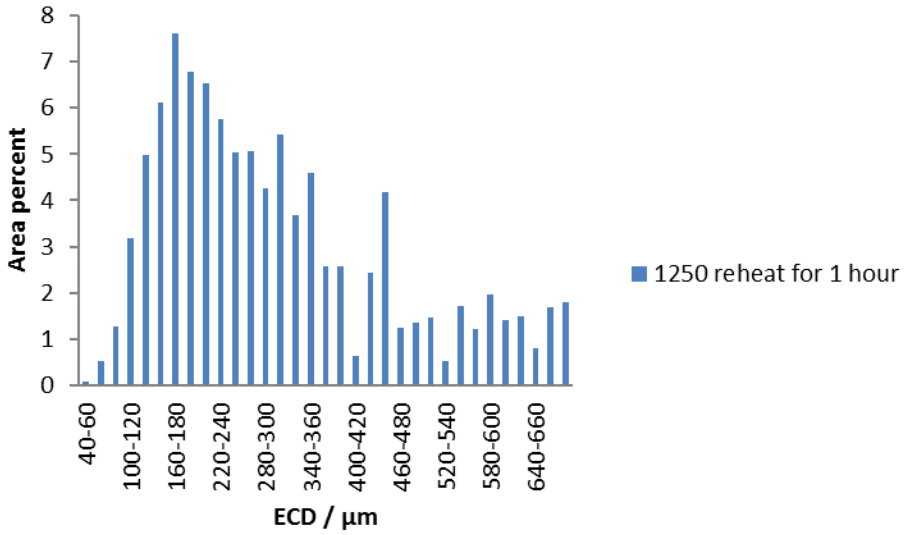

(b)

Figure 4.4: (a) Heat treated Fe - 30 wt - % Ni sample to 1250 °C for an hour (a) Micrograph (b) Bimodal grain size distribution.

Figures 4.5 and 4.6 illustrate the fact that grain growth is influenced by both the reheat temperature and holding time; at higher reheating temperatures and longer holding times grain coarsening is achieved. For heat treatments carried out at 1000 ^{o}C and 1050 ^{o}C there is no increase in the observed mode and largest grain size in the distribution (50 - 60 μm) as temperature is increased. However, an increase in the area percent of the largest grain size in a given distribution is noted as the reheat temperature is increased (at a reheat of 1050 ^{o}C for 30 minutes an area percent of 2.3 is obtained whereas an area percent of 1 is obtained for the sample reheated at 1000 ^{o}C for 30 minutes). The dependency of grain growth on reheat holding time and temperature has also been observed in the literature, for example, Abdollah-Zadeh [18] reheated Fe - 30 wt - % Ni steel at different temperatures ranging from 800 ^{o}C to 1150 ^{o}C (with a holding time of 30 minutes) and found that the reheated grain size increased (from an initial mode grain size of 42 μm to 160 μm at 1150 ^{o}C) with reheating temperature, as shown in Figure 4.7. The results obtained in this work are very similar to that of Abdollah-Zadeh [18], Figure 4.7, with a slight delay in the onset of grain coarsening to higher temperature.

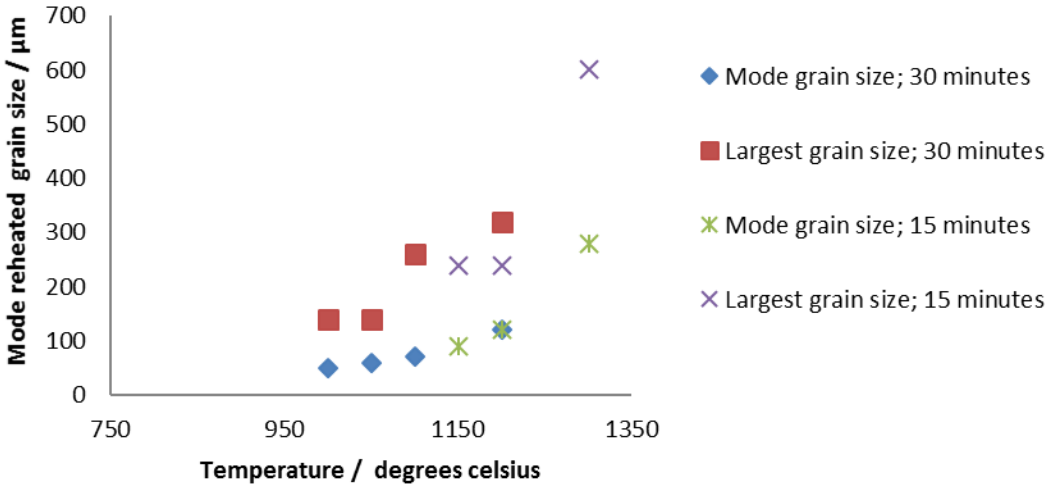

Figure 4.5: Effect of reheating temperature on the reheated grain size (i.e. the mode and largest grain size in a distribution) for the Fe - 30 wt - % Ni steel using different soaking times (15 and 30 minutes).

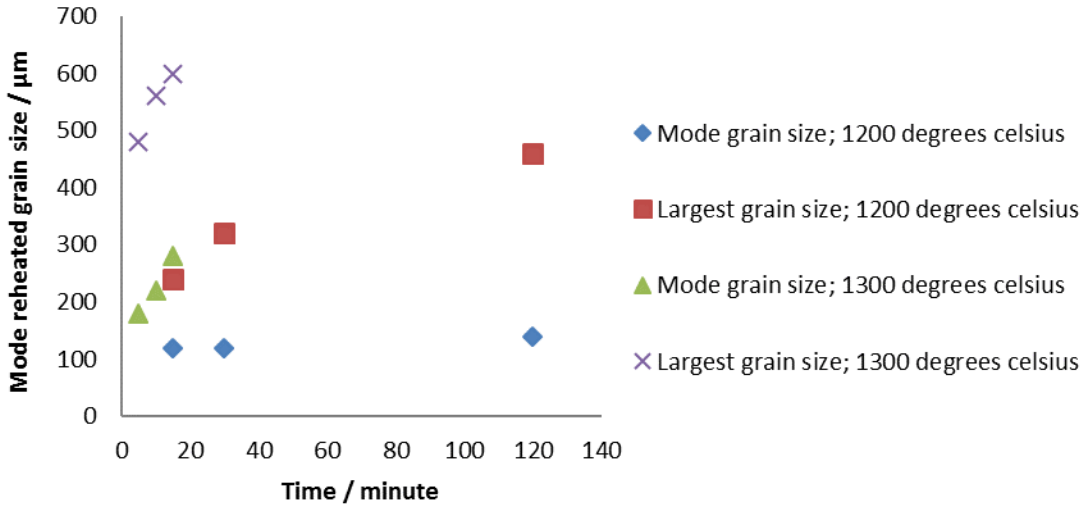

Figure 4.6: Effect of soaking time on the reheated grain size (i.e. the mode and largest grain size in a given distribution) for the Fe - 30 wt - % Ni steel at different reheat temperatures (1200 and 1300 ^{o}C).

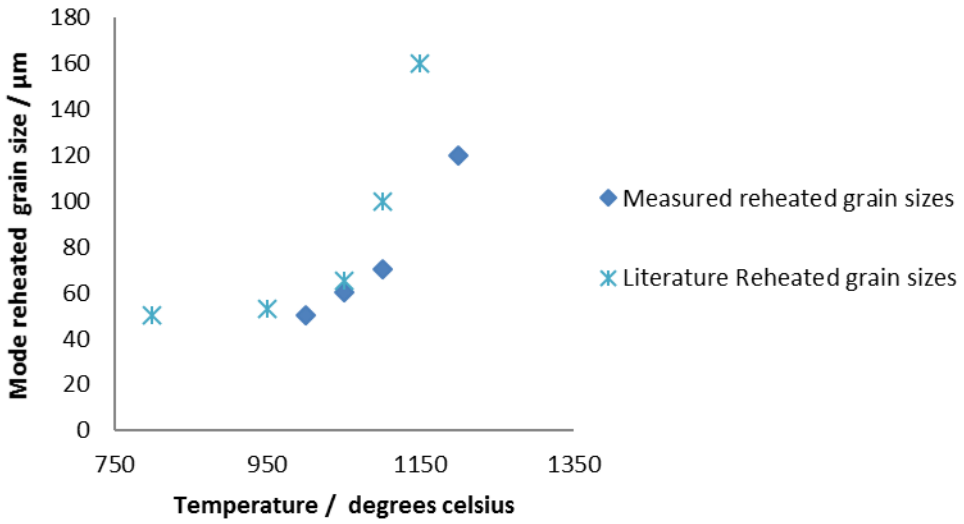

Figure 4.7: Comparison of measured and literature [18] reheated mode grain sizes obtained at different temperatures using a holding time of 30 minutes for Fe - 30 wt - % Ni steel.

For the subsequent deformation tests, it was desired to use three different initial grain size distributions to allow its influence on recrystallised grain size to be determined. The heat-treated samples of 1200 °C for 15 minutes and 1300 °C for 5 minutes were selected as they gave uniform and normal grain growth with mode grain sizes of 110 - 120 µm and 160 - 180 µm respectively. For a finer initial grain size distribution (mode grain size of 50 - 60 µm) three potential conditions were identified: sample heat treated at 1050 °C for 30 minutes (largest grain size in distribution; 140 µm); as-received sample (largest grain size in distribution; 130 µm), and heat treated sample at 1200 °C for 15 minutes and deformed to a strain of 0.3 strain and fully recrystallised (largest grain size in distribution; 120 µm) – the grain size distributions for the three conditions are given in Figure 4.8. The sample heat treated at 1200 °C for 15 minutes, deformed to a strain of 0.3 and fully recrystallised was selected as it had a slightly more uniform distribution as compared to the other two samples. The selected reheated grain size distributions prior to deformation are shown in Figure 4.9.

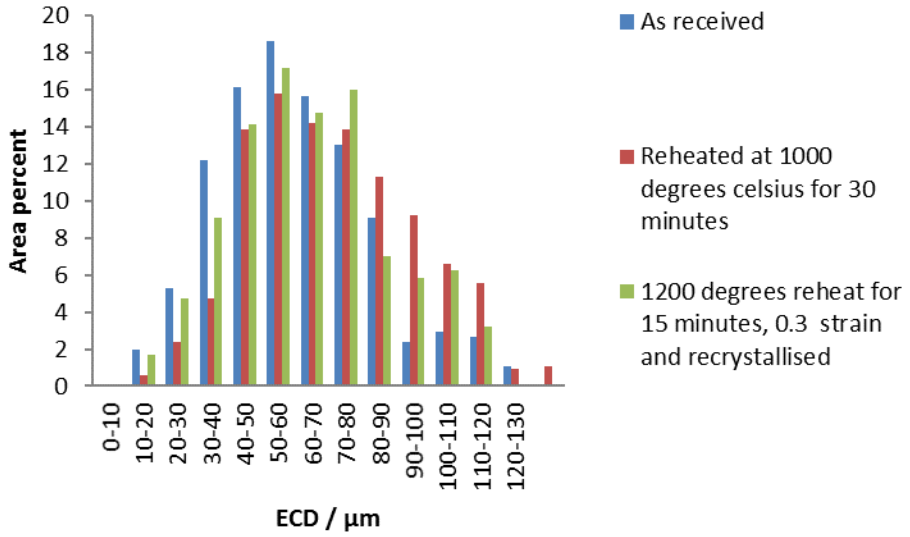

Figure 4.8: Grain size distributions for samples for the as-received sample, reheated at 1000 ^{o}C for 30 minutes and reheated at 1200 ^{o}C for 15 minutes, deformed to a strain of 0.3 and recrystallised at 850 ^{o}C.

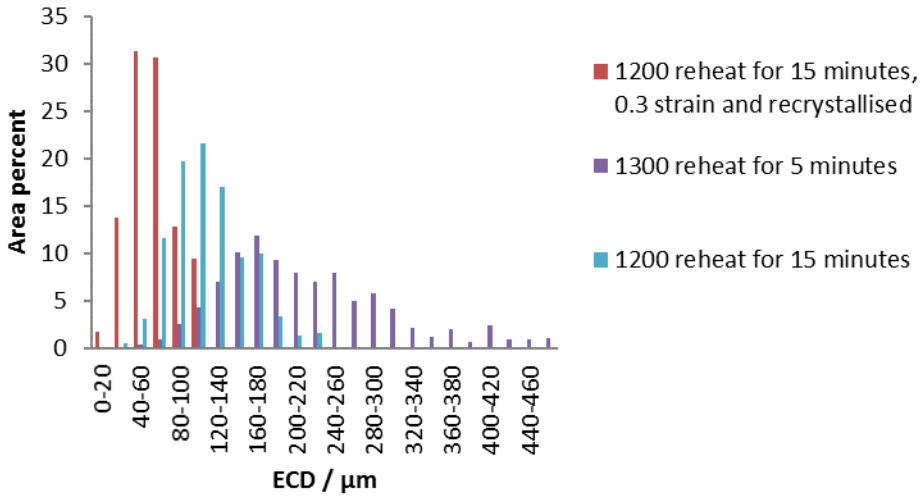

Figure 4.9: Typical grain size distributions for three samples with different initial grain size distributions selected for deformation tests.

4.2 Deformation

4.2.1 Comparison of room temperature and hot uniaxial compression tests

It is known that differences in flow stresses exist when a sample is deformed cold or hot and that other differences are observed, such as non-uniform distribution of strain in the deformed sample [32]. The non-uniform strain is caused by barrelling of the hot deformed samples due to a lack of adequate lubrication at elevated temperatures between the anvils and the sample. The barrelling coefficient (B), which is the ratio of the final test-piece dimensions and the initial test-piece dimensions, is often used to determine whether excessive barrelling has occurred and is given by the following equation [198]:

$$B = h_f d^2_f / h_i d_i^2 \quad (4.1)$$

Where h_f is the final height after deformation, d_f is final diameter measured at the mid length of the deformed sample, h_i is the initial height (15 mm) and d_i is the initial diameter (10 mm) [198].

A barrelling coefficient value between 0.9 and 1.1 generally indicates that the deformation test is valid [198, 166], while a value of 1 indicates that barrelling has not occurred. Tables 4.2 and 4.3 show that the calculated values for the barrelling coefficients are all below 1.1, and as such the deformation tests are valid. Comparison of the values given in Table 4.2 for samples deformed uniaxially at room temperature (RT) to those given in Table 4.3 for samples hot deformed (to equivalent strains) shows that barrelling is more evident in the samples that were hot deformed. This is because hot deformed samples seem to have slightly higher barrelling coefficients (1.02 - 1.06) compared to the barrelling coefficient of 1 for cold deformed samples indicating the absence of barrelling; this could be due to the lubrication not being as efficient [32, 193].

Table 4.2: Barrelling coefficients for the room temperature deformed uniaxial compression samples (initial diameter and height: 10 mm *15 mm).

Strain	Diameter after RT deformation /mm	Barrelling coefficient
0.08	10.45	1.01
0.17	10.94	1.01
0.22	12.12	0.99

Table 4.3: Barrelling coefficients for hot deformed uniaxial compression samples (initial diameter and height: 10 mm *15 mm).

Strain	Diameter after hot deformation /mm	Barrelling coefficient
0.15	10.65	1.02
0.3	12.23	1.05
0.45	13.29	1.06

Measurements of the recrystallised grain size in the room temperature deformed samples (to equivalent strains), (Table 4.4), and hot deformed samples by carrying out uniaxial compression testing, (Table 4.5), showed that the mode grain size is slightly smaller for the hot deformed samples. This is consistent with a non-uniform strain distribution from barrelling in hot deformed samples, resulting in a higher local strain in the sample centre where grain size measurements were made. Watson [166] showed that a 9Cr forging steel deformed to a strain of 1 at a strain rate of 1 / s exhibited non-uniform distribution of strain (difference in flow lines) with the non-uniformity also being predicted using Q-form software using the measured amount of barrelling [166], as shown in Figure 4.10. It was shown that the highest strain (higher stored energy and hence finer recrystallised grain size) of 1.1 is predicted in the centre of the deformed sample, while a strain of 0.5 is predicted near the anvil (dead zone).

Table 4.4: Measured recrystallised mode grain size following room temperature deformation (uniaxial compression).

Strain	D_{rex} / µm
0.08	80 - 90
0.17	50 - 60
0.22	40 - 50

Table 4.5: Measured recrystallised mode grain size following hot (850 °C) deformation (uniaxial compression).

Strain	D_{rex} / µm
0.15	70 - 80
0.3	40 - 50
0.45	30 - 40*

**Dynamically recrystallised*

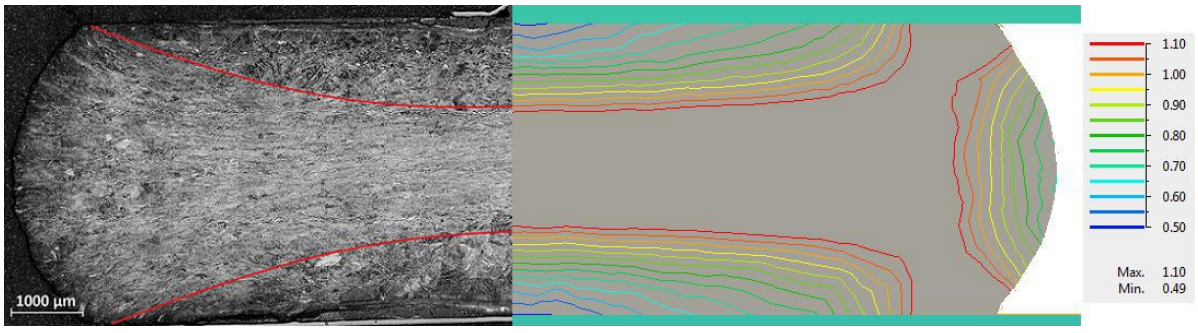

Figure 4.10: Predicted using Q-form and deformed 9Cr forging steel at 900 °C to a strain of 1 at a strain rate of 1 / s exhibiting non-uniform distribution of strain [166].

The presence of very large grains (in the dead zone) in the Fe - 30 wt - % Ni steel reheated at 1200 ^{o}C for 15 minutes and deformed to a strain of 0.45 at a strain rate of 1 / s at 850 ^{o}C and thereafter held for 130 seconds at this temperature (for full recrystallisation to take place) is depicted in Figure 4.11, which indicates that non-uniform deformation has occurred in the sample. It must be stated here that the presence of large grains near the anvil is not due to insufficient holding time at 850 ^{o}C, as evidenced by the stress relaxation curve (Figure 4.12 a) and plot of recrystallised fraction vs. time (Figure 4.12 b) which indicates that within the given holding time of 130 seconds complete recrystallisation is achieved (recrystallisation fraction of 1 is reached). It must be noted here that apart from non-uniform distribution of strain, the sample deformed to a strain of 0.45 recrystallises dynamically, as shown in Figure 4.13 (for the Fe - 30 wt - % Ni steel deformed at 850 ^{o}C to a strain of 0.9 at a strain rate of 1 / s where it is indicated that dynamic recrystallisation occurs at strains above 0.42). This will affect the recrystallised grain size as nucleation and grain growth of new grains will occur during deformation, as compared to static recrystallisation where recrystallisation will occur after deformation for a specified amount of holding time [46, 47] and hence making the cold deformed sample (0.22 strain) in Table 4.4 and hot deformed sample (0.45 strain) in Table 4.5 incomparable. Comparisons for room temperature strains of 0.3 and hot deformation (850 ^{o}C) strains of 0.7 were not carried out due to the fact that applying such high strains during hot deformation gives dynamic recrystallisation as discussed for the sample deformed to a strain of 0.45. The grain size distributions for the room temperature (0.17 strain) and 850 °C uniaxially deformed (0.3 strain) samples, i.e. equivalent strains, after full recrystallisation are shown in Figure 4.14.

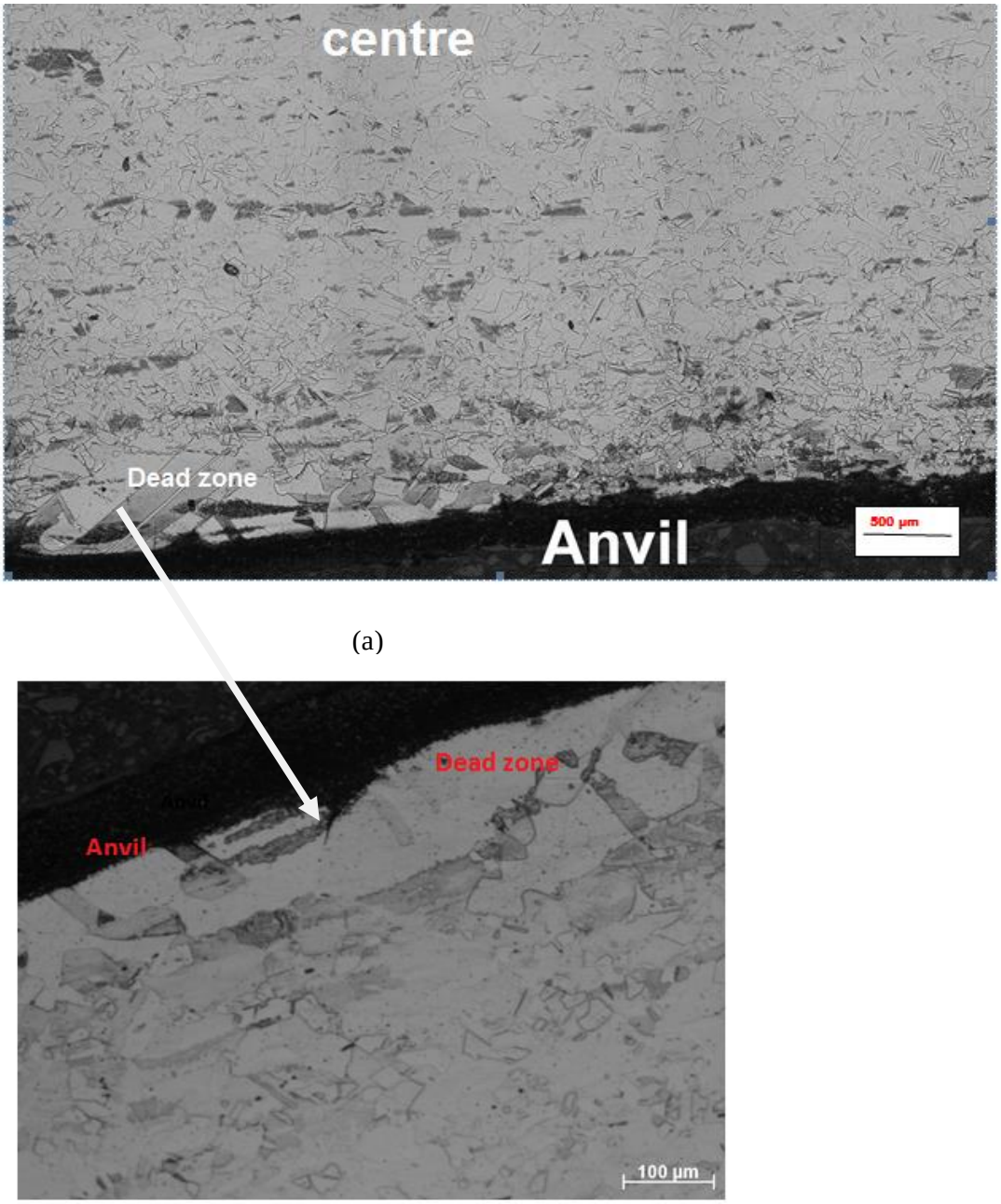

Figure 4.11: Fe - 30 wt - % Ni steel deformed at 850 ^{o}C to a strain of 0.45 at a strain rate of 1 / s and held for 130 seconds (a) Optical micrograph exhibiting large grains in the dead zone (b) Enlarged optical micrograph showing large grains in the dead zone.

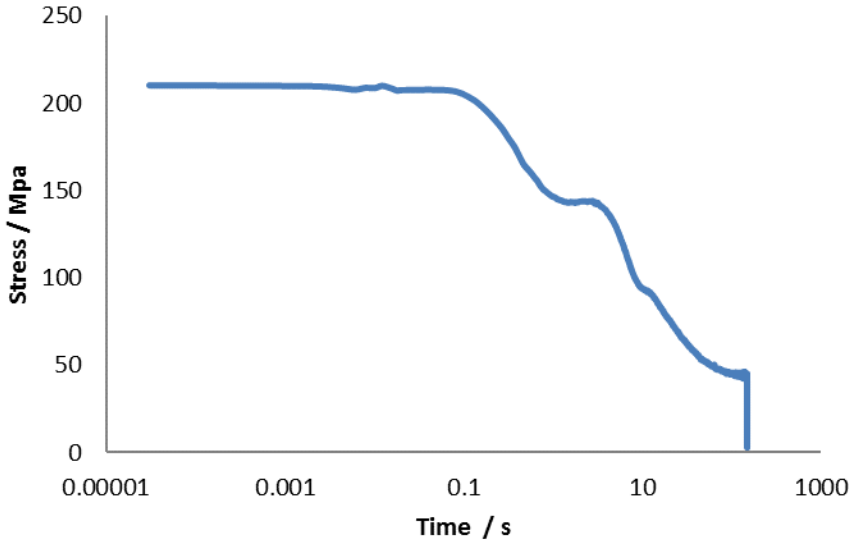

(a)

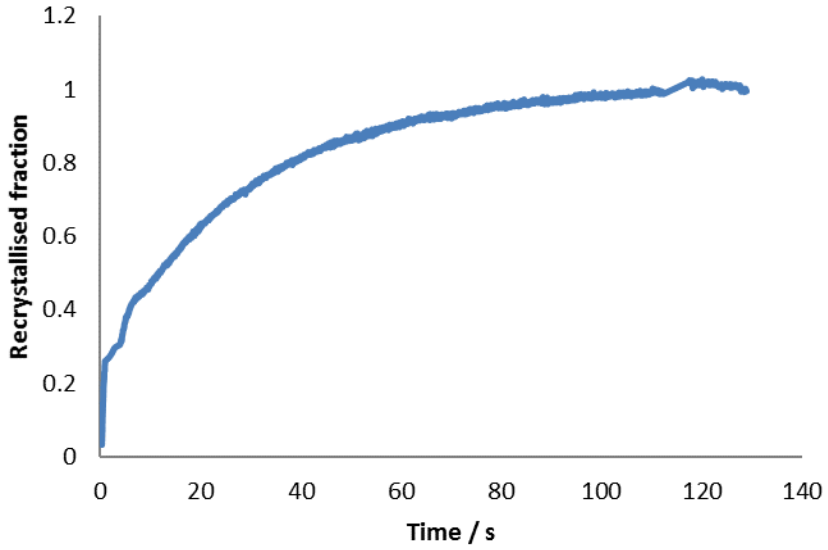

(b)

Figure 4.12: Fe - 30 wt - % Ni steel deformed at 850 ^{o}C to a strain of 0.45 at a strain rate of 1 / s and held for 130 seconds (a) Stress relaxation curve (b) Recrystallised fraction.

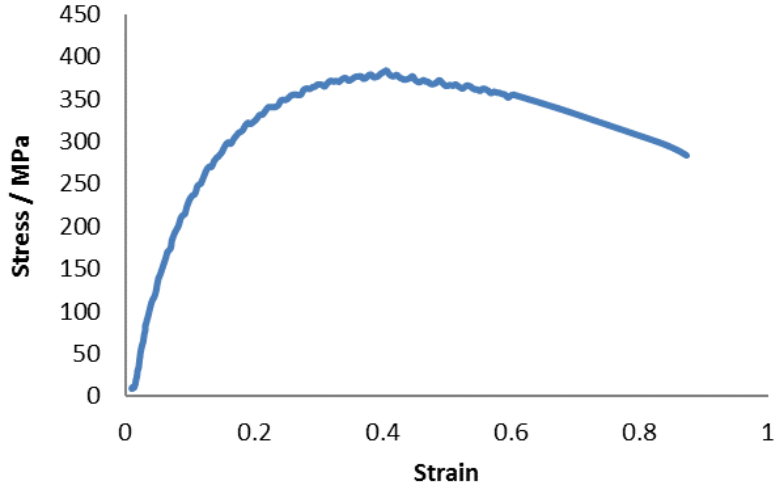

Figure 4.13: Flow stress for Fe - 30 wt - % Ni steel with an initial grain size of 110 - 120 µm deformed to a strain of 0.9 at 850 °C.

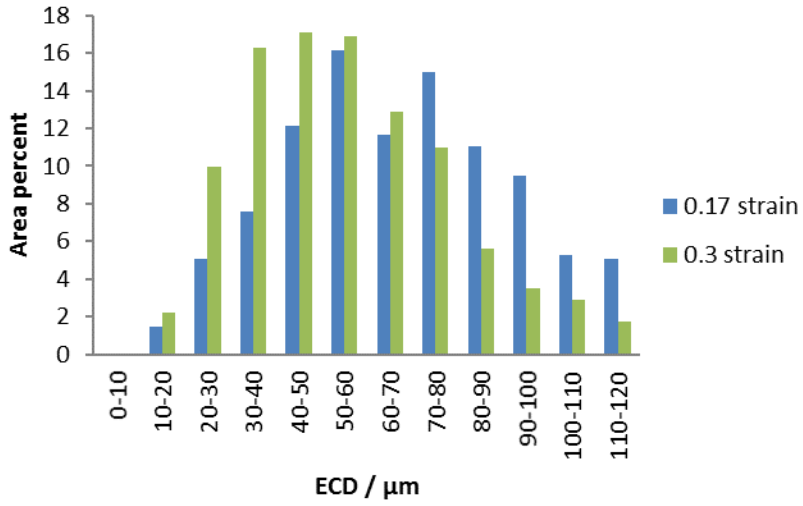

Figure 4.14: Grain size distributions for fully recrystallised samples following room temperature (0.17 strain) and 850 °C (0.3 strain) uniaxial compression testing, i.e. equivalent strain (initial mode grain size of 110 - 120 µm).

4.2.1.1 Effect of temperature gradient on the recrystallised grain size

Apart from non-uniform strain due to barrelling, other factors such as a temperature gradient across the sample may lead to differences in recrystallisation kinetics. However, this effect is not expected to be significant as the test samples used in this work were relatively small and steel has a relatively high thermal conductivity; in addition, the anvils used in the Gleeble are designed to become hot and as such minimising temperature loss. Samples were also allowed to soak for about 5 seconds to ensure uniform temperature throughout the specimen volume. Using the same Gleeble 3500 thermo-mechanical simulator as the one used in this work, Watson [166] measured the temperature along a 12Cr forging steel (8 mm diameter * 12 mm height) by spot welding four thermo-couples to the test-piece surface (about 1.5 mm apart from the centre to the outer edge of the test-piece) and observed that there was only a temperature variation of 6 ^{o}C along the longitudinal surface of the test-piece (temperature of the sample was hottest nearer the anvil / test-piece) and as such no significant effect of temperature gradient on the recrystallised grain size is expected as the variation in temperature is minimal. Therefore, the most likely cause of the differences in recrystallised grain sizes observed in the centre of the hot and cold deformed samples may be due to non-uniform strain (as the strain influences the amount of energy stored which consequently influences the recrystallised grain size).

4.2.2 Comparison of room temperature and hot plane strain compression tests

Table 4.6 shows that similar mode and largest grain sizes are obtained when plane strain compression is carried out. The grain size distributions for the room temperature (0.17 strain) and 850 °C plane strain deformed (0.3 strain) samples, i.e. equivalent strains, after full recrystallisation are shown in Figure 4.15. From the similarity in the results given in Table 4.6 the cold deformation and recrystallisation results in this thesis will be converted into

equivalent hot (i.e. 850 °C) strain values to be directly compared to hot deformation plane strain and torsion test data from the literature [3, 4], where the sample design shows more uniform strain distribution [32]. Comparison to literature hot uniaxial compression sample data may give some differences due to test procedure (barrelling in hot tests leading to finer recrystallised grain sizes as noted in Section 4.2.1).

Table 4.6: Comparison between the measured recrystallised mode and largest grain size following room temperature and hot (850 °C) deformation (plane strain compression) to equivalent strains.

RT Strain	RT deformation (D_{mode}) / µm	RT deformation (D_{max}) / µm	850 °C Strain	850 °C deformation (D_{mode}) / µm	RT deformation (D_{max}) / µm
0.08	80 - 90	200 - 210	0.15	80 - 90	200 - 210
0.17	50 - 60	110 - 120	0.3	50 - 60	110 - 120

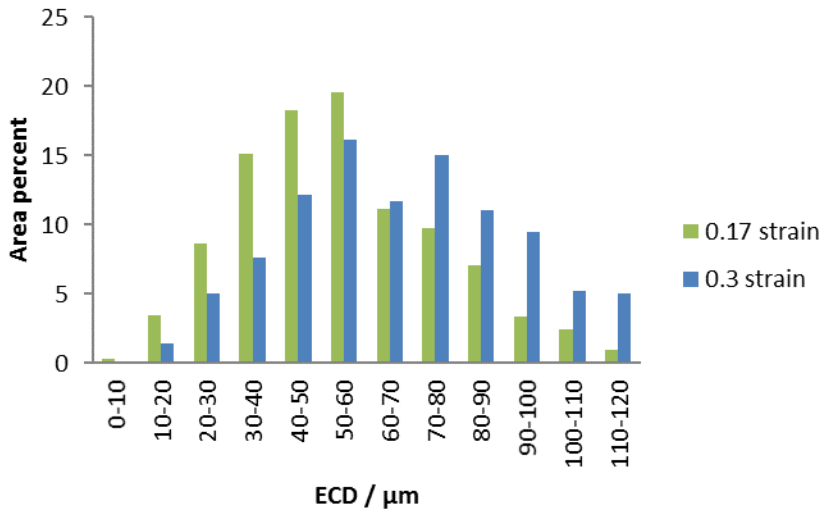

Figure 4.15: Grain size distributions for fully recrystallised samples following room temperature (0.17 strain) and 850 °C (0.3 strain) deformation (plane strain compression testing), i.e. equivalent strain (initial mode grain size of 110 - 120 µm).

4.2.3 Effect of strain and initial grain size on the recrystallised grain size

Table 4.7 gives the predicted recrystallised mode grain sizes (40 - 50 μm to 80 - 100 μm) at 0.3 strain for initial grain sizes ranging from 50 - 180 μm using Sellars equation (Equation 2.29) with *D'* values of 0.35 and 0.83 (with x = 0.67 and y = 1), which are the reported values used for C - Mn steels [5].

Table 4.7: Predicted and measured recrystallised mode grain sizes for Fe - 30 wt - % Ni steel with different initial grain sizes deformed to 0.3 strain using Equation 2.29 [5].

Initial grain size / μm	**Measured / μm**	**Predicted recrystallised grain size / μm**	
		***D'* = 0.83**	***D'* = 0.35**
50 - 60	40 - 50	40 - 50	10 - 20
110 - 120	50 - 60	60 - 70	20 - 30
160 - 180	80 - 100	80 - 100	20 - 40

Equation 2.29 was applied by splitting the initial grain size distribution into classes and determining the recrystallised grain size of each class using Equation 2.29; each split grain size class was weighted by its corresponding initial area fraction. A strain of 0.3 has been considered since most deformation in the literature has been carried out at such a strain [4, 5, 58]. It can be seen from Table 4.7 that a larger *D'* value of 0.83 predicts that the recrystallised mode grain sizes will be larger (40 - 100 μm) while a *D'* value of 0.35 predicts finer recrystallised mode grain sizes (10 - 40 μm) for all the initial grain sizes examined. In regard to the comparison of the measured and the predicted mode grain sizes, Table 4.7 also shows that Equation 2.29 generally predicts the recrystallised mode grain size well after 0.3 strain when a *D'* constant of 0.83 is employed. When a comparison of the measured and predicted grain size distribution for the 50 - 60 μm sample deformed to 0.3 using Equation 2.29 with a *D'* of 0.83 is made (Figure 4.16), it can be seen that there are significant differences,

particularly for the larger grain sizes in the distribution (NRMS error of 0.75) even though the mode grain size is well predicted; the equation predicts that the largest grain size would be 60 - 70 µm instead of the 90 - 100 µm grain size measured.

To ensure that the larger measured grains compared to the predicted distribution are not because of grain growth following recrystallisation the effect of heat treatment on grain growth was considered. The grain size distribution of a sample heat treated at 1000 °C for 30 minutes was compared to that of the as-received sample. Figure 4.17 shows that the sample heated at 1000 °C for 30 minutes has the same mode grain size (50 - 60 µm) and with slightly larger maximum grain size (130 - 140 µm compared to 120 - 130 µm) which indicates that there has been little grain growth. The recrystallised samples have been heat treated at lower temperatures (850 °C) and for shorter times (maximum time of 28 minutes), therefore, all recrystallised grain sizes that have been measured are taken as the 'true' recrystallised sizes.

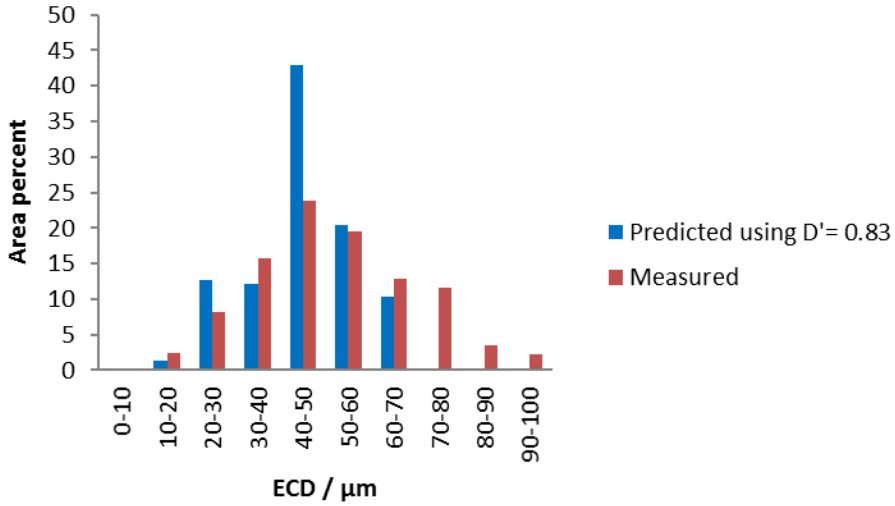

Figure 4.16: The recrystallised grain size distributions for a sample with an initial mode grain size of 50 - 60 µm deformed to a 0.3 strain and the predicted distribution based on Sellars equation ($D' = 0.83\ \mu m^{0.33}$, x = 0.67 and y = 1) [5].

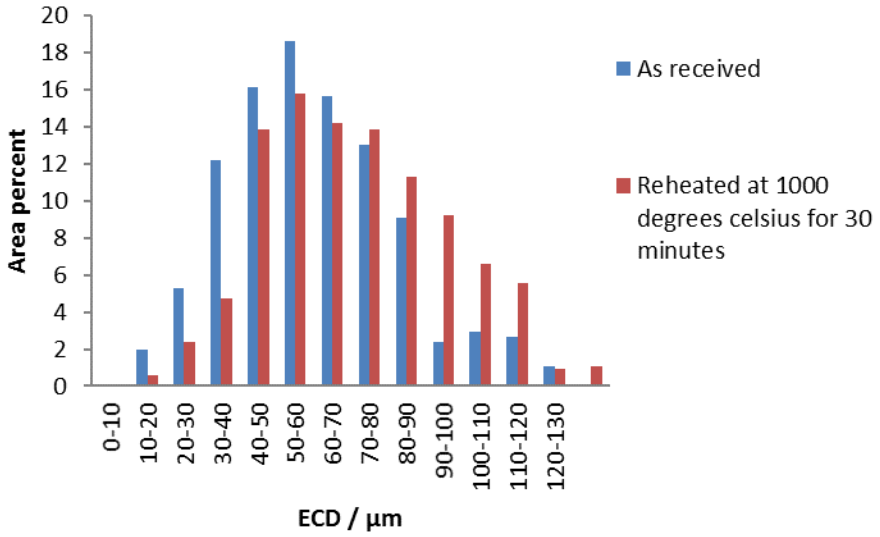

Figure 4.17: Grain size distributions for samples for the as-received sample and reheated at 1000 °C for 30 minutes.

A number of mechanisms drive grain refinement as discussed in Section 2.3.1. As deformation proceeds dislocations are generated and interact in a number of ways. The rate of change of the dislocation density is governed by generation and annihilation reactions. The generation rate is governed by the operation of Frank-Read sources that may originate at grain boundaries or because of dislocation reactions (formation of junctions). The annihilation rate is determined by reactions that remove or pin moving dislocations. This can occur through a number of mechanisms such as annihilation of opposite signed dislocations (resulting in removal of dislocation line segments) and the formation of dipole pairs. The latter can lead to the formation of stable dislocation configurations such as sub-grain structures that lower the overall energy state of the system as discussed in Section 2.3.4 [28]. The generation and annihilation / trapping rates will evolve until steady state is reached where they completely balance leading to nucleation of new grains. The formation of new grains involves growth of nucleated grains (discussed in Section 2.3.6.2) which results in the removal of dislocations as

the interface of the new grain expands – thereby further reducing the energy of the system [28].

As discussed in section 2.3.9.1 a finer recrystallised mode and maximum grain size (refined grain size distribution) is obtained as strain is increased and the initial grain size decreased, [7, 8] which is also seen in this work, as shown in Table 4.8. A finer recrystallised mode and maximum grain size is obtained as the initial grain size is decreased due to the fact that for small grains there is more available grain boundary area per unit volume, which provides a higher number density of nucleation sites. Higher strains lead to an increase in dislocation densities and as such an increase in stored energy as discussed in Section 2.3.3. Typical grain size distributions showing the effect of using different strains (for the Fe - 30 wt - % Ni steel with an initial grain size of 50 - 60 μm) and initial grain sizes (for the Fe - 30 wt - % Ni steel deformed to a strain of 0.3) on the recrystallised grain size distribution are shown in Figure 4.18 and 4.19 respectively.

Table 4.8: Measured mode and maximum recrystallised grain sizes.

Strain	50 - 60 µm		110 - 120 µm		160 - 180 µm	
	mode grain size / µm	**Maximum grain size / µm**	**mode grain size / µm**	**Maximum grain size / µm**	**mode grain size / µm**	**Maximum grain size / µm**
0.15	50 - 60	110 - 120	80 - 90	210 - 220	160 - 180	420 - 440
0.22	40 - 50	100 - 110	60 - 70	150 - 160	100 - 120	240 - 260
0.3	40 - 50	90 - 100	50 - 60	110 - 120	80 - 100	220 - 240
0.45	40 - 50	80 - 90	40 - 50	100 - 110	60 - 80	200 - 220
0.7	30 - 40	70 - 80	30 - 40	80 - 90	40 - 60	140 -160

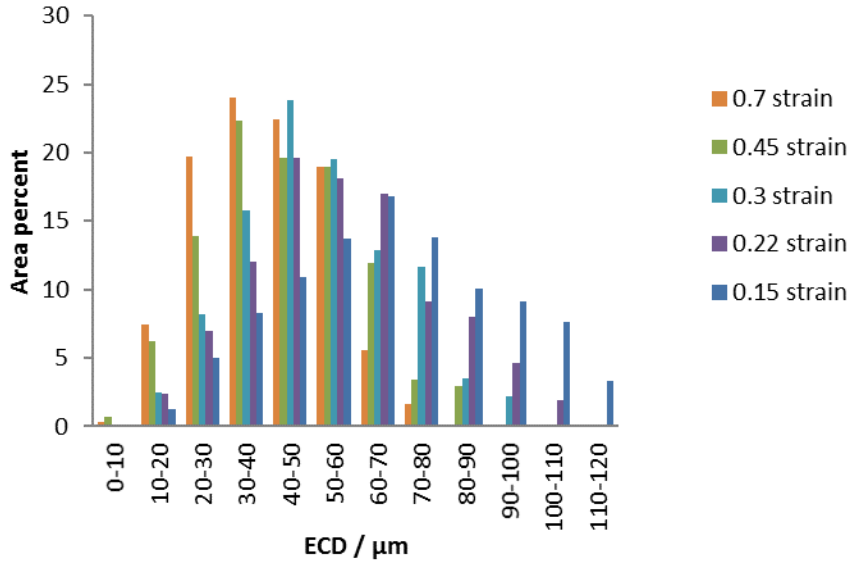

Figure 4.18: The recrystallised grain size distributions for samples with an initial mode grain size of 50 - 60 µm deformed to a range of strains (0.15 to 0.7).

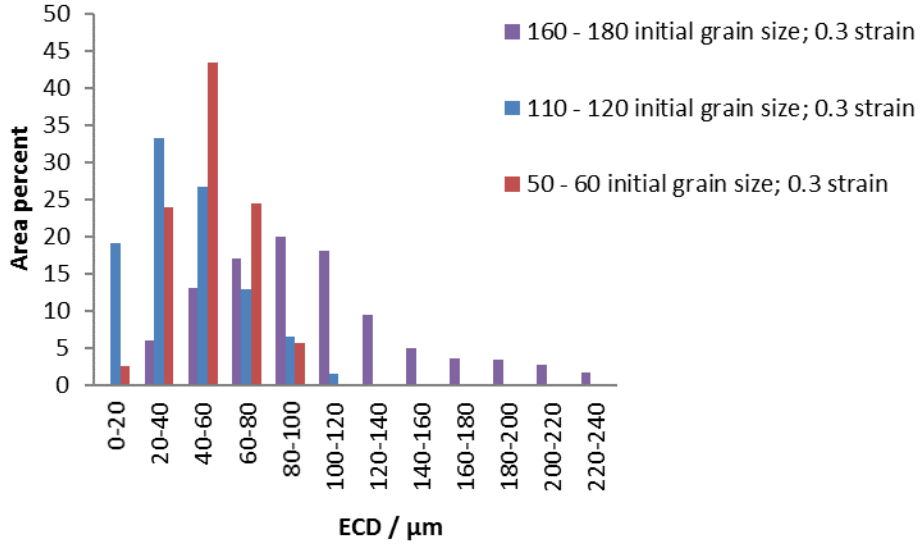

Figure 4.19: The recrystallised grain size distributions for samples with initial grain sizes ranging from 50 - 180 µm deformed to a strain of 0.3.

Figure 4.20 shows that the recrystallised mode grain size decreases with an increase in strain for all initial grain sizes during a single-stage hot deformation, which is qualitatively consistent with results published in the open literature [3 - 8]. The percentage decrease of 50 % observed when the reheated original grain size distributions of 110 - 120 µm and 160 - 180 µm are deformed to strains of 0.3 is similar to that observed by Kundu [4] at similar strains for a 0.046 wt - % Nb microalloyed steel with an initial grain size of 240 - 280 µm.

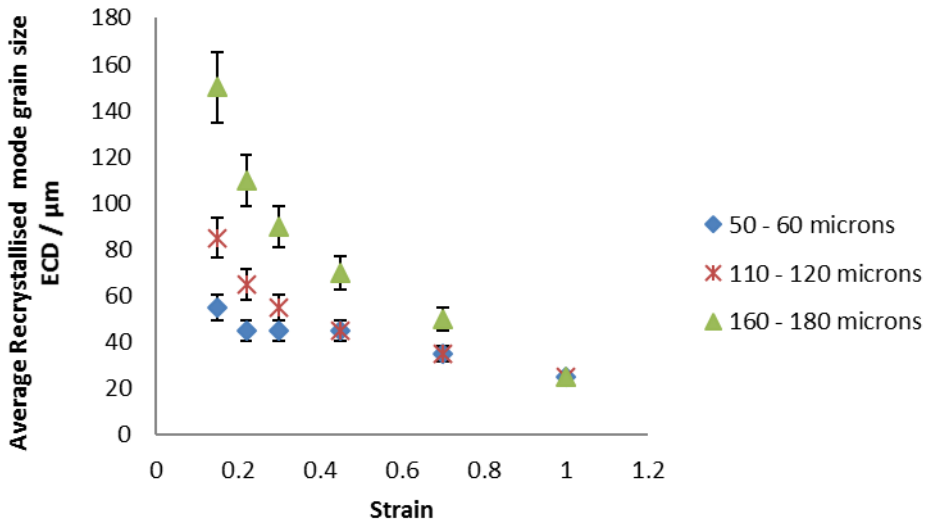

Figure 4.20: Relationship between the recrystallised grain size (middle of the recrystallised mode grain size) value) and the applied strain for samples with initial mode grain sizes of 50 - 60 µm, 110 - 120 µm and 160 - 180 µm.

Comparison of measured mode and maximum grain sizes and those predicted using Equation 2.29 is given in Tables 4.9 - 4.11. Table 4.9 shows that for the 50 - 60 µm sample, Equation 2.29 over predicts the mode grain size for deformations carried out at 0.15 and 0.22 strains, however at a strain of 0.3 the mode grain size is predicted well. At higher strains (0.45 and 0.7) the recrystallised mode grain size is under predicted by 20 µm. The largest grain size in all the distributions examined are under predicted, except for the sample deformed to a 0.15

strain where the largest grain size is over predicted by 20 μm. Computed NRMS errors ranged from 0.60 - 1.83. For the sample with an initial grain size of 110 - 120 μm, Equation 2.29 over predicts the measured mode grain size at lower strains (0.15 - 0.3), Table 4.10. At a strain of 0.45 the mode grain size is predicted well, however, it is under predicted at a strain of 0.7. The largest grain size in the distribution is under predicted for all conditions examined. Computed NRMS errors ranged from 0.72 - 1.2. Table 4.11 highlights the fact that the mode grain size is predicted well for the 160 - 180 μm samples deformed to 0.15 - 0.3 strain. Above a strain of 0.3 the recrystallised mode grain sizes are under predicted by 20 μm. The largest grain size in the distributions is under predicted for conditions examined. Computed NRMS errors ranged from 0.54 - 1.36.

Tables 4.9 - 4.11 show that generally the recrystallised mode grain sizes are predicted well at a strain of 0.3 for all grain sizes investigated; which is within the range of strains used by Sellars [5] to develop Equation 2.29. However, the maximum grain sizes are not very well predicted (under predicted) using Sellars equation for all conditions investigated in this work. Generally, it can also be noted from Tables 4.9 - 4.11 that samples deformed to lower strains (0.15 - 0.3) seem to be predicted with less discrepancies as the calculated NRMS errors (0.54 - 1) are lower than for samples deformed to strains of 0.45 - 0.7 (1.06 - 1.83 NRMS) except for the 110 - 120 sample were the NRMS errors are higher at both lower (1.07 - 1.20) and higher strains (0.99 - 1.2) with the exception of the sample strained to a strain of 0.3. Overall no specific trend is observed in the calculated NRMS errors with regards to initial grain sizes.

Table 4.9: Comparison of the measured mode and maximum grain sizes to those predicted by using Sellars equations using $D' = 0.83$ for the 50 - 60 μm sample.

Strain	Measured mode grain size / μm	Predicted mode grain size / μm	measured maximum grain size / μm	Predicted maximum grain size / μm	NRMS error
0.15	55	80	115	145	1.00
0.22	45	50	105	90	0.60
0.3	45	45	95	65	0.75
0.45	45	25	85	45	1.16
0.7	35	15	75	30	1.83

Table 4.10: Comparison of the measured mode and maximum grain sizes to those predicted by using Sellars equations using $D' = 0.83$ for the 110 - 120 μm sample.

Strain	Measured mode grain size / μm	Predicted mode grain size / μm	measured maximum grain size / μm	Predicted maximum grain size / μm	NRMS error
0.15	95	145	215	215	1.07
0.22	65	95	155	145	1.20
0.3	55	65	115	105	0.72
0.45	45	45	105	75	0.99
0.7	35	15	85	45	1.20

Table 4.11: Comparison of the measured mode and maximum grain sizes to those predicted by using Sellars equations using $D' = 0.83$ for the 160 - 180 μm sample.

Strain	Measured mode grain size / μm	Predicted mode grain size / μm	measured maximum grain size / μm	Predicted maximum grain size / μm	NRMS error
0.15	170	170	430	350	0.86
0.22	110	110	250	230	0.54
0.3	90	90	230	170	0.57
0.45	70	50	210	110	1.06
0.7	50	30	150	70	1.36

It can be deduced from Figure 4.20 that whilst the mode grain size decreased as the applied strain increases, the rate of refinement decreases and the initially different grain size values converge at high strains. For example, the finest initial grain size condition (mode grain size 50 - 60 μm) shows little refinement on recrystallisation even at high strains (between 0.22 and 0.45 strain no refinement is seen whilst for strains of 0.7 and above the recrystallised mode grain size is only refined to 30 - 40 μm). Whilst the mode grain size for the 50 - 60 μm samples remains unchanged for strains between 0.22 and 0.45 when the full grain size distributions are considered, Table 4.8, refinement of the larger grain classes in the distribution occurs thereby giving a more uniform microstructure. Increasing the strain to 0.7 seems to further refine the larger grains in particular; this suggests that even though a limiting mode grain size may occur [7, 8] a more uniform (narrower, unimodal grain size distribution) microstructure can be realised through further recrystallisation, which may lead to better toughness with reduced scatter in properties. However, Sellars equation [5] (Table 4.9) predicts that for strains between 0.22 and 0.45 the recrystallised mode grain size will decrease with an increase in strain for the sample with an initial mode grain size of 50 - 60 μm which is contrary to what has been observed at such strains in this work. Grain size distributions are rarely reported in the literature and as such the reasons why larger grain classes in the distribution continue to be refined are not very well known. The above discussion emphasises the importance of being able to predict the full grain size distribution on recrystallisation. It should be noted that when a hot rolling schedule is used for microalloyed steels, higher strains of 0.7 cannot necessarily be applied due to limitations in mill loading and also because this may give dynamic recrystallisation.

The recrystallised grain size distributions obtained for the Fe - 30 wt - % Ni steel deformed to a range of strains (0.15 - 07) have been used to examine the accuracy of literature equations in

predicting the recrystallised grain size as well as validate the individual grain size class approach (discussed in Section 4.2.4) used for predicting a full grain size distribution.

4.2.4 Predicting the recrystallised grain size distribution using the individual grain size class approach

The limit and validity of the individual grain size class approach has been evaluated using Fe - 30 wt - % Ni steel. This approach was shown to successfully predict the full grain size distribution in a 0.046 wt - % Nb microalloyed steel deformed to a 0.3 strain (discussed in Chapter 2, Section 2.4). The individual grain size class approach was applied (by splitting the grain size distribution into individual grain size classes and halving the original reheated grain size distribution, each split grain size class was weighted by its corresponding initial area percent [4]) to the samples tested with different mode grain sizes (50 - 60 μm, 110 - 120 μm, 160 - 180 μm) of the Fe - 30 wt - % Ni steel. The predicted and measured grain size distributions for samples with initial mode grain sizes of 110 - 120 μm and 160 - 180 μm samples deformed to a strain of 0.3 and fully recrystallised are shown in Figure 4.21 a and b, and it can be seen that the individual grain size class approach does predict the recrystallised grain size distribution reasonably well (NRMS error of 0.41 and 0.37). However, Figure 4.22 demonstrates that for a similar strain of 0.3 the recrystallised grain size distribution for the finer initial grain size of 50 - 60 μm is not well predicted as both the mode grain size and largest grain sizes in the distribution are under predicted (NRMS error of 1) when the individual grain size approach is employed. This may be due to the fact that even though a sample with a finer initial grain size distribution has greater total stored energy, most of it goes to accommodate grain boundaries and therefore the available energy to drive recrystallisation is reduced [86] and as such, the finer grains have not halved (20 - 30 μm) but

instead have recrystallised to a larger grain size (40 - 50 µm) than predicted by halving the original reheated grain size distribution.

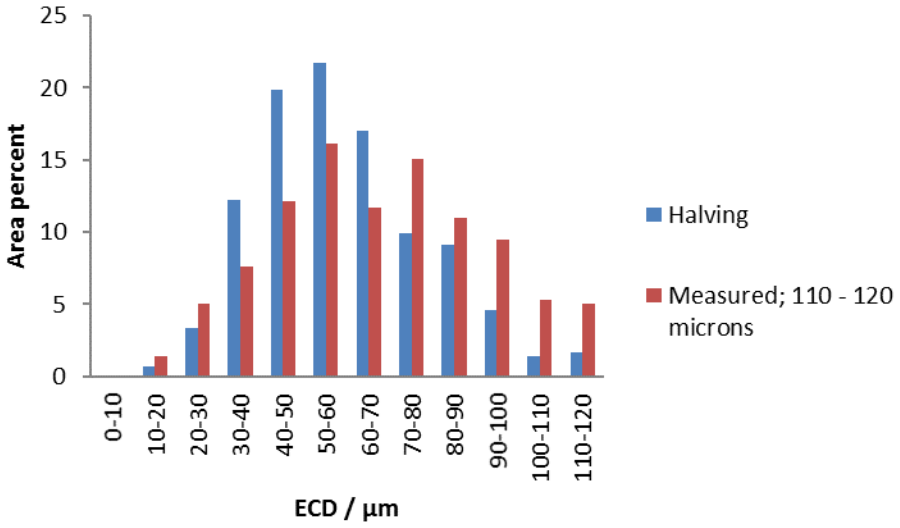

(a)

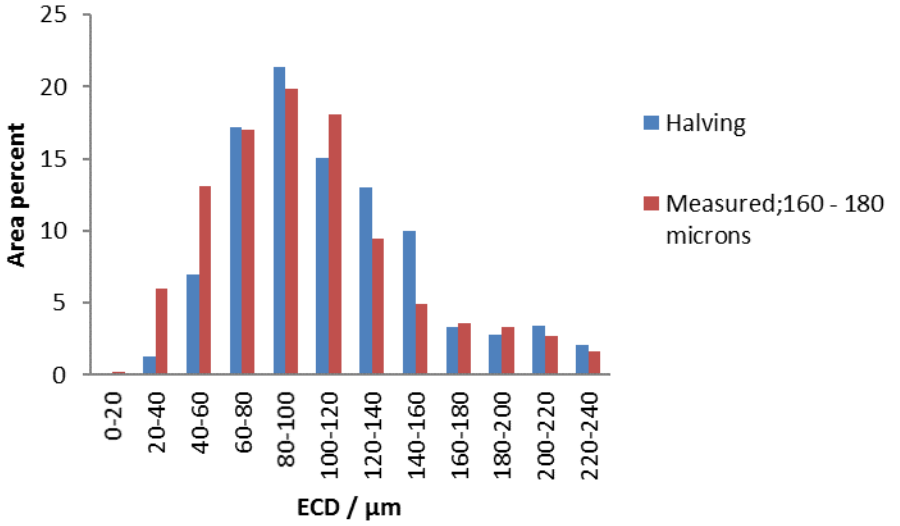

(b)

Figure 4.21: The recrystallised grain size distributions for the Fe - 30 wt - % Ni steel deformed to a 0.3 strain and the predicted distribution based on the 'halving' approach proposed by Kundu [4] (a) 110 - 120 µm initial mode grain size (b) 160 - 180 µm initial mode grain size.

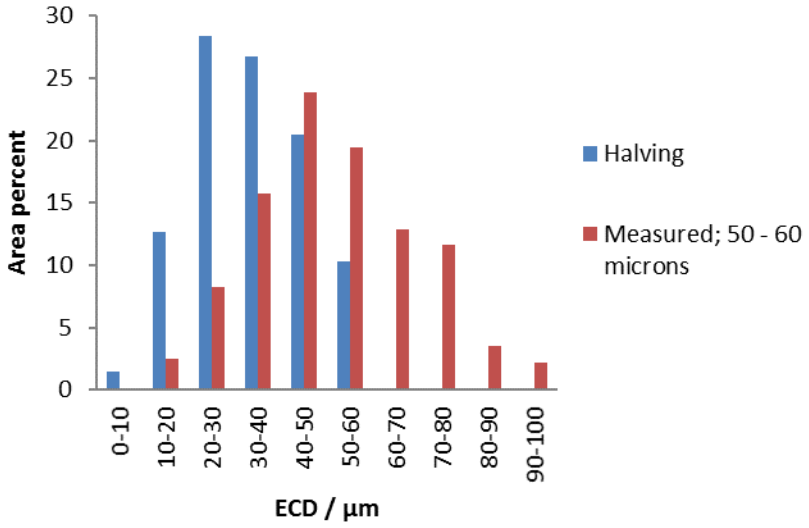

Figure 4.22: The recrystallised grain size distributions for the Fe - 30 wt - % Ni steel with an initial mode grain size of 50 - 60 µm deformed to a 0.3 strain and the predicted distribution based on the 'halving' approach proposed by Kundu [4].

At higher strains (0.7) the grain size distributions for the larger initial grain sizes (110 - 120 µm and 160 - 180 µm) are not well fitted as both the mode and largest grain size in the distributions are under predicted with NRMS errors of 0.79 and 1.23 respectively (Figures 4.23 and 4.24). However, at a strain of 0.7 the finer (50 - 60 µm) initial grain sample is reasonably fitted with a NRMS error of 0.42, although larger grains are under predicted as shown in Figure 4.25. The discrepancies seen when predicting samples with initial grain sizes of 110 - 120 µm and 160 - 180 µm may arise as the approach does not take into account the effect of high strain values on nucleation site density, and was only proposed and validated for a strain of 0.3. An increase in strain leads to more dislocations being introduced in the sample, and therefore more available nucleation sites, which influences the rate of nucleation [24, 124]. As there are more available nucleation sites at high strain a simple assumption can be made that grain refinement is by a greater degree, if refinement by a third is considered; this then gives a much better fit for the 110 - 120 µm and 160 - 180 µm grain size material

(0.41 and 0.28 NRMS respectively) to the measured grain size distribution (as illustrated in Figure 4.26 for the 110 - 120 µm sample deformed to a 0.7 strain) than the 'halving' approach (0.79 and 1.23 NRMS respectively) shown in Figures 4.23 and 4.24. It was found that this approach was only appropriate for strains of 0.7 and for the samples with an initial mode grain size above 100 µm (110 - 120 µm and 160 - 180 µm) as highlighted in Table 4.12. However, for finer initial grain sizes (50 - 60 µm) the 'halving' approach can be used to predict the recrystallised grain size distribution when higher strains (0.7) are employed (0.42 NRMS error).

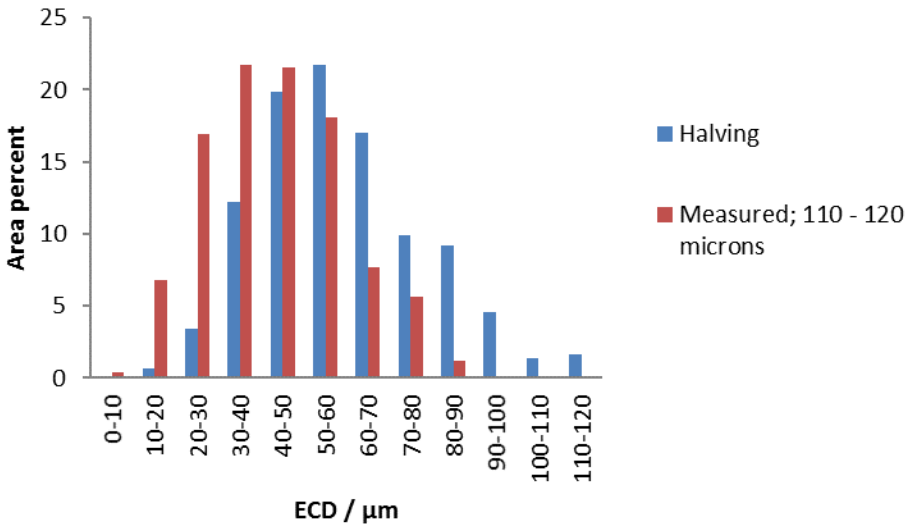

Figure 4.23: The recrystallised grain size distributions for the Fe - 30 wt - % Ni steel with an initial mode grain size of 160 - 180 µm deformed to 0.7 strain and the predicted distribution based on the 'halving' approach proposed by Kundu [4].

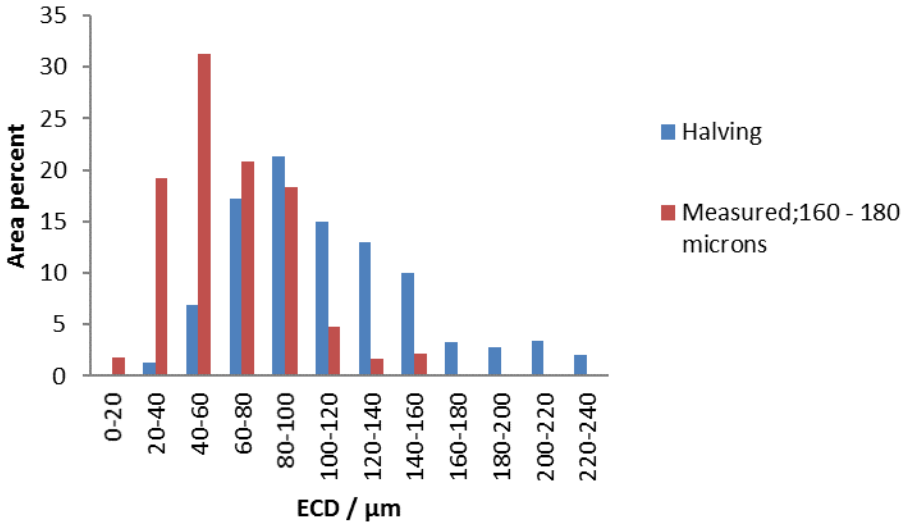

Figure 4.24: The recrystallised grain size distributions for the Fe - 30 wt - % Ni steel with an initial mode grain size of 160 - 180 µm deformed to a 0.7 strain and the predicted distribution based on the 'halving' approach proposed by Kundu [4].

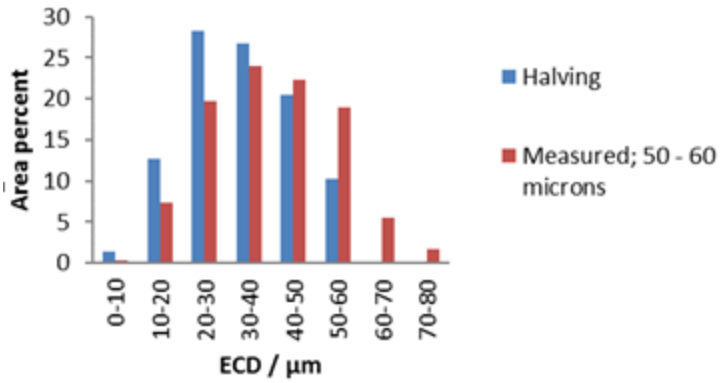

Figure 4.25: The recrystallised grain size distributions for the Fe - 30 wt - % Ni steel with an initial mode grain size of 50 - 60 µm deformed to a 0.7 strain and the predicted distribution based on the 'halving' approach proposed by Kundu [4].

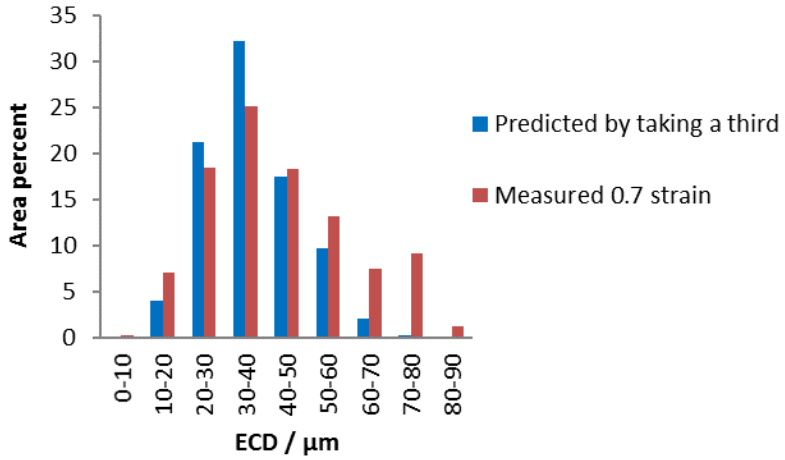

Figure 4.26: The recrystallised grain size distributions for Fe - 30 wt - % Ni steel with an initial mode grain size of 110 - 120 µm deformed to a 0.7 strain and the predicted distribution based on grain refinement by a third.

The best fit simple functions (1:1 relationship, halving and a third using the individual grain size approach) that can be used in predicting the grain size distributions for the different strains and initial mode grain sizes in this study are given in Table 4.12 for the Fe - 30 wt - % Ni steel. For all investigated grain sizes above 100 µm (i.e. 110 - 120 µm and 160 - 180 µm) the recrystallised grain size is predicted well by the 'halving' approach at strains of 0.22, 0.3 and 0.45. Although recrystallised grain sizes are predicted well for grain sizes above 100 µm, discrepancies in the predicted grain size classes are observed, for example, when the individual grain size class approach is applied to the 110 - 120 µm sample deformed to a strain of 0.22 by halving the original reheated grain size distribution the maximum grain size is under predicted by 40 µm (Table 4.12). Discrepancies in the degree of fit (NRMS errors) between the predicted and measured grain size distributions seem to decrease with an increase in strain, as shown in Table 4.12. At higher strains of 0.7 investigated grain sizes above 100 µm tend to be better fitted (with NRMS errors of 0.41: 110 - 120 µm) and 0.28:160 - 180 µm) if grain refinement is assumed to be by a third. Assuming a 1:1 relationship (i.e. making an

assumption that the recrystallised grain size recrystallises back to its initial grain size distribution) gives better fits (0.23 - 0.55 NRMS errors) than if halving is assumed (1.24 - 1.49 NRMS errors) at 0.15 strains for all investigated grain sizes. Samples with initial grain sizes below 100 μm exhibit a different behaviour at higher strains (0.45 and 0.7) compared to samples with initial grain sizes above 100 μm deformed to similar strains, as the grain size distributions for the fine-grained sample are predicted with reduced errors when halving is assumed (0.42 and 0.68 NRMS errors) instead of assuming a 1:1 relationship (0.93 and 1.16 NRMS error). Grain sizes below 100 μm show that a 1:1 relationship gives the best fit distribution for 0.15 - 0.3 strains (0.23 - 0.69 NRMS error) given in Table 4.12 as compared to the 'halving' approach (1 - 1.49 NRMS error) given in Table 4.13. However even though assuming a 1:1 relationship gives reduced errors than when the 'halving' approach is applied, it is evident that some of the grain size classes have been refined; for example, for the sample strained to 0.3, it is clear that the largest grain size is refined to 90 - 100 μm from 110 - 120 μm and the mode grain size is refined to 40 - 50 μm from 50 - 60 μm.

Although the above discussion shows that the best fit functions (1:1 relationship, halving and a third) can be used to determine the grain size distribution reasonably well, there are still inaccuracies in the predictions (in terms of the predicted $D_{5\%}$, mode grain size and the largest grain size in the distribution). It is generally highlighted in Table 4.12 that the use of simple best fit functions will not predict the recrystallised grain size distribution very well for all ranges of grain size and strain. Furthermore, it is difficult to know which simple relationship (i.e. 1:1 relationship, halving or a third etc.) to use for any new prior austenite grain size that maybe generated (e.g. if initial grain sizes > 200 μm are generated).

Table 4.12: Best fit simple functions used in predicting the grain size distributions for different strains and initial grain sizes.

Initial mode grain size	Strain	Measured mode grain size / µm	Predicted mode grain size / µm	Measured $D_{5\%}$ / µm	Predicted $D_{5\%}$ / µm	Measured D_{max} / µm	Predicted D_{max} / µm	Prediction method	NRMS error
50 - 60	0.15	50 - 60	50 - 60	20 - 30	20 - 30	110 - 120	110 - 120	1/1	0.23
	0.22	40 - 50	50 - 60	20 - 30	20 - 30	100 - 110	110 - 120	1/1	0.51
	0.3	40 - 50	50 - 60	10 - 20	20 - 30	90 - 100	110 - 120	1/1	0.69
	0.45	40 - 50	50 - 60	10 - 20	20 - 30	80 - 90	110 - 120	1/2	0.68
	0.7	30 - 40	30 - 40	10 - 20	10 - 20	70 - 80	50 - 60	1/2	0.42
110 - 120	0.15	80 - 90	110 - 120	40 - 50	20 - 30	200 - 210	230 - 240	1/1	0.55
	0.22	60 - 70	50 - 60	30 - 40	20 - 30	150 - 160	110 - 120	1/2	0.54
	0.3	50 - 60	50 - 60	20 - 30	20 - 30	110 - 120	110 - 120	1/2	0.41
	0.45	40 - 50	50 - 60	20 - 30	20 - 30	100 - 110	110 - 120	1/2	0.37
	0.7	30 - 40	30 - 40	10 - 20	20 - 30	80 - 90	70 - 80	1/3	0.41
160 - 180	0.15	160 - 180	160 - 180	100 - 120	80 - 100	440 - 460	420 - 440	1/1	0.53
	0.22	100 - 120	100 - 120	40 - 60	40 - 60	240 - 260	220 - 240	1/2	0.52
	0.3	80 - 100	100 - 120	20 - 40	40 - 60	220 - 240	220 - 240	1/2	0.37
	0.45	60 - 80	100 - 120	20 - 40	40 - 60	200 - 220	220 - 240	1/2	0.33
	0.7	40 - 60	40 - 60	20 - 40	20 - 40	140 - 160	140 - 160	1/3	0.28

Table 4.13: Summary of NRMS error values for predicted grain size distributions using the 'halving' approach [4] and Equation 2.29 [5].

Initial grain size / µm	Strain	NRMS errors	
		'Halving' approach	Constant *D'* approach (0.83) using Equation 2.29
50 - 60	0.15	1.49	1.00
	0.22	1.20	0.60
	0.3	1.00	0.75
	0.45	0.68	1.16
	0.7	0.42	1.83
110 - 120	0.15	1.32	1.07
	0.22	0.54	1.20
	0.3	0.41	0.72
	0.45	0.37	0.99
	0.7	0.79	1.20
160 - 180	0.15	1.24	0.86
	0.22	0.52	0.54
	0.3	0.37	0.57
	0.45	0.33	1.06
	0.7	1.23	1.36

4.2.5 Comparison of the accuracy of individual grain size class approach and Equation 2.29 (*D'* = 0.83, x = 0.67, y = 1) in predicting the recrystallised grain size distribution

In order to make a comparison of how well the two literature approaches discussed in Section 4.2.3 and 4.2.4 predict recrystallised grain size distributions, the individual grain size approach ('halving' approach) [4] and Equation 2.29 using a *D'* of 0.83 and exponents reported for C - Mn steels (x = 0.67, y = 1) [5] have been compared, as highlighted in Table 4.13 (NRMS errors computed for Equation 2.29 were initially tabulated in Tables 4.9 - 4.11 and have just been repeated for the purposes of comparison to the individual grain size approach). Table 4.13 shows that for the 50 - 60 µm sample deformed to lower strains (0.15 - 0.3) the computed NRMS error values are reduced (0.60 - 1.00 NRMS) when Equation 2.29

with a constant *D'* of 0.83 is employed, as compared to when the 'halving' approach is used (1 - 1.49 NRMS error), where an increase in computed NRMS error values is observed at lower strains. At higher strains (0.45 - 0.7) the trend is reversed with the 'halving' approach giving better fits (0.42 - 0.68 NRMS error) than Equation 2.29 with a constant *D'* of 0.83, where the discrepancies are increased (1.16 - 1.83 NRMS error). It is generally highlighted in Table 4.13 that the 'halving' approach will not predict the recrystallised grain size distribution for all ranges of grain size and strain, however it does generally give reduced errors (0.33 - 1.49 NRMS error) for all conditions examined compared to the use of Equation 2.29 with a constant *D'* of 0.83 (0.54 - 1.83 NRMS error) [5]. Typical measured and predicted grain size distributions using the individual grain size class approach ('halving' approach) and Equation 2.29 with *D'* value of 0.83 [5] for the 110 - 120 µm sample are given in Figure 4.27.

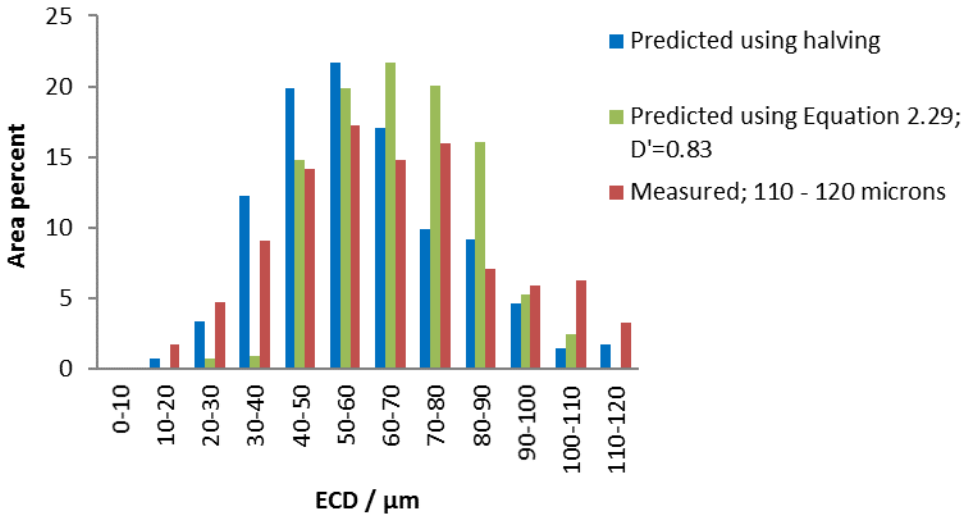

Figure 4.27: The recrystallised grain size distributions for a sample with an initial mode grain size of 110 - 120 µm deformed to a 0.3 strain and the predicted distribution based on Equation 2.29 (D' = 0.83 $\mu m^{0.33}$, x = 0.67 and y = 1) [5] and the individual grain size class approach ('halving' approach) [4].

Comparison of the individual grain size class approach using different simple functions (1:1 relationship, halving and a third) given in Table 4.12 with Equation 2.29 (NRMS errors given in Table 4.13) shows that applying the individual grain size class approach using different simple functions gives better fits. Whilst this shows that the individual grain size class approach (NRMS errors given in Table 4.12) can be used to determine the grain size distribution if different simple functions (1:1 relationship, halving and taking a third) are applied across all strains and grain sizes, there are still inaccuracies observed in the predicted grain size distributions. Therefore, consideration of how Equation 2.29 can be used for predicting grain size distributions has been made based on the classical theory for the rate of nucleation (presented and discussed in Chapter 5, Section 5.1).

4.3 Summary

- Different grain size distributions with mode grain sizes ranging from 50 μm to 160 μm were generated for the Fe - 30 wt - % Ni steel using heat treatments with or without prior deformation.
- Grain growth after recrystallisation has been investigated and it has been shown that there is no significant grain growth; therefore, all recrystallised grain sizes that have been measured are 'true' recrystallised sizes.
- The influence of strain (up to 0.7) and initial grain size (mode grain sizes of 50 - 60, 110 - 120 and 160 - 180 μm) on the recrystallised grain size distributions has been examined using the Fe - 30 wt - % Ni steel. Results obtained for the recrystallised mode grain size after deformation show that it decreases with an increase in strain and decrease in the initial mode grain size, which is consistent with the results in the literature. However, whilst the mode grain size decreased as the applied strain

increased, the rate of refinement decreased and the initially different grain size values converged at high strains.

- Greater refinement of large grains in the distribution compared to the mode grain size (leading to narrower grain size distributions) has been observed.
- Sellars equation ($D_{rex} = D' D_o^{0.67} \varepsilon^{-1}$) [5] predicts mode grain sizes well for strains of 0.3 and a *D'* of 0.83. However, errors arise when predicting the largest grain sizes in the distribution as well as when strains higher than 0.3 are employed.
- The accuracy of the individual grain size class approach ('halving' approach) [4] in predicting the recrystallised grain size distribution has been assessed and compared to Equation 2.29: $D_{rex} = D' D_o^{0.67} \varepsilon^{-1}$) [5].
- The individual grain size approach ('halving' approach) only predicted the recrystallised grain size distribution well at strains of 0.3 and 0.45 for initial grain sizes of 110 - 120 μm and 160 - 180 μm, whereas for the initial grain size of 50 - 60 μm it was only valid at the higher strain of 0.7.
- Using different best fit simple functions such as assuming a 1:1 relationship, halving and taking a third to predict the measured recrystallised grain size improves the degree of fit between the measured and predicted grain size distributions. At a lower strain of 0.15 a 1:1 relationship gives good fits for all the grain sizes examined. For strains of 0.22 - 0.45 grain sizes above 100 μm are fitted well when an assumption is made that the grains have refined by halving whereas at 0.7 strains an assumption that the grains have refined by a third gives better fits. For grain sizes below 100 μm an assumption that the grains have not refined (that is assuming a 1:1 relationship between the recrystallised and initial grain size) gives better fits for the samples deformed to strains of 0.22 - 0.3) while at strains of 0.45 and 0.7 the 'halving' approach gives better fits.

CHAPTER – 5

Modelling recrystallised grain size distributions

The accuracy of Equation 2.29 (with parameters D' = 0.83, x = 0.67 and y = 1) [5] and the individual grain size class approach [4], discussed in Chapter 2, in predicting the full grain size distribution have been assessed in Section 4.2.3 and 4.2.4 where it was concluded that Equation 2.29 predicts the mode grain size reasonably well, but discrepancies are observed when it is employed in the prediction of a full grain size distribution, while the individual grain size class approach predicts the grain size distribution well at strains of 0.3 and 0.45 for the larger grain size distributions (mode grain size of 110 - 120 μm and 160 - 180 μm). For finer grain sizes (mode grain size of 50 - 60 μm) the individual grain size class approach is only valid at strains of 0.7. Using classical nucleation theory, this section will consider modifying Equation 2.29 in order to improve prediction of grain size distributions at different strains and initial grain sizes.

5.1 Prediction of the recrystallised grain size and distribution using a modified Equation 2.29

The recrystallised grain size is strongly linked to the nucleation rate of new grains in the deformed structure. Since nucleation is assumed to occur on grain boundaries (via strain induced grain boundary migration) [122, 130, 131] and so the parameters that affect nucleation rate should also affect the relationship between the recrystallised and original grain size. Therefore, it is reasonable to consider nucleation rate equations (given in literature) in order to derive or modify already existing equations [5] for predicting recrystallised grain size

distributions after deformation. Cahn [199, 200] proposed that the boundary nucleation rate is represented by the rate of nucleation in the form of Equation 5.1.

$$N_V = C_4 v exp - \left(\frac{\Delta G^*}{kT}\right) \exp - \left(\frac{\Delta G}{kT}\right) \quad \text{nuclei } m^{-3}s^{-1} \qquad (5.1)$$

Where ΔG^* is the critical free energy for nucleation, ΔG is the free energy of activation for diffusion, v is the nucleation (Debye) frequency factor, C_4 is the factor that represents the number of nucleation sites per unit volume, N_V is the number of nuclei per unit volume per unit time (nucleation rate), T is the absolute temperature and k is the Boltzmann constant [20, 24, 124, 191].

The classical theory for rate of nucleation, Equation 5.1, gives a dependency on nucleation sites (grain boundary area) per unit volume (D_o^2 / D_o^3) for grain boundary nucleation after deformation to strain, ε (Equation 5.2) [24].

$$N_V \propto D_o^2 / D_o^3 \qquad (5.2)$$

5.1.1 Determination of the strain exponent in Equation 2.29

Based on the assumption that the grains are spherical, ΔG^* for a given critical radius (r^*) is given by Equation 5.3, which indicates that the nucleation barrier (ΔG^*) is inversely proportional to ΔG^2_V (volumetric free energy). Derivation of Equation 5.3 is given in Appendix B.

$$\Delta G^* \propto 16\pi\gamma_2^3 / 3\Delta G^2_V \qquad (5.3)$$

Where γ_2 is the interfacial surface energy per unit area. ΔG_V is assumed to be the driving force for nucleation and as such an assumption is made that ΔG^* is inversely proportional to (stored

energy) [2]. During deformation stored energy is approximately proportional to the square of strain;

Therefore, stored energy $\propto \varepsilon^2$ (5.4)

Hence; $\Delta G^* \propto 1 / \varepsilon^2$ (5.5)

Equation 5.5 suggests that there is a quadratic strain dependency on the driving force for nucleation (ΔG^2_V). However, nucleation site density is dependent on strain suggesting that there is also a strain dependency of 1 and as such Equation 5.2 becomes as follows:

Nucleation sites / unit volume $\propto (\varepsilon * D_o^2) / D_o^3$ (5.6)

Therefore, the strain exponent, y in Equation 2.29 becomes 1.

5.1.2 Determination of the initial grain size exponent in Equation 2.29

To establish the dependency of nucleation rate on grain size an assumption that there is an inverse relationship between D_{rex} and N_V is made. This is based on the fact that fewer nuclei per unit time per unit volume leads to a larger recrystallised grain size being formed whereas more nuclei per unit time per unit volume leads to a finer recrystallised grain size being formed [24]. Therefore, D_{rex} is assumed to be directly proportional to D_o^3 / D_o^2 (Equation 5.7) since N_V has been shown to be proportional to D_o^2 / D_o^3 (Equation 5.2).

$D_{rex} \propto D_o^3 / D_o^2$ (5.7)

Therefore, *x* and *y* in Equation 2.29 should both be unity so that Equation 5.8 would apply.

$D_{rex} = D' D_o \varepsilon^{-1}$ (5.8)

D' then becomes dimensionless and represents the 'efficiency' of nucleation of new grains. The analysis above assumes uniform strain and stored energy in the deformed grains.

5.1.3 Determination of the best fitted *D'* values using recrystallised grain size distributions for the Fe - 30 wt - % Ni steel

Grain size distributions from the cold deformed and recrystallised Fe - 30 wt - % Ni steel samples were used to determine the best fitted values for *D'* using Equation 5.8. The predicted grain size distributions were based on measured values for $D_{5\%}$ (grain size class constituting the first 5 % of the total area measured), D_{mode} (mode grain size class) and D_{max} (largest grain size class in the distribution). The *D'* values were obtained for the $D_{5\%}$, D_{mode} and D_{max} for the model alloy via fitting iterations with measured data and error checking for each strain level. In order to determine what *D'* values to use for the intermediate grain size classes (i.e. grain sizes other than $D_{5\%}$, D_{mode} and D_{max}), the obtained *D'* values for $D_{5\%}$, D_{mode} and D_{max} were used to make a plot of *D'* versus initial grain size for the $D_{5\%}$, D_{mode} and D_{max} (Figures 5.1 - 5.3). A linear equation was fitted to the obtained data as a linear relationship deemed appropriate from initial examination of the plots. The equation was used to determine *D'* values for intermediate grain size classes. The obtained *D'* values were used in Equation 5.8 in order to determine to what grain size class (D_{rex}) each initial grain size class had recrystallised. Thereafter, the area percents contributed by each initial grain size class to the recrystallised individual grain size class were summed, enabling the construction of the recrystallised grain size distribution from the initial grain size distribution.

Figure 5.4 illustrates the procedure for the modelling approach. This procedure of determining the recrystallised grain size distribution has been applied throughout this work and will be referred to as the variable *D'* approach; unless otherwise stated. As stated in Chapter 3

(Section 3.3.2) no stereological grain size correction has been carried out for the $D_{5\%}$, D_{mode} and D_{max} values due to the fact that Equation 2.29 was developed for 2-dimensional (2D) grain sizes and therefore, consideration of 2D grain size is appropriate for use in modifying the existing equations to account for grain size distributions.

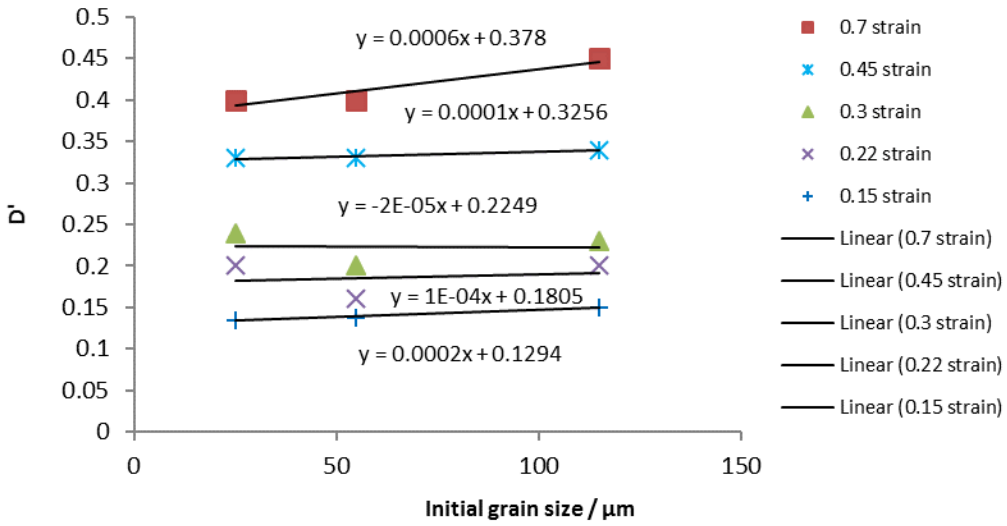

Figure 5.1: Plot of fitted *D'* values (for the $D_{5\%}$, D_{mode} and D_{max}) for different applied strains (0.15 - 0.7) against the grain size distribution (i.e. $D_{5\%}$, D_{mode} and D_{max}) for the sample with an initial grain size of 50 - 60 µm.

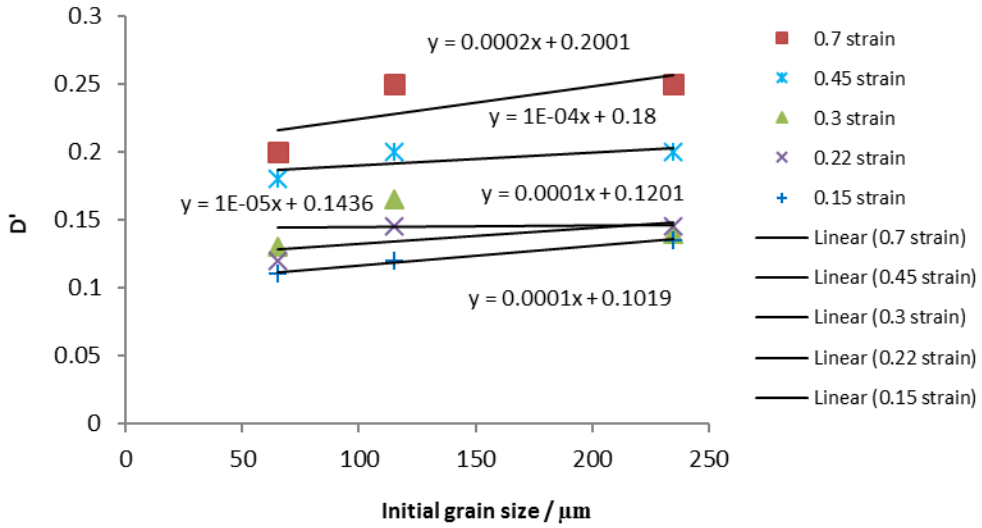

Figure 5.2: Plot of fitted *D'* values (for the $D_{5\%}$, D_{mode} and D_{max}) for different applied strains (0.15 - 0.7) against the grain size distribution (i.e. $D_{5\%}$, D_{mode} and D_{max}) for the sample with an initial grain size of 110 - 120 µm.

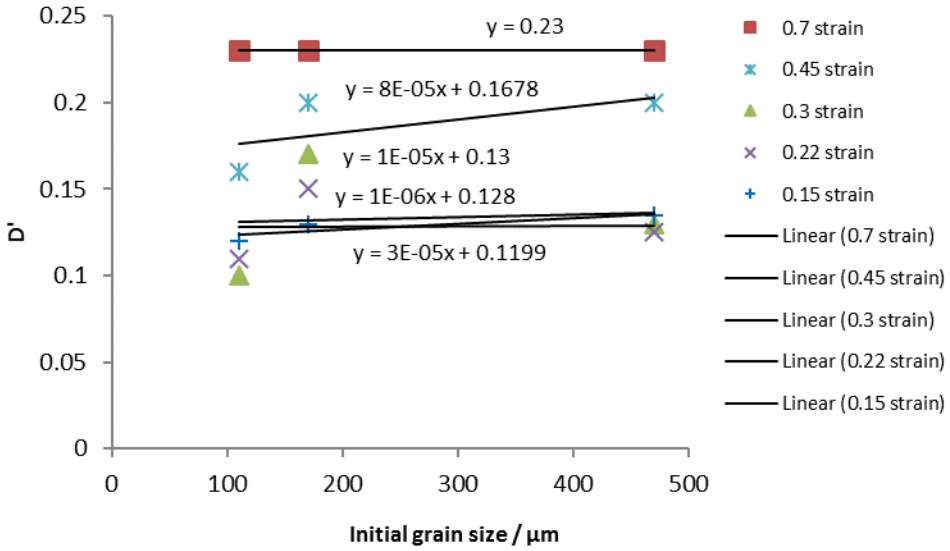

Figure 5.3: Plot of fitted *D'* values (for the $D_{5\%}$, D_{mode} and D_{max}) for different applied strains (0.15 - 0.7) against the grain size distribution (i.e. $D_{5\%}$, D_{mode} and D_{max}) for the sample with an initial grain size of 160 - 180 µm.

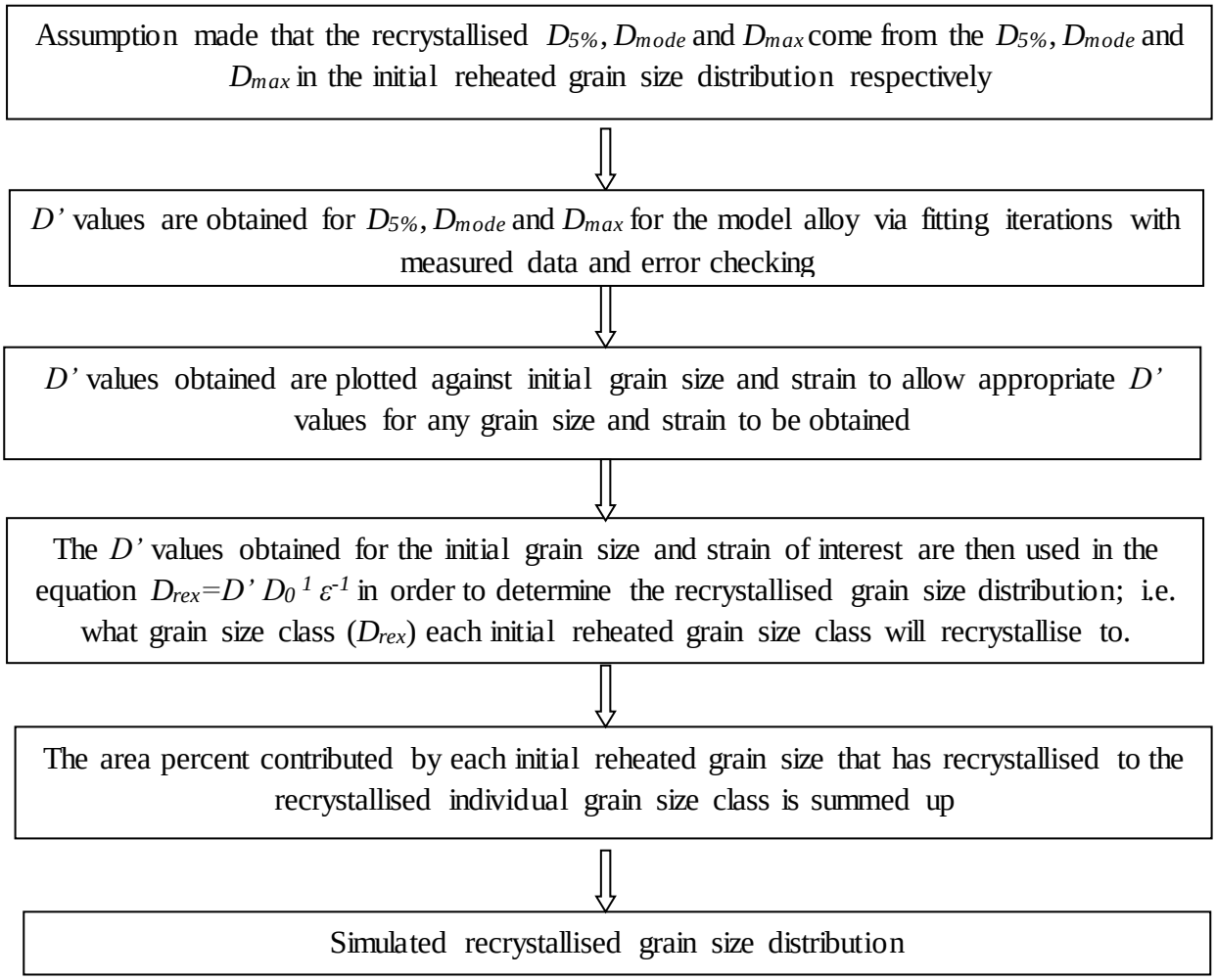

Figure 5.4: Flow diagram illustrating the modelling approach used to predict the recrystallised grain size distribution after deformation.

The values of *D'* varied from 0.1 to 0.45 to give the best fit possible to the measured data and are given in Tables 5.1 - 5.3 for the range of strains and initial grain sizes tested. It can be seen from Tables 5.1 - 5.3 that for the different strains and different grain sizes in the distribution, *D'* is a function of grain size and strain, that is, *D'* is $f\{D^*, \varepsilon\}$, where D* is the relative position of the grain size in the grain size range, i.e. *D'* is not the same for one grain size class when deformed to a single strain, but depends on where that grain size class is in the distribution. For example, for the 110 - 120 µm sample deformed to 0.15 strain, different *D'* values are required for the $D_{5\%}$ (0.11), D_{mode} (0.12) and D_{max} (0.14) to fit the recrystallised grain size distribution, Tables 5.1 - 5.3. The general trends for *D'* are that, the values increase with increasing strain and decreasing grain size. The observed trends for *D'* values in relation to strain and initial grain size will be discussed in detail in Section 5.1.5.

Table 5.1: Best *D'* for predicting the $D_{5\%}$ in a distribution for different applied strains.

Initial mode grain size / µm	**Initial $D_{5\%}$ grain size / µm**	**Strain**				
		0.15	**0.22**	**0.3**	**0.45**	**0.7**
50 - 60	20 - 30	0.14	0.2	0.24	0.33	0.4
110 - 120	60 - 70	0.11	0.12	0.13	0.18	0.2
160 - 180	100 - 120	0.12	0.11	0.1	0.16	0.23

Table 5.2: Best *D'* for predicting the D_{mode} in a distribution for different applied strains.

Initial mode grain size / µm	Strain				
	0.15	**0.22**	**0.3**	**0.45**	**0.7**
50 - 60	0.14	0.16	0.2	0.33	0.4
110 - 120	0.12	0.15	0.17	0.2	0.25
160 - 180	0.13	0.13	0.17	0.2	0.23

Table 5.3: Best *D'* for predicting the D_{max} in a distribution for different applied strains.

Initial mode grain size / µm	Initial D_{max} grain size / µm	Strain				
		0.15	**0.22**	**0.3**	**0.45**	**0.7**
50 - 60	110 - 120	0.15	0.2	0.25	0.34	0.45
110 - 120	230 - 240	0.14	0.15	0.14	0.2	0.25
160 - 180	440 - 460	0.14	0.13	0.13	0.2	0.23

Table 5.4 gives a comparison between the measured and fitted grain size classes using the variable *D'* approach, and it can be seen that the grain size classes are fitted well (mostly the correct grain size class is given by Equation 5.8, with occasional differences of up to 20 microns). Typical fitted and measured grain size distributions for different samples (50 - 60 µm, 110 - 120 µm and 160 - 180 µm) deformed to a strain of 0.7 are given in Figures 5.5 - 5.7.

Table 5.4: Comparison of the predicted (using best fit *D'* values given in Tables 5.1 - 5.3) and measured grain size distributions in terms of $D_{5\%}$, D_{mode} and D_{max}.

Initial mode grain size / µm	**Strain**	**Measured $D_{5\%}$ / µm**	**Predicted $D_{5\%}$ / µm**	**Measured mode grain size / µm**	**Predicted mode grain size / µm**	**Measured D_{max} / µm**	**Predicted D_{max} / µm**
50 - 60	0.15	20 - 30	20 - 30	50 - 60	50 - 60	110 - 120	110 - 120
	0.22	20 - 30	20 - 30	40 - 50	40 - 50	100 - 110	100 - 110
	0.3	10 - 20	10 - 20	40 - 50	40 - 50	90 - 100	90 - 100
	0.45	10 - 20	10 - 20	40 - 50	40 - 50	80 - 90	80 - 90
	0.7	10 - 20	10 - 20	30 - 40	30 - 40	70 - 80	70 - 80
110 - 120	0.15	40 - 50	40 - 50	80 - 90	100 - 110	200 - 210	200 - 210
	0.22	30 - 40	30 - 40	60 - 70	60 - 70	150 - 160	150 - 160
	0.3	20 - 30	20 - 30	50 - 60	50 - 60	110 - 120	110 - 120
	0.45	20 - 30	20 - 30	40 - 50	40 - 50	100 - 110	100 - 110
	0.7	10 - 20	10 - 20	30 - 40	30 - 40	80 - 90	80 - 90
160 - 180	0.15	100 - 120	80 - 100	160 - 180	160 - 180	420 - 440	420 - 440
	0.22	40 - 60	40 - 60	100 - 120	100 - 120	240 - 260	260 - 280
	0.3	20 - 40	20 - 40	80 - 100	60 - 80	220 - 240	220 - 240
	0.45	20 - 40	20 - 40	60 - 80	60 - 80	200 - 220	200 - 220
	0.7	20 - 40	20 - 40	40 - 60	40 - 60	140 - 160	140 - 160

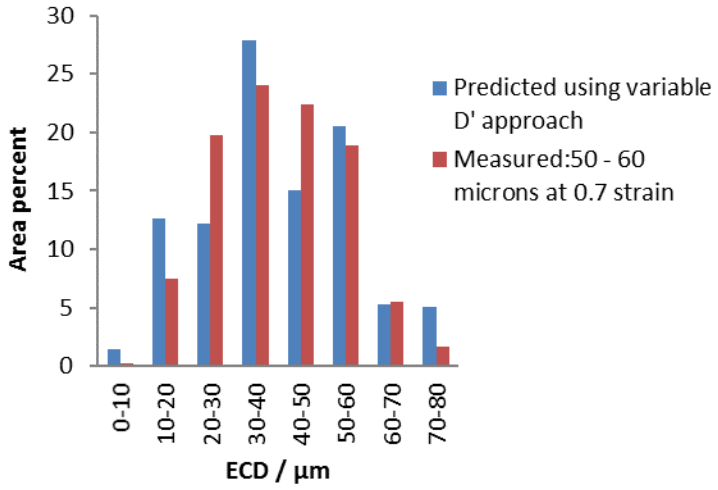

Figure 5.5: The recrystallised grain size distributions for the Fe - 30 wt - % Ni steel with an initial grain size of 50 - 60 µm deformed to a 0.7 strain and the predicted distribution based on the variable *D'* approach.

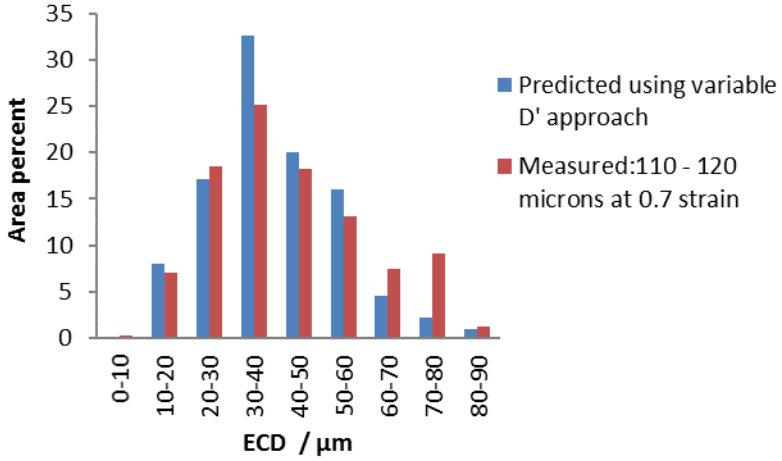

Figure 5.6: The recrystallised grain size distributions for the Fe - 30 wt - % Ni steel with an initial grain size of 110 - 120 µm deformed to a 0.7 strain and the predicted distribution based on the variable *D'* approach.

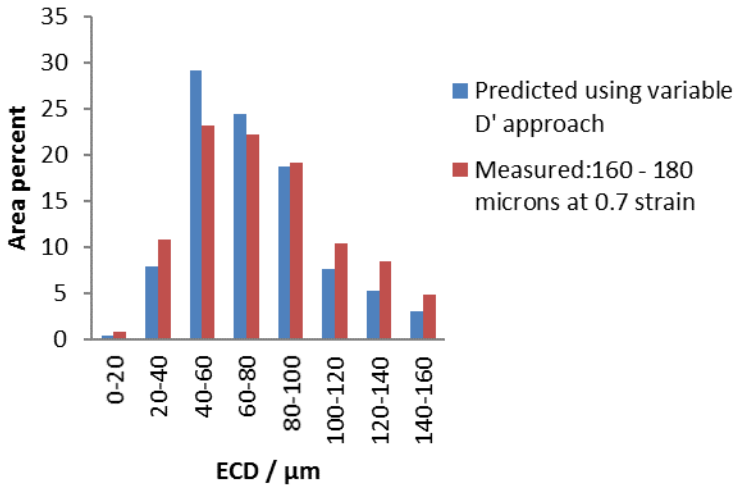

Figure 5.7: The recrystallised grain size distributions for the Fe - 30 wt - % Ni steel with an initial grain size of 160 - 180 µm deformed to a 0.7 strain and the predicted distribution based on the variable *D'* approach.

A comparison of NRMS error values obtained when Equation 5.8 and Equation 2.29, with the later using exponents determined for C - Mn steels (D' = 0.83, x = 0.67 and y = 1) are used is shown in Table 5.5. The values for NRMS errors obtained when Equation 2.29 is applied were initially given in Tables 4.8 - 4.10 in Chapter 4.

Table 5.5: Comparison of NRMS error values for the variable *D'* and constant *D'* (0.83) approach.

Grain size / μm	Stain	NRMS error	
		Variable *D'* approach (using Equation 5.8)	Constant *D'* approach (0.83) using Equation 2.29
50 - 60	0.15	0.19	1.00
	0.22	0.34	0.60
	0.30	0.29	0.75
	0.45	0.56	1.16
	0.70	0.36	1.83
110 - 120	0.15	0.49	1.07
	0.22	0.54	1.20
	0.30	0.36	0.72
	0.45	0.50	0.99
	0.70	0.34	1.20
160 - 180	0.15	0.58	0.86
	0.22	0.34	0.54
	0.3	0.27	0.57
	0.45	0.41	1.06
	0.70	0.24	1.36

5.1.3.1 Discussion on the sensitivity of grain size distribution fits to changes in *D'* values

Grain size distribution fits are sensitive to changes in *D'* values, for example for the 110 - 120 μm grain size material deformed to a strain of 0.15, a change in the *D'* value of 0.01 (from the best fit value of 0.11) leads to the largest grain size and the mode grain size being under predicted by 10 μm and 20 μm respectively, with an increase in NRMS error value of 0.12.

Furthermore, Tables 5.6 - 5.8 highlight the sensitivity of the fits to changes in *D'* values for different samples (in terms of the largest grain size (D_{max})) deformed to a strain of 0.3.

Table 5.6: *D'* sensitivity for the 50 - 60 µm sample (D_{max}) deformed to 0.3 strain.

Measured (D_{max}) / µm	***D'***	**Predicted / µm**	**NRMS**
90 - 100	0.2	80 - 90	0.45
	0.24	80 - 90	0.35
	0.25	90 - 100	0.29
	0.3	100 - 110	0.50

Table 5.7: *D'* sensitivity for the 110 - 120 µm sample (D_{max}) deformed to 0.3 strain.

Measured (D_{max}) / µm	***D'***	**Predicted / µm**	**NRMS**
110 - 120	0.09	70 - 80	0.86
	0.13	100 - 110	0.60
	0.14	110 - 120	0.36
	0.19	130 - 140	0.43

Table 5.8: *D'* sensitivity for the 160 - 180 µm sample (D_{max}) deformed to 0.3 strain.

Measured (D_{max}) / µm	***D'***	**Predicted / µm**	**NRMS**
220 - 240	0.08	160 - 180	0.34
	0.12	180 - 200	0.33
	0.13	220 - 240	0.27
	0.18	240 - 260	0.45

For the 50 - 60 μm sample a difference in NRMS errors ranging from 0.06 to 0.21 between the measured and the predicted grain size distributions is computed when *D'* values are either lowered (by 0.01 or 0.05) or increased (by 0.05). The changes in *D'* lead to D_{max} being either under predicted (by 10 μm for a *D'* change of 0.01 or 0.05) or over predicted (by 10 μm when *D'* is increased by 0.05) as shown in Table 5.6. Using different *D'* values for the 110 - 120 μm sample leads to variation in the NRMS error values (differences of 0.07 to 0.5 observed between different *D'* values) as shown in Table 5.7. The use of different *D'* values also leads to the largest grain size being over predicted by 20 μm when the *D'* value is increased by 0.05, and under predicted by 10 μm when the *D'* value is reduced by 0.01. If a lower *D'* value (by 0.05) than the proposed best fit value is used in Equation 5.8 in order to predict the recrystallised grain size, the largest grain size is under predicted by 40 μm as shown in Table 5.7.

Variation in the degree of fit (NRMS error value) when *D'* values other than the proposed best fit value (*D'* = 0.13) are also observed for the sample with an initial grain size of 160 - 180 μm deformed to a 0.3 strain as given in Table 5.8. Differences in the computed NRMS errors (degree of fits) range from 0.01 to 0.18. Varying different *D'* values also lead to the largest grain size being over predicted by 20 μm when the *D'* is increased by 0.05 and it is under predicted by 40 μm when *D'* is reduced by 0.01. The sensitivity of fits to changes in *D'* are less pronounced when *D'* values are increased (by 0.05) as compared to when they are lowered (by 0.05) for all grain sizes examined (in terms of the largest grain size). Generally, the sensitivity of fits to changes in *D'* values is less in the 110 - 120 μm (except for a decrease in *D'* of 0.05) and 50 - 60 μm material and more pronounced in the 160 - 180 μm sample.

5.1.4 Comparison of Equation 5.8 (x = 1, y = 1) and Equation 2.29 (x = 0.67, y = 1) in predicting recrystallised grain size distributions - varying *D'*

In order to make comparison between predictions made using Equation 5.8 with those made using Equation 2.29, with the exponents determined for C - Mn steels (x = 0.67 and y = 1) [5] because the steel used in this work does not contain Nb as discussed in Section 2.3.9. When the exponents (x = 0.67 and y = 1) proposed by Sellars [5] for C - Mn steels are used as inputs in Equation 2.29, it becomes Equation 5.9 (this is just for the purposes of this discussion). Equation 5.9 was therefore used to predict the grain size distributions based on values for $D_{5\%}$, D_{mode} and D_{max}.

$$D_{rex} = D' D_o^{0.67} \varepsilon^{-1} \qquad (5.9)$$

The values of *D'* varied from 0.45 to 1.75 $\mu m^{0.33}$ to give the best fit possible to the measured data for Fe - 30 wt - % Ni steel using Equation 5.9 for the range of strains and initial grain sizes tested, Figures 5.8 - 5.10.

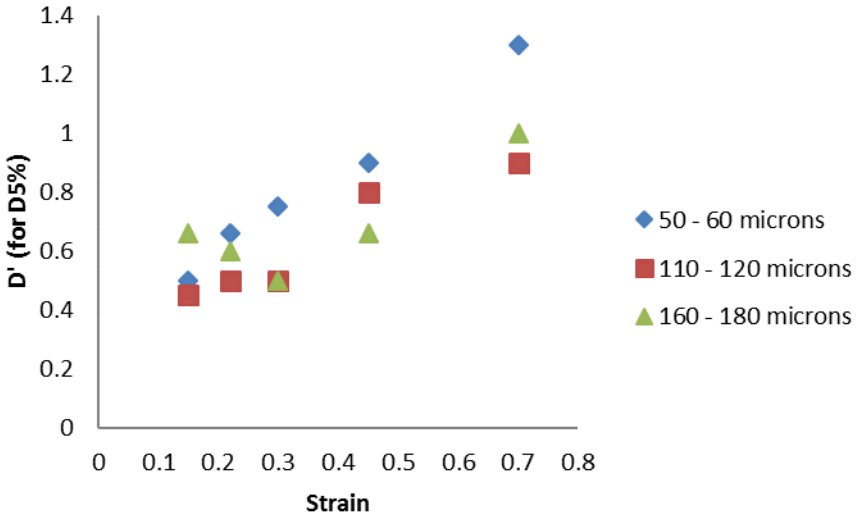

Figure 5.8: Relationship between *D'* and applied strain for the $D_{5\%}$ for different initial grain sizes using Equation 5.9.

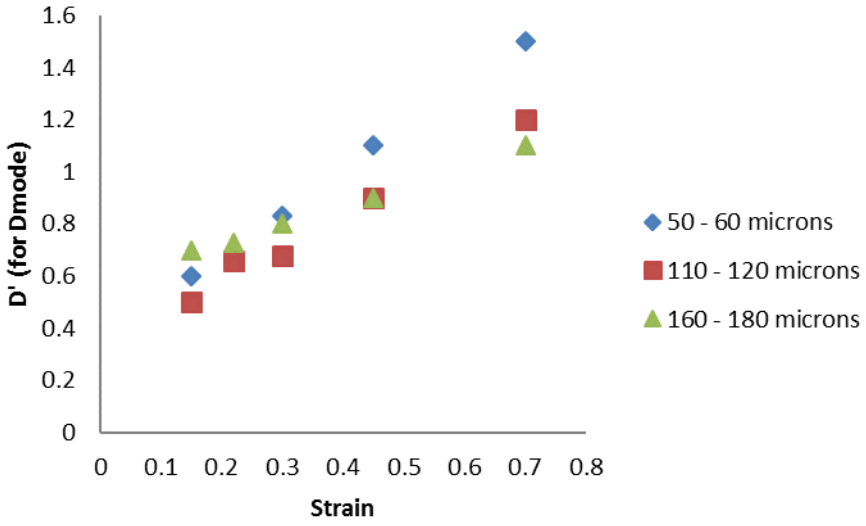

Figure 5.9: Relationship between *D'* and applied strain for the D_{mode} for different initial grain sizes using Equation 5.9.

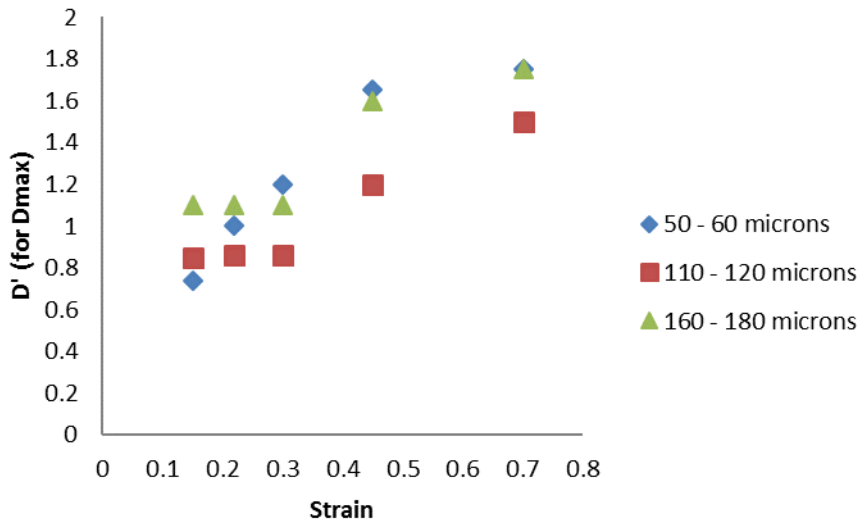

Figure 5.10: Relationship between *D'* and applied strain for the D_{max} for different initial grain sizes using Equation 5.9.

A comparison of NRMS errors obtained when Equation 5.8 and Equation 5.9 (using the best fit *D'* value) are used is shown in Table 5.9. The errors are reduced for all conditions when a D_o exponent of 1 (Equation 5.8) instead of 0.67 (Equation 5.9) is used. Similar trends for the

D' values with respect to strain and grain size are observed when Equation 5.9, shown in Figures 5.8 - 5.10 and Equation 5.8, shown in Figures 5.11 - 5.13, are applied, therefore the discussion that follows applies to both equations; the only difference being that the values for *D'* are much lower when Equation 5.8 is used compared to Equation 5.9.

Table 5.9: Comparison of NRMS error values for different D_o exponents.

Grain size / µm	Stain	NRMS error	
		Variable *D'* approach (using Equation 5.8)	**Variable *D'* approach (using Equation 5.9)**
50 - 60	0.15	0.19	0.23
	0.22	0.34	0.34
	0.30	0.29	0.54
	0.45	0.56	0.68
	0.70	0.36	0.36
110 - 120	0.15	0.49	0.61
	0.22	0.54	0.54
	0.30	0.36	0.52
	0.45	0.50	0.68
	0.70	0.34	0.48
160 - 180	0.15	0.58	0.75
	0.22	0.34	0.54
	0.3	0.27	0.4
	0.45	0.41	0.65
	0.70	0.24	0.44

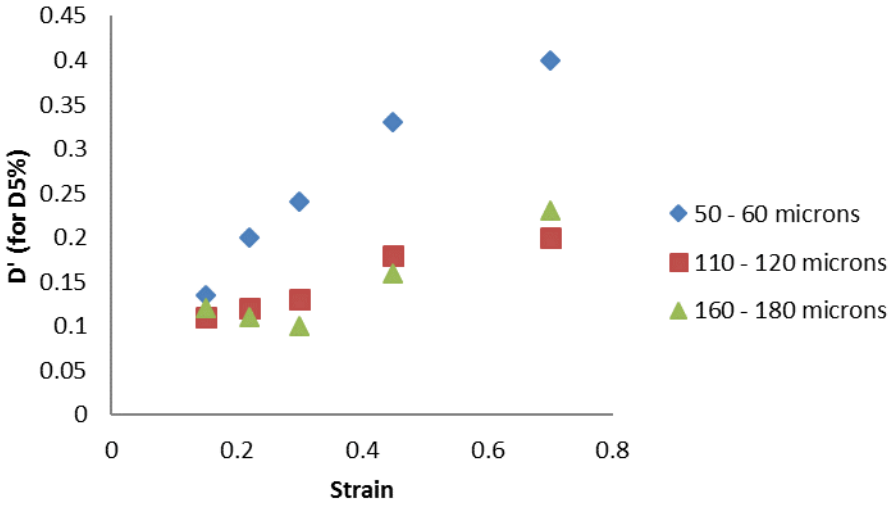

Figure 5.11: Relationship between *D'* and applied strain for the $D_{5\%}$ for different initial grain sizes using Equation 5.8.

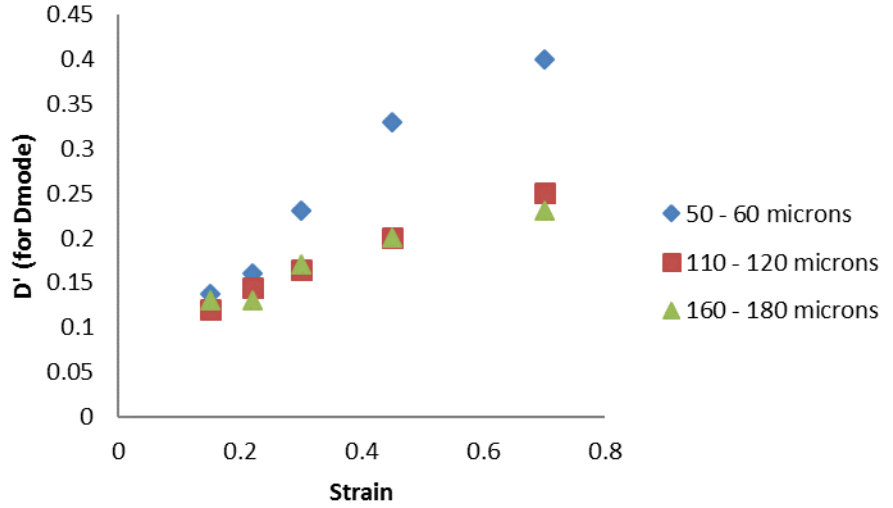

Figure 5.12: Relationship between *D'* and applied strain for the D_{mode} for different initial grain sizes using Equation 5.8.

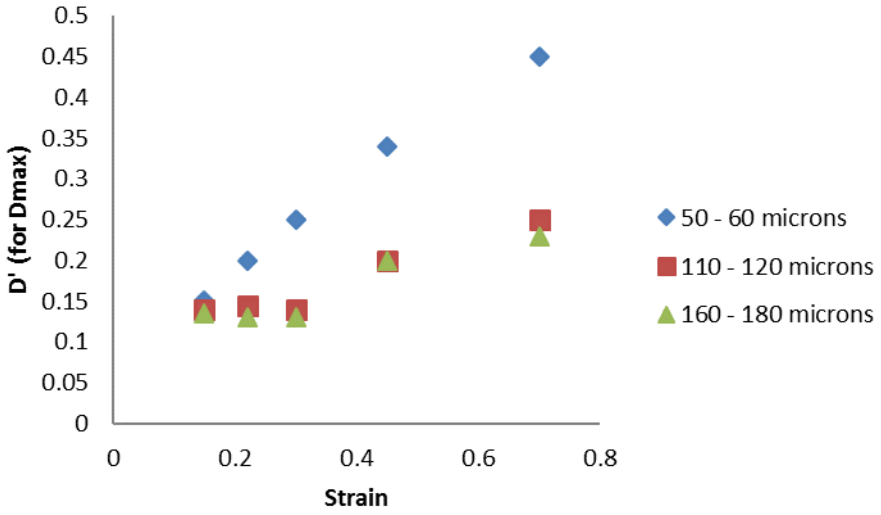

Figure 5.13: Relationship between *D'* and applied strain for the D_{max} for different initial grain sizes using Equation 5.8.

5.1.5 Factors influencing *D'* values

5.1.5.1 Effect of initial grain size on *D'* values

Comparison of the best fit *D'* values obtained for the different initial grain sizes using Equation 5.8 in Figures 5.11 - 5.13 show that D_o has a weaker effect for an increase in grain size for the larger grain size samples, that is from 110 - 120 µm to 160 - 180 µm, because the difference in *D'* values between 110 - 120 µm and 160 - 180 µm samples (in terms of D_{max}, D_{mode} and $D_{5\%}$) is observed to be about 0.01 at lower strains and 0.02 at higher strains. However, for a decrease in initial grain size to grain sizes below 100 µm (that is to 50 - 60 µm) a larger effect of D_o on *D'* is observed at higher strains (0.3, 0.45, 0.7) where, for example, a difference of 0.2 is observed between best fit *D'* values used in predicting the 50 - 60 µm sample (in terms of $D_{5\%}$) deformed to a strain of 0.7 and larger grain sizes ($D_{5\%}$ for 110 - 120 µm sample) deformed to a similar strain. At lower strains of 0.15 and 0.22, differences in *D'* values of up to 0.08 are observed between the finest initial grain size sample and samples with larger initial grain sizes. Overall *D'* is not very sensitive to change in D_o for

grains above 100 µm for all strains examined; however, it is very sensitive to changes in grain sizes at higher strains. Figures 5.11 to 5.13 generally show that for the 50 - 60 µm initial mode grain size *D'* values for the $D_{5\%}$, D_{mode} and D_{max} are higher than for the larger grains (110 - 120 µm and 160 - 180 µm) which might be due to differences in strain dependency (effectiveness of grain refinement) for example, in Chapter 4 it was shown that at a strain of 0.7 the 50 - 60 µm sample refined by 50 %, while the sample with a larger initial grain size had refined by 70 % at a similar strain due to the sample with a finer initial grain size not having enough available driving force for recrystallisation compared to the sample with a larger initial grain size. Finer grains will store more energy on deformation and so they should have a larger driving force (as already discussed in Section 2.3.3.2 [71 - 74, 76]), hence more efficient nucleation and refinement is expected, however, the larger stored energy is not as effective for fine grain sizes, when the strain is very high (0.7). This could be consistent with the higher strain triggering recovery and so provide less driving force for recrystallisation.

5.1.5.2 Effect of strain on *D'* values

Although the values of *D'* for the different initial grain size samples with respect to strain, Figures 5.14 - 5.16, show scatter, there is a general trend that *D'* values for all grain size categories considered ($D_{5\%}$, D_{mode} and D_{max}) and all initial mode grain sizes increase with increasing strain.

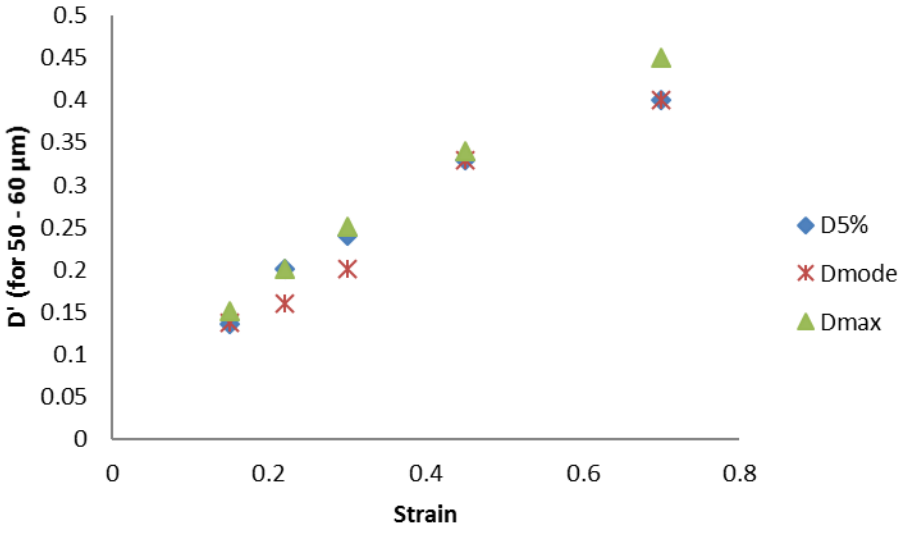

Figure 5.14: Effect of strain on the *D'* values for the Fe - 30 wt - % Ni steel with an initial grain size of 50 - 60 µm.

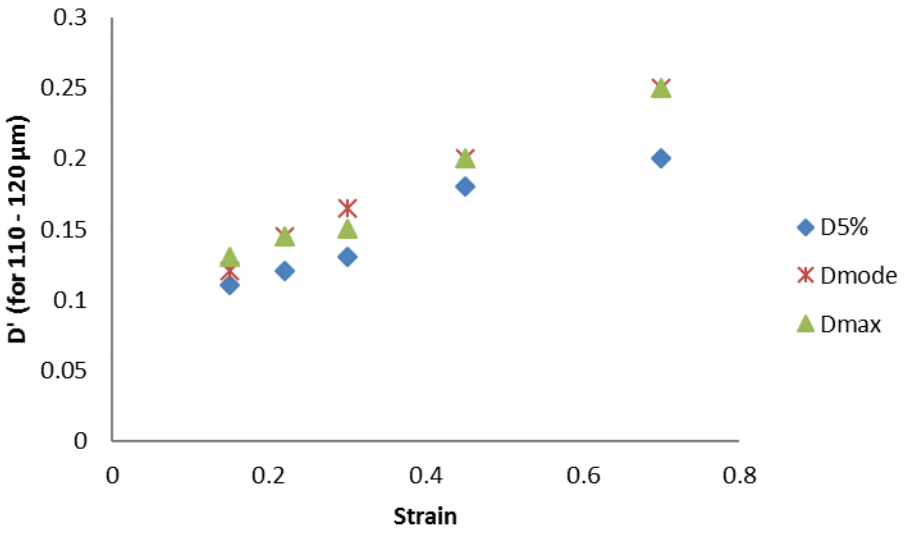

Figure 5.15: Effect of strain on the *D'* values for the Fe - 30 wt - % Ni steel with an initial grain size of 110 - 120 µm.

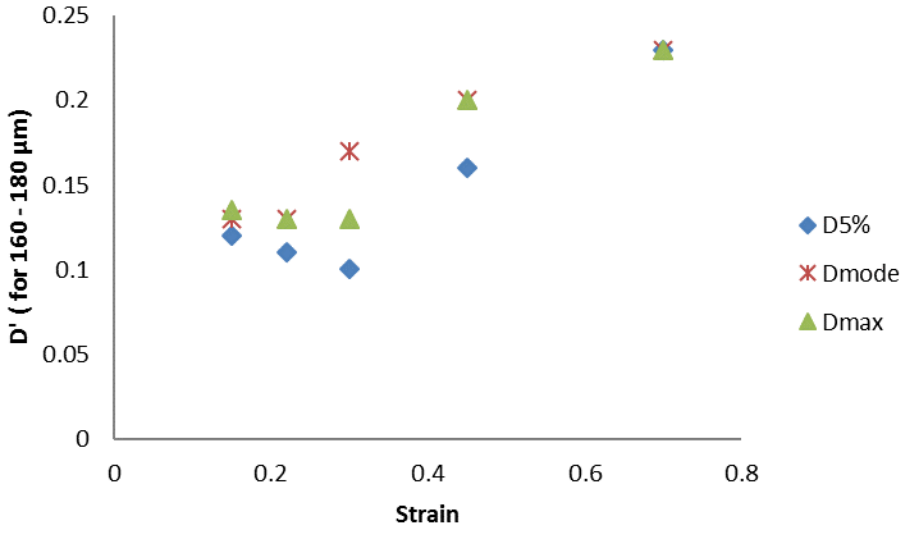

Figure 5.16: Effect of strain on the *D'* values for the Fe - 30 wt - % Ni steel with an initial grain size of 160 - 180 µm.

For the 50 - 60 µm grain size *D'* values increase (i.e. less effective nucleation as strain increases) with strain for the $D_{5\%}$, D_{mode} and D_{max}. For example, a change in strain from 0.3 to 0.45 leads to a change in *D'* of 0.09, 0.13 and 0.09 for the $D_{5\%}$, D_{mode} and D_{max} respectively. At higher strains the *D'* value for the D_{max} is higher (i.e. less effective nucleation) than for D_{mode} and $D_{5\%}$ which may be due to faster nucleation of smaller grains, which would lead some of the potential nucleation sites for the larger grains being used up, and hence less effective nucleation than expected, leading to an increase in *D'*, Figure 5.14. Preliminary in-situ recrystallisation investigations carried out using EBSD from a parallel study [171] on the Fe - 30 wt - % Ni steel with and without Nb have shown that finer grains recrystallise first. The Fe - 30 wt - % Ni steel used in [171] is the same material as used in this study. For the 110 - 120 µm initial grain size sample it is observed that at lower strains (0.15 - 0.3) the increase (0.01) in *D'* is less as compared to *D'* values computed at higher strains (0.45 - 0.7) where the increase in *D'* is slightly greater (differences between *D'* values are in the range of 0.03 - 0.06) than at low strains as shown in Figure 5.15. A change in strain from 0.3 to 0.45

for the 110 - 120 µm sample requires an increase in *D'* of 0.06 in order for the D_{max} to be reasonably predicted. For the 160 - 180 µm grain size the *D'* values for D_{mode} and D_{max} are higher than the $D_{5\%}$ except at 0.7 strain were *D'* values for $D_{5\%}$, D_{mode} and D_{max} converge (*D'* = 0.23). Below and up to a strain of 0.22 the values for *D'* decreases (by 0.01) and then increase rapidly (by 0.07) from 0.3 to 0.45 strain for the $D_{5\%}$ D_{mode} and D_{max}. Above 0.45, the rate of increase is reduced, as only an increase of 0.03 is observed for the D_{mode} and D_{max} as shown in Figure 5.16.

Generally, it can be seen in both Figure 5.15 and 5.16 that there is a very similar trend of *D*' increasing with increasing strain apart from the highest strain for the 110 - 120 µm and 160 - 180 µm. The data in Figure 5.14 for the 50 - 60 µm is more varied. To verify that the 50 - 60 µm sample behaves differently (in terms of nucleation) from the 110 - 120 µm and 160 - 180 µm grain sizes, stress-strain curves for the three different grain size samples (50 - 60 µm, 110 - 120 µm and 160 - 180 µm) deformed to a cold strain of 0.3 (0.7 equivalent hot strain), shown in Figure 5.17, were examined. From Figure 5.17, it can be seen that the finest initial grain size distribution (50 - 60 µm) material shows a greater work hardening rate of 0.51 than the other samples (0.46 and 0.48 for the 110 - 120 µm and 160 - 180 µm). This would suggest that the finest mode grain size distribution would be most different and the other two would be more similar. The rate of work hardening reflects the difference in stored energy in the different grain sizes because the rate of work hardening is influenced by the density of dislocations during deformation, which consequently influences the amount of energy stored (finer grains having a larger grain boundary area and hence a higher dislocation density), as discussed in Section 2.3.3.2 [16].

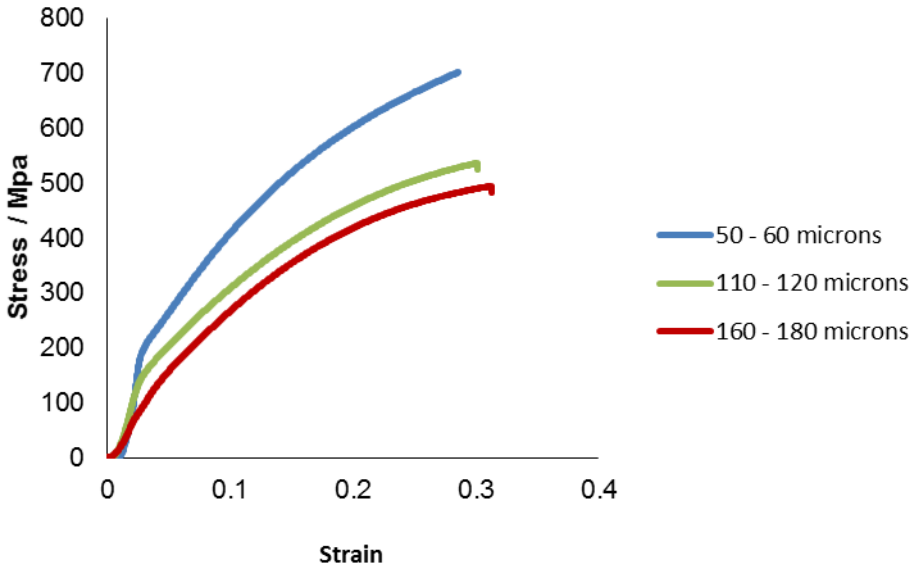

Figure 5.17: Stress-strain curves for three different initial mode grain sizes (50 - 60 µm, 110 - 120 µm and 160 - 180 µm) for the Fe - 30 wt - % Ni steel deformed to a cold strain of 0.3 (0.7 equivalent hot strain).

Furthermore, for the finer grain size there is a similar behaviour for the three *D'* values (for $D_{5\%}$, D_{mode} and D_{max}) with increasing strain except for the highest strain level. *D'* for the $D_{5\%}$ is more clearly lower for the 110 - 120 µm sample (Figure 5.15) than for the 50 - 60 µm sample (Figure 5.14). These trends show that (for all grain classes) the effectiveness of increased strain on grain size refinement is decreased as the strain increases (over the whole strain range for the 50 - 60 µm sample (Figure 5.14) but mostly above 0.3 for the 110 - 120 µm sample (Figure 5.15). This means that the nucleation rate does not increase at the same rate as strain increases, which could be due to a lower driving force, i.e. recovery increases as strain increases [83] or that the increase in strain does not activate a commensurate increased number of nucleation sites (or a combination of the two). While the latter may apply for the mode and maximum grain size classes it is unlikely to be the sole factor for the finest grain size classes as it has been argued that finer grains recrystallise first [171]. Generally, for the

larger samples (greater than 100 μm) it can be stated that *D'* is not sensitive to strain at low strains; however, it is a function of strain at higher strains.

5.1.5.3 Effect of the relative position of the grain size class within the grain size range on *D'* values

Figure 5.14 illustrates that, there is no specific trend observed in the behaviour of the *D'* values for the $D_{5\%}$, D_{mode} and D_{max} (in relation to the position of the grain size class in the distribution) for the sample with 50 - 60 μm initial grain size. It can be seen from Figure 5.14 that there are no significant differences observed between *D'* values used to predict the $D_{5\%}$, D_{mode} and D_{max} at strains of 0.15 (*D'* values range from 0.14 to 0.15) and 0.45 (*D'* values range from 0.33 - 0.34). At 0.22 and 0.3 strains, there is a difference of 0.04 observed between the $D_{5\%}$ and both the D_{mode} and D_{max}. At higher strains the *D'* value for predicting D_{max} is higher than that for predicting the D_{mode} and $D_{5\%}$. However, from Figure 5.15 it can be seen that for the 110 - 120 μm samples the *D'* values for D_{mode} and D_{max} are higher than the $D_{5\%}$ by at least 0.02 - 0.05. Similarly, for the 160 - 180 μm sample the *D'* values for D_{mode} and D_{max} are consistently higher than that for the $D_{5\%}$ but only up to 0.45 strain as shown in Figure 5.16. The D_{max} and D_{mode} values are higher by 0.02 - 0.04 across all the strains.

Even though, no specific trend is observed in the behaviour of the *D'* values for the $D_{5\%}$, D_{mode} and D_{max} (with regard to the position of the grain size class in the distribution), nucleation of recrystallised grains from boundaries of deformed fine grains would, where these abut coarser grains, remove potential nucleation sites so that, when the coarser grains in the distribution do recrystallise, they do so to a smaller number of recrystallised grains than theoretically possible for their grain boundary area. Therefore, the refinement for these grain size classes is not as much as would be expected if they had been the $D_{5\%}$ or the mode of a

distribution making the 'efficiency' of grain nucleation less and so leading to an increase in *D'*. Hence, the *D'* value for a given grain size may generally differ depending on where that grain size class is positioned in the grain size distribution.

5.1.6 Comparison of *D'* values used to predict the recrystallised mode grain size for literature data

To verify the effect of strain on *D'* observed while investigating the Fe - 30 wt - % Ni steel Equation 5.8 has been fitted to recrystallised mode grain sizes in the literature [18] in order to determine the best fit *D'* values. Literature data for the Fe - 30 wt - % Ni steel with an initial grain size of 310 microns shows that the *D'* value increases with strain [18]. The effect of strain on *D'*, that is, the increase in *D'* values with strain, observed in this work (Section 5.1.5.2) agrees with that observed from fitting Equation 5.8 to recrystallised mode grains reported in [18] as shown in Table 5.10. Consideration of the *D'* values for different grain size classes in a distribution has not yet been reported. The observations so far suggest that a constant *D'* cannot simply be used to predict the entire grain size distribution as it depends on where the grain size class is in a distribution (as well as depending on strain and initial grain size).

Table 5.10: *D'* used in predicting the mode grain size for Fe - 30wt - % Ni steel from literature data for an initial mode grain size of 310 μm [18].

Strain	D_{rex} / μm	*D'*
0.25	102	0.10
0.5	73	0.24

5.1.7 Effect of grain size on the stored energy after deformation

As discussed in Chapter 2 (Section 2.3.3), the energy of deformation is stored in the form of statically stored dislocations and geometrically necessary dislocations [68, 71, 86]. At lower strains (less than 0.4 [71, 72]) the initial grain size influences the stored energy after deformation as the dislocation density at these low strains has been shown to be dependent on both strain and initial grain size (grain boundary per unit volume), as shown in Equation 2.10 in Section 2.3.3.3. A fine grain-sized material has been reported to have a higher stored energy as compared to a coarse grain-sized material for a given plastic strain. This has been argued to be due a fine-grained material having a greater grain boundary area per unit volume (higher dislocation density) as compared to the coarse-grained material as discussed in Section 2.3.3.2 [71 - 74, 76].

Table 5.11 shows measured (using differential scanning calorimetry) stored energy values for different initial grain sizes (mode grain size classes of 50 - 60 µm, 110 - 120 µm and 160 - 180 µm deformed to a cold strain of 0.3 (0.7 equivalent hot strain)). It can be seen from Table 5.11 that the material with the smallest initial mode grain size has a higher measured stored energy (2.8 J / g); this is due to reasons given in previous paragraphs and discussed in detail in Section 2.3.3.2, which are consistent with observations in literature reports [71 - 74, 76].

Table 5.11: Measured stored energies using DSC for different initial grain sizes.

Grain size / µm	Average measured / J / g	Standard deviation for measured values
50 - 60	2.8	1
110 - 120	2.45	1
160 - 180	1.63	0.7

Recrystallisation start and finish temperatures were observed to be slightly different for the grain sizes examined. For instance, for the 50 - 60 µm grain size the recrystallisation range was approximately 360 ^{o}C to 830 ^{o}C whereas for the 160 - 180 µm initial grain size the recrystallisation range was approximately 400 ^{o}C to about 850 ^{o}C, which further supports the stored energy differences observed in the deformed samples with different initial grain sizes. Typical DSC curves (first and second DSC runs on the sample) are shown in Figures 5.18 - 5.20 for a Fe - 30 wt - % Ni steel with initial grain sizes ranging from 50 - 60 µm to 160 - 180 µm deformed to a cold strain of 0.3 (0.7 equivalent hot strain). For example, Figure 5.8 demonstrates that recrystallisation starts from around 390 ^{o}C and ends around 840 ^{o}C for the sample with an initial grain size of 110 - 120 µm. It can be seen from Figures 5.18 - 5.20 that only one exothermic peak (corresponding to recrystallisation) occurs in the first run, while no exothermic peaks are observed in the second run, suggesting that all the stored energy has been used up; DSC curves were discussed in detail in Section 2.3.3.

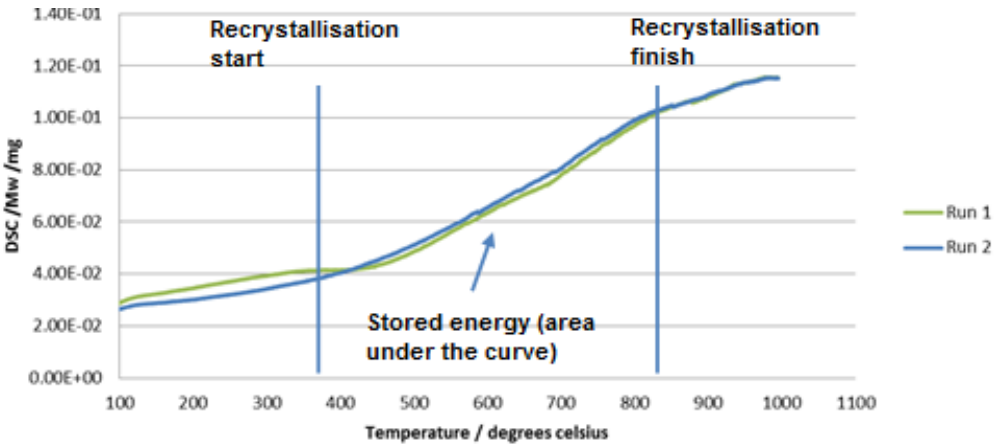

Figure 5.18: Typical DSC curves for sample deformed to 0.3 (0.7 equivalent hot strain) with an initial grain size of 50 - 60 µm heat treated from 50 to 1000 ^{o}C at a heating rate of 10 ^{o}C / minute.

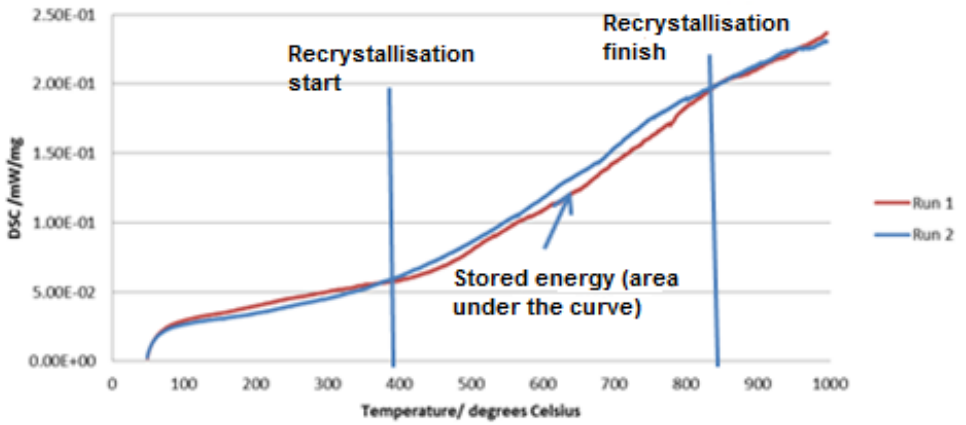

Figure 5.19: Typical DSC curves for sample deformed to 0.3 (0.7 equivalent hot strain) with an initial grain size of 110 - 120 µm heat treated from 50 to 1000 °C at a heating rate of 10 °C / minute.

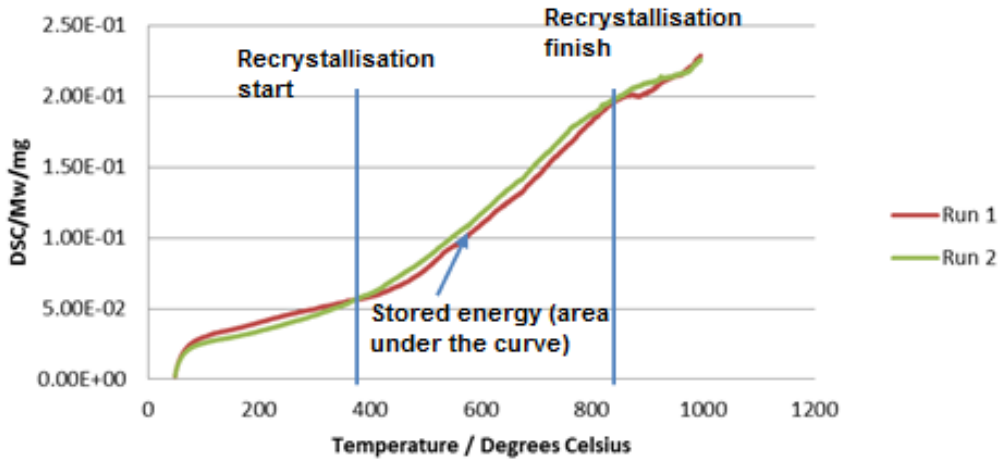

Figure 5.20: Typical DSC curves for sample deformed to 0.3 (0.7 equivalent hot strain) with an initial grain size of 160 - 180 µm heat treated from 50 to 1000 °C at a heating rate of 10 °C / minute.

To verify whether the specimens had completely softened or not, interrupted DSC tests were carried out at temperatures between 400 °C and 850 °C. The hardness values for the samples from interrupted DSC tests were measured, as well as for the annealed samples (reheated at

1300 °C for 5 minutes), and the deformed samples (0.7 equivalent hot strain). Although, hardness measurements cannot be used to accurately determine the fraction recrystallised as they do not distinguish recovery, they can however be used to indicate whether dislocation annihilation (stored energy consumed / softening) has occurred or not; relatively similar hardness values for an annealed sample to that of a deformed and annealed sample (with a similar grain size) would indicate that there is no residual strain in the deformed sample after recrystallisation and all the stored energy has been used up as discussed in Section 2.3.7 [60, 61, 169]. Table 5.12 shows the results obtained from micro hardness tests on interrupted, deformed and annealed samples. The hardness values for the annealed samples and the DSC samples (160 - 180 µm deformed to a strain of 0.7 equivalent hot strain) heated up to 850 °C are similar indicating that the specimen heated to 850 °C was fully softened while the samples (deformed 160 - 180 µm) heated treated up to 600 °C were partially softened based on the hardness values obtained in comparison to the hardness values for the annealed sample. This verifies earlier suggestions in previous paragraphs that complete softening (recrystallisation) occurs around 850 °C for the sample with an initial grain size of 160 - 180 µm. Hardness tests were only carried out for the sample with an initial grain size of 160 - 180 µm and as such more tests need to be carried out for samples with initial grain sizes of 50 - 60 µm and 110 - 120 µm deformed to a cold strain of 0.3 (0.7 equivalent hot strain).

Table 5.12: Micro hardness values from interrupted DSC tests for the 160 - 180 µm sample.

Sample condition	Average micro hardness value (HV0.3)	Standard deviation
Annealed	116	3.1
50 - 600 °C (DSC run)	204	3.7
50 - 850 °C (DSC run)	116	9.5
Deformed (0.3 strain)	220	14.9

5.2 Summary

In this chapter, Equation 2.29 ($D_{rex} = D' D_o^{0.67} \varepsilon^{-1}$) has been modified in order to predict the recrystallised grain size distribution based on classical theory for the rate of nucleation and compared to the modified equation. Equation 5.8 ($D_{rex} = D' D_o^{1} \varepsilon^{-1}$) has been proposed for predicting recrystallised grain size distributions in order to predict the entire recrystallised grain size distribution considering all strain and grain size ranges.

When considering the optimum *D'* value to fit the $D_{5\%}$, D_{mode} and D_{max} values it has been found that at low strain values (up to 0.3) *D'* is not very sensitive to strain; however, it is sensitive to strain at higher strains for all initial grain sizes examined, except for the 50 - 60 μm where sensitivity of *D'* to strain is observed even at lower strains. Generally, the dependency of *D'* on strain seems not to follow a specific trend with strain levels and initial grain sizes. *D'* is also sensitive to the relative position of the grain size in the grain size range (D*); *D'* values are consistently higher for D_{max} and D_{mode} than $D_{5\%}$ for all grain sizes examined (except for the 50 - 60 μm initial grain size were no specific trend is observed). Therefore, generally *D'* is a function of strain and relative position of grain size ($f\{\varepsilon, D^*\}$).

CHAPTER – 6

Prediction and verification of grain size distributions in different steel grades

An analysis of grain size distributions before and after recrystallisation in the model Fe - 30 wt - % Ni steel was used to develop the relationship between *D'* using the modified Equation 5.8 (presented and discussed in Chapter 5) and strain and grain size within the distribution. Three initial mode grain sizes were considered: 50 - 60 μm, 110 - 120 μm and 160 - 180 μm. In order to verify and establish limits for the use of the modified Equation 5.8 in predicting recrystallised grain size distributions after deformation, the variable *D'* approach has been applied to grain size distributions (ranging from 50 - 60 μm to 360 - 380 μm) for different steel grades available in the open literature (HSLA steel [4] and 9Cr forging steel [189]) and from other material available at the University of Birmingham (high strength strip steel, and Fe - 30 Ni - 0.044 Nb steel). Initial grain size distributions for all the examined steels are given in Figure 6.1 and 6.2. Figures 6.1 and 6.2 show that the grain size distributions for the steels examined are all unimodal, albeit skewed to larger grain sizes. Table 6.1 summarises the initial mode grain sizes, heat treatment conditions, precipitates present and their dissolution temperatures (predicted using Thermo-Calc software) for the steels considered. Information on precipitate dissolution temperatures for the different steels has been used in this chapter to establish whether there is an influence of precipitates (e.g. Nb (C, N) and TiN) and alloying elements in solution (such as Nb) on the recrystallised grain size.

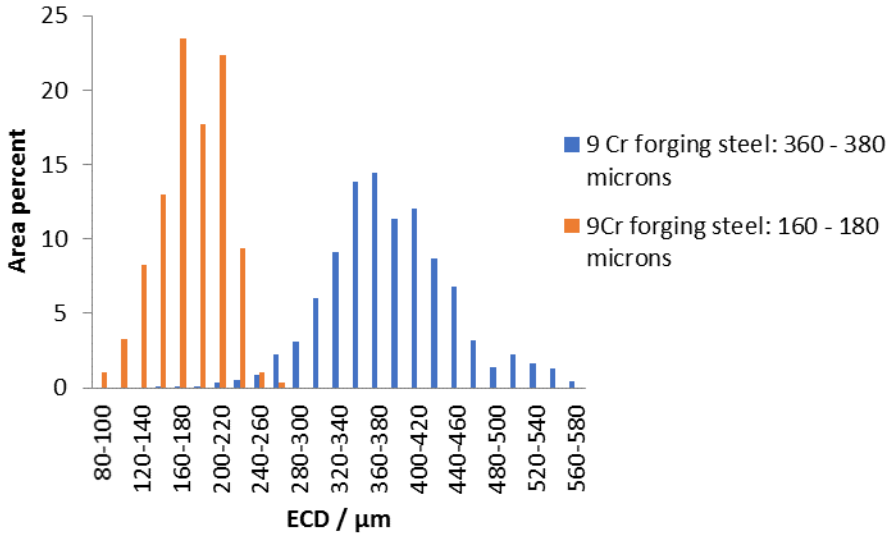

(a)

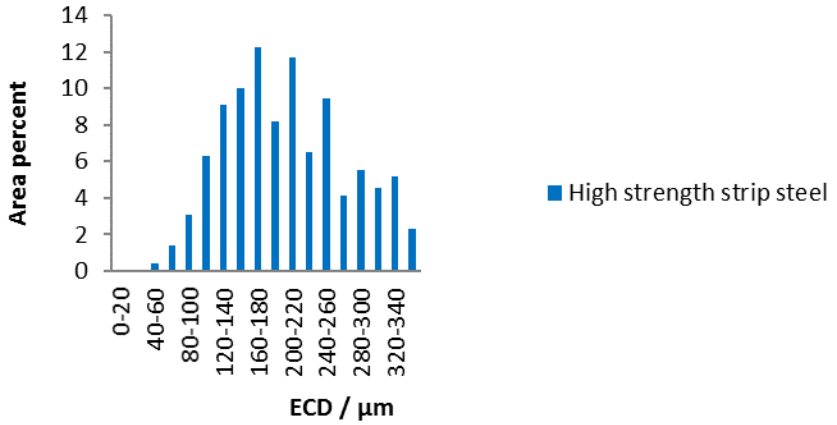

(b)

Figure 6.1: Initial grain size distributions for highly microalloyed steels (a) 9Cr forging steel [189] (b) high strength strip steel.

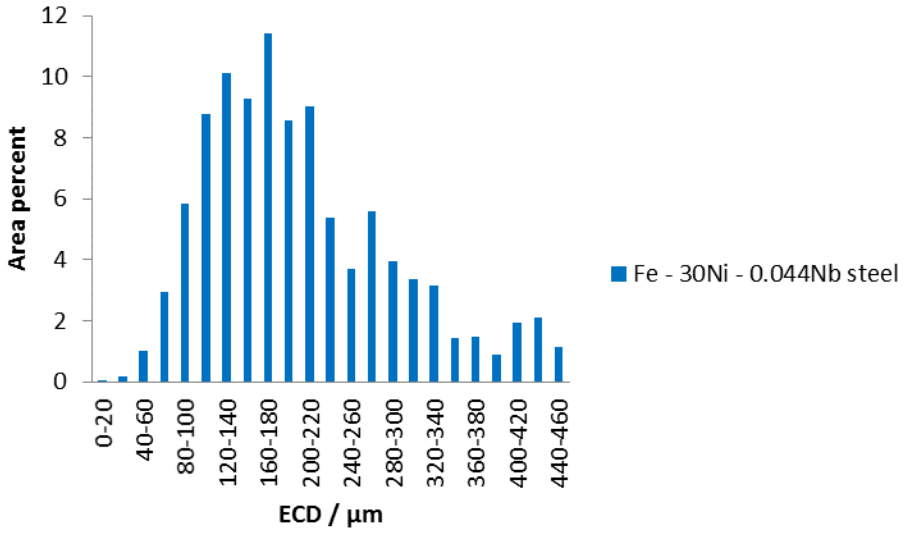

(a)

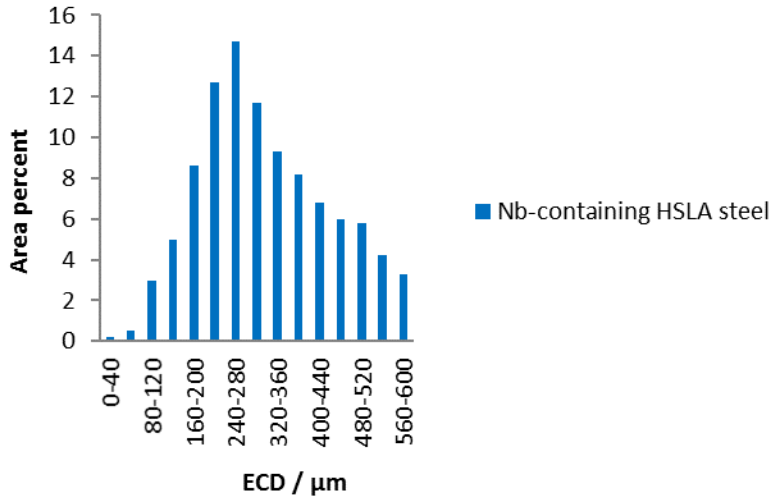

(b)

Figure 6.2: Initial grain size distributions for Nb microalloyed steel (a) Fe - 30Ni - 0.044Nb steel (b) Nb-containing HSLA steel [4].

Table 6.1: Summary of generated and literature mode grain sizes, heat treatment conditions and predicted precipitate dissolution temperatures for different materials.

Material	**Mode grain size / μm**	**Heat treatment Temperature / °C**	**Predicted precipitate dissolution temperatures / °C**
Fe - 30Ni - 0.044Nb	110 - 120	1150 °C for 4 hours, 0.15 strain and recrystallised	TiN; 1185 °C
	160 - 180	1150 °C for 4 hours	Nb (C, N); 1020 °C
HSLA steel [4]	240 - 280	1225 °C for 60 minutes	(Nb, Ti, V) (C, N); 1210 °C
9Cr forging steel [189]	170 - 180	Reheated to 1200 °C then deformed	(V, Cr) (C, N); 1185 °C
	360 - 380		Nb (C, N); 1140 °C
High strength strip steel	160 - 180	1200 °C for 5 minutes	Nb (C, N); 1135 °C TiN; 1370 °C

The simple variable *D'* approach developed in Chapter 5, based on the observation that the best fit value for *D'* in Equation 5.8, generally increases with grain size class in a grain size distribution at a given strain, has been used in this work to predict the recrystallised grain size distributions after deformation for the steels listed in Table 6.1. The procedure used in determining the full grain size distribution for any steel grade, strain and initial grain size using the simple variable *D'* approach is given in Chapter 5. This procedure is based on an assumption that the recrystallised $D_{5\%}$, D_{mode} and D_{max} grain classes come from the $D_{5\%}$, D_{mode} and D_{max} grain classes in the initial grain size distribution respectively. Based on observations from grain size measurements carried out in this work, only grain sizes above 5 μm are optically resolvable and hence initial grain sizes (D_o) of 5 μm will be considered to be the minimum (D_o > 5 μm). Normalised root mean square (NRMS) errors obtained when the variable *D'* values are used in predicting the measured grain size distribution for the Fe - 30 wt - % Ni steel range from 0.19 to 0.58, as shown in Table 5.5 in Chapter 5, as such any NRMS errors below and up to 0.60 are taken as representing a good fit between the measured and predicted grain size distribution in this work and anything above a NRMS error of 0.60 would indicate that the measured and the predicted grain size distributions are not fitted very well.

6.1 Verification and prediction for Nb microalloyed steel

The variable *D'* approach was applied to predict the recrystallised grain size distributions for the HSLA Nb microalloyed steel [4] and the Fe - 30 wt - % Ni - 0.044 wt - % Nb steel (data produced in this project). It must be noted here that in literature different strain exponent values are used for the Nb steels (y = 0.67) and C - Mn (y = 1) which suggests that the Nb microalloyed steel has a greater dependence on strain than C - Mn steels. This means that the Nb-containing steel is expected to refine more than C - Mn steels [5]. However, the same

initial grain size exponent value (x = 0.67) is used in Equation 2.29 for both Nb and C - Mn steels [5]. In the current study the same value of strain exponent (y = 1) and initial grain size exponent (x = 1) is proposed based on classical theory for rate of nucleation.

6.1.1 Predicting recrystallised grain size distributions for the Fe - 30 wt - % Ni - 0.044 wt - % Nb steel

When the variable *D'* approach is used to predict the recrystallised grain size distribution for a Nb-containing Fe - 30 wt - % Ni steel with initial mode grain sizes of 100 - 120 μm and 160 - 180 μm deformed to 0.15 strain, Figure 6.3 and 6.4, there is a reasonable agreement with the measured data (NRMS error of 0.49) for the smaller initial mode grain size, Figure 6.3, however, for the sample with an initial grain size of 160 - 180 μm, Figure 6.4, the fit is not as good (NRMS error of 0.86) as the largest grain size is predicted to be 400 - 420 μm (which is about 8 % grain refinement) instead of the measured 240 - 260 μm (44 % grain refinement). However, when Equation 2.29 is employed using the exponents reported in the literature for Nb-containing steels (D' = 1.1 μm $^{0.33}$, x = 0.67 and y = 0.67 [5]) an improvement in the fit is observed for the 160 - 180 μm grain size material (NRMS error of 0.53) although the agreement is not as good for the 100 - 120 μm grain size material (NRMS error of 0.75). A *D'* value of 1.1 μm $^{0.33}$ is used as it represents better agreement between the measured and predicted recrystallised grain size distributions compared to when *D'* values of 0.66 and 1.86 μm $^{0.33}$ (also proposed in the literature [5] for Nb-containing steels) are used; for example, for the 160 - 180 μm sample deformed to a strain of 0.3, NRMS errors of 1.5, 0.5 and 1.86 are computed when *D'* values of 0.66 [10], 1.1[9] and 1.86 μm $^{0.33}$ [7] are used in Equation 2.29 respectively. Furthermore, a *D'* value of 1.1 μm $^{0.33}$ is used because the grain size for the Fe - 30Ni steel - 0.044 Nb (100 - 120 μm and 160 - 180 μm) falls within the grain size range (55 -

220 μm) used to obtained a *D'* value of 1.1, information on different *D'* values proposed in the literature is given in Table 2.15 in Chapter 2. A *D'* value of 1.1 μm $^{0.33}$ was applied to all the steels examined in this chapter, unless otherwise stated. Possible reasons for the poorer agreement of the variable *D'* approach for the larger mode grain size material will be discussed in Section 6.1.1.1.

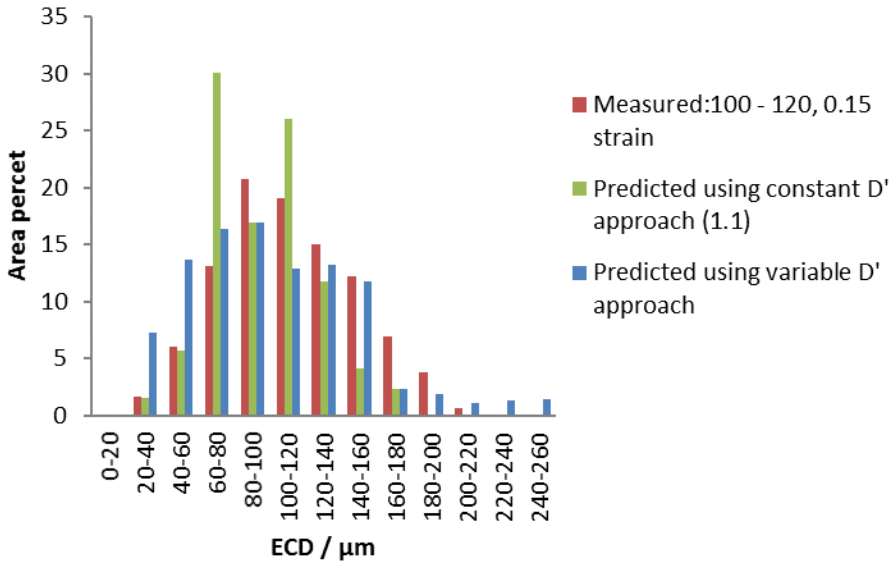

Figure 6.3: Recrystallised grain size distributions for the Nb - containing Fe - 30Ni steel with an initial mode grain size of 100 - 120 μm deformed to a 0.15 strain and predicted distributions based on the variable *D'* approach and Equation 2.29 (*D'* = 1.1 μm$^{0.33}$, x = 0.67 and y = 0.67).

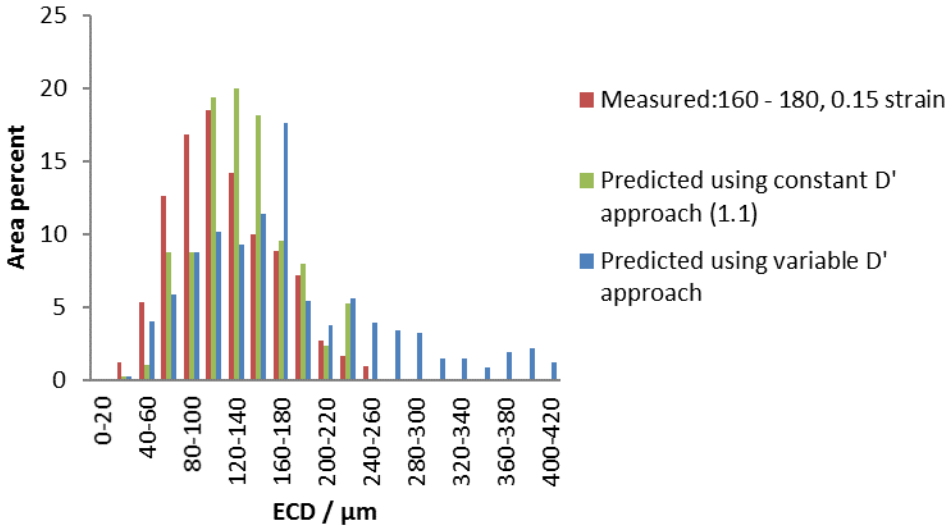

Figure 6.4: Recrystallised grain size distributions for the Nb - containing Fe - 30Ni steel with an initial mode grain size of 160 - 180 µm deformed to a 0.15 strain and predicted distributions based on the variable *D'* approach and Equation 2.29 (*D'* = 1.1 $\mu m^{0.33}$, x = 0.67 and y = 0.67).

It is apparent from Figure 6.5 a and b that all the grain size classes in the grain size distribution for the samples with an initial mode grain size of 160 - 180 µm and deformed to a strain of 0.3 and 0.7 are very well predicted (using the variable *D'* approach) with a NRMS error of 0.31 and 0.4. Overall, for all conditions examined for the Nb-containing Fe - 30Ni steel, the variable *D'* approach seems to predict reasonably well the smallest ($D_{5\%}$) and mode grain size in a given distribution, however the largest grain sizes are not very well fitted (for strains lower than 0.3) as shown in Figure 6.4 and 6.5.

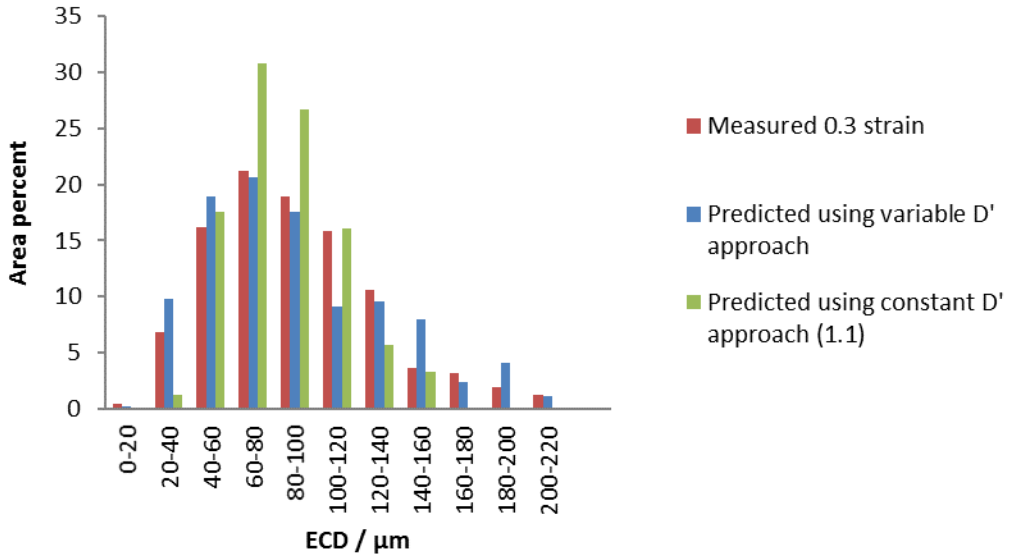

(a)

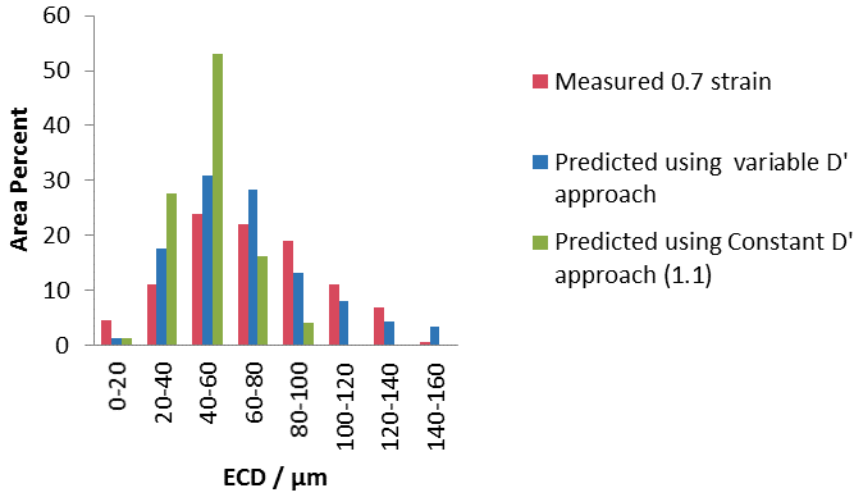

(b)

Figure 6.5: Recrystallised grain size distributions for the Nb-containing Fe - 30Ni steel with an initial mode grain size of 160 - 180 µm deformed to a range of strains and predicted distributions based on the variable *D'* approach and Equation 2.29 (*D'* = 1.1 $\mu m^{0.33}$, x = 0.67 and y = 0.67) for (a) 0.3 strain and (b) 0.7 strain.

6.1.1.1 Discussion on the causes of discrepancy between predicted and measured grain size distributions for the Fe - 30 wt - % Ni steel containing Nb

Discrepancies observed between the measured and predicted grain size distributions in terms of large grain sizes in the distribution using the variable *D'* approach could be due to a number of factors. Inaccuracies in the measured initial grain size distribution as the prediction of the recrystallised grain size distribution is based on the measured initial grain size could lead to discrepancies in the fits. This would affect all strains, however inaccuracies in the measured initial grain size in the current study were reduced by considering a large number of grains (about 700 - 1000 grains) when constructing a grain size distribution [4]. This would be similar for all the steels / conditions examined, however no consistent error has been observed in the current work. The reasons for the poorer agreement of the variable *D'* approach for the larger mode grain size material deformed to 0.15 strain may therefore be due to the stored energy of deformation being underestimated when equivalent cold strains were determined, which could affect the sample with a larger initial grain size (160 - 180 μm) more than the sample with a finer initial grain size (100 - 120 μm) deformed to a similar strain (0.15) as the larger grain size sample would have more available stored energy compared to the finer grain size sample and therefore a narrower distribution would be realised for the initial larger grain size. This is due to finer initial grain sized samples having a larger grain boundary area, which means that most of the stored energy goes into maintaining grain boundary compatibility during plastic deformation leaving less energy to drive recrystallisation. It is also possible that discrepancies in predicting the larger initial grain size deformed at lower strains (0.15) may occur due to the fact that strain may still be inhomogeneous, which could affect the sample with an initial grain size of 160 - 180 μm more than the sample with an initial grain size of 100 - 120 μm.

The influence of precipitates and solute atoms on the recrystallised grain size could be another source of disparities in the fits. Table 6.1 shows that TiN and Nb (C, N) precipitates can form in the Nb-containing Fe - 30Ni steel and that Nb will be completely in solution at 1020 ^{o}C while TiN can provide grain boundary pinning up to 1185 ^{o}C. The heat treatment for this steel was carried out at 1150 ^{o}C and so Nb would be expected to be in solution and as a result solute drag (reduction in the mobility of grain boundaries due to segregation of microalloying elements such as Nb and V to the grain boundaries) might occur which may retard recrystallisation kinetics. It was discussed in Section 2.3.6.2 that some researchers argue that solute drag does not affect the recrystallised grain size because solute atoms only have an effect on the growth process rather than recrystallisation nucleation [5, 11, 12, 24, 26, 28, 39, 56]. It was also discussed in Section 2.3.8.2 that strain induced precipitates can pin moving boundaries through the formation of fine Nb (C, N) precipitates (about 4 - 10 nm [4, 18]) during deformation, thereby also retarding the recrystallisation kinetics (increasing the recrystallisation stop temperature, RST) [4, 5, 18, 24, 47, 170].

Contrary to the reports that solute drag has no effect on recrystallisation nucleation, Miao *et al.* [55] claimed that for steels with very high Nb content (0.1 wt - % Nb) the slow growth rate of the recrystallised grain size due to solute drag and / or strain induced precipitation can lead to a finer recrystallised grain size after deformation, as compared to steels with low Nb contents (0.063 wt - % Nb and 0.012 wt - % Nb) as discussed in Section 2.3.6.2. The amount of Nb (0.044 wt - %) present in the Nb-containing steel examined in the current work is less than that which was examined (0.063 wt - % Nb to 0.1 wt - % Nb) in [55]. Therefore, it is not expected that solute drag would lead to greater refinement of the recrystallised grain size via decrease in the efficiency of recovery. In addition, recovery is not expected in this steel as it has a low stacking fault energy as discussed in Section 2.3.5. Solute drag may not be

significant in the current study as preliminary characterisation of particles carried out in a parallel project [190] shows that strain induced precipitates (7 nm) are present in the sample deformed to a strain of 0.7 at 950 ^{o}C (determination of the volume fraction of the particles is still underway) and as such, takes some of the Nb out of solution thereby reducing the solute drag effect. However, it has been reported in the literature that at strains lower than 0.2 and deformation temperatures higher than 1050 ^{o}C solute drag is more effective than precipitate pinning [4] which may affect the samples deformed to a 0.15 strain.

Sellars [5] observed that for a Nb-containing steel with an initial grain size of 250 μm deformed to strains of 1 - 1.6 below 1000 ^{o}C (where recrystallisation and precipitation were expected to interact) the recrystallised grain sizes had a greater strain dependence (greater degree of refinement) which he said reflected an effect on the distribution of precipitates and consequently influenced the grain size. It is also worth noting here that similar values for the initial grain size exponents ($x = 0.67$; which is related to nucleation site density) are proposed for use in the Sellars equations for both the Nb-containing steel (above 950 ^{o}C) and C - Mn steel as mentioned earlier in Section 6.1 which would indicate that below 950 ^{o}C nucleation site density may vary for the Nb-containing steel. Different strain exponents, that is, 0.67 for Nb-containing steels and 1 for C - Mn steels, were proposed by Sellars [5] which also indicates that the dependency of the recrystallised grain size on strain may vary with composition, with Nb microalloyed steels having a greater grain size refinement than C - Mn steels as mentioned in Section 6.1.

Conflicting views to those reported by Miao *et al.* [55] and Sellars [5], were made by Abdollah-Zadeh [18], who stated that within the solute drag regime the recrystallised grain size for the Nb free steel was finer (94 μm) than the recrystallised mode grain size for the Nb-

containing steel (116 μm) at 0.25 strain. They examined Fe - 30Ni steel with 0.02 wt - % Nb and without Nb with an initial grain size of 310 μm deformed at 850 - 1000 ^{o}C. They argued that niobium in solution and / or in the form of Nb (C, N) (strain induced precipitation) retards the rate of nucleation of recrystallisation leading to fewer nuclei and consequently to coarser austenite grain sizes after completion of recrystallisation. At higher strains of 0.5 they observed that the difference between the measured mode grain size for the Fe - 30Ni steel with (39 μm) and without Nb (48 μm) was even smaller (9 μm difference). From the above discussion, it is clear that there may not be significant differences between the results for the Fe - 30Ni steel with and without Nb at strains of 0.25 and 0.5 strain if errors are accounted for which was not presented in [18].

From the current study comparison of the recrystallisation finish times for the Fe - 30Ni steels with (8 minutes) and without (5 minutes) Nb, with a similar initial grain size of 160 - 180 μm deformed to a 0.7 strain and furnace recrystallised at 850 ^{o}C, indicated that the Nb - containing steel takes longer to recrystallise than the Nb free steel, which is consistent with the literature findings [5, 18, 55], however it seems the final recrystallised mode grain size after deformation and annealing is not influenced by SIP (strain induced precipitation) as the recrystallised mode grain size (40 - 60 μm) and largest grain size (140 - 160μm) are the same for both steels, as shown in Figure 6.6. This would suggest that even though grain boundary migration is slowed down, most likely by SIP, recrystallisation nucleation should not be influenced. SIP is likely to occur because the samples were furnace recrystallised at 850 ^{o}C for higher strains (0.7) and 950 ^{o}C for lower strains ranging from 0.15 to 0.3 (where it is predicted that precipitation will influence recrystallisation, based on the Dutta - Sellars equations [170]).

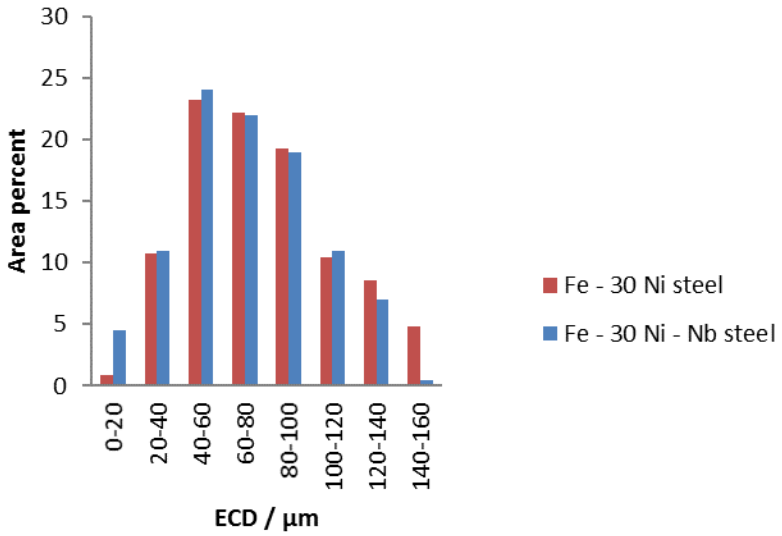

Figure 6.6: Recrystallised grain size distributions for the Fe - 30Ni steel with and without Nb both with an initial mode grain size of 160 - 180 µm deformed to a strain of 0.7 at 850 °C.

A small amount (volume fraction of < 2 x 10^{-5}) of TiN is predicted to be present up to temperatures of 1185 °C for the Nb - containing Fe - 30 wt - % Ni steel using Thermo-Calc software, therefore TiN may provide some grain boundary pinning up to 1185 °C. However, given the predicted volume fraction, TiN particles with an assumed (based on literature reports for TiN forming after solidification [196]) size (side length) of about 50 - 100 nm would have number densities of about 636 / mm^2 to 2548 / mm^2. The pinning force is estimated to be about 6.36*10^{-11} N / m^2 to 5*10^{-10} N / m^2, calculated using the Zener equation (Equation 2.5), with an interfacial energy of 0.5 J / m^2 [197]. The limiting grain size (diameter) for these pinning forces is calculated to be approximately 3 mm to 7 mm using Equation 2.6 [26], suggesting that grain growth is unlikely to be inhibited.

The 160 - 180 µm Nb - containing Fe - 30 wt - % Ni sample deformed at 0.15 strain seems to show different nucleation behaviour (44 % grain refinement) from that of the Fe - 30Ni steel without Nb (13 % grain refinement) at a similar strain and the same initial grain size. It must

be noted here that the obtained recrystallised grain size distribution for the 160 - 180 μm Fe - 30 wt -% Ni - 0.044 wt - % Nb sample deformed to a strain of 0.15, where poorer agreement is observed between the predicted and measured grain size distributions, was also measured by another researcher [190]. The measured grain size distribution obtained for the 160 - 180 μm Fe - 30Ni - 0.044Nb sample deformed at 0.15 strain is therefore accurate. Therefore, it is not clear at this moment what exact influence Nb has on the recrystallised grain size refinement at 0.15 strains, and as such further work is required to establish the reasons for the apparent difference in nucleation behaviour between the Fe - 30Ni steel with and without Nb at 0.15 strains because at higher strains similarity in grain refinement is seen for both steels (50 % for the samples strained to a 0.3 strain and 70 % grain refinement for the sample strained to a 0.7 strains).

The degree of fit (NRMS errors) for the different conditions is given in Table 6.2, where it can be seen that normalised root mean square errors are less than the NRMS error of 0.60, specified to be the limiting case for 'reasonable 'agreement (discussed in Section 6.1) when the variable *D'* approach is employed at all grain sizes and strains examined, except at lower strains of 0.15 where the NRMS error is above (0.86) the specified value (0.60) for 'reasonable' agreement. A comparison between the degrees of fit for the Fe - 30Ni steel with and without Nb when the variable *D'* approach is applied is given in Table 6.2, where it can be noted that generally the Nb-free grade is slightly better predicted than the Nb-containing model steel, as expected as the *D'* values were determined for the Nb - free steel.

Table 6.2: NRMS error values for predicted grain size distributions for the Fe - 30 wt - % Ni - 0.044 wt - % Nb and Fe - 30 wt - % Ni steel and using the variable *D'* and constant *D'* approach (*D'* = 1.1 for Fe - 30 wt - % Ni - 0.044 wt - % Nb steel and 0.83 for Fe - 30 wt - % Ni steel).

Initial mode grain size / μm	**Alloy type**	**Strain**	**NRMS error**	
			Variable *D'*	**Constant *D'* approach (*D'* = 0.83 for Fe - 30Ni steel; *D'* = 1.1 for Fe - 30Ni - 0.044Nb steel)**
100 - 120	Fe - 30 wt - % Ni - 0.044 wt - % Nb	0.15	0.49	0.75
	Fe - 30 wt - % Ni	0.15	0.49	1.07
160 - 180	Fe - 30 wt - % Ni - 0.044 wt - % Nb	0.15	0.86	0.53
		0.30	0.31	0.50
		0.70	0.40	1.10
	Fe - 30 wt - % Ni	0.15	0.58	0.86
		0.30	0.27	0.57
		0.70	0.24	1.36

6.1.2 Predicting recrystallised grain size distributions for a Nb-containing HSLA steel

The variable *D'* approach was applied to a Nb-containing HSLA steel (0.046 wt - %) with an initial mode grain size of 240 - 280 μm deformed to 0.3 strain at 1075 ^{o}C [3, 4]. Figure 6.7 shows that the variable *D'* approach does give a better fit (NRMS of 0.46) to the measured recrystallised grain size as compared to Equation 2.29 with *D'* = 1.1 $\mu m^{0.33}$, x = 0.67 and *y* = 0.67 (NRMS error of 1). The variable *D'* approach seems to reasonably well predict the smallest and mode grain sizes in the distribution, however the largest grain sizes are least fitted (under predicted by 40 μm), Figure 6.7. The simple variable *D'* approach predicted that the largest grain size class would be 240 - 260 μm instead of the measured grain size class of 280 - 300 μm, as compared to the 180 - 200 μm predicted using Equation 2.29. Despite the largest grain sizes not being fitted well when the variable *D'* approach is employed, the computed NRMS error value of 0.46 is within the acceptable range (NRMS error value of > 0.60 for reasonable agreement). The degree of fit (NRMS errors) for the different approaches used to predict the recrystallised grain size distributions is given in Table 6.3.

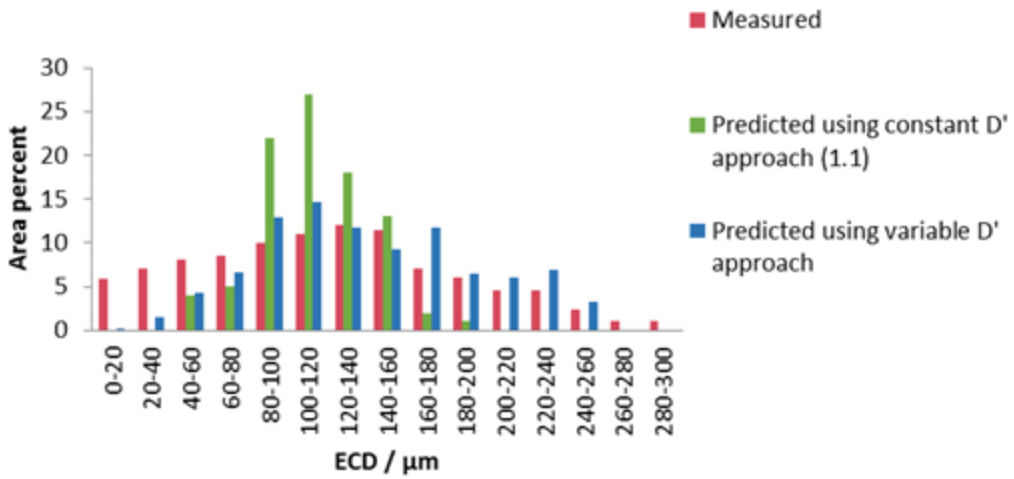

Figure 6.7: Recrystallised grain size distributions for the Nb-containing HSLA steel with an initial mode grain size of 240 - 280 µm deformed to a 0.3 strain at 1075 °C [4] and the predicted distribution based on the variable *D'* approach and Equation 2.29 (*D'* = 1.1 $\mu m^{0.33}$, x = 0.67 and y = 0.67).

Table 6.3: NRMS error values for predicted grain size distributions in Nb microalloyed HSLA steels.

Alloy type	Initial mode grain size / µm	Strain	NRMS error (Variable *D'*)	NRMS error (Constant *D'* (1.1))
0.046 wt - % Nb	240 - 280	0.3	0.46	1

6.1.2.1 Discussion on the causes of discrepancy between predicted and measured grain size distributions for the HSLA steel containing Nb

Table 6.1 shows that (Nb, Ti, V) (C, N) precipitates in this steel will be completely in solution at around 1210 °C. Heat treatment for this steel prior to deformation was carried out at 1225 °C to ensure all the precipitates were in solution which consequently would lead to microalloying elements such as V and Nb giving solute drag or lead to the formation of strain induced precipitation (precipitates with particle size distribution ranging from 2 nm to 20 nm

with a volume fraction of 0.00012 were found in the steel at a deformation temperature of 1075 ^{o}C [4]). Therefore, the precipitates formed would only retard recrystallisation kinetics but not affect the recrystallised grain size as discussed in Section 6.1.1.1. Despite heat treatments being carried out at temperatures above the precipitate dissolution temperature, it was reported that Nb (C, N) (ranging from 0.1 - 0.4 μm in diameter) and undissolved TiN (side length > 0.4 μm) with an area percent of 0.0003 were still present in the steel, which could also affect the recrystallised grain size as undissolved precipitates may tend to pin grain boundaries (Zener drag) [4]. No discussion on any influence of these undissolved precipitates on the recrystallised grain size was reported, however, it has been reported in the literature that coarse (> 0.5μm side length) precipitates will not have an influence on the recrystallised grain size as they will not pin the grain boundaries [4]. In Section 2.3.6.2 it was discussed that undeformed particles may lead to strain incompatibility between the deforming matrix, which can be accommodated by the generation of geometrically necessary dislocations at the particle-matrix interface thereby increasing dislocation density [28, 86]. It was stated that particles larger than 1 μm will lead to the formation of deformation zones which are a source of particle stimulated nucleation of recrystallisation and may affect the recrystallised microstructure [28, 56]. Therefore, it is expected that the undissolved precipitates will not have any influence on the recrystallised grain size distribution since the precipitate size is below 1 μm, however, recrystallisation kinetics will be retarded by strain induced precipitation and solute drag.

6.2 Verification and prediction for highly microalloyed steel

6.2.1 Comparison of literature equations is predicting recrystallised grain size distributions for highly microalloyed steel

Equations for predicting the recrystallised grain size distribution for highly alloyed steels are not readily available in the literature. Literature equations were applied and their accuracy to predict the recrystallised grain size distributions for highly microalloyed steels (that is, besides Nb the steel contains alloying elements such as Ti, V, Mo and B) compared. The following steels were studied: Nb-containing high strength strip steel (data produced in this project) and 9Cr forging steel [189].

Sha *et al.* [6] proposed Equation 6.1 (with parameters D' = 0.88 $\mu m^{0.41}$, x = 0.59 and y = 0.98) for predicting the recrystallised mode grain size which is similar to Equation 2.29 [5], where the only difference is the values for the exponents and D' values. Equation 6.1 was developed for predicting the recrystallised mode grain size for highly microalloyed steel containing 0.06 wt - % Nb, 0.014 wt - % Ti, 0.23 wt - % Mo and 0.030 wt - % V with a coarse-grained austenite initial grain size (700 - 810 µm).

$$D_{rex} = 0.88\, D_o^{0.59}\, \varepsilon^{-0.98} \qquad (6.1)$$

A comparison is made between Equation 2.29 using exponents for a Nb-containing steel (D' = 1.1 $\mu m^{0.33}$, x = 0.67 and y = 0.67) [5] and Equation 6.1 (D' = 0.88 $\mu m^{0.41}$, x = 0.59 and y = 0.98) [6] to establish the accuracy of these equations in predicting the recrystallised grain size distribution for the high strength strip steel as shown in Table 6.4. Equation 2.29 is compared to Equation 6.1 because the composition for the high strength strip steel (0.04 wt - % Nb, 0.239 wt - % Mo, 0.002 wt - % Ti and 0.051 wt - % V) and that used by Sha *et al.* [6] (given in the previous paragraph) are quite similar. It can be seen in Table 6.4 that using Equation 6.1

[6] leads to discrepancies (1.2 to 2.4 NRMS error) as the measured grain size distribution is generally under predicted. Equation 2.29 [5] also under predicts the recrystallised grain size distribution (0.9 - 1.6 NRMS error) with the exception of samples deformed to a strain of 0.15, where only the mode grain size is predicted well.

A comparison is also made for the 9Cr forging steel between Equation 2.29 using exponents for a Nb-containing steel (D' = 1.1 $\mu m^{0.33}$, x = 0.67 and y = 0.67) [5] and Equation 6.1 (D' = 0.88 $\mu m^{0.41}$, x = 0.59 and y = 0.98) [6] to establish the accuracy of these equations in predicting the recrystallised grain size distribution, as shown in Table 6.5. It can be seen from Table 6.5 that using Equation 6.1 [6] leads to errors (0.79 to 2.98 NRMS) as the measured grain size distribution is generally under predicted, except at lower strains of 0.15 where the largest grain size (D_{max}) is predicted well and the NRMS error is slightly lower (0.79 NRMS error) than when exponents proposed by Sellars [5] are employed (0.88 NRMS error). It must however be noted here that errors (0.88 - 1.80 NRMS error) in predicting the recrystallised grain size distribution using Equation 2.29 [5] may arise from the fact that the amount of Nb (0.051 wt - %) in the 9Cr forging steel is outside the range (0.015 - 0.045 wt - %) for which Equation 2.29 was developed. On the other hand, the amount of Cr in the 9Cr forging steel is also much higher (9 - 9.5 wt - % Cr) than that used (0.068 wt - % Cr) in developing Equation 2.29. Equation 2.29 gives reduced errors from 2.42 - 2.98 NRMS error when Equation 6.1 is used to about 1.1 - 1.8 NRMS error (for samples deformed to 0.3 and 0.45 strain).

The NRMS errors for both the high strength strip steel and 9Cr forging steels [189] get bigger as strain and grain size increase which would suggest that changing the strain exponent (to y = 1 used for C - Mn steels) would not solve the problem as errors would get worse at low strains, for example for the 9Cr deformed to 0.3 strain the error increases by 44 %. For the high strength strip steel, when the strain exponent is changed from 0.67 to 1, discrepancies are

reduced by only 5 % and significant discrepancies are still observed as the mode grain size and the largest grain sizes are over predicted by 140 and 100 μm respectively.

The accuracy of the variable *D'* approach in predicting recrystallised grain size distributions for both the Nb-containing high strength strip steel and 9Cr forging steel [189] will therefore be compared to Equation 2.29, using the exponents (x = 0.67 and y = 0.67) and *D'* values (1.1) determined for Nb-containing steel [5] instead of Equation 6.1 [6].This is due to significant discrepancies observed when Equation 6.1 is used to predict recrystallised grain size distributions for the Nb-containing high strength strip steel and 9Cr forging steel [189].

Table 6.4: Comparison between Equation 2.29 (*D'* = 1.1, x = 0.67, y = 0.67) [5] and Equation 6.1 (*D'* = 0.88, x = 0.59, y = 0.98) [6] in predicting the recrystallised grain size in the high strength strip steel.

Strain	**Measured**		**Equation 2.29**		**NRMS**	**Equation 6.1**		**NRMS**
	D_{mode} / µm	**D_{max} / µm**	**D_{mode} / µm**	**D_{max} / µm**	**error**	**D_{mode} / µm**	**D_{max} / µm**	**Error**
0.15	140 - 160	280 - 300	140 - 160	180 - 200	0.9	120 - 140	160 - 180	1.2
0.3	120 - 140	220 - 240	80 - 100	120 - 140	1.4	40 - 60	80 - 100	2.0
0.45	80 - 100	200 - 220	60 - 80	80 - 100	1.6	40 - 60	60 - 80	2.4

Table 6.5: Comparison between Equation 2.29 (D' = 1.1, x = 0.67, y = 0.67) [5] and Equation 6.1 (D' = 0.88, x = 0.59, y = 0.98) [6] in predicting the recrystallised grain size in the 9Cr forging steel.

Initial grain size / µm	**Strain**	**Measured**		**Equation 2.29**		**NRMS error**	**Equation 6.1**		**NRMS error**
		D_{mode}	**D_{max}**	**D_{mode}**	**D_{max}**		**D_{mode}**	**D_{max}**	
170 - 180	0.15	110 - 120	150 - 160	120 - 130	150 - 160	0.88	110 - 120	150 - 160	0.79
	0.3	90 - 100	120 - 130	80 - 90	90 - 100	1.10	60 - 70	70 - 80	2.43
	0.45	70 - 80	100 - 110	50 - 60	70 - 80	1.39	40 - 50	50 - 60	2.42
360 - 380	0.3	180 - 200	260 - 280	120 - 140	180 - 200	1.80	80 - 100	120 - 140	2.98

6.2.2 Predicting the recrystallised grain size distribution for a high strength strip steel using the variable *D'* approach

The variable *D'* approach was applied to the high strength strip steel with an initial mode grain size of 160 - 180 μm and deformed to strains of 0.15, 0.3 and 0.45 at 1200 ^{o}C. This approach was compared to Equation 2.29, using the exponents determined for Nb-containing steels [5] as the steel contains Nb and since Equation 2.29 gives reduced errors compared to Equation 6.1 as discussed in Section 6.2.1.

It can be seen from Figure 6.8 that the *D'* variable approach reasonably predicts the measured grain size distribution at 0.15 strain (0.41 NRMS error as shown in Table 6.6). At higher strains (0.3 and 0.45) the fits are not very good as the errors are higher (NRMS errors of 0.84 and 0.77) than specified for reasonable agreement (0.60 NRMS error), as illustrated in Figure 6.9 and Figure 6.10. The variable *D'* approach is seen to generally predict well the measured $D_{5\%}$ at higher strains (whilst at strains of 0.15 it is under predicted by 20 μm), whilst it under predicts both the mode grain size and largest grain size in the distribution (by 20 - 60 μm) at 0.3 and 0.45 strains. The mode grain size at 0.15 strain is predicted well, whereas the largest grain size is under predicted by 20 μm.

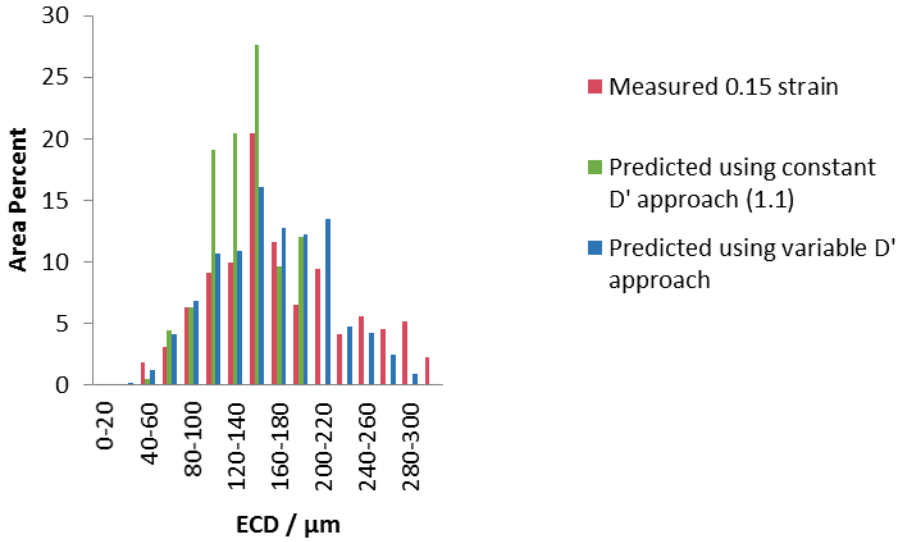

Figure 6.8: Recrystallised grain size distributions for the high strength strip steel with an initial grain size of 160 - 180 µm deformed at 1200 °C to a 0.15 strain and predicted distributions based on the variable *D'* approach and using Equation 2.29 (*D'* = 1.1 $\mu m^{0.33}$, x = 0.67 and y = 0.67).

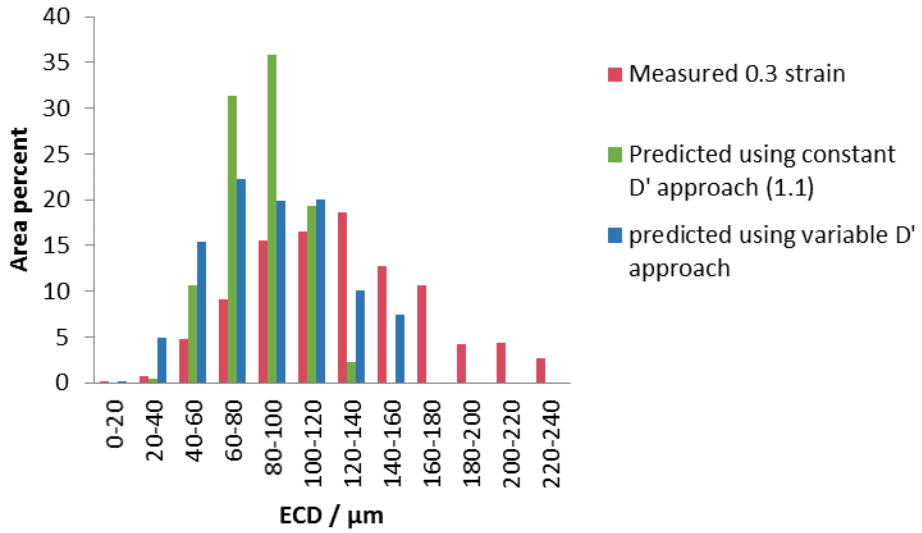

Figure 6.9: Recrystallised grain size distributions for the high strength strip steel with an initial grain size of 160 - 180 µm deformed at 1200 °C to a 0.3 strain and predicted distributions based on the variable *D'* approach and using Equation 2.29 (*D'* = 1.1 $\mu m^{0.33}$, x = 0.67 and y = 0.67).

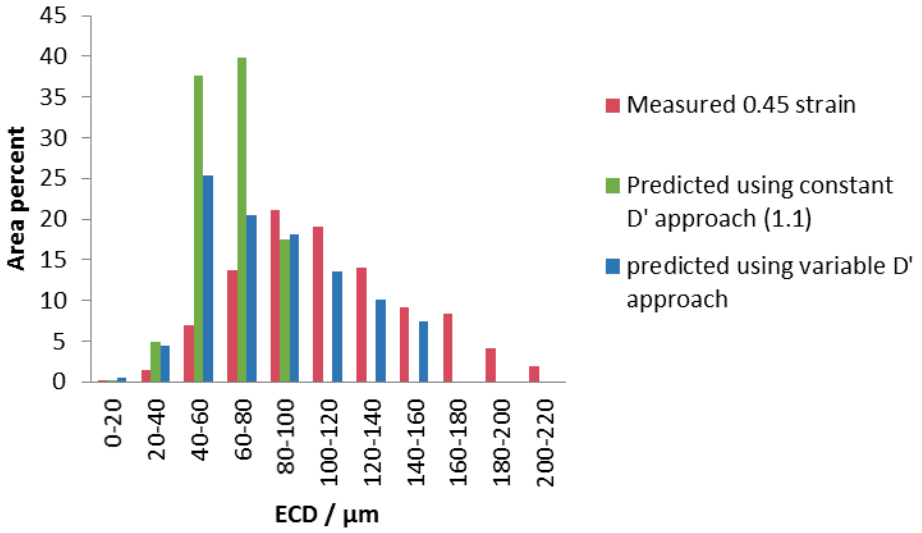

Figure 6.10: Recrystallised grain size distributions for the high strength strip steel with an initial grain size of 160 - 180 µm deformed at 1200 °C to a 0.45 strain and predicted distributions based on the variable *D'* approach and using Equation 2.29 (*D'* = 1.1 $\mu m^{0.33}$, x = 0.67 and y = 0.67).

Table 6.6: NRMS errors for predicted grain size distributions in high strength strip steels using the variable *D'* approach.

Alloy type	Initial mode grain size / µm	Strain	NRMS error
Strip steel	160 - 180	0.15	0.41
		0.3	0.84
		0.45	0.77

6.2.2.1 Discussion on the causes of discrepancy between predicted and measured grain size distributions for the high strength strip steel

Nb (C, N) will be in solution at the deformation temperature of 1200 ^{o}C as the dissolution temperature for the high strength strip steel is predicted to be around 1135 ^{o}C, and TiN will be undissolved as its dissolution temperature is predicted to be around 1370 ^{o}C (data given in Table 6.1). Therefore, it is expected that the microalloying (predominantly Nb) elements in solution should influence grain boundary mobility and the undissolved TiN may pin grain boundaries. It was discussed in Section 6.1.1.1 that solute drag does not have any influence on the recrystallised grain size for samples with Nb contents below 0.06 wt - %, therefore, since the Nb content (0.044 wt - %) in the high strength strip steel is below 0.06 wt - % no influence of solute drag on the recrystallised grain size is expected. Based on literature data [4] for steel with a similar Ti weight percent (0.002) with a slight difference in the nitrogen content of 0.003 wt - % N (i.e. 0.008 wt - % N for HSLA steel [4] and 0.005 wt - % N for the high strength strip steel), TiN particles with particle size of 0.4 μm and area percent of about 0.0003 are expected to be present in the steel. This low volume fraction of precipitates is not expected to be effective in pinning the grain boundaries or influence the final recrystallised grain size. Du *et al.* [144] examined a similar strip steel with 0.006 wt - % Ti and found that no coarse (greater than 0.5) particles of TiN were present in the steel, which indicates that TiN particles will not act as a source for particle stimulated nucleation for recrystallisation as the particles are not large enough (> 1 μm).

Therefore, the reasons for the variable *D'* approach predicting the high strength strip steel sample deformed to a 0.15 strain well and not samples deformed at higher strains (0.3 and 0.45) may be because the two samples behave in a similar manner (in terms of grain refinement of the largest grain size in the distribution). The high strength strip steel is refined

by 10 % while the Fe - 30Ni steel deformed to a similar strain is refined by 13 %. As earlier mentioned in Section 6.1.1.1 comparison of the degree of refinement is made to the Fe - 30Ni steel since it was used to obtain the best fit *D'* values used in the variable *D'* approach. At strains of 0.3 and 0.45 the high strength strip steel samples have refined by only 22 % and 41 % (in terms of the largest grain sizes) compared to 50 % and 52 % for the Fe - 30Ni steel deformed to similar strains of 0.3 and 0.45 respectively. The difference in degree of refinement (nucleation behaviour) observed between the Fe - 30Ni steel and high strength strip steel deformed to similar strains may be because the Fe - 30Ni steel has been cold deformed whereas the high strength strip steel has been hot deformed at 1200 ^{o}C, and as such it is possible that recovery (discussed in Chapter 2) could play a role and thereby reduce the amount of stored energy available for recrystallisation.

The other source of error might be due to the fact that the equivalent cold strain for the hot strain at 1200 °C may be less than for deformation at 850 °C, which may affect the amount of driving force for recrystallisation. This is because at higher temperatures some of the dislocations may be annihilated, leading to a lower flow stress and consequently a lower amount of driving force for recrystallisation than at lower temperatures, as discussed in Section 2.3.3.2 [18, 84]. Therefore, tests are required at different deformation temperatures to improve the accuracy of the variable *D'* approach.

6.2.3 Predicting recrystallised grain size distributions for the 9Cr forging steel using the variable *D'* approach

The variable *D'* approach was applied to the 9Cr forging steel with an initial mode grain size of 170 - 180 µm deformed to 0.15, 0.3 and 0.45 strain. The variable *D'* approach was also applied to the 9Cr forging steel sample with a larger initial grain size of 360 - 380 µm

deformed to a 0.3 strain [189]. Figure 6.11 shows that, for the samples deformed to a strain of 0.15, the variable *D'* approach does not predict the recrystallised grain size distribution very well (NRMS error of 1.6). The $D_{5\%}$, mode grain size and largest grain size in the distribution are all not fitted well (over predicted). However, the error is reduced (0.88 NRMS error) when Equation 2.29 is used with *D'* = 1.1 $\mu m^{0.33}$, *x* = 0.67 and *y* = 0.67 [5], although the mode grain size is slightly over predicted (120 - 130 µm predicted instead of 110 - 120 µm). Reasons for the poor agreement observed between the measured and predicted grain size distributions when the variable *D'* approach is applied to the 9Cr forging steel deformed to a 0.15 strain will be given in Section 6.2.3.1.

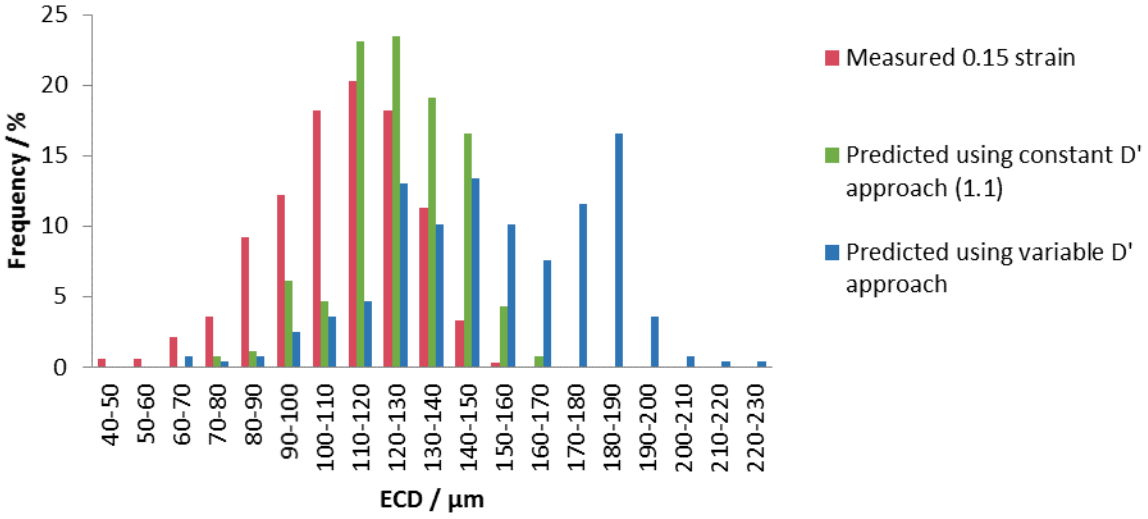

Figure 6.11: Recrystallised grain size distributions for the 9Cr forging steel with an initial grain size of 170 - 180 µm deformed at 1200 °C to a 0.15 strain [189] and predicted distributions based on the variable *D'* approach and using Equation 2.29 (*D'* = 1.1 $\mu m^{0.33}$, x = 0.67 and y = 0.67).

The variable *D'* approach was also applied to samples deformed to a 0.3 strain and the results in Figure 6.12 show that the approach does not give very good fits to the measured recrystallised grain size distributions (0.92 NRMS error, given in Table 6.7); despite this the mode grain size is predicted well however, $D_{5\%}$ and the largest grain size is least fitted (under predicted by 10 µm). Moreover, it can be seen from Figure 6.12 that the variable *D'* approach does give reduced discrepancies (0.92 NRMS) in the fits as compared to Equation 2.29 with *D'* = 1.1 $\mu m^{0.33}$, x = 0.67 and *y* = 0.67 (1.1 NRMS error). Figure 6.13 for the sample deformed to a strain of 0.45, shows that the variable *D'* approach gives a good fit (0.38 NRMS error) to the measured recrystallised grain size as compared to Equation 2.29 with *D'* = 1.1 $\mu m^{0.33}$, x = 0.67 and *y* = 0.67 (1.39 NRMS error). It is apparent from Figure 6.13 that the mode grain size is better fitted than the largest grain size (over predicted by 10 µm) while the $D_{5\%}$ is under predicted.

Figure 6.14 shows that for a 9Cr forged steel sample with an initial grain size of 360 - 380 µm and deformed to a strain of 0.3, the variable *D'* approach does not give a very good fit (0.95 NRMS error) to the measured grain size distribution. However, the variable *D'* approach gives a much better fit than when Equation 2.29, with the exponents determined for Nb steels (*D'* = 1.1 $\mu m^{0.33}$, *x* = 0.67 and *y* = 0.67 [5]) is used (1.8 NRMS error given in Table 6.7). The results in Figure 6.14 also show that when the variable *D'* approach is employed, the $D_{5\%}$, mode and largest grain size in the distribution are all under predicted by 40 µm and 20 µm respectively.

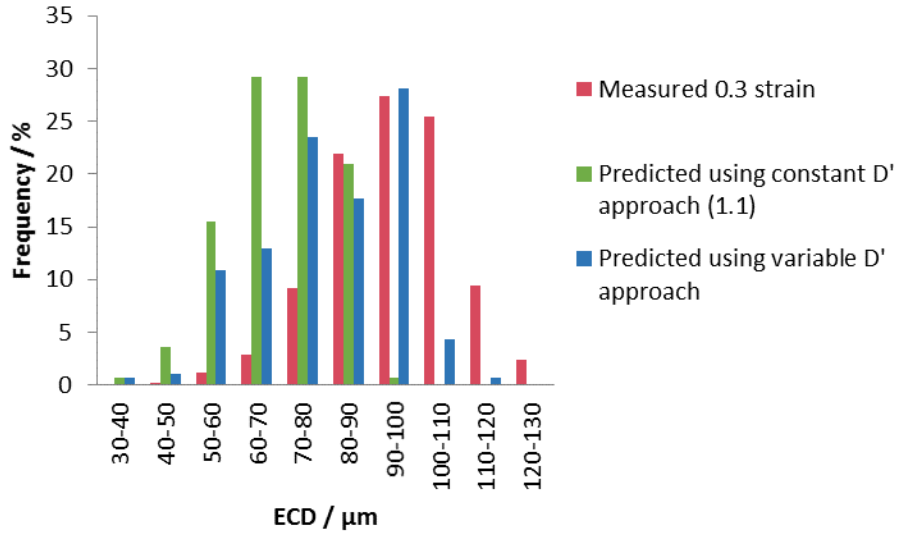

Figure 6.12: Recrystallised grain size distributions for the 9Cr forging steel with an initial grain size of 170 - 180 µm deformed at 1200 °C to a 0.3 strain [189] and predicted distributions based on the variable *D'* approach and using Equation 2.29 (*D'* = 1.1 $\mu m^{0.33}$, x = 0.67 and y = 0.67).

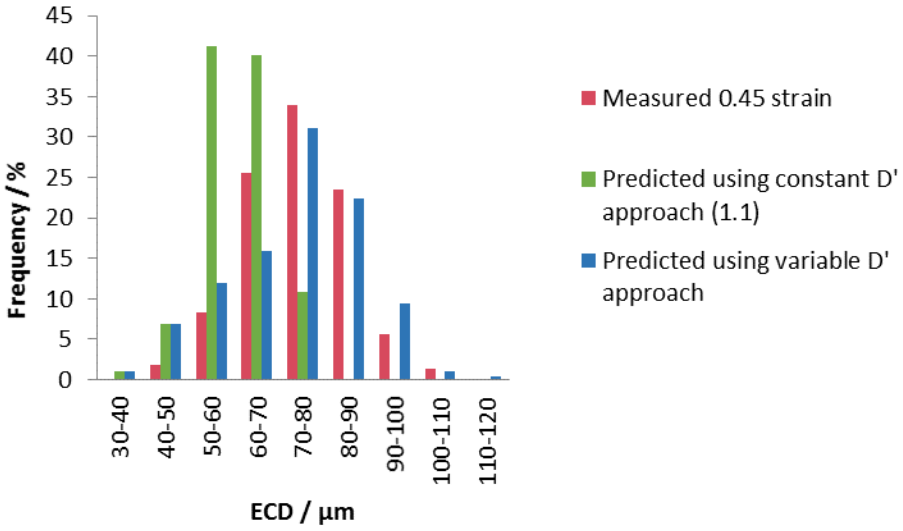

Figure 6.13: Recrystallised grain size distributions for the 9Cr forging steel with an initial grain size of 170 - 180 µm deformed at 1200 °C to a 0.45 strain [189] and predicted distributions based on the variable *D'* approach and using Equation 2.29 (*D'* = 1.1 $\mu m^{0.33}$, x = 0.67 and y = 0.67).

Table 6.7: NRMS errors for predicted grain size distributions in 9Cr forging steel using the variable *D'* approach.

Alloy type	Initial mode grain size / µm	Strain	NRMS error
9Cr forging steel	170 - 180	0.15	1.60
		0.3	0.92
		0.45	0.38
	360 - 380	0.3	0.95

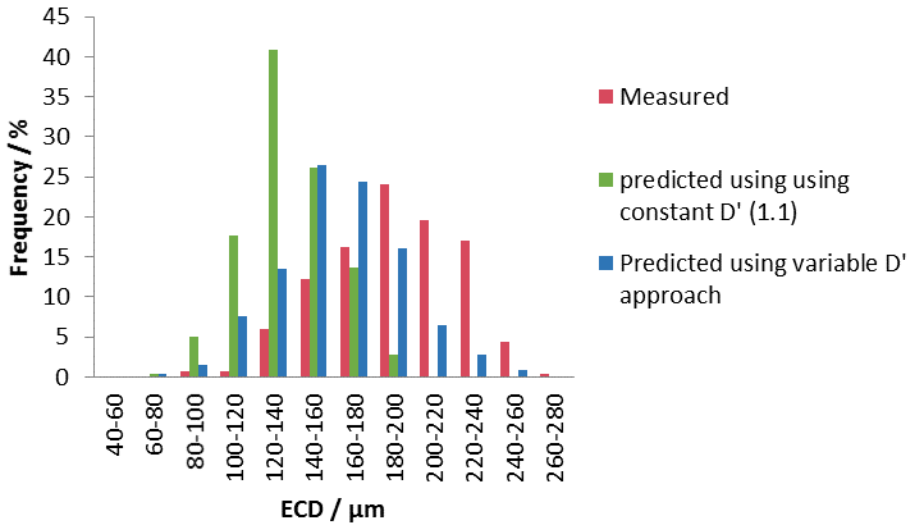

Figure 6.14: Recrystallised grain size distributions for the 9Cr forging steel with an initial grain size of 360 - 380 µm deformed at 1200 °C to a 0.3 strain [189] and predicted distribution based on the variable *D'* approach and using Equation 2.29 (*D'* = 1.1 $\mu m^{0.33}$, x = 0.67 and y = 0.67).

6.2.3.1 Discussion on the causes of discrepancy between predicted and measured grain size distributions for the 9Cr forging steel

For the range of strains and initial grain sizes examined for the 9Cr forging steel, the variable *D'* approach seems to give reasonable fits at higher strains (0.45 strain) for the 170 - 180 μm sample. Major discrepancies are observed for the 170 - 180 μm sample deformed to a 0.15 strain where the fit to the measured grain size distribution is poor, as discussed in the preceding sections. The degree of fit (NRMS errors) for the different conditions is given in Table 6.7, where it is shown that the variable *D'* gives reduced errors at all strains examined, compared to when the constant *D'* approach (1.1) is employed, except at a strain of 0.15, where a constant *D'* approach gives reduced discrepancies.

The discrepancies observed in the 9Cr forging steel could be due to the steel's highly microalloyed nature, which would affect all strains. Most of the microalloying elements such as Nb, and V are expected to be in solution at 1200 ^{o}C (reheating temperature) as the dissolution temperature for (Nb, V, Cr) (C, N) was predicted to be 1185 ^{o}C for this steel using Thermo-Calc software [189], and as such, the growth rate of the recrystallised grains might be slower than expected, which will affect recrystallisation kinetics as earlier mentioned in Section 6.1.1.1. It is likely that there may be a strong drag effect in the 9Cr forging steel due to the fact that the sample will contain a lot of microalloying elements in solution such as V, Nb, Cr etc. It has also been reported that solute drag is more prevalent at higher deformation temperatures (the samples were deformed at 1200 ^{o}C). This may cause a decrease in the efficiency of recovery, leading to greater refinement of the recrystallised grain size at all strains, despite the fact that the amount of Nb (0.051 wt - %) present in the 9Cr forging steel is less than that proposed (0.1 wt - % Nb) by Miao *et al.* [55], for refinement of grain sizes to occur as a result of solute drag. The solute drag parameter (SRP) is estimated to be about 29

% for the 9Cr forging steel [189] compared to an SRP of 3 % for the 0.1 wt - % containing steel used by Miao *et al.* [55]. For more details on how SRP is computed the reader is referred to Akben *et al.* [201]. It has been reported in the literature [4] that solute drag is more effective in samples deformed to strains below 0.2 and at high temperatures, therefore it is possible that there would be a stronger solute drag effect in the 9Cr forging steel deformed to a strain of 0.15 leading to a significant degree of grain refinement than at higher strains. Therefore, it is also likely that as solute drag slows down the growth rate of the recrystallised grains, more nucleation sites may be activated and consequently refining the recrystallised grain size [55]. This is expected to affect all strains.

Strain induced precipitation is not expected to occur as deformation was carried out at 1200 ^{o}C, which is well above the deformation temperature (1080 ^{o}C) where strain induced precipitation is predicted (using Dutta-Sellars equations [5, 170]) to interfere with recrystallisation [189]. However, it has not yet been ascertained for the 9Cr forging steel whether there are any undissolved precipitates present as the work in still ongoing [189]. In any case, even if precipitates were present this would affect all strains, although so far discrepancies are different at various strains. At higher deformation temperatures recovery is expected to occur, which would lead to a reduction in the driving force for recrystallisation as discussed in Section 2.3.3. This would lead to a large recrystallised grain size being obtained after deformation. However, the recrystallised grain sizes for the 9Cr forging steel with an initial grain size of 170 - 180 µm have significantly refined by 43 %, 54 % and 61 % at strains ranging from 0.15 - 0.45 whereas, the 9Cr forging steel with an initial grain size of 360 - 380 µm refined by 50 %, suggesting that the effect of recovery on the recrystallised grain size may not be very significant.

The reasons for the discrepancies observed may also be due to differences in the dependence of the recrystallised grain size on strain between the 9Cr forging steel and the Fe - 30Ni steel (used to determine *D'* values for use in Equation 5.8). At a 0.15 strain the 9Cr forging steel with an initial grain size of 170 - 180 µm had refined by 43 %, whereas the Fe - 30Ni steel had refined by 13 % which may lead to the discrepancies observed in predicting the measured grain size distribution. At strains of 0.3 and 0.45 the 9Cr forging steel samples refined by 54 % and 61 %, compared to 50 % and 52 % for the Fe - 30Ni steel deformed to similar strains of 0.3 and 0.45 respectively. As discussed in previous paragraphs, this could be due to the steel's highly microalloyed nature which would affect all strains.

6.3 Overall discussion / summary of the simple variable *D'* approach and literature equations in predicting the recrystallised grain size distributions in a range of steel grades.

Comparison of the variable *D'* approach and literature equations in predicting the recrystallised grain size distributions in a range of steel grades has been carried out to establish if there are any general trends occurring. As earlier stated in the introductory part of this chapter NRMS error values less than, and up to 0.60 are taken as representing a good fit in this work; anything above a NRMS error of 0.60 would indicate that the measured and predicted distributions are not fitted very well.

6.3.1 Discussion on grain size distribution fits obtained for the different steel grades using the variable *D'* approach

Table 6.8 shows that at a lower strain of 0.15, the grain size distributions for the 110 - 120 µm and 160 - 180 µm samples have been over predicted by 40 µm and 160 µm (with regards to the largest grain size in the distribution) for the Fe - 30Ni - 0.044Nb steel, whereas the largest

grain size was predicted reasonably well at higher strains (0.3 and 0.7 strain). The measured $D_{5\%}$ and mode grain sizes for the Fe - 30Ni - 0.044Nb steel are reasonably predicted for the 0.3 and 0.7 strained samples. The largest grain size for the HSLA steel deformed to a 0.3 strain [4] is under predicted, while both $D_{5\%}$ and mode grain sizes are reasonably predicted, Table 6.8. As discussed in Section 6.1.1, there is a need for further investigations at lower strains of 0.15 as the sample exhibits a greater degree of refinement when compared to the Fe - 30Ni steel without Nb, especially the sample with an initial grain size of 160 - 180 μm. At higher strains (0.3 and 0.7) similar degrees of grain refinement are observed (50 % and 70 %) in the Fe - 30 wt - % Ni steel with and without Nb.

For the high strength strip steel, Table 6.8 shows that the $D_{5\%}$ is predicted well at all strains examined except at a strain of 0.15 were it is under predicted, while the mode grain sizes are all under predicted except at strains of 0.15 where they are well predicted. The largest grain sizes in the distributions for the high strength strip steel are under predicted (by 60 μm) at strains of 0.3 and 0.45 whereas, they are under predicted at lower strains of 0.15 (by 20 μm). It can also be seen from Table 6.8 that the $D_{5\%}$ in the grain size distribution for the 9Cr forging steels are all under predicted (10 to 20 μm) except for the 170 - 180 μm sample strained to 0.15 (over predicted by 30 μm), whereas the mode grain sizes are predicted well at 0.3 and 0.45 strain for the 170 - 180 μm sample except for the sample with an initial grain size of 360 - 380 μm, where at a strain of 0.3 the mode grain size is under predicted by 40 μm. A variation in prediction using variable *D'* approach was observed in that the grain size distributions examined for both the high strength strip steel and 9Cr forging steel were either under predicted or over predicted (in terms of the largest grain size); discrepancies might be

due to the highly microalloyed nature of the steels examined. For the high strength strip steel errors may also arise due to recovery.

Overall, the variable *D'* approach deteriorates as the complexity of the alloy increases. Therefore, there is need for further studies in order to improve the accuracy in predicting recrystallised grain size distributions using the proposed variable *D'* approach, more especially at low strains (0.15).

6.3.2 Comparison between the variable *D'* approach and literature equations in predicting recrystallised grain size distributions in a range of steel grades

Tables 6.2 and 6.3 (given in Section 6.1.1 and 6.1.2 respectively) highlight how well the predicted grain size distribution using the simple variable *D'* approach and Equation 2.29 fits the measured grain size distribution based on computed NRMS error values for the Nb - microalloyed steels investigated. Tables 6.2 and 6.3 generally show that using the simple variable *D'* approach gives reduced errors compared to the use of Equation 2.29 with *D'* = 1.1 $\mu m^{0.33}$, x = 0.67 and y = 0.67 for steels with Nb except at lower strain of 0.15 were Equations 2.29 predicts the recrystallised grain size better (0.53 NRMS error) than the variable *D'* approach (0.86 NRMS error).

It was generally shown in Tables 6.6 (given in Section 6.2.2) and 6.7 (given in Section 6.2.3) that using the simple variable *D'* approach leads to a decrease in errors compared to the use of Equation 2.29 with *D'* = 1.1 $\mu m^{0.33}$, x = 0.67 and y = 0.67 for highly microalloyed steels examined. It was shown in Table 6.6 that the variable *D'* approach predicts well the high strength strip steel sample deformed to a strain of 0.15 (0.41 NRMS error), as compared to samples strained at higher strains (0.77 - 0.84 NRMS error). It was observed for complex alloys (9Cr forging), Table 6.7, that using Equation 2.29 (*D'* =1.1) for predicting the

recrystallised grain size does not work well (1.1 - 1.39 NRMS errors) at higher strains (0.3 - 0.45). The variable *D'* approach however works well at high strains (at a strain of 0.45 for the sample with an initial grain size of 170 - 180 μm) but not very well at lower strains (0.15 - 0.3 for both the finer and larger initial grain size). The variable *D'* approach is therefore generally more appropriate for predicting recrystallised grain size distributions for the Nb and highly microalloyed steel grades investigated than its alternative.

Table 6.8: Grain size distribution fits for the high strength strip, 9Cr forging steel and Nb microalloyed steels using the variable *D'* approach.

Alloy type	Initial mode grain size / µm	Strain	$D_{5\%}$	Difference between measured and predicted D_{rex} / µm	D_{mode}	Difference between measured and predicted D_{rex} / µm	D_{max}	Difference between measured and predicted D_{rex} / µm
Strip steel	160 - 180	0.15	Under predicted	20	Good	-	Under predicted	20
		0.3	Good	-	Under predicted	60	Under predicted	80
		0.45	Good	-	Under predicted	20	Under predicted	60
9Cr forging [189]	170 -180	0.15	Over predicted	30	Over predicted	30	Over predicted	80
		0.3	Under predicted	10	Good	-	Under predicted	10
		0.45	Under predicted	10	Good	-	Over predicted	10
	360 - 380	0.3	Under predicted	20	Under predicted	40	Under predicted	20
Fe-Ni-0.044Nb	110 - 120	0.15	Under predicted	20	Good	-	Over predicted	40
		0.15	over predicted	20	Over predicted	60	Over predicted	160
	160 - 180	0.3	Good	-	Good	-	Good	-
		0.7	Good	-	Good	-	Good	-
HSLA (4)	240 - 280	0.3	Good	-	Good	-	Under predicted	40

6.4 Summary

The approaches from the literature used to predict the recrystallised grain sizes ($D_{rex} = 0.88 D_o^{0.59}\varepsilon^{-0.98}$ for high alloyed steels [6] and $D_{rex} = 1.1D_o^{0.67}\varepsilon^{-0.67}$ for Nb-containing steels [5]) have been assessed and compared. It was found that $D_{rex} = 1.1D_o^{0.67}\varepsilon^{-0.67}$ reduced errors as compared to $D_{rex} = 0.88 D_o^{0.59}\varepsilon^{-0.98}$. Therefore, the approaches from the literature used to predict the recrystallised grain sizes ($D_{rex} = D' D_o^{0.67}\varepsilon^{-1}$ for non-Nb containing steels and $D_{rex} = D' D_o^{0.67}\varepsilon^{-0.67}$ for Nb-containing steels [5]) where D' values of 0.83 $\mu m^{0.33}$ and 1.1 $\mu m^{0.33}$ have been used for non-Nb and Nb-containing steels respectively [5], have been assessed and compared to the variable D' approach using $D_{rex} = D' D_o^{1}\varepsilon^{-1}$ described in Chapter 5.

The variable D' approach generally gives good agreement for the model Fe - 30Ni - based steels (both with and without Nb) except at 0.15 strain for the larger grain size (160 - 180 μm). It also gives good agreement for the Nb-containing HSLA steel deformed to a 0.3 strain. The fit between measured and predicted grain size distributions for the variable D' approach generally deteriorates as the complexity of the alloy increases and at lower strain values for the 9Cr forging steel, although in almost all cases the fit was better than for a constant D' approach. The fit between measured and predicted grain size distributions for the variable D' approach is still acceptable as reasonable agreement between predicted and measured grain size distribution is achieved for the high strength strip steel deformed to a 0.15 strain and for the 9Cr forging steel deformed to a strain of 0.45.

CHAPTER – 7

Conclusions

This thesis has investigated the following main areas:

(i) Validity of the individual grain size approach from the literature and other literature equations (based on the Sellars equation) in predicting recrystallised grain size distributions after hot deformation and the effect of strain and initial grain size on the recrystallised grain size after deformation.

(ii) Modelling recrystallised grain size distributions after hot deformation using a modified Sellars equation developed using results from a Fe - 30 wt - % Ni steel with different initial grain sizes and deformed to different strain levels.

(iii) Prediction of the recrystallised grain size distributions for different steel grades, initial grain sizes and applied strain in order to verify and establish the limits for the proposed new approach.

The main conclusions from the work in these three areas are given below:

Validity of the individual grain size approach and Sellars based equations from the literature and the effect of strain and initial grain size on the recrystallised grain size after deformation:

- The recrystallised mode grain size after deformation decreased with an increase in strain and decrease in the initial mode grain size, which is consistent with literature results. However, whilst the mode grain size decreased as the applied strain increased, the rate of refinement decreased and the initially different grain size values converged at high strains.

- Greater refinement of large gains in the distribution compared to the mode grain size has been observed.
- The Sellars equation ($D_{rex} = D' D_o^{0.67} \varepsilon^{-1}$) [5] predicts mode grain sizes well for strains of 0.3 and *D'* of 0.83; however, errors arise when predicting the largest grain sizes in the distribution as well as when strains higher than 0.3 are employed.
- Modified Sellars equations (varying *D*', D_o exponent and strain exponent) developed in the literature, whilst accurate in predicting recrystallised grain sizes for the steels and conditions the equations were developed for, were not robust when used to predict the grain size distributions for a range of different steels and conditions (using data obtained in the literature and during this project).
- The individual grain size class approach ('halving' method) proposed in the literature [4] only predicted the recrystallised grain size distribution well at strains of 0.3 and 0.45 for initial grain sizes of 110 - 120 μm and 160 - 180 μm whereas for the initial grain size of 50 - 60 μm it was only valid at a higher strain of 0.7.
- Using the individual grain size class approach with different best fit simple functions such as assuming a 1:1 relationship, halving and a third to predict the measured recrystallised grain size improves the degree of fit between the measured and predicted grain size distributions. At a lower strain of 0.15 a 1:1 relationship gives good fits for all the grain sizes examined. For strains of 0.22 - 0.45 grain sizes above 100 μm are fitted well when an assumption is made that the grains have refined by halving whereas at 0.7 strains an assumption that the grains have refined by a third gives better fits. For grain sizes below 100 μm an assumption that the grains have not refined (that is assuming a 1:1 relationship between the recrystallised and initial grain

size) gives better fits for the samples deformed to strains of 0.22 - 0.3 while at strains of 0.45 and 0.7 the 'halving' approach gives better fits.

Modelling of the recrystallised grain size distribution using Fe - 30 wt - % Ni steel:

- The equation proposed by Sellars ($D_{rex} = D' D_o^{0.67} \varepsilon^{-1}$) was modified in order to predict the recrystallised grain size distribution; the modification was to use a D_o exponent of 1, based on classical theory for the rate of nucleation, and variable *D'* values.

- $D_{rex} = D' D_o^{1} \varepsilon^{-1}$ has been proposed for predicting recrystallised grain size distributions considering all strain and grain size ranges. When considering the optimum *D'* value to predict the $D_{5\%}$, D_{mode} and D_{max} values it has been found that at low strain values (up to 0.3) *D'* is not very sensitive to strain; however, it is a function of strain at higher strains for all initial grain sizes examined except for small initial grain sizes (50 - 60 μm) where sensitivity of *D'* to strain is observed even at lower strains. *D'* is also a function of the relative position of the grain size in the grain size range (D*); *D'* values are consistently higher for D_{max} and D_{mode} than $D_{5\%}$ for all grain sizes examined (except for the 50 - 60 μm initial grain size were no specific trend is observed) which is explained by considering that the fine grain sizes in the distribution should recrystallise first affecting the available nucleation sites for subsequent recrystallisation of the larger grains. Therefore, in general *D'* is a function of strain and relative position of grain size ($f\{\varepsilon,$ D*}).

Prediction and verification of grain size distribution in different steel grades, initial grain sizes and applied strain:

- The variable *D'* approach generally gives good agreement for the model Fe - 30Ni - based steels (both with and without Nb) except at 0.15 strain for the larger grain size (160 - 180 μm). Comparison of the variable *D'* approach to the constant *D'* approach (using $D_{rex} = 1.1D_o^{0.67}\varepsilon^{-0.67}$ for Nb - containing steels and $D_{rex} = 0.83D_o^{0.67}\varepsilon^{-1}$ for non - Nb containing steels based on the best fit literature equations) was carried out and the variable *D*' approach gave more accurate predictions.

- The fit between measured and predicted grain size distributions for the variable *D'* approach generally deteriorates as the complexity of the alloy (i.e. alloying additions) increases and at lower strain values for the 9Cr forging steel, although in almost all cases the fit was better than for a constant *D'* approach.

CHAPTER – 8

Further Work

From this study, the following suggestions for further research can be made:

1. Greater refinement of large grains in the distribution compared to the finer (mode) grain size in the distribution has been observed which might lead to improved mechanical properties in materials. Therefore, more studies are required in future to investigate how much refinement of larger grains in grain size distributions after refinement of the finer grains becomes saturated can be achieved. Consideration of the strain required for maximum refinement of the coarser grains could influence the rolling schedules used when processing steels, particularly if high reheating temperatures are used to dissolve microalloy precipitates leading to a coarse reheated grain structure.
2. Equivalent hot (850 ^{o}C) deformation strains to the cold strain values used in the current work have been determined based on equivalence of stored energies using flow stress data. However, more studies need to be carried out to establish the equivalence of hot strains to cold strains at different deformation temperatures (above 850 ^{o}C) and hence improve the accuracy of equivalent hot strains. This is due to the fact that at higher deformation temperatures lower flow stresses are obtained than at lower deformation temperatures which may influence the driving force for recrystallisation and consequently recrystallised grain sizes.
3. It has been suggested in Chapter 5 that smaller grains may be recrystallising first and as such in situ EBSD could be utilised in order to verify that the smallest grain sizes in the distribution are recrystallising first as well as to measure the stored energy of

deformation. For example, the Fe - 30Ni steel would be ideal for in-situ studies as cold deformation can be used then the sample heated in the SEM with EBSD used to confirm initiation and progression of recrystallisation. Some very recent work has been initiated in this area in a parallel project [171].

4. It was shown in Chapter 6 that the simple variable *D'* approach does not predict the recrystallised grain size distribution well when used to predict recrystallised grain size distribution after deformation for complex alloys; there is, therefore a need to examine highly microalloyed steels further to increase the range of applicability of the variable *D'* approach. It is unclear whether the high alloy content is affecting the recrystallised grain boundary motion, therefore affecting the number of initiating recrystallised grains that can grow or is affecting the number of nuclei that form.

5. There is a need for further studies at lower strains (0.15) and larger grain sizes than 160 - 180 μm investigated in this work because the variable *D'* approach does not give reasonable agreement under these conditions. This may be due to underestimation of effective stored energy when equivalent strains were determined.

6. So far in this work the largest grain size examined using the variable *D'* approach has been the data obtained from [4] (240 - 280 μm) and 360 - 380 μm from [189], therefore examination of grain size distributions with larger initial mode grain sizes (> 300 μm) to establish the limits for the variable *D'* approach is required.

CHAPTER – 9

References

1. Rehman, K.; "Modelling the microstructure evolution during hot deformation of microalloyed steels"; Ph. D Thesis, McMaster University, (2014).
2. Vervynckt, K., Verbeken, B., Lopez, B., Jonas, J. J.; "Modern HSLA steels and role of non-recrystallisation temperature"; International Materials Review, v.57, n 4, (2012), pp. 187 - 207.
3. Kundu, A., Davis, C. L. and Strangwood, M.; "Modelling of grain size distributions during single hit deformation of a Nb-containing Steel"; Metallurgical and Materials Transaction A, v 41 A, (2010), pp. 994 - 1001.
4. Kundu, A.; "Grain structure development during casting, reheating and deformation of Nb-microalloyed steel"; Ph. D Thesis, The University of Birmingham, (2011).
5. Sellars, C. M.; "The physical metallurgy of hot working', Proceedings of the Conference on 'Hot working and forming processes"; (eds. C. M. Sellars, G. L. Davies), Book 264, The metals society, London, (1980), pp.3 - 15.
6. Sha, Q., Li, G. and Li, D.; "Static recrystallized grain size of coarse-grained austenite in an API-X70 pipeline steel"; Materials Engineering and Performance, v 22, (2013), pp. 3626 - 3630.
7. Weiss, H., Gittings, A., Brown, G. G. and McTeggart, W. J.; "Recrystallisation of a Niobium-Titanium steel in austenite range"; The Iron and Steel Institute, 211**, (**1973), pp. 703 - 708.

8. Priestner, R.; "Observations on behaviour of austenite during hot working of some Low-Carbon steels"; The Iron and Steel Institute, v 206 (1968), pp. 1252 - 1262.

9. Kozasu, I., Ouchi, C. Sampei, T. and T. Okita, T.; "Hot rolling as a high-temperature thermo-mechanical process"; Microalloying 75 - Proceedings International symposium 'on high strength low alloy steels', v 1, (1975), pp. 120 - 135.

10. Le Bon, A., Rofes-Vernis, J. and Rossard, C.; "Recrystallisation and precipitation induced by high-temperature"; Les Memoires Scientifiques de la Revue de Me'tallurgie, v 70**, (**1973), pp. 577 - 588.

11. Cuddy, L. J.; "Grain Refinement of Nb Steels by control of recrystallisation during hot rolling"; Metallurgical Transactions, v 15A, n 1, (1984), pp. 87 - 98.

12. Cuddy, L. J.; "Microstructures developed during thermomechanical treatment of HSLA Steels"; Metallurgical Transactions A, v 12A, n 7, (1981), pp. 1313 - 1320.

13. Thomas, G., Kim, J. K., Manojlovic, D. and Milovic, R.; "Development of high strength and toughness microcomposite HSLA Fe/Cr/Mn/C steel with and without Nb. Processing"; Microstructure and Properties of HSLA steels, (1987).

14. Sellars, C. M. and Whiteman, J. A.; "Recrystallisation and grain growth in hot rolling"; Metal Science, v 13, n 3-4, (1979), pp. 187 – 194.

15. Vervynckt, S., Verbeken, K., Thibaux, P., Houbaert, Y.; "Characterisation of the Austenite recrystallisation by comparing double deformation and stress relaxation tests, Steel Research"; v 81, n 3, (2010), pp. 234 - 244.

16. Hodgson, P. D. and Gibbs, R. K.; "A mathematical model to predict the mechanical properties of hot rolled C - Mn and microalloyed steels"; ISIJ International, v 32, n 12, (1992), pp. 1329 - 1338.

17. Chakrabarti, D.; "Development of bimodal grain structures and their effect on toughness in HSLA steel"; PhD thesis, the University of Birmingham, (2007).

18. Abdollah-Zadeh, A.; "The investigation of deformation, recovery, recrystallization and precipitation in austenite HSLA steel analogue alloys"; Ph. D Thesis, University of Wollongong, (1996).

19. Cuddy, L. J., Raley, J. C.; "Austenite Grain Coarsening in microalloyed steels"; Metallurgical Transactions A, v 14A, (1983), pp. 1989 - 1995.

20. Porter, D. A. and Eastering, K.E. and Sherif, M.Y.; "Phase transformations in metals and alloys"; CRC Press, Taylor and Francis group, 3rd Edition, ISBN: 978 - 1- 4200 - 6210 - 6, (2010) pp. 264 - 277.

21. Flemings, M. C.; "Solidification process"; McGraw - Hil, (1974), ISNB: 0 - 07-021283.

22. Strangwood, M. and Davis C. L.; "Modelling grain size distributions during TMCR of Nb-microalloyed steels"; International Journal of Metallurgical Engineering, v 2, (2013), pp. 125 - 129.

23. Miller, O.; "Influence of Austenitizing time and temperature on austenite grain size of steel"; Transactions of the American Society for metals, v 43, (1951), pp. 260 - 289.

24. Martin, J. W., Doherty R. D. and Cantor, B.; "Stability of microstructure in metallic systems"; 2nd Edition, Cambridge University Press, ISBN 0-521-42316-3, (1997), pp. 147 - 218.

25. Callister, W. D., Jr.; "Materials Science and Engineering: An introduction"; John Wiley and Sons, 7th Edition, ISBN-0471-73696-1, (2007).

26. Gladman, T.; "The Physical Metallurgy of Microalloyed Steels"; The Institute of Materials, London, Book 615, ISBN 0910716812, (1997).

27. Ralph, B.; "Grain growth"; Materials Science and Technology, v 6, (1990), pp. 1139 - 1144.

28. Humpreys, F. J. and Hatherly, M.; "Recrystallisation and related annealing phenomena"; Elsevier Ltd, 2nd Edition, ISBN: 978-0-08-044164-1, (2004).

29. Zhang, S. S., Li, M. Q., Liu, Y. G., Luo, J. and Liu, T. Q.; "The grain growth behaviour of austenite grain in the heating process of 300M steel"; Materials Science and Engineering A, v 528, (2011), pp. 4967 - 4972.

30. Zhao, Y., Shi, J., Cao, W., Wang, M. and Xie, G.; "Kinetics of austenite grain growth in medium carbon niobium - bearing steel"; Journal of Zhejiang University - Science A, v 12, n 3, (2011), pp. 171 - 176.

31. Sha, Q. Y., Sun, Z. Q. and Li, L. F.; "Refinement of coarse grained austenite in Nb - V - Ti microalloyed steel during roughing rolling"; Iron and Steelmaking, v 42, n 1, (2015), pp. 74 - 80.

32. Dieter, G. E., Kuhn, H. A. and Semiatin, S. L.; "Handbook of workability and process design"; ASM International, ISBN 0 - 87170 - 778 - 0, (2003), pp 40 - 70.

33. Wang, L., Quian, D. Guo, J. and Pan, Y.; "Austenite grain growth behaviour of AISI 4140 alloy steel"; Advances in Mechanical Engineering, (2013), pp. 1 - 7.

34. Ruibal, E., Urcola, J. J. and Fuentes, M.; "Static recrystallisation kinetics, recrystallised grain size and grain growth kinetics after hot deformation of a low alloy steel"; Zeitschrift Fur Metallkunde, v 76, n 8, (1985), pp. 568 - 578.

35. Huang, Y. and Humpreys, F. J.; "Measurements of grain boundary mobility during recrystallisation of a single - phase Aluminium alloy"; Acta Materialia, v 47, n 7, (1999), pp. 2259 - 2268.
36. Kwon, O. and DeArdo, A. J.; "Interactions between recrystallisation and precipitation in hot - deformed microalloyed steels"; Acta Metallurgical Materials, v 39, n 4, (1991), pp. 529 - 538.
37. Rollett, A. D., Srolovitz, D. J. and Anderson, M.P.; "Simulation and theory of abnormal grain growth-anisotropic grain boundary energies and mobilities"; Acta Metallurgica, v 37, n 4, (1989), pp. 1227 - 1240.
38. Davis, C.; "The effect of microalloying precipitates on final product mechanical properties"; Transaction Indian Institute of Metals, v 59, n 5, (2006), pp. 1-16.
39. May, J. E. and Turnbull, D.; "Secondary recrystallization in Silicon Iron"; Transaction of the A.I.M.E., v 212, (1958), pp. 769 - 781.
40. Rios, P. R.; "Abnormal grain growth development from uniform grain size distributions"; Acta Materialia, v 45, n 4, (1997), pp. 1785 - 1789.
41. Beck, P. A, Holzworth, M.L. and Sperry, P.R.; "Effect of a dispersed phase on grain growth in Al - Mn alloys"; Transactions of A.I.M.E, v 180, (1949), pp. 163 - 192.
42. Hillert, M.; "On the theory of normal and abnormal grain growth"; Acta Metallurgica, v 13, n 3, (1965), pp. 227.
43. Gladman, T.; "On the theory of effect of precipitate particles on grain growth in metals"; Proceedings of the royal Society of London Series A- Mathematical and Physical Sciences, v 294, n 1438, (1966), pp. 298.

44. Fernandez, A. I., Uranga, P., Lopez, B., Rodriguez-Ibabe, J. M.; "Static recrystallisation behaviour of a wide range of austenite grain sizes in microalloyed steels"; ISIJ International, v 40, n 9, (2000), pp. 893 - 901.

45. Medina, S. F., Quispe, A.; "Improved model for static recrystallisation kinetics of hot deformed austenite in low alloy and Nb/V microalloyed steels"; ISIJ International, v 41, (2001), pp. 774 - 781.

46. Mannan, P, Kostryzhev, A. G., Zurob, H. and Perloma, E. V.; "Hot deformation behaviour of Ni - 30Fe - C and Ni - 30Fe - Nb - C model alloys"; Materials Science and Engineering A, v 641, (2015), pp. 160 - 171.

47. Laasraoui, A. and Jonas, J. J.; "Prediction of steel flow stresses at high temperatures and strain rates"; Metallurgical Transactions A, v 22A, (1991), pp. 1545 - 1558.

48. Li, G., Maccagno, T. M., Bai, D. Q. and Jonas, J. J.; "The effect of initial grain size on the static recrystallisation kinetics of Nb microalloyed steels"; ISIJ International, v 36, n 12,1996, pp. 1479 - 1485.

49. Medina, S. F. and Mancilla, J. E.; "Determination of static recrystallisation critical temperature of austenite in microalloyed steels", ISIJ International, v 33, n 12, (1993), pp. 1257 - 1264.

50. Sun, W. P. and Hawbolt, E. B.; "Comparison between static and metadynamic recrystallisation - an application to the hot rolling of steel"; ISIJ International, v 37, n 10, (1997), pp. 1000 - 1009.

51. Perttula, J. S. and Karjalaninen, L. J.; "Recrystallisation rates in austenite measured by double compression and stress relaxation methods"; Materials Science and Technology, v14, n 7, (1998), pp. 626 - 630.

52. Quispe, A., Medina, S. F., Gomez, M. and Chaves, J. I.; "Influence of austenite grain size on recrystallisation-precipitation interaction in a V - microalloyed steel"; Materials Science and Engineering A, v 447, (2007), pp. 11 - 18.

53. Dong, D., Chen, F. and Cui, Z.; "Static recrystallisation behaviour of SA508 - III steel during hot deformation"; Journal of Iron and steel research international, v 25, n 5, (2016), pp.466 - 474.

54. Palmiere, E. J., Bai, F., Poths, R. M., Turner, J., Vagarajan, V., Wynne, B. P. and Rainforth W. M.; "The use of model systems based on Fe - 30%Ni for studying the microstructural evolution during the hot deformation of austenite"; Material Science Forum, v 638/642, (1999), pp. 2694 - 2699.

55. Miao, C. L., Shang, C. J., Zurob, H. S., Zhang, G. D. and Subramanian, S. V.; "Recrystallisation, precipitation behaviours and refinement of austenite grains in high Mn, High Nb steel"; Metallurgical and Materials Transactions A, v 43A, (2012), pp. 665 - 676.

56. Doherty, R. D., Hughes, D. A., Humpreys, F. J., Jonas, J. J., Juul Jensen, D. Kassner, M. E., King, W. E., McNelley, T. R, McQueen, H. J. and Rollett, A. D.; "Current issues in recrystallization: a review"; Materials Science and Engineering, v A238, (1997), pp. 219 - 274.

57. Uranga, P., Gutierrez, I. and Lopez, B.; "Determination of recrystallisation kinetics from plane strain compression tests"; Materials Science and Engineering A, v 578, (2013), pp. 174 - 180.

58. Uranga, P., Fernández, A. I., Lopez, B. and Rodriguez-Ibabe, J. M.; "Modelling of austenite grain size distribution in Nb microalloyed steels processed by thin slab

casting and direct rolling (TSDR) route"; ISIJ International, v 44, n 8, (2004), pp. 1416 - 1425.

59. Taylor, A. S., Cizek, P. and Hodgson, P. D.; "Comparison of 304 stainless steel and Ni-30wt.% Fe as potential model alloys to study the behaviour of austenite during thermomechanical processing"; Acta Materialia, v 59, (2011), pp. 5832 - 5844.

60. Kazeminezhad, M.; "On the modelling of the static recrystallisation considering the initial grain size effects"; Materials Science and Engineering A, v 486, (2008), pp. 202 - 207.

61. Saidi, P., Shahandeh, S. and Hoyt, J.; "Relationship between recrystallization kinetics and the inhomogeneity of stored energy"; Metallurgical and Materials Transactions A, v 46A, (2015), pp. 2975 - 2985.

62. Ravi Kumar, B. and Sharma, S.; "Recrystallisation characteristics of cold rolled austenitic stainless steel during repeated annealing"; Materials Science Forum, v 753, (2013), pp. 157 - 162.

63. Le Bon, A., Rofes - Vernis, J., Rossard, C.; "Recrystallization and precipitation during hot working of a Nb-bearing HSLA steel"; Metal Science, v 9, n 1, (1975), pp. 36 - 40.

64. Sarkar, A. and Chakravartty, J. K.; "Investigation of progress in dynamic recrystallisation in two austenitic stainless steels exhibiting flow softening"; International Journal of Metallurgical Engineering, v 2, n 2, (2013), pp. 130 - 136.

65. Rainforth, W. M., Black, M. P., Higgison, R. L., Palmiere, E. J., Sellars, C. M., Prabst, I., Warbichler P. and Hofer, F.; "Precipitation of NbC in a model austenitic steel"; Acta Materialia, v 50, (2002), pp. 735 - 747.

66. Xu, W. and Ferry, M.; "Recrystallisation processes in cold low carbon steel strip containing different starting microstructures"; Materials Science and Technology, v 26, n 3, (2010), pp. 333 - 342.

67. Titchener, A. L. and Bever, M. B.; "The stored energy of cold work"; Progress in Metal Physics, v 7, (1958), pp. 247 - 337.

68. Bever, M. B., Holt, D. L. and Titchener, A. L.; "The stored energy of cold work"; Progress in Materials Science, v 17, (1973), pp.5 -177.

69. Bailey, J. E.; "The dislocation density, flow stress and stored energy in deformed polycrystalline copper"; Philosophical Magazine A, v 8, (1963), pp. 223 - 236.

70. Bailey, J. E. and Hirsch, P. B.; The dislocation distribution, flowstress and stored energy in cold - worked polycrystalline silver"; v 13, n 12, (1960), pp. 1115 - 1115.

71. Baker, I., Liu, L. and Madal, D.; "The effect of grain size on the stored energy of cold work as a function of strain for polycrystalline Nickel"; Scripta Metallurgica et Materialia, v 32, n 2, (1995), pp.167 - 171.

72. Madal, D. and Baker, I.; "The influence of grain boundaries on the stored energy of cold-work and recrystallization kinetics"; Materials Science Forum, v 207 - 209, (1996), pp. 521 - 524.

73. Clarebrough, L. M., Hargreaves, M. E. and Loretto, M. H.; "The influence of grain size on the stored energy and mechanical properties of Copper"; Acta Metallurgica, v 6, (1958), pp. 725 - 735.

74. Williams, R.O.; "The stored energy in deformed Copper: The effect of grain size and Silver content"; Acta Metallurgica, v 9, (1961), pp. 949 - 957.

75. Gordon, P.; "Microcalorimetric investigation of recrystallisation of copper"; Transactions of the American Institute of Mining, Metallurgical and Petroleum Engineers, v203, (1955), pp. 1043 - 1052.

76. Loretto, M. H. and White, A. J.; "The influence of grain size on the energy stored in deformed Copper"; Acta Metallurgica, v 9, (1961), pp. 512 - 513.

77. Hazra, S. S., Gazder, A. and Pereloma, E. V.; "Stored energy of a severely deformed interstitial free steel"; Materials Science and Engineering A, v 524, (2009), pp. 158 - 167.

78. Deng, C., Liu, S. F., Hao, X. B. Ji, L. J., Zhang, Z. Q. and Liu, Q.; "Orientation dependence of stored energy release and microstructure evolution in cold rolled tantalum"; International journal of refractory Metals and Hard Materials, v 46, (2014), pp. 24 - 29.

79. Clarebrough, L. M., Hargreaves, M. E., Michell, D. and West, G. W.; "The determination of the energy stored in a metal during plastic deformation"; Proceedings of the Royal Society of London, Series A, Mathematical and physical Sciences, v 215, n 1123, (1952), pp. 507 - 524.

80. Titchener, A. L.; "The stored energy of cold work in relation to grain size and other variables"; Acta Metallurgica, v 9, (1961), pp. 379 - 382.

81. Suzuki, T.; "The release of energy associated with crystal restoration in cold-worked polycrystalline Copper"; Science Rep. Research Institute, Tohoku University, A1, (1949), pp. 193.

82. Taylor, G. I. and Quinney, H.; "The latent energy remaining in a metal after cold working"; Proceeding of the Royal Society, v A143, (1934), pp. 307 - 326.

83. Clarebrough, L. M., Hargreaves, M. E. and West, G. W.; "The determination of the energy stored in a metal during plastic deformation"; Proceedings of the Royal Society of London series A - Mathematical and Physical Siences, v 232, n 1189, (1955), pp. 252 - 270

84. Greenfield, P. and Bever, M. B.; "The evolution of the energy stored by a Gold - Silver alloy cold - worked at 195 - Degrees - C and at room temperature"; Acta Metallurgica, v 4, (1956), pp. 433 - 439.

85. Palmiere, E. J., Garcia, C. I. and DeArdo, A. J.; "Influence of niobium supersaturation in austenite on the static recrystallization behaviour of low carbon microalloyed steels"; Metallurgical and Materials Transactions A, v 27A, n 4, (1996), pp. 951 - 960.

86. Ashby M. F.; "The deformation of plastically non-homogeneous materials"; Philosophical Magazine, 'structure and properties of condensed matter', v 21, (1970), pp. 399 - 422.

87. Keh, A. S.; "Conference on direct observations of lattice defects in crystals"; AIME, (New York; Interscience publishers), pp. 213.

88. Vandermeer, R. A. and Juul Jensen, D.; "Recrystallisation in hot vs cold deformed commercial aluminium: a microstructure path comparison"; Acta Materialia, v 51, (2003), pp. 3005 - 3018.

89. Vicente Alvarez, M. A., Marchena, M. and Perez. T.; "Recovery kinetics of cold - deformed Cr - Mo steels"; Metallurgical and Materials Transactions A, v 39A, (2008), pp. 3283 - 3290.

90. Sandstrom, R.; "On recovery of dislocations in subgrains and subgrain coalescence"; Acta Metallurgica, v 25, (1977), pp. 897 - 904.

91. Furu, T., Orsund, R. and Nes, E.; "Subgrain growth in heavily deformed aluminium – experimental investigation and modelling treatment"; Acta Metallurgica et Materialia, v 43, n 6, (1995), pp. 2209 - 2232.

92. Vandermeer, R. A. and Hansen, N.; "Recovery kinetics of nanostructured aluminium: Model and experiment"; Acta Materialia, v 56, (2008), pp. 5719 - 5727.

93. Yu, T. and Hansen, N.; "Recovery kinetics in commercial purity aluminium deformed to ultrahigh strain: model and experiment"; Metallurgical and Materials Transactions A, v 47A, (2016), pp. 4189 - 4196.

94. Hansen, N. and Juul Jesen, D.; "Deformed metals - structure, recrystallisation and strength"; Materials Science and Technology, v 27, n 8, (2011), pp. 1229 - 1240.

95. Haessner, F. and Schmidt, J.; "Recovery and recrystallisation of different grades of high purity aluminium determined with low temperature calorimeter"; Scripta Metallurgica, v 22, (1988), pp. 1917 - 1922.

96. Barraclough, D. R. and Sellars, C. M.; "Static recrystallisation and restoration after hot deformation of type 304 stainless steel"; Metal Science, v 13, (1979), pp. 257 - 267.

97. Karjalaninen, L. P.; "Stress relaxation method for investigation of softening kinetics in hot deformed steels"; Materials Science and Techonology, v 11, (1995), pp. 557-565.

98. Martinez-de-Guerenu, A., Arizti, F. and Gutierrez, I.; "Recovery during annealing in a cold rolled low carbon steel. Part I: Kinetics and microstructural characterisation"; Acta Materialia, v 52, (2004), pp. 3657 - 3664.

99. Beck, P. A.; "Annealing of cold worked metals"; Advances in Physics, v 3, n 11, (1954), pp. 245 - 324.

100. Martinez-de-Guerenu, A. Arizti, F. and Gutierrez, I.; "Recovery during annealing in a cold rolled low carbon steel. Part II: Modelling and kinetics"; Acta Materialia, v 52, (2004), pp. 3665 - 3670.

101. Nes, E.; "Recovery revisited"; Acta Metallurgica et Materialia, v 43, n 6, (1995), pp. 2189 - 2207.

102. Friedel, F., quoted by Humpreys, F. J. and Hatherly, M.; "Recrystallisation and related annealing phenomena"; Elsevier Ltd, 2nd Edition, ISBN: 978-0-08-044164-1, (2004).

103. De Campos, M. F.; "Selected values for the stacking fault energy of face centred cubic metals"; Materials Science Forum, v 591 - 593, (2008), pp. 708 - 711.

104. Jenkins, M. L.; "Measurement of the stacking - fault energy of gold using the weak – beam technique of electron microscopy"; Philosophical Magazine, v 26, (1972), pp. 747 - 751.

105. Cockayne, D. J. H., Jenkins, M. L. and Ray, I. L. F.; "The measurement of stacking - fault energies of pure face centred cubic metals"; Philosophical Magazines, v 24, (1971), pp. 1383 - 1392.

106. Mills, M. J. and Stadelmann, P.; "A study of the of the structure of lower and 60 - degrees dislocations in aluminium using high - resolution transmission electron - microscopy"; Philosophical magazine A - Physics of condensed matter structure defects and mechanical properties, v 60, n 3, (1989), pp. 355 - 384.

107. Gallagher, P. C. J.; "The influence of alloying, temperature and related effects on the stacking fault energy"; Metallurgical Transaction, v 1, n 9, (1970), pp. 2429 - 2461.

108. Charnock, W. and Nutting, J.; "The effect of Carbon and Nickel upon the stacking fault energy of Iron"; Journal of Materials Science, v 1, n 1, (1967), pp. 123 - 127.

109. Rhodes, C. G. and Thompson, A. W.; "The composition dependence of stacking fault energy in austenitic stainless steels"; Metallurgical Transactions A, v 8A, (1977), pp. 1901 - 1906.

110. Dillamore, I. L.; "The stacking fault energy dependence of the mechanisms of deformation in FCC metals"; Metallurgical Transactions, v 1, (1970), pp. 2463 - 2470.

111. Dumay, A., Chateau, J. P., Allain, S., and Bouaziz, O.; "Influence of addition elements on the stacking - fault energy and mechanical properties of an austenitic Fe - Mn - C steel"; Materials Science and Engineering A, v 483 - 484, (2008), pp. 184 - 187.

112. Harmida, J. D.; "Stacking fault energy decrease in austenitic stainless steels induced by hydrogen pairs formation"; v 39, n 8, (1998), pp. 1145 - 1149.

113. Schramm, R. E. and Reed, R. P.; "Stacking fault energies of seven commercial austenitic stainless steels"; Metallurgical Transactions A, v 6A, (1975), pp. 1345 - 1351.

114. Lecroisey, F. and Pineau, A.; "Martensitic transformations induced by plastic - deformation in Fe - Ni - Cr - C system"; Metallurgical Transactions, v 3, (1972), pp.387 - 396.

115. Pontini, A. E. and Hermida, J. D.; "X-Ray diffraction measurement of the stacking fault energy reduction induced by hydrogen in an AISI 304 steel"; Scripta Materialia, v 37, n 11, (1997), pp. 1831 - 1837.

116. Doherty, R. D.; "The deformed state and nucleation of recrystallisation"; Metal Science, v 8, (1974), pp. 132 - 142.

117. Dillamore, I. L., Morris, P. L., Smith, C. J. E and Hutchinson, W. B.; "Transition bands and recrystallisation in metals"; Proceedings of the Royal Society of London, Series A - Mathematical and Physical Sciences, v 329, n 1579, (1972), pp. 405 - 420.

118. Humphreys, F. J.; "A unified theory of recovery, recrystallisation and grain growth based on the stability and growth of cellular microstructures - I. The basic model"; Acta Materialia, v 45, n 10, (1997), pp. 4231 - 4240.

119. Swan, P. R.; "Electron microscopy and strength of crystals"; New York (Interscience publishers) edited by Thomas, G. and Washburn, J., (1963), pp. 131 - 181.

120. Furu, T., Orsund, R. and Nes, E.; "Subgrain growth in heavily deformed aluminium - experimental investigation and modelling treatment"; Acta Metallurgica et Materialia, v 43, n 6, (1995), pp. 2209 - 2232.

121. Hurley, P. J. and Humpreys, F. J.; "The application of EBSD to the study of substructural development in a cold rolled single-phase aluminium alloy"; Acta Materialia, (2003), v 51, pp. 1087 - 1102.

122. Bailey, J. E. and Hirsch, P. B.; "Recrystallisation process in some polycrystalline metals"; proceedings of the royal society of London Series A, v A267, n 1328, (1962), pp. 11 - 30.

123. Honeycombe, R. W. K.; "The plastic deformation of metals"; 2nd Edition, ASM, Metal Park, OH, (1984), pp. 287.

124. Turnbull, D. and Fisher, J. C.; "Rate of nucleation in condensed systems"; Journal of Chemical physics, v 17, (1949), pp. 71-73.

125. Burke, J. E. and Turnbull, D.; "Recrystallisation and grain growth "; Progress in Metal Science, v 3, (1952), pp. 220 - 292.

126. Byrne, J. G.; "Recovery, Recrystallisation and Grain growth"; MacMilla series in Materials Science, New York, (1965).

127. Cahn, R. W.; "Physical Metallurgy"; editions by Cahn, R. W. and Hansen, P. North-Hallard Physics publishing, New York, (1983), pp.1595.

128. Doherty, R. D.; "Recrystallization and grain growth of multi-phase and particle containing materials"; Proceedings of the 1st RISO International symposium on Metallurgy and Materials Science, editions by Hansen, N., Jones, A. R., and Leffers, T., (1980), pp. 57.

129. Cahn, R. W.; "Recrystallisation, grain growth and textures"; New York, Ny, H. Margolin edition ASM, Metal Park, OH, (1966), pp. 99.

130. Beck, P. A. and Sperry, P. R.; "Effect of recrystallization texture on grain growth"; Transactions of A.I.M.E, v 185, (1949), pp. 240 - 241.

131. Hosford, W. F.; "Physical Metallurgy"; CRC Press, Taylor and francis group 2nd Edition, ISBN: 978-1-4398-1361- 4, (2010), pp. 152.

132. Beck, P. A. and Sperry, P. R.; "Strain induced grain boundary migration in high purity aluminium"; Journal of Applied Physics, v 21, (1950), pp. 150 - 152.

133. Bellier, S. P. and Doherty, R. D.; "Structure of deformed aluminium and its recrystallization - investigations with transmission Kossel diffraction"; Acta Metallurgica., v 25, n 5, (1977), pp. 521 - 538.

134. Paggi, A., Angella, G. and Donnini, R.; "Strain induced grain boundary migration effects on grain growth of an austenitic stainless steel during static and metadynamic recrystallisation"; v 107, (2015), pp. 174 - 181.

135. Andrade, H. L., Akben, M. G. and Jonas, J. J.; "Effect of molybdenum, niobium and vanadium on static recovery and recrystallisation and on solute strengthening microalloyed steels"; Metallurgical Transaction A - Physical Metallurgy and Materials Science, v 14, n 10, (1983), pp. 1967 - 1977.

136. Smith, C. S.; "Grains, phases and interphases, an interpretation of microstructure"; Transactions of Metallurgical Society of AIME, v 175, (1948), pp. 47.

137. White, M. J. and Owen, W. S.; "Effects of vanadium and nitrogen on recovery and recrystallisation during and after hot-working some HSLA steels"; Metallurgical Transactions A, 11A, n 4, (1980), pp. 597 - 604.

138. Cordea, J. N. and Hook, R. E.; "Recrystallisation behaviour in deformed austenite of high strength low alloy (HSLA) steels"; Metallurgical Transactions, v 1, n 1, (1970), pp. 111 - 118.

139. Vercammen, S. Blanpain, B., De cooman, B. C. and Wollants, P.; "Cold rolling behaviour of an austenitic Fe - 30Mn-3Al - Si TWIP - steel: the importance of deformation twinning"; Acta Materialia, , (2004), pp. 2005 - 2012.

140. Bai, D. Q., Yue, S., Sun, W. P. and Jonas, J. J.; "Effect of deformation parameters on the no - recrystallisation temperature in Nb-bearing steels";

Metallurgical and Materials Transaction A-Physical Metallurgy and Materials Science), v 24, n 10, (1993), pp. 2151 - 2159.

141. Siwecki, T.; "Modelling of microstructure evolution during recrystallisation controlled rolling"; ISIJ International, v 32, n 3, (1992), pp. 368 - 376.

142. Cho, S.; "Static recrystallisation kinetics of 304 stainless steel"; Journal of Materials Science, v 36, (2001), pp. 4273 - 4278.

143. Cho, S., Lang, K. and Jonas, J. J.; "The dynamic, static and metadynamic recrystallisation of a Nb-microalloyed steel"; ISIJ International, v 41, n 1, (2001), pp. 63 - 69.

144. Du, J., Strangwood, M. and Davis, C. L.; "Effect of TiN particles and grain size on the Charpy impact transition temperature in steels"; Journal of Materials Science and Technology, v 28, n10, (2012), pp. 878 - 888.

145. Weiss, I. and Jonas, J. J.; "Dynamic precipitation and coarsening of niobium carbonitrides during the hot compression of HSLA steels"; Metallurgical Transactions A - Physical Metallurgy and Materials Science, v 11, n 3, (1980), pp. 403 - 410.

146. Leduc, L. A. and Sellars, C. M.; "In Thermomechanical processing of microalloyed austenite"; (edited by DeArdo, A. J., Ratz, G. A. and Wray, P. J.), Metallurgical Society of AIME, (1982), pp. 641.

147. Humphreys, F.J.; "The nucleation of recrystallisation at second phase particles in deformed aluminium"; Acta Metallurgica, v 25, n 11, (1977), pp. 1323 - 1344.

148. Humphreys, F. J. and Kalu, P. N.; "Dislocation particle interactions during high temperature deformation of 2 - phase aluminium - alloys"; Acta Metallurgica, v 35, n 12, (1987), pp. 2815 - 2829.

149. Humphreys, F.J. and Kalu, P. N.; "The plasticity of particle - containing polycrystals"; Acta Metallurgica et Materialia, v38, n 6, (1990), pp. 917 - 930.

150. Gomez, M., Rancel, L., Fernandez, B. J. and Medina, S. F.; "Evolution of austenite static recrystallization and grain size during hot rolling of a V-microalloyed steel"; Materials Science Engineering A, v 501, n 1 - 2 (2009), pp. 188 - 196.

151. Bracke, L., Verbeken, K., Kestens, L. and Penning, J.; "Microstructure and texture evolution during cold rolling and annealing of a high Mn TWIP steel"; Acta Materialia, v 57, n 5, (2009), pp. 1512 - 1524.

152. Jiang, L., Humphreys, A. O. and Jonas, J. J.; "Effect of silion on the interaction between recrystallisation and precipitation in niobium microalloyed steel"; ISIJ International, v 44, n 2, (2004), pp. 381 - 387.

153. Vervynckt, S., Verbeken, K., Thibaux, P. and Houbaert, Y; "Evaluation of the austenite recrystallisation by multi-deformation and double deformation tests"; Steel Research, v 82, (2011), pp. 369 - 378.

154. Dzubinsky, M., Husain, Z. and van Haaften, W. M; "Comparison of recrystallisation kinetics determined by stress relaxation, double hit, optical metallography and EBSD approaches"; Materials Characterisation, v 52, (2004), pp. 93 - 102.

155. Devadas, C., Samarasekera, I. V. and Hawbolt, E. B.; "The thermal and metallurgical state of steel strip during hot rolling.3. microstructural evolution"; Metallurgical and Materials Transaction A, v 22, 2, (1991), pp. 335 - 349.

156. Bleck, W., Herzig, C. and Venkatraman, M.; "Softening behaviour after deformation in the austenite-ferrite two phase-region"; Steel Research International, v 74, n 5, (2003), pp. 311- 317.

157. McQueen, H. J. and Jonas, J. J.; "In 'Metal forming: interrelation between theory and practice"; New York, Plenum Press, (1971), pp. 393 - 428.

158. Airaksinen, K., Karjalainen, L. P, Porter, D. and J. Perttula, J.; "Recrystallisation kinetics of microalloyed steels determined by two mechanical testing techniques"; Materials Science Forum, v 284 - 286, (1998), pp. 119-126.

159. Liu, W. J. and Akben, M. G.; "Softening behaviour of 2 Ti bearing steels during torsional simulation of rolling"; Canadian Metallurgical Quarterly, v 26, n 2 (1987), pp. 145 - 153.

160. Yanagida, A. and Yanagimoto, J.; "Formularization of softening fractions and related kinetics for static recrystallisation using inverse analysis of double compression test"; Materials Science Engineering A - Structural materials properties microstructure and processing, v 487, n 1 - 2 (2008), pp. 510 - 517.

161. Iparraguirre, C., Ferna´ndez, A. I., Lo´pez, B., Scott, C., Rose, A., Kranendonk, W., Soenen, B. and Paul, G.; "Characterisation of strain induced precipitation of Nb in microalloyed austenite"; Materials Science Forum, v 500 - 501, (2005), pp. 677 - 684.

162. Quidort, D., Lotter, U., Lorenz, U., Vandekinderen, H., Zufia, A. and van Haafteen, W. M; "New concepts for understanding and modelling the influence of austenite state on phase transformations in hot rolled steels"; Final report of the ECSC Steel RTD Programme, IRSID, Maizie`res-le`s-Metz, France, (2003).

163. Samarasekera, I. V. and Hawbolt, E. B; "Overview of modelling the microstructural state of steel strip during hot rolling"; The South African Institute of Mining and Metallurgy, (1995), ISSN 0038-223X, pp. 157-165.

164. Irvine, K. J. and Pickering, F. B., Gladman, T.; "Grain-refined C-M steels"; Iron and Steel Institute-Journal., v 205, n 2, (1967), pp. 161 - 182.

165. Fernandez, A. I., Lopez, B. and Rodriguez - Ibabe, J. M.; "Relationship between the austenite recrystallized fraction and the softening measured from the interrupted torsion test technique"; Scripta Materialia, v 40, n 5, (1999), pp. 543 - 549.

166. Watson, C.; "Modelling high integrity steel forgings for turbine applications in the power generation industry"; Ph. D Thesis, The University of Birmingham, (2015).

167. Jonas, J. J.; "Mechanical testing for the study of austenite recrystallization and Carbo-nitride precipitation"; Woolongong, Australia, (1984), pp. 80 - 91.

168. Almaguer, S., Sellars, C. M. and Rainforth, W. M.; "Study of the static recrystallization of an Fe-30%Ni alloy and comparison with plain Carbon steel"; Proceedings of the First Joint International Conference, (2001), pp. 831 - 836.

169. Oyarzabal, M., Martinez de Guerenu, A., and Gutierrez, I.; "Effect of stored energy and recovery on the overall recrystallization kinetics of a cold rolled low Carbon steel"; Materials Science and Engineering A, v 485, n 1-2, (2008), pp. 200 - 209.

170. Dutta, B. and Sellars, C. M.; "Effect of composition and process variables on Nb (C, N) precipitation in niobium microalloyed austenite"; Materials Science and Technology, v 3, n 3, (1987), pp. 197 - 206.

171. Ji, M., Janik, V., Strangwood, M., and Davis C. L.; "Effect of grain size distribution on recrystallisation kinetics in a Fe - 30 Ni Alloy"; 6th International Conference on Recrystallization and Grain Growth, (2016), Pittsburgh, USA.

172. Luo, H. and Zwaag, S.; "An analytical approach to model heterogonous recrystallisation kinetics taking into account the natural spatial inhomogeneity of deformation"; Metallurgical and Materials Transaction A, v 47A, (2016), pp. 231 - 238.

173. Medina, S. F. and Fabregue, P.; "Activation energy in the static recrystallisation of austenite "; Journal of Materials Science, v 26, (1991), pp. 5427 - 5432.

174. Zurob, H. S., Brechet, Y. and Purdy, G.; "A model for the competition of precipitation and recrystallisation in deformed austenite"; Acta Materialia, v 49, (2001), pp. 4183 - 4190.

175. Jonas, J. J. and Weiss, I.; "Effect of precipitation on recrystallisation in microalloyed steels"; Metal Science, v 13, n 3 - 4, (1979), pp. 238 - 245.

176. Weiss, I and Jonas, J. J.; "Interaction between recrystallisation and precipitation during the high temperature deformation of HSLA steel"; Metallurgical Transactions A, v 10, n7, (1979), pp. 831 - 840.

177. DeArdo, A. J.; "Niobium in modern steels"; International Materials Reviews, v 48, n 6, (2003), pp. 371 - 402.

178. Cai, S. and Boyd, J. D.; "Mechanism of microstructural bonding in hot rolled microalloyed steels"; Materials Science Forum, v 500 - 501, (2005), pp. 171 - 178.

179. Dutta, B. and Palmiere, E.J.; "Effect of prestrain and deformation temperature on the recrystallisation behaviour of steels microalloyed with niobium"; Metallurgical and Materials Transactions A, v 34A, n 6, (2003), pp. 1237 - 1247.

180. Courtois, E., Epicier, T. and Scott, C.; "Characterisation of Niobium carbide and carbonitride evaluation within ferrite contribution of transmission electron microscopy and advanced associated techniques"; Materials Science Forum, v 500 - 501, (2005), pp. 669 - 677.

181. ZaJac, S.; "Precipitation of microalloying carbo - nitrides prior durig and after g / a transformation"; Materials Science Forum, v 500 - 501, (2005), pp. 75 - 86.

182. Hodgson, P. D., Beladi, H., Barnet, M. R.; "Grain refinement in steels through thermomechanical processing"; Materials Science Forum, v 500 - 501, (2005), pp. 39 - 48.

183. Abad, R., Fernandez, A. I, Lopez, B. and Rodriguez-Ibabe, J. M.; "Interaction between recrystallisation and precipitation during multipass rolling in a low Carbon Niobium microalloyed steel"; ISIJ International, v 41, n 11, (2001) pp. 1373 - 1382.

184. Kim, S., Lee, Y. and Jang, B.; "Modelling of recrystallisation and austenite grain size for AISI 316 stainless steel and its application to hot bar rolling"; Materials Science and Engineering, v A357, (2003), pp. 235 - 239.

185. Chen, J., Lv, M. Y., Tang, S., Liu, Z. Y. and Wang, G. D.; "Influence of thermomechanical control process on the evolution of austenite grain size in a low - carbon Nb - Ti - bearing bainitic steel"; Journal of Materials Engineering and Performance, v 24, n 10, (2015), pp. 3852 - 3861.

186. Pareda, B., Uranga, P., Lopez, B., Rodriguez - Ibabe, J.M., Arantes - Rebellato, M. and Nagarajan, V.; "Mill data based microstructural modelling for Thin

Slab Direct Rolling of Nb microalloyed steels"; Proceedings of the 4th international conference on Thermo - mechanical simulation and processing of steels (simPro 16), India, (2016), pp. 196 - 206.

187. Wu, S. J and Davis, C. L.; "Effect of duplex ferrite grain size distribution on local fracture stresses of Nb - microalloyed steels"; Materials Science and Engineering A, v 387 - 389, (2004), pp. 456 - 460.

188. Abbod, M. F., Sellars, C. M., Cizek, P., Linkens D. A. and Mahfouf, M.; "Modelling the flow behaviour, recrystallisation, and crystallographic texture in hot-deformed Fe - 30 wt pct Ni austenite"; Metallurgical and Materials Transaction A, v 38A, (2007), pp. 2400 - 2409.

189. Kalinowski, P., Strangwood M. and Davis, C. L.; "Recrystallisation and grain size development during forging in power generation steels"; proceedings of the 6th International Conference Steelsim, (2015).

190. Ji, M.; "Effect of precipitation on recrystallisation of HSLA steels"; Ph. D research project, (on going).

191. Du, J.; "Development of high strength hot rolled strip products with Baintic / Martenisitic microstructures"; PhD research project, (2016).

192. Reardon, A.; "Metallurgy for Non - Metallurgists"; 2nd Edition, ASM International, (2011), ISBN 1-61503-821- 3 pp. 120 - 121.

193. Shipway, P. H. and Bhadeshia, H. K. D. H.; "Mechanical stabilisation of Bainite"; Materials Science and Technology, v 11, (1995), pp. 1116 - 1128.

194. Karhausen, K. F. and Roters, F.; "Development and application of constitutive equations for the multi-stand hot rolling of Al-alloys"; Journal of Materials Processing Technology, (2002), pp. 155 - 166.

195. Attallah, M.; "Microstructure-property development in friction stir welds of aluminium-based alloys"; Ph. D Thesis, The University of Birmingham, (2007).

196. Zhang, L. P., Davis, C. L. and Strangwood, M.; "Assessment of microstructural development during continuous casting of microalloyed bars"; Proceeding from conference on 'Thermomechanical processing of steels', published by IoM Communications, ISBN I-86125-122-X, London, (2000), pp. 764 - 775.

197. Dutta, B., Palmiere, E. J. and Sellars, C. M.; "Modelling the kinetics of strain induced precipitation in Nb microalloyed steels"; Acta Materialia, v 49, (2000), pp.785 - 794.

198. Roebuck, B., Lord, J. D., Brooks, M., Loveday, M. S., Sellars, C. M. and Evans, R. W.; "Measuring flow stress in hot axisymmetric compression tests"; ed. Teddington: National Physical Laboratory, (2002), pp.1 - 62.

199. Cahn, J. W.; "The kinetics of grain boundary nucleated reactions"; v 4, Acta Metallurgica, (1956), pp. 449 - 459.

200. Cahn, J. W.; "Nucleation on dislocations"; Acta Metallurgica, v 5, (1957), pp. 169 - 172.

201. Akben, M. G, Bacroix, B. and Jonas, J. J.; "Effect of vanadium and molybdenum addition on high temperature recovery, recrystallisation and precipitation behaviour of niobium - based microalloyed steels"; Acta Metallurgica, v 31 (1983), pp. 161 - 174.

202. Brook, C.R.; "Principles of the heat treatment of plain Carbon and low alloy steels"; ASM International, ISBN: 0-87170-538-9, (1999), pp. 270 - 271.

Appendix A

A.1 Rationale behind the use of the NRMS error approach

The reasons for using NRMS (normalised root mean square) error approach instead of RMS (root mean square) error approach are considered in the following paragraph. The following paragraph also justify why the number of bins for the widest grain size is employed in the normalised root mean square approach.

For grain size distributions that perfectly match (in terms of area percent and grain size classes) the NRMS error will be zero. From Table A.1 it can be seen that if grain size distributions (i.e. predicted and measured) have an equal number of bins for grain size classes, the value for the NRMS error does not differ as significantly as the RMS error approach does. A difference of 0.02 is observed when the NRMS error approach is used whereas for the RMS error approach a difference of 7.7 is observed. However, when the number of bins for grain size classes for the measured and predicted grain size distributions are very different, example distributions are given Figure A.1; the difference between computed NRMS error values increases slightly.

Table A.1: RMS and NRMS error values for different bin sizes for matching distributions (in terms of number of grain size classes in a distribution). Bin size is in microns.

RMS		**NRMS**	
Bins of 10	Bins of 20	Bins of 10	Bins of 20
10.3	18	0.92	0.90

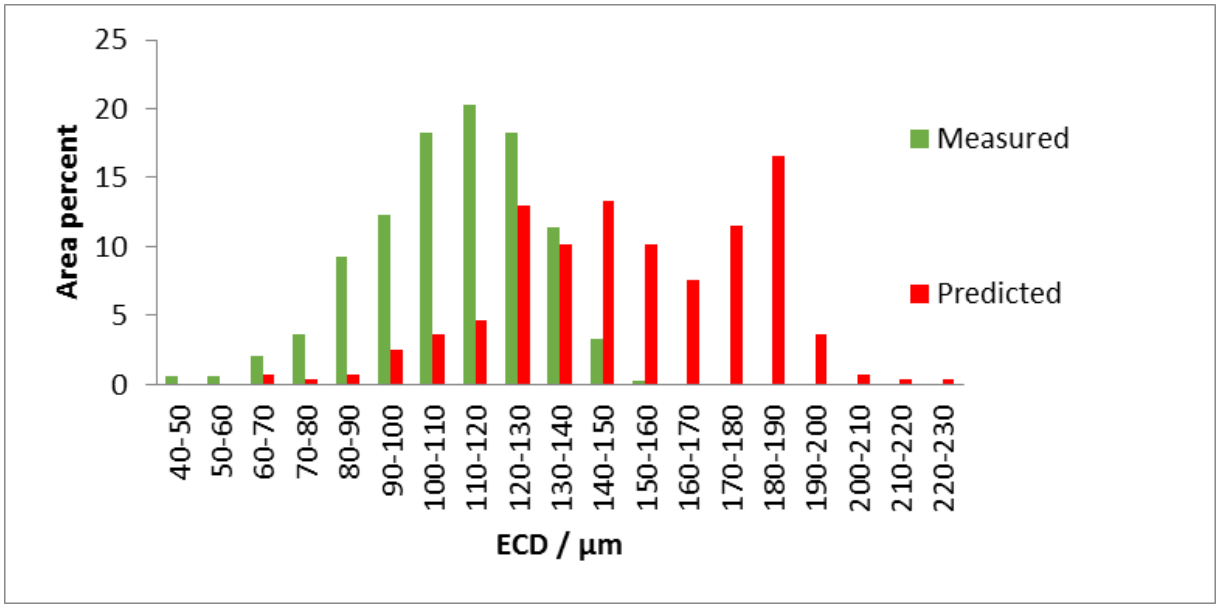

Figure A.1: Non-matching distributions in terms of number of grain size bins for the predicted and measured distribution.

Greater variation is observed in the NRMS error values when the measured and predicted number of bins (for the widest grain size distribution) are swapped around, that is, using the number of bins for the measured grain size distribution to determine the RMS error while the number of bins for the predicted grain size distribution (number of bins for the widest grain size distribution) is used to determine the mean for the total area percent, which is consequently used to compute the NRMS error and vice versa as shown in Tables A.2 and A.3.

Table A.2: RMS and NRMS error values for different bin sizes for non-matching distributions (in terms of number of grain size classes in a distribution); RMS error values determined using the number of grain size bins for the measured grain size distribution and NRMS error determined using the number of grain size bins for the predicted grain size distribution (widest distribution). Bin size in microns.

RMS		**NRMS**	
Bins of 10	Bins of 20	Bins of 10	Bins of 20
8.9	15.6	1.1	0.95

Table A.3: RMS and NRMS errors for different bin sizes for un-matching distributions (in terms of number of grain size classes in a distribution); RMS determined using the number of grain size bins for the predicted grain size distribution (widest distribution) and NRMS error determined using number of grain size bins for the measured grain size distribution in order to determine NRMS error. Bin size in micron.

RMS		**NRMS**	
Bins of 10	Bins of 20	Bins of 10	Bins of 20
10.58	20.3	1.8	2

Swapping the number of bins in order to determine either RMS and NRMS error values for the same grain size distribution should not give different values of NRMS error as these distributions are essentially the same (in terms of discrepancy between grain size distributions) and as such the same value of NRMS error should be computed. However, as can be seen from Tables A.2 and A.3 the errors are twice as much when the number of bins is swapped around. It can be seen from Tables A.2 and A.3 that if predicted and measured grain size distributions do not have the same number of bins the value for the NRMS error does not differ as much as it does when the RMS error approach is employed. When grain size bins are

varied, differences of 0.15 - 2 between NRMS error values are observed while for the RMS error approach differences of 6.7 - 9.72 are observed as shown in Tables A.2 and A.3. The effect of varying the number of bins is reduced when the NRMS error approach is applied as compared to when RMS error approach is used. Although differences between NRMS errors increase slightly when non - matching grain size distributions are considered the differences between NRMS errors are better than when the RMS error approach is applied. Since the difference in error values (0.02) is not as significant when matching distributions are considered, that is, using the number of bins for the widest grain size distribution to compute both the RMS error and the mean for the total area percent, this work has therefore used the number of bins for the widest grain size distribution in order to compute both the RMS error and the mean for the total area percent used in order to compute NRMS errors. Therefore, NRMS error approach has been used to calculate errors between the measured and the predicted area percent values for the grain size distributions as it is not as dependent on the number of bins as is the RMS error approach.

Appendix B

B.1 Determination of the strain and initial grain size exponents

B.1.1 Strain exponent determination

Stored energy is approximately proportional to hot strain (ε), and from classical nucleation, the nucleation rate (N_V) is proportion to $\exp(\frac{\Delta G^*}{kT})$ which is approximately $1 - \frac{\Delta G^*}{kT}$, where ΔG^* is the nucleation barrier (Equation B.1) [24, 131, 191, 200].

$$N_V = C_4 v \exp - (\frac{\Delta G^*}{kT}) \exp - (\frac{\Delta G}{kT}) \quad m^3 s^{-1} \qquad (B.1)$$

Where v is frequency factor, C_4 is the factor that represents the number of nucleation sites per unit volume, ΔG* is the critical free energy or activation energy for nucleation, ΔG is the free energy of activation for diffusion, N_V is the number of nuclei per unit volume per unit time (nucleation rate), T is the absolute temperature and k is the Boltzmann constant [20, 24, 124, 199].

As a nucleus with radius r forms, the change in Gibbs free energy (ΔG(r)) is given by Equation B.2.

$$\Delta G(r) = \frac{4}{3}\pi r^3 \Delta G_v + 4\pi r^2 \gamma_2 \qquad (B.2)$$

For nucleus formation, the Gibbs free energy change is balanced by the two competitive factors, the volume free energy (ΔG_v, which represents the driving for nucleation) and

interfacial energy (γ_2) due to formation of a new phase as shown in Figure B.1.

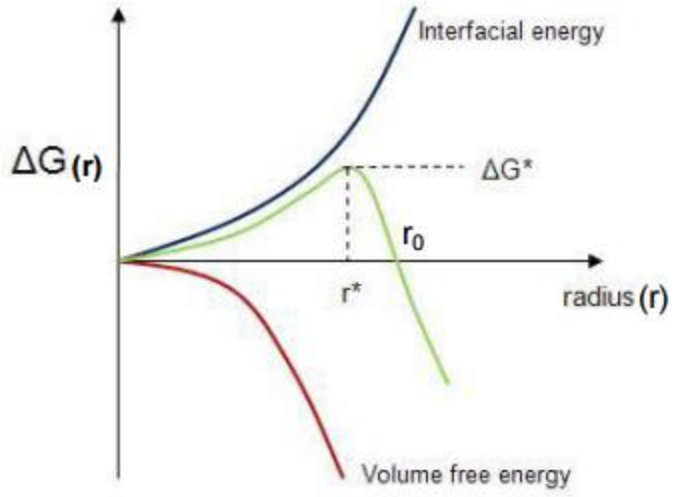

Figure B.1: Schematic plot of Gibbs free energy versus nucleus radius, on which is shown the critical free energy change (ΔG^*) and the critical nucleus radius (r*); schematic curves for volume free energy and interfacial energy are also shown [25].

As r increases initially for small r, $r^2 > r^3$, so $\Delta G(r) > 0$; for large r, $r^2 < r^3$, $\Delta G(r) < 0$. Thus, $\Delta G(r)$ must go through a maximum.

At the maximum,

$$\left.\frac{d\Delta G(r)}{dr}\right|_{r^*} = 0 \qquad \text{(B.3)}$$

This yields Equation B.4:

$$4\pi r^{*2}\Delta G_v + 8\pi r^*\gamma_2 = 0 \qquad \text{(B.4)}$$

Making r* the subject of Equation B.4 leads to Equation B.5 and substituting the expression obtained for r* into Equation B.2 yields Equation B.6.

$$r^* = -\frac{2\gamma_2}{\Delta G_V} \qquad \text{(B.5)}$$

$$\Delta G^* = \frac{16\pi\gamma_2^3}{3\Delta G_V^2} \quad \text{(B.6)}$$

Therefore, for a critical radius of growth the critical free energy for nucleation (nucleation barrier) is inversely proportional to the square of volumetric free energy (ΔG_V). Thus, the nucleation rate is also influenced by the volumetric free energy which is assumed to be the driving force for nucleation.

$$\Delta G^* \propto \frac{1}{\Delta G_V^2} \quad \text{(B.7)}$$

During deformation, the difference in stored energy between two grains is the driving force for recrystallisation, and stored energy is assumed to be approximately proportional to strain the following relationship is assumed:

$$\Delta G_V \propto \varepsilon^2 \implies \Delta G^* \propto \frac{1}{\varepsilon^2} \quad \text{(B.8)}$$

Equation B.8 suggests that the strain exponent in Sellars ($D_{rex} = D' D_o^x \varepsilon^{-y}$) equations should be equal to - 2 (y = - 2). However, nucleation rate is also dependant on strain therefore the nucleation rate (nucleation sites per unit volume) is proportional to ($\varepsilon * D_o^2$) / D_o^3 which means that there is a strain dependency of 1 giving a combined strain exponent (y) of -1. However, there is a dependence of the actual useful stored energy on grain size as some of the stored energy goes into maintaining the boundaries (in form geometrically necessary dislocations), which so far has not been taken into account. Therefore, either x must be dependent on D_o and ε or can be accounted for in *D'*, hence *D'* must be a function of ε and D_o, $f\{\varepsilon, D_o\}$. This dependence should be independent of alloy content when there is no recovery.

B.1.2 Initial grain size exponent determination

From classical nucleation, the nucleation rate (i.e. nuclei per unit time per unit volume) represented by Equation B.1 is shown to be dependent on the initial grain size which is related to the jump frequency and the number of nucleation sites (Nucleation rate $\propto$ Number of nucleation sites. A decrease in the prior austenite grain size leads to an in increase in the boundary area (higher nucleation sites density per unit volume) and as such an increase nucleation rate leads to a finer recrystallised grain size [202]. Few nuclei per unit time per unit volume leads to a bigger grain size being formed due to the fact that the few nuclei that are formed given a grain boundary area per unit volume are allowed to grow into big grains until impingement as compared to when there is more nuclei formed per unit time [24, 131]. Therefore, nucleation rate, is proportional to nucleation sites per unit volume ($D_o^2/ D_o^{3)}$ leading to nucleation rate being proportional to D_o^{-1}, but the recrystallised grain size (D_{rex}) is inversely proportional to the nucleation rate, and as such, since nucleation rate $\propto D_o^{-1}$ and $D_{rex} \propto \frac{1}{N_V}$ then D_{rex} is proportional to D_o^1. Hence a D_o exponent of 1 is proposed for use in Sellars equations. Therefore, the following equation: $D_{rex} = D' D_o \varepsilon^{-1}$ is proposed for predicting the recrystallised grain size.